

Tiago Ancelmo de Carvalho Pires de Oliveira

# FIRE RESISTANCE OF COMPOSITE COLUMNS MADE OF CONCRETE FILLED CIRCULAR HOLLOW SECTIONS AND WITH RESTRAINED THERMAL ELONGATION

Thesis presented in fulfillment of the requirements for the Degree of Doctor of  
Philosophy (PhD) in "Construção Metálica e Mista" - Dept. of Civil Engineering -  
Faculty of Sciences and Technology of the University of Coimbra

2013



UNIVERSIDADE DE COIMBRA



**FCTUC** DEPARTAMENTO DE ENGENHARIA CIVIL  
FACULDADE DE CIÊNCIAS E TECNOLOGIA  
UNIVERSIDADE DE COIMBRA



Institute for Sustainability and  
Innovation in Structural Engineering



# **FIRE RESISTANCE OF COMPOSITE COLUMNS MADE OF CONCRETE FILLED CIRCULAR HOLLOW SECTIONS AND WITH RESTRAINED THERMAL ELONGATION**

**Thesis presented in fulfillment of the requirements for the Degree of Doctor of  
Philosophy (PhD) in “Construção Metálica e Mista” – Dept. of Civil Engineering –  
Faculty of Sciences and Technology of the University of Coimbra**

**Author**

**Tiago Ancelmo de Carvalho Pires de Oliveira**

**Supervisors**

**Prof. João Paulo Correia Rodrigues**  
University of Coimbra, Portugal.

**Prof. José Jéferson do Rêgo Silva**  
Federal University of Pernambuco, Brazil.

**Coimbra, September 2013**

## ACKNOWLEDGEMENTS

To my supervisors Professors João Paulo Correia Rodrigues and José Jéferson do Rêgo Silva for their tireless dedication to the supervision of this work, it was indispensable to the success of this research.

The PhD scholarship of Erasmus Mundus in the framework of the “Improving Skills Across Continents (ISAC)” Programme, the Portuguese Foundation for Science and Technology (FCT) due to financial for the research in the framework of PTDC ECM 65696/2006 research project, Metalcardoso S.A. and A. da Costa Cabral for providing steel profiles at a reduced price for the experimental tests and other enterprises that contributed to the research.

Professors, employees and friends of the PhD program “Construção Metálica e Mista” of the University of Coimbra, the Division of International Relations at the University of Coimbra and other bodies of the University of Coimbra who contributed immensely to the realization of this work.

To the University of Coimbra, Coimbra city and the Portuguese State who welcomed me during this period.

To my friend and Professor Dayse Duarte of the Federal University of Pernambuco – Brazil, which was always encourage my academic career.

To the friends I met on this journey, which facilitated the adaptation and coexistence stay in Coimbra, Portugal.

To my uncles, cousins, brothers, friends, who directly or indirectly took part in all this.

Finally, but not least to my family: Dad, Mom, Camila and Dede, you more than anyone else lived this journey by minors. Thanks for your patience, I apologize for my shortcomings, and I dedicate this work to you.

## ABSTRACT

Composite columns made of Concrete Filled Circular Hollow (CFCH) sections or CFCH columns become popular principally in high-rise and industrial buildings as a good solution for fire situation due advantages such as high load-bearing capacity, high seismic resistance; attractive appearance, slenderness, fast construction times and reduced costs.

Despite several research studies on fire resistance of CFCH columns, its behaviour in fire is not completely understood. Most of these studies did not consider the restraining to column thermal elongation, important parameter for behaviour of the column on fire when that one is inserted in a structure.

This thesis presents the results of a series of forty fire resistance tests on CFCH columns with axial and rotational restraining to thermal elongation. Parameters such as the slenderness of the column, its load level, the stiffness of the surrounding structure, the ratio of steel reinforcement and the degree of concrete filling inside the column, were tested. Circular Hollow Sections (CHS) columns (*i.e.* steel columns) were tested also for comparison.

A three-dimensional nonlinear finite element model developed in ABAQUS (2011) to predict the behaviour in fire of these columns is presented and validated in comparison with the fire tests. The model includes the relevant parameters tested experimentally.

The research is complemented with a numerical analysis that includes a range of practical values of load level, diameter of the column and ratio of reinforcement for the columns. Based on this study, simple equations to evaluate the critical time of the CFCH columns are proposed. Finally, a comparison between the research results and the simple methods proposed by EN1994-1-2 (2005) is presented.

The thesis shows critical times smaller than the fire resistance suggested in literature for the studied CFCH columns. The stiffness of the surrounding structure does not lead to major changes in the critical times. The numerical model presents results in close agreement with the experimental data. Based on numerical data simplified equations to evaluate the critical time of these columns with restrained thermal elongation were proposed. The tabulated data method may be unsafe and the simple calculation model is conservative to evaluate the fire resistance of CFCH column in the fire.

Keywords: fire, column, steel, concrete, resistance, thermal restraining.



## RESUMO

As colunas tubulares em aço de secção circular preenchidas por betão (CFCH) tornaram-se populares na indústria da construção civil, especialmente em plantas industriais ou prédios altos, como uma boa solução em situação de incêndio. Isto deve-se a sua alta capacidade de carga, resistência sísmica, elegância, esbeltez, tempos e custos de construção reduzidos.

Apesar de vários estudos de investigação sobre a resistência ao fogo de colunas CFCH, o seu comportamento em caso de incêndio ainda não é completamente compreendido. A maioria destes estudos não considera a restrição ao alongamento térmico do pilar, parâmetro importante para seu desempenho ao fogo quando este se encontra inserido em uma estrutura.

Este trabalho apresenta os resultados de uma série de quarenta ensaios de resistência ao fogo realizados em colunas CFCH com restrição a rotação e a deformação axial durante o alongamento térmico. Parâmetros como a esbeltez da coluna, seu nível de carga, a rigidez da estrutura circundante, a taxa de armadura e o grau de preenchimento com betão no interior da coluna, foram testados. Colunas tubulares em aço de secção circular (CHS) também foram testadas como referência.

Um modelo tridimensional não linear em elementos finitos desenvolvido na ABAQUS (2011) para prever o comportamento do fogo das referidas colunas é apresentado e validado em comparação com os resultados experimentais. Os parâmetros testados experimentalmente mais relevantes para o comportamento ao fogo dos pilares foram considerados no modelo.

A pesquisa é complementada com uma análise numérica que abordou diferentes valores de níveis de carga, diâmetros externos e taxa de armadura para as colunas. Baseado nestes resultados equações simples para avaliar o tempo crítico das colunas CFCH foram propostas. Por último, é apresentada uma comparação entre os resultados da pesquisa e os métodos simplificados da EN1994-1-2 (2005).

As colunas apresentaram tempos críticos inferiores aos divulgados na literatura. A rigidez da estrutura circundante não influenciou os tempos críticos. O modelo numérico apresentou resultados em conformidade com os experimentos. Baseados nestes resultados foram propostas equações simplificadas para o cálculo do tempo crítico de colunas com restrição ao alongamento térmico e em situação de incêndio. O método tabular pode ser inseguro para alguns casos, já o método simplificado proposto pela referida norma mostrou-se conservativo para avaliar a resistência ao fogo de colunas CFCH em situação de incêndio

Palavras-chave: fogo, colunas, aço, betão, resistência, restrição à dilatação.

---

**SUMMARY**

ACKNOWLEDGEMENTS	ii
ABSTRACT	iii
RESUMO	iv
SUMMARY	v
LIST OF FIGURES	viii
LIST OF TABLES	xii
NOTATION	xiii
1. INTRODUCTION	1
1.1 General Considerations	1
1.2 Objectives	5
1.2.1 General objective	5
1.2.2 Specific objectives	6
1.3 Scope of thesis	6
2. STATE OF THE ART	8
2.1 Introduction	8
2.2 Experimental researches	10
2.3 Numerical and analytical researches	20
2.4 EN1994-1-2 – Tabulated data and simple calculation method	39
2.5 Chapter remarks	42
3. FIRE RESISTANCE TESTS ON CONCRETE FILLED CIRCULAR HOLLOW COLUMNS	44
3.1 Introduction	44

---

3.2	Experimental programme	44
3.2.1	Test set-up	44
3.2.2	Test columns	50
3.2.3	Test plan	54
3.3	Results	57
3.3.1	Evolution of temperatures	57
3.3.2	Restraining forces	61
3.3.3	Axial deformations	67
3.3.4	Critical times	72
3.3.5	Failure mode	76
3.4	Chapter remarks	80
4.	<b>NUMERICAL ANALYSIS OF CONCRETE FILLED CIRCULAR HOLLOW COLUMNS SUBJECTED TO FIRE</b>	<b>82</b>
4.1	Introduction	82
4.2	Numerical model	82
4.2.1	Geometry	82
4.2.2	Thermal and mechanical properties	83
4.2.3	Analysis procedure	84
4.2.4	Interaction	85
4.2.5	Load and boundary conditions	86
4.2.6	Mesh	87
4.3	Validation of the model	88
4.3.1	Critical times	91
4.3.2	Maximum relative restraining forces	95
4.3.3	Maximum axial deformation	97
4.3.4	Failure mode	98
4.4	Chapter remarks	100

---

---

5.	AN ANALYSIS BASED ON NUMERICAL DATA OF CONCRETE FILLED CIRCULAR HOLLOW COLUMNS SUBJECTED TO FIRE	102
5.1	Introduction	102
5.2	Numerical data – discussion and simplified equations	103
5.3	Comparison with simple methods of EN1994-1-2 (2005)	110
5.3.1	Tabulated data method	110
5.3.2	Simple Calculation Model	113
5.4	Chapter remarks	116
6.	CONCLUSIONS	118
	REFERENCES	122
	APPENDIX A – Mechanical properties of concrete and steel at ambient temperature and other tests	129
	APPENDIX B – Evolution of temperatures in the tests	132
	APPENDIX C – Lateral deflections of tested columns	172
	APPENDIX D – Deformed shapes of tested columns	192
	APPENDIX E – Fire tests on fibre reinforced concrete filled circular hollow (CFCH-FRC) columns	202

---

## LIST OF FIGURES

Figure 1.1 – Fires by location group in UK (Department for Communities and Local Government, 2012).	2
Figure 1.2 – Fatalities from fires by location group in UK (Department for Communities and Local Government, 2012).	2
Figure 2.1 – Stages during the heating of a CFH column (Espinosa <i>et al.</i> 2010).	9
Figure 2.2 – Typical fire resistance of CFH columns (Kodur, 1999).	11
Figure 2.3 – Axial deformation of tested CFCH-PC columns (Adapted from Han <i>et al.</i> 2003b).	15
Figure 2.4 – Typical failure mode of CFH-PC columns (Han <i>et al.</i> , 2003b).	16
Figure 2.5 – A comparison of fire resistance calculated by Han's <i>et al.</i> formula and test results (Adapted from Han <i>et al.</i> , 2003b).	17
Figure 2.6 – A comparison of results between those that were calculated using Lie's model and tests results for column 1 (Lie, 1994).	21
Figure 2.7 – A comparison of results between those that were calculated using Lie's model and tests results for column 2 (Lie, 1994).	21
Figure 2.8 – Influence of the external diameter of a column on fire resistance (Lie and Kodur, 1996).	23
Figure 2.9 – Influence of the effective length of a column on fire resistance (Lie and Kodur, 1996).	23
Figure 2.10 – Influence of load applied on fire resistance (Lie and Kodur, 1996).	24
Figure 2.11 – Fire resistance calculated by Lie and Kodur's equation and numerical predictions (Lie and Kodur, 1996).	24
Figure 2.12 – Fire resistance calculated by Lie and Kodur's equation and test results (Lie and Kodur, 1996).	25
Figure 2.13 – Fire resistance calculated by Han's model and test results (Han, 2001).	28
Figure 2.14 – Influence of the dimension on fire resistance (Han, 2001).	28
Figure 2.15 – Influence of the slenderness on fire resistance (Han, 2001).	29
Figure 2.16 – Temperature calculated using Ding and Wang's model and test results (Ding and Wang, 2008).	30
Figure 2.17 – Results calculated using Ding and Wang's model and test results (Ding and Wang, 2008).	31
Figure 2.18 – Temperature calculated using Hong and Varma's model and test results (Hong and Varma, 2009).	32
Figure 2.19 – Axial deformation calculated by Hong Varma's model and test results (Hong and Varma, 2009).	33
Figure 2.20 – Fire resistances calculated using the Schaumann <i>et al.</i> model and test results (Schaumann <i>et al.</i> , 2009).	35
Figure 2.21 – Axial deformation calculated using the model by Espinosa <i>et al.</i> and test results (Espinosa <i>et al.</i> , 2010).	38
Figure 2.22 – Fire resistances calculated using the model by Espinosa <i>et al.</i> and tests results (Espinosa <i>et al.</i> , 2010).	38

---



Figure 2.23 – Temperatures calculated by Espinos <i>et al.</i> and test results (Espinos <i>et al.</i> , 2010). .....	39
Figure 3.1 – Restraining steel beams and M27 threaded rods.....	45
Figure 3.2 – Upper restraining steel beams.....	45
Figure 3.3 – Upper restraining frame assembly.....	45
Figure 3.4 – Furnace modules.....	45
Figure 3.5 – Furnace assembly.....	46
Figure 3.6 – 2D reaction frame assembly.....	46
Figure 3.7 – 3D restraining frame assembly.....	46
Figure 3.8 – Final configuration of test apparatus.....	46
Figure 3.9 – General view of testing set up.....	47
Figure 3.10 – Scheme of testing set up.....	48
Figure 3.11 – Axial stiffness of the 3D restraining frame.....	49
Figure 3.12 – Rotational stiffness of the 3D restraining frame.....	50
Figure 3.13 – Reinforcing steel bars and stirrups (steel reinforcement).....	51
Figure 3.14 – CFCH-RC column with concrete ring before casting.....	51
Figure 3.15 – Steel reinforcement with Styrofoam cylinder.....	51
Figure 3.16 – Stiffeners welded at the base/top of a CFCH column.....	51
Figure 3.17 – Columns before the casting.....	52
Figure 3.18 – Curing of the CFCH columns.....	52
Figure 3.19 – Casting of the CFCH columns.....	52
Figure 3.20 – Position of thermocouples on the columns by height and cross-section.....	53
Figure 3.21 – Evolution of furnace temperature as a function of time for all the tests.....	57
Figure 3.22 – Distribution of temperature in cross-section S3 for test column A17 <sub>219-TOT-RC-30%-Klow</sub> .....	58
Figure 3.23 – Distribution of temperature in cross-section S3 for test column A19 <sub>219-RING-RC-30%-Klow</sub> .....	58
Figure 3.24 – Effect of filling in steel tube temperature of CFCH columns with d = 168.3mm at cross-section S3.....	59
Figure 3.25 – Effect of filling in steel tube temperature of CFCH columns with d = 219.1mm at cross-section S3.....	60
Figure 3.26 – Distribution of temperature over height at the moment of failure for column A17 <sub>219-TOT-RC-30%-Klow</sub> .....	60
Figure 3.27 – Distribution of temperature along the cross-section at the moment of failure for column A17 <sub>219-TOT-RC-30%-Klow</sub> .....	61
Figure 3.28 – Restraining forces for a load level of 70%, column diameter of 168.3 mm and axial stiffness of the surrounding structure of 13 kN/mm.....	62
Figure 3.29 – Restraining forces for a load level of 70%, column diameter of 168.3 mm and axial stiffness of the surrounding structure of 128 kN/mm.....	63
Figure 3.30 – Restraining forces for a load level of 70%, column diameter of 219.1 mm and axial stiffness of the surrounding structure of 13 kN/mm.....	63
Figure 3.31 – Restraining forces for a load level of 70%, column diameter of 219.1 mm and axial stiffness of the surrounding structure of 128 kN/mm.....	64

Figure 3.32 – Restraining forces for a load level of 30%, column diameter of 168.3 mm and axial stiffness of the surrounding structure of 13 kN/mm.....	65
Figure 3.33 – Restraining forces for a load level of 30%, column diameter of 168.3 mm and axial stiffness of the surrounding structure of 128 kN/mm.....	65
Figure 3.34 – Restraining forces for a load level of 30%, column diameter of 219.1 mm and axial stiffness of the surrounding structure of 13 kN/mm.....	66
Figure 3.35 – Restraining forces for a load level of 30%, column diameter of 219.1 mm and axial stiffness of the surrounding structure of 128 kN/mm.....	66
Figure 3.36 – Axial deformations for a load level of 70%, column diameter of 168.3 mm and axial stiffness of the surrounding structure of 13 kN/mm.....	67
Figure 3.37 – Axial deformations for a load level of 70%, column diameter of 168.3 mm and axial stiffness of the surrounding structure of 128 kN/mm.....	68
Figure 3.38 – Axial deformations for a load level of 70%, column diameter of 219.1 mm and axial stiffness of the surrounding structure of 13 kN/mm.....	68
Figure 3.39 – Axial deformations for a load level of 70%, column diameter of 219.1 mm and axial stiffness of the surrounding structure of 128 kN/mm.....	69
Figure 3.40 – Axial deformations for a load level of 30%, column diameter of 168.3 mm and axial stiffness of the surrounding structure of 13 kN/mm.....	69
Figure 3.41 – Axial deformations for a load level of 30%, column diameter of 168.3 mm and axial stiffness of the surrounding structure of 128 kN/mm.....	70
Figure 3.42 – Axial deformations for a load level of 30%, column diameter of 219.1 mm and axial stiffness of the surrounding structure of 13 kN/mm.....	71
Figure 3.43 – Axial deformations for a load level of 30%, column diameter of 219.1 mm and axial stiffness of the surrounding structure of 128 kN/mm.....	71
Figure 3.44 – Comparison of the critical times of columns obtained for the lower surrounding structure stiffness with the critical times of other columns for the higher stiffness. ....	73
Figure 3.45 – Comparison of the critical times of columns obtained for the load level of 30% with columns bearing a load level of 70%. ....	74
Figure 3.46 – Comparison of the critical times obtained for columns with diameter of 219.1 mm with columns that have a diameter of 168.3 mm.....	75
Figure 3.47 – Comparison of the critical times of CFCH columns obtained for the completely filled columns with the critical times for partially filled columns (concrete ring). ....	76
Figure 3.48 – Comparison of the critical times obtained for the CFCH columns with steel bars reinforcement with those without. ....	77
Figure 3.49 – Deformed shape of tested columns. ....	78
Figure 3.50 – Local buckling in tested columns.....	79
Figure 3.51 – Percentage of columns tested that presented local buckling.....	79
Figure 4.1 – Three-dimensional finite element model for CFCH columns .....	87
Figure 4.2 – Experimental vs. numerical restraining forces for a load level of 30% and 70%, a column diameter of 168.3mm and axial stiffness of the surrounding structure of 13 kN/mm	89
Figure 4.3 – Experimental vs. numerical axial deformations for a load level of 30% and 70%, a column diameter of 168.3mm and axial stiffness of the surrounding structure of 13 kN/mm .....	89

Figure 4.4 – Experimental vs. numerical restraining forces for a load level of 30% and 70%, a column diameter of 168.3mm and axial stiffness of the surrounding structure of 128 kN/mm .....	90
Figure 4.5 – Experimental vs. numerical axial deformations for a load level of 30% and 70%, a column diameter of 168.3mm and axial stiffness of the surrounding structure of 128 kN/mm .....	90
Figure 4.6 – Numerical vs. experimental critical times .....	92
Figure 4.7 – Frequency of the num-exp critical time difference .....	92
Figure 4.8 – Temperatures in the middle height cross-section of column A01 <sub>168-TOT-PC-70%-Klow</sub> .....	93
Figure 4.9 – Numerical vs. experimental maximum relative restraining forces .....	96
Figure 4.10 – Frequency of the difference in num-exp maximum relative restraining forces .....	96
Figure 4.11 – Numerical vs. experimental maximum axial deformation.....	97
Figure 4.12 – Frequency of num-exp maximum axial deformation differences .....	98
Figure 4.13 – Num-exp deformed shapes of CFCH columns .....	99
Figure 5.1 – Critical times arising from a load level of CFCH columns with a reinforcement ratio of 0%.....	103
Figure 5.2 – Critical times arising from a load level of CFCH columns with a reinforcement ratio of 3%.....	104
Figure 5.3 – Critical times arising from a load level of CFCH columns with a reinforcement ratio of 6%.....	104
Figure 5.4 – Critical times arising from CFCH column diameters with 3% steel reinforcement .....	106
Figure 5.5 – Influence of diameter on the failure mode of the CFCH column .....	108
Figure 5.6 – Number of CFCH columns that presented local buckling.....	108
Figure 5.7 – Critical times arising from a reinforcement ratio for CFCH columns with a diameter of 168.3mm .....	109
Figure 5.8 – Critical times arising from the CFCH load level .....	110
Figure 5.9 – Tabulated method vs. experimental critical time of CFCH columns .....	112
Figure 5.10 – Tabulated method vs. numerical study of the critical time of the CFCH columns .....	112
Figure 5.11 – Simplified equations vs. experimental critical time of the CFCH columns ....	113
Figure 5.12 – Critical times for SMC, experimental tests and simplified equation for a CFCH-PC column total filled which has a diameter of 219.1mm .....	114
Figure 5.13 – Critical times for SMC, experimental tests and simplified equation for a CFCH-RC column total filled which has a diameter of 219.1mm.....	115
Figure 5.14 – Critical times for SMC, experimental tests and simplified equation for a CFCH-PC column total filled which has a diameter of 168.3mm .....	115
Figure 5.15 – Critical times for SMC, experimental tests and simplified equation for a CFCH-RC column total filled which has a diameter of 168.3mm.....	116

---

## LIST OF TABLES

Table 1.1 – Direct losses and deaths due fires (Adapted from <a href="#">segurancaonline@</a> , 2012) .....	3
Table 2.1 – Characteristics and material mechanical properties of CFH columns tested in Han <i>et al.</i> (2002) and Han and Huo (2003). .....	12
Table 2.2 – Residual strength of the CFH columns tested in Han <i>et al.</i> (2002) and Han and Huo (2003). .....	13
Table 2.3 – Characteristics and material mechanical properties of the CFH columns tested in Han <i>et al.</i> (2003a and 2003b) .....	14
Table 2.4 – Fire resistance and steel critical temperature of the CFH-PC columns tested in Han <i>et al.</i> (2003a and 2003b) .....	16
Table 2.5 – Fire resistance of the CFCH columns tested in Romero <i>et al.</i> (2011). .....	19
Table 2.6 – Failure times calculated using Hong Varma’s model and test results (Adapted from Hong and Varma, 2009) .....	34
Table 2.7 Standard fire resistance and minimum requirements for CFH columns (EN1994-1-2, 2005) .....	40
Table 3.1 – Mechanical properties of the concrete at ambient temperature .....	52
Table 3.2 – Mechanical properties of the steel at ambient temperature .....	53
Table 3.3 – Test plan, critical times and failure modes. ....	55
Table 4.1 – Parameters for the thermal model .....	85
Table 4.2 – Mesh details for the numerical models .....	88
Table 4.3 – Exp vs. Num - Critical times and Maximum axial deformation .....	94
Table 5.1 – Standard fire resistance and critical times for CFCH columns .....	111

## NOTATION

### *Latin symbols*

$A_a$	Cross-sectional area of the steel profile or steel hollow section
$A_c$	Cross-sectional area of the concrete
$A_s$	Cross-sectional area of the reinforcing bars
$E_a$	Modulus of elasticity of structural steel at ambient temperature
$E_c$	Effective modulus of elasticity for concrete at ambient temperature
$E_s$	Modulus of elasticity of reinforcing bars at ambient temperature
$E_{a,\theta,\sigma}$	Tangent modulus of stress-strain relationship for structural steel at temperature $\theta$ and for a stress $\sigma_{a,\theta}$
$E_{c,\theta,\sigma}$	Tangent modulus of stress-strain relationship for concrete at temperature $\theta$ and for a stress $\sigma_{c,\theta}$
$E_{s,\theta,\sigma}$	Tangent modulus of stress-strain relationship for reinforcing bars at temperature $\theta$ and for a stress $\sigma_{s,\theta}$
$(EA)_{eff}$	Effective axial stiffness
$(EI)_{eff}$	Effective flexural stiffness
$I_a$	Moment of inertia of the steel profile or steel hollow section, related to the central axis y or z of the composite cross-section
$I_c$	Moment of inertia of the concrete, related to the central axis y or z of the composite cross-section
$I_s$	Moment of Inertia of the reinforcing bars, related to the central axis y or z of the composite cross-section
$K$	Stiffness of the surrounding structure
$K_{as}$	Axial stiffness of the surrounding structure
$K_{rs,i}$	Rotational stiffness of the surrounding structure in “i” direction
$K_{as,c}$	Axial stiffness of the column
$K_{rs,c}$	Rotational stiffness of the column
$L$	Real length of the column
$L_e$	Buckling length of the column
$N_{ed}$	Design value of the buckling load at room temperature
$N_{pl,Rk}$	Characteristic value of the plastic resistance of the composite section to compressive normal force at room temperature
$N_{cr}$	Elastic critical or Euler buckling load at room temperature
$N_{fi,rd}$	Design axial buckling load at elevated temperature
$N_{fi,cr}$	Elastic critical or Euler buckling load at elevated temperature
$N_{fi,pl,rd}$	Design value of the plastic resistance to axial compression of the total cross-section
$P$	Applied load on the column
$P_0$	Initial applied load on the column



---

$b$	Width of the steel section
$d$	Diameter of the column
$e$	Thickness of steel wall profile
$f_{ay}$	Yield strength of structural steel at ambient temperature
$f_{au}$	Ultimate tensile strength of structural steel at ambient temperature
$f_{cu,j}$	Compressive cube strength of concrete at “j” days
$f_{c,j}$	Compressive cylinder strength of concrete at “j” days
$f_{sy}$	Yield strength of reinforcing bars at ambient temperature
$f_{su}$	Ultimate tensile strength of reinforcing bars at ambient temperature
$h$	Depth or height of the steel section
$h_c$	Convective heat transfer coefficient
$l_{\theta}$	Relevant buckling length in fire situation
$t$	Fire duration time
$u_s$	Axis distance of reinforcing bars
$u_{m\acute{a}x}$	Maximum axial deformations of the column

*Greek symbols*

$\alpha$	Degree of axial restraint
$\beta_i$	Degree of rotational restraint in “i” direction
$\varepsilon_m$	Emissivity of the material
$\varepsilon_f$	Emissivity of fire
$\phi$	Diameter (size) of a steel reinforcing bars
$\phi_r$	Radiation configuration factor
$\bar{\lambda}$	Relative slenderness
$\eta$	Load level
$\eta_{fi,t}$	Load level for fire design
$\rho$	ratio of reinforcement with reinforcing steel bars
$\sigma$	Stephan-Boltzmann constant
$\sigma_{a,\theta}$	Stress in structural steel at temperature $\theta$
$\sigma_{c,\theta}$	Stress in concrete at temperature $\theta$
$\sigma_{s,\theta}$	Stress in reinforcing bars at temperature $\theta$
$\gamma_{M,fi,a}$	Partial safety factor of structural steel for fire design
$\gamma_{M,fi,c}$	Partial safety factor of concrete for fire design
$\gamma_{M,fi,s}$	Partial safety factor of reinforcing bars for fire design
$\theta$	Temperature of material
$\theta_0$	Initial temperature

## 1. INTRODUCTION

### 1.1 General Considerations

The Fire Safety Engineering had a large development in the 80s, important regulations and reference documents were addressed around the world such as the European Recommendations for the Fire Safety of Steel Structures – ECCS (1983).

In the 90s, the European Committee for Standardization (CEN) published the first editions of the parts concerned with Fire Safety Design of the Eurocodes. Actually, these documents were:

- Eurocode 1: Actions on Structures. Part 1.2: General Actions – Actions on Structures Exposed to fire (EN 1991-1-2:2002);
- Eurocode 2: Design of Concrete Structures. Part 1.2: General Rules – Structural Fire Design (EN 1992-1-2:2004);
- Eurocode 3: Design of Steel Structures. Part 1.2: General Rules – Structural Fire Design (EN 1993-1-2:2005);
- Eurocode 4: Design of Composite Steel and Concrete Structures. Part 1.2: General Rules – Structural Fire Design (EN 1994-1-2:2005);
- Eurocode 5: Design of Timber Structures. Part 1.2: General Rules – Structural Fire Design (EN 1995-1-2:2004);
- Eurocode 6: Design of Masonry Structures. Part 1.2: General Rules – Structural Fire Design (EN 1996-1-2:2005);
- Eurocode 9: Design of Aluminium Alloy Structures. Part 1.2: General Rules – Structural Fire Design (EN 1999-1-2:2007);

However since a long time ago and until nowadays, fires cause numerous and irreparable losses to the world heritage these are financial, life, cultural, environmental and others losses.

Figure 1.1 presents the number of fires and Figure 1.2 the number of deaths related to fires by location group registered in Great Britain (UK) according the fire statistics of Department for Communities and Local Government. Most of deaths were in dwellings fires (Figure 1.2).

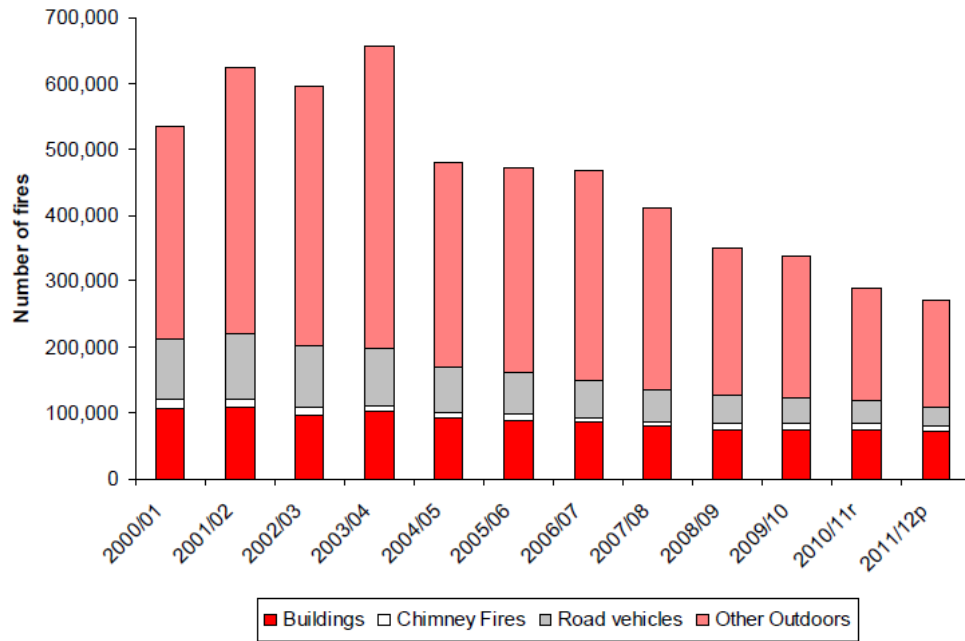


Figure 1.1 – Fires by location group in UK (Department for Communities and Local Government, 2012).

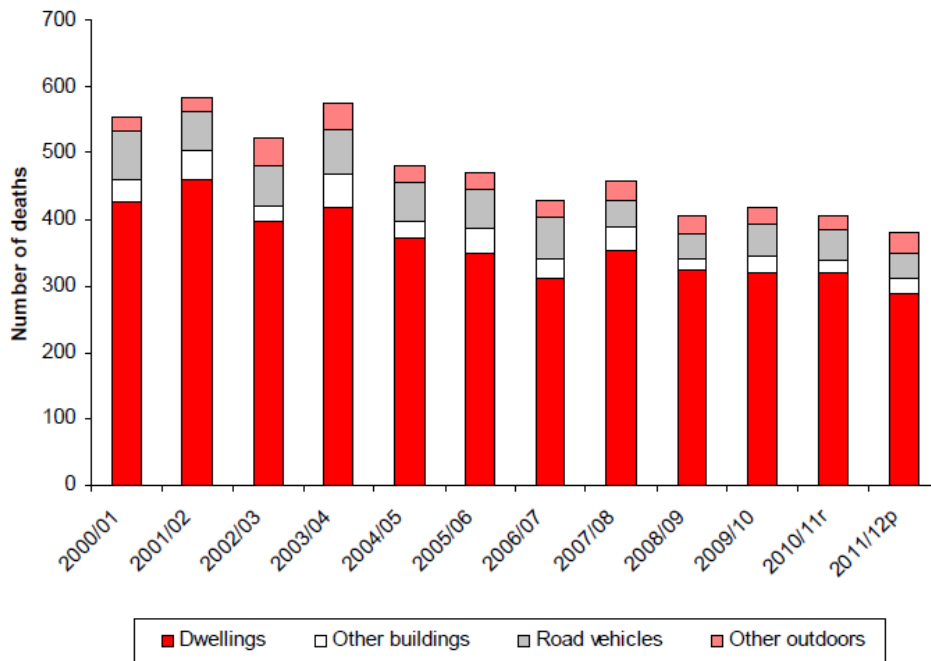


Figure 1.2 – Fatalities from fires by location group in UK (Department for Communities and Local Government, 2012).

The United States of America (USA) registered 1.6 millions of fires in 2005 with 3677 deaths, 83% of these deaths occurred in dwellings fires (Seito *et al.* 2008).

Each year hundreds of deaths and billions of dollars in property losses occur due to fires (Buchanan, 2001). Drysdale (1998) reported that in the United Kingdom (UK) direct losses such as physical property, human life, and in the production line due fires exceed more than £ 1 billion of sterling pounds and over than 800 deaths each year.

In USA the financial losses due fire are around 85 billions of dollars according Quintiere (1998). Later, Hall Jr. (2005) points out that these costs were 93.9 billions of dollars in 2003.

The Canada has an annual cost due fires in the order of 11 billions of Canadian dollars based on 1991 values according Schaenman et al (1995). Denmark in 1998 had damages due fires around 10,825 millions of Danish kroner (Moller, 2001).

The fire costs represented 0.813% of USA Gross Domestic Product (GDP), 0.864% of Denmark GDP and 0.729% of UK GDP according to Ramachandran (1998).

Table 1.1 presents the costs with direct losses and deaths due fires in years from 2005 up to 2007 according The Geneva Association *apud* [segurancaonline@](mailto:segurancaonline@) (2012).

Table 1.1 – Direct losses and deaths due fires (Adapted from [segurancaonline@](mailto:segurancaonline@), 2012)

Country	Direct losses (in billions of Euros)				Deaths			
	2005	2006	2007	%GDB	2005	2006	2007	Deaths /1000 hab.
<b>Germany</b>	2.9	3.3	3.4	0.13	605	510	-	0.68
<b>EUA</b>	8.3	9.0	11.4	0.10	4000	3550	3750	1.23
<b>France</b>	3.4	3.3	3.4	0.19	660	620	605	1.02
<b>UK</b>	2.1	1.8	1.8	0.3	515	515	465	0.82
<b>Japan</b>	2.3	2.4	2.1	0.12	2250	2100	2050	1.67

Unfortunately the inexistence of a standard form to collect, analyze and publish these statistics and the fact that not all fires are taken into account introduce some vies in analysis making so difficult a comparison. However it is clearly the high cost to society of fire damages and the necessity of a fire risk management.

The modern fire risk management models include the behaviour in fire situation of structures such as the model based on performance proposed by Fitzgerald (2003). In this way the analysis of the structure subject to fire is an important step of a fire risk management model.

In last decade the use of composite structures and in particular composite columns made of Concrete Filled Circular Hollow (CFCH) sections or to keep it simple CFCH columns become popular in high-rise and industrial buildings as a good solution for fire situation.

This choice is justified by the advantages of this type of column such as the high load-bearing capacity and high seismic resistance; the attractive appearance and better use of the built space due to the possibility of use columns with smaller cross-sections; the fast construction technology and reduction in costs due to avoid formworks; and finally, its good fire performance. Therefore, these columns seem to be an adequate construction solution in terms of load-bearing capacity at ambient temperature and in fire

The behaviour of CFCH columns when subjected to fire has been studied by several authors for years in experimental approaches such as the tests of National Research Council of Canada summarized in Kodur (1999), the tests realized by Han *et al.* (2003a and 2003b) and the tests presented by Romero *et al.* 2011. Numerical researches such as the presented by Lie (1994), Ding and Wang (2008), Hong and Varma (2009), Schaumann *et al.* (2009) and Espinos *et al.* (2010), complemented the experimental researches.

However most of these studies did not consider the restraining to column thermal elongation. The response of these columns when inserted in a building structure is different than when isolated. Restraints on the thermal elongation of the column, provoked by the building surrounding structure, plays a key role on columns stability, since it induces different forms of interaction between the heated column and the cold adjacent structure. The increase in the stiffness of the surrounding structure to the column subjected to fire increases not only the axial but also the rotational restraining, while the former reduces the critical time (also the critical temperature) of the columns, the latter increase them (Ali *et al.*, 1998; Valente and Neves, 1999; Rodrigues *et al.*, 2000 and Neves *et al.*, 2002).

Thereby the restraining to thermal elongation is an important parameter on fire performance of structures that was not considered in previously researches and its influence on the behaviour of CFCH columns subjected to fire is one of the main aims of this research.

On the other hand, there are important differences on the experimental and numerical models presented in literature such as the column failure criteria, the thermo-mechanical model applied for steel and concrete materials or in the simulation of relevant aspects as the thermo-mechanical behaviour in the interface between the steel tube and concrete core. These

---



differences make difficult a comparison between the results and lead to divergences in the fire resistance of the columns.

This thesis presents the results of a series of forty fire resistance tests on CFCH columns with axial and rotational restraining to thermal elongation. The columns were filled with plain concrete (CFCH-PC) and reinforcing concrete (CFCH-RC). Relevant parameters that had influence in fire resistance of the columns were tested, such as: slenderness and cross-sectional external diameter of the column; load level; stiffness of the surrounding structure which imposes restraining to thermal elongation of the column; percentage of steel bar reinforcing; and degree of concrete filling inside the column. Circular Hollow Sections (CHS) columns (*i.e.* steel columns) were tested also for comparison.

A three-dimensional nonlinear finite element model developed with ABAQUS (2011) to predict the behaviour of these columns is also presented, verifying its more relevant parameters, and considering the restraints of columns to their thermal elongation that adds a rather difficult step to the problem analysis. The model is validated in comparison with the experimental fire tests results.

The study of the behaviour in fire of CFCH columns with restrained thermal elongation was complemented with an analysis based on numerical data obtained with the proposed numerical model. A range of practical values of load level, diameter of the column and ratio of reinforcement was studied. Based on numerical data simplified equations to evaluate the critical time of CFCH columns with restrained thermal elongation were proposed.

In addition, a comparison between experimental results and a set of simplified equations proposed with the tabulated and the simple calculation methods proposed by EN1994-1-2 (2005) are presented in order to verify the capacity of these methods to assess the structural behaviour in fire of CFCH columns with axial and rotational restraining to thermal elongation.

## **1.2 Objectives**

### **1.2.1 General objective**

Aggregate knowledge on the structural performance of steel and composite steel and concrete structures in fire.

In particular analyse the behaviour in fire of CFCH columns with axial and rotational restraining to thermal elongation testing the main parameters that had great influence in its fire performance.

### **1.2.2 Specific objectives**

1. Carry out an experimental research by fire resistance tests on CFCH columns with restraining to thermal elongation;
2. Develop and validate a numerical finite element model to assess the fire performance of these columns in fire;
3. Review of the state of the art in the behaviour of CFCH columns in fire;
4. Compare the results with the simple methods proposed for these columns in EN1994-1-2 (2005) and suggest improvements;
5. Contribute to a standard method to assess the fire resistance of CFCH columns closer than a real situation;

### **1.3 Scope of thesis**

This thesis is divided in the following chapters:

Chapter 1 presents the introduction to the problem and the necessity to study fire risk management of structures in particular the behaviour in fire of CFCH columns. Also the objectives and an overview of this research are presented in this chapter.

Chapter 2 presents the state of the art in the behaviour of CFCH columns subjected to fire. An overview of the studies published in international papers and conference proceedings concerning the object of study of this thesis (*i.e.* CFCH columns subjected to fire) is presented. In addition others researches were added for a better understanding of the fire behaviour of these columns.

Chapter 3 describes the experimental programme carried out with details of the experimental method and the parameters tested. Then results of temperatures, restraining forces, axial deformation, critical times and failure modes are showed.

Chapter 4 presents the numerical model developed in ABAQUS and its features implemented. The results are presented in a comparison with the experimental tests in order to validate the model.

Chapter 5 presents a numerical analysis to complement the study of the behaviour of CFCH columns in fire. Equations to evaluate the critical time of these columns are presented. In addition a comparison with the simple calculation methods presented in EN1994-1-2 (2005) is presented.

Chapter 6 presents the general conclusions of this research also the prospects of future studies.

Chapter 7 contains a list of bibliography used in this thesis.

## 2. STATE OF THE ART

### 2.1 Introduction

Concrete Filled Hollow (CFH) columns have a good fire performance (*i.e.* fire resistance above 60 minutes). That does not mean that they do not need to be designed for fire situations. In this situation, their behaviour is totally different from that at an ambient temperature.

First of all, the reduction in mechanical properties and changes in the characteristics of the materials (*i.e.* steel and concrete) due to the high temperatures reduce the resistance of the columns.

However the concrete infill, the thermal conductivity of which is less than that of steel, delays the rise in temperatures in the cross-section, thus benefiting its fire resistance. On the other hand the steel tube protects the concrete core from direct exposure to fire, thus retaining its integrity and reducing the probability of spalling. Furthermore the concrete core reinforced by steel bars or steel fibres may support the load for longer and, consequently, increase the fire resistance of the columns.

Some authors (Lu *et al.*, 2009, Ding and Wang, 2009 and Espinos *et al.*, 2010) divide the behaviour of these columns during heating into 4 stages: (1) the steel tube directed exposed to fire heats and expands more than the concrete core leading to a loss of contact between the concrete core and the loading plate thus transferring all the applied load to the steel tube. (2) After reaching its critical temperature, local buckling of the steel tube occurs and it starts to shorten until the concrete core returns into contact with the loading plate. (3) After this, the load is progressively transferred to the concrete core thus starting its major contribution since due to the high temperature of the steel tube, its resistance is very low. (4) Finally with the increase of temperature in the concrete core, the concrete mechanical properties degrade and the column fails. Figure 2.1 illustrates the stages described above.

In addition, restraints on the thermal elongation of the column, provoked by the surrounding structure, plays a key role in column stability and influences the deformation of the axial column and the restraining forces that act on the columns.

The response of these columns when inserted into a building structure induces different forms of interaction between the heated column and the cold adjacent structure. The increase in the stiffness of the structure surrounding the column subjected to fire increases not only axial but also rotational restraining, while the former reduces the critical time (and also the critical

temperature) of the columns, the latter increase them (Ali *et al.*, 1998; Valente and Neves, 1999; Rodrigues *et al.*, 2000 and Neves *et al.*, 2002).

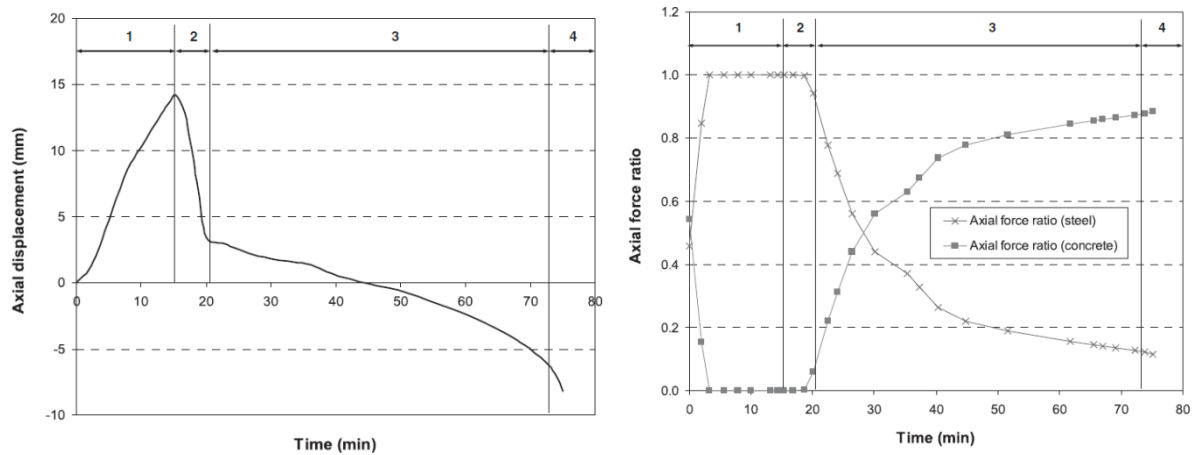


Figure 2.1 – Stages during the heating of a CFH column (Espinosa *et al.* 2010).

Parameters such as loading level, cross-sectional dimensions, length of buckling, slenderness, degree of concrete filling and type of concrete used to fill the column (*i.e.* plain concrete – CFH-PC, steel bar reinforced concrete – CFH-RC or steel fibre reinforced concrete – CFH-FRC) have a significant influence on the fire resistance of the CFH columns.

The influence of other parameters, such as the strength of the concrete and steel, the type of aggregates and the eccentricity of the load is moderate. On the other hand, the ratio of steel reinforcement, the thickness of the steel tube wall and the distance from the axis of the reinforcing bars to the internal wall surface of the steel tube, have little influence on the fire resistance of the columns. The influence of the stiffness of the surrounding structure on the behaviour of these columns subjected to fire has been little studied and remains unclear.

Over the last 20 or so years, there have been a number of research studies on the behaviour of CFH columns subjected to fire. The sub-sections below give an overview of the main experimental and numerical research studies, in chronological order. This overview focuses principally on Concrete Filled Circular Hollow (CFCH) columns with infill of plain concrete (CFCH-PC) or steel bar reinforced concrete (CFCH-RC) since these are the main objective of study of this thesis. However, research on other types of CFH columns, steel columns and steel elements is also presented for a better understanding of the behaviour of these columns in fire. Finally, a brief overview of the tabular method and simplified method proposed by



---

EN1994-1-2 (2005) is presented to enable a comparison to be made with the numerical and experimental results obtained in this thesis.

## 2.2 Experimental researches

An extensive experimental programme in the fire behaviour of concrete filled hollow columns was carried out at the National Research Council of Canada (NRCC) and the test results can be found in Lie and Chabot (1990), Chabot and Lie (1992), Lie *et al.* (1992), Lie and Irwin (1992), Lie and Chabot (1992), Kodur and Lie (1995), and Kodur and Lie (1996). From now on these tests will be reported as NRCC tests.

Kodur (1999) summarized the NRCC tests. They are a series of 75 fire tests in CFH-PC, CFH-RC and CFH-FRC columns with circular and square cross-sections. The external diameters varied from 141 to 406mm for the circular columns and the width from 152 to 305mm for the square ones. The thickness of the tube wall was between 4.8 and 12.7mm and the length of the columns was 3810 mm.

The parameters studied were the cross-sectional dimension, the thickness of the tube wall, load level, end conditions, concrete strength, type of aggregate in the concrete and the infill material (PC, RC or FRC). The strength of the concrete at 28 days varied between 30 and 50 MPa and the ratio of steel fibre reinforcement was 1.77% by mass. The load level applied was between 10% and 45% of the compression resistance at ambient temperature of the composite column and the heating rate followed the standard fire curve, ASTM E119 (1990) or CAN/ULC-S101 (1989).

In these tests the load was kept constant and the failure criterion was when the column could no longer sustain the load. The maximum displacement rate of the hydraulic jack was 76 mm/min.

The results of these tests showed that the fire resistance of the CFH-PC columns was between 1h and 2h, while for those filled with RC or FRC, this reached 3h (Figure 2.2). These levels of fire resistance is much higher than those obtained from columns not filled with concrete (*i.e.* steel columns) and without fire protection which resisted for around 15 minutes.

Also these tests showed that the load applied on CFH- PC columns had to be reduced in order to obtain practical fire resistances and failure in these occurred due to the rapid propagation of cracking in the concrete core, thus impairing its strength. A sensitivity to eccentric loads of such columns was also found. The infill of the CFH-RC and CFH-FRC columns avoided this

cracking and thus increased the load bearing capacity and consequently the fire resistance but RC infill is not recommended for columns with small dimensions due to the space being restricted.

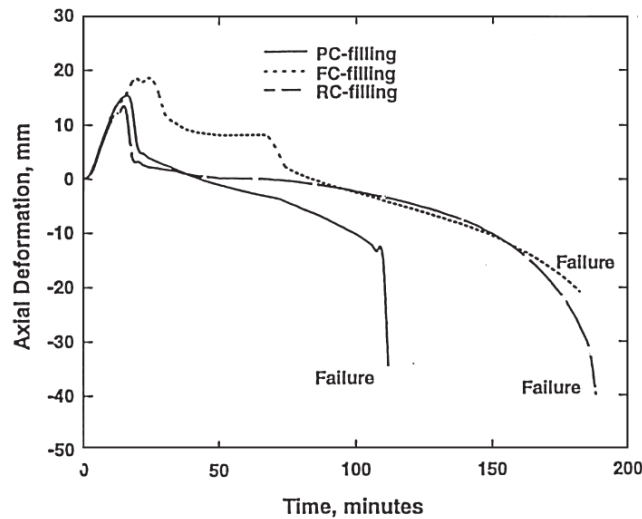


Figure 2.2 – Typical fire resistance of CFH columns (Kodur, 1999).

The failure modes varied from compression to buckling due to the size of the column and the type of filling. In the case of CFH-PC columns, the most common failure mode was buckling, principally in columns with a cross-section dimension of less than 203mm.

Rodrigues *et al.* (2000) published results obtained from a series of 168 fire resistance tests on compressed steel elements (*i.e.* small scale samples) with restrained thermal elongation. Parameters were tested such as the slenderness of the elements, load eccentricity, stiffness of the surrounding structure and type of end supports. It was concluded that for the case of pin-ended elements with centred loading, the higher the axial stiffness of the surrounding structure is, the lower is the critical temperature.

A series of experimental tests on residual strength of 18 CFH columns after exposure to the ISO834 (1975) standard fire was presented in Han *et al.* (2002) and Han and Huo (2003). CFH columns with circular, rectangular and square cross-sections were tested. All columns were filled with PC. Some columns were fire protected by intumescent sprayed mortar to a thickness of 25mm. Other parameters studied were the slenderness of the columns and the eccentricity of the load applied.

Table 2.1 presents a summary of the characteristics of the specimens such as cross-section dimensions, wall thickness of steel tube and the effective buckling length of the columns as well as the mechanical properties of the materials used in the columns tested. In all concrete compositions, the fine aggregate used was silica-based sand and the coarse aggregate was carbonate stone.

Table 2.1 – Characteristics and material mechanical properties of CFH columns tested in Han *et al.* (2002) and Han and Huo (2003).

<i>Property/ characteristic</i>	<i>Rectangular cross-section</i>	<i>Circular cross-section</i>	<i>Square cross-section</i>
<b>Cross-section (mm)</b>	100x80 and 120x90	108	100
<b><i>e</i> (mm)</b>	2.93	4.32	2.93
<b><i>L</i> (mm)</b>	900 and 1200	600, 900 and 1200	600, 900 and 1200
<b>Slenderness</b>	26.0 - 41.6	22.2 - 44.4	20.8 - 41.6
<b><i>f<sub>ay</sub></i> (MPa)</b>	294	356	294
<b><i>E<sub>a</sub></i> (GPa)</b>	195	201	195
<b><i>f<sub>c, 28day</sub></i> (MPa)</b>	34.4	70.2	34.4
<b><i>f<sub>c, test day</sub></i> (MPa)</b>	36.2	71.3	34.8
<b><i>E<sub>c</sub></i> (GPa)</b>	27.4	31.1	27.4
<b>Concrete mix (kg/m<sup>3</sup>):</b>			
<i>Cement</i>	457	536	457
<i>Water</i>	206	176	206
<i>Sand</i>	1129	1099	1129
<i>Coarse aggregate</i>	608	589	608

According to the authors, the heating rate followed the ISO834 (1975) standard fire curve during 90min for the composite columns without fire protection and 180min for those that did. After heating, the columns were loaded to failure and the residual strength of the columns was determined. Table 2.2 presents the residual strength as a percentage of the column resistance at ambient temperature as laid down in EN1994-1-1 (1996).

The authors of these research studies pointed out the smaller loss of strength in the columns with fire protection. The predominant failure mode was global buckling and due to the infill, the columns behaved in a relative ductile manner and thus testing proceeded in a smooth and controlled way.

Table 2.2 – Residual strength of the CFH columns tested in Han *et al.* (2002) and Han and Huo (2003).

<i>CFSH columns</i>	<i>Rectangular cross-section</i>	<i>Circular cross-section</i>	<i>Square cross-section</i>
<b>Without fire protection</b>	40.1% - 62.5%	45% - 68.4%	45% - 78.3%
<b>Fire protected</b>	64.1% - 89.6%	92.3% - 94.7%	87.7 - 99.7%

Also the authors stated that the dimension of cross-section, slenderness and heating time have a great influence on the residual strength of the columns. The higher the cross-sectional dimensions are, the higher the residual strength of the columns is. In the other parameters, inverse fire behaviour takes place (*i.e.* the higher the slenderness or heating time, the lower the residual strength of the columns). The steel ratio, load eccentricity ratio, width-to-depth ratio, and strength of concrete and steel have a moderate influence on the residual strength of the columns.

Finally the authors suggested formulae for calculating the residual strength of composite columns made of CFH sections after exposure to ISO834 (1975) fire standard curve. They concluded that the results calculated were in reasonable accordance with the experimental tests and mathematical model presented in greater detail in Han (2001).

In the following year a series of tests on the fire behaviour of CFH columns with and without fire protection submitted to axial and eccentric loads were presented in Han *et al.* (2003a and 2003b). These tests are different from the others presented above by the same author because they were not residual tests realized after exposure to fire.

The heating rate followed the typical ISO834 (1975) standard curve and the failure criteria of the columns was the maximum axial contraction of 0.01 L in mm or the maximum rate of axial contraction of 0.003 L in mm/min as per ISO834 - Part 1 (1975). As the length of the columns tested in this research was 3810mm, these failure values were 38mm and 11.4mm/min respectively.

It is important to point out that even with columns of the same length these failure values are smaller than those adopted in the NRCC tests previously cited. Neither of studies considered restrained thermal elongation.

The main parameters considered in this research were the shape of the cross-section (*i.e.* rectangular, square or circular), the cross-section dimensions, the thickness of the wall of the tube and fire protection, slenderness and finally the eccentricity of the load applied.

The columns were loaded with 77% of the design load of the member at room temperature and two 20mm semi-circular holes were provided as vent holes for the water vapour pressure. Just 3000mm of the columns were heated, the rest of the column being outside the furnace. In all concrete compositions, the fine aggregate used was silica-based sand and the coarse aggregate was carbonate stone. Other details of the columns and concrete mixes are given in Table 2.3.

Table 2.3 – Characteristics and material mechanical properties of the CFCH columns tested in Han *et al.* (2003a and 2003b)

<i>Property/ characteristic</i>	<i>Rectangular cross-section</i>	<i>Circular cross-section</i>	<i>Square cross-section</i>
<b>Cross-section (mm)</b>	300x200 and 300x150	150 - 478	219 and 350
<b><i>e</i> (mm)</b>	7.96	4.6 - 8.0	5.3 and 7.7
<b><i>L</i> (mm)</b>	3810	3810	3810
<b><i>f<sub>ay</sub></i> (MPa)</b>	341	259, 293 and 381	246 and 284
<b><i>E<sub>a</sub></i> (GPa)</b>	187	168 and 201	200 and 183
<b><i>f<sub>c, 28day</sub></i> (MPa)</b>	47.3	39.6/68.8	17.8
<b><i>f<sub>c, test day</sub></i> (MPa)</b>	49.0	-	18.7
<b><i>E<sub>c</sub></i> (GPa)</b>	30.2	27.8/29.4	26.7
<b>Concrete mix (kg/m<sup>3</sup>):</b>			
<i>Cement</i>	425	713/542	318
<i>Water</i>	170	449/151	171
<i>Sand</i>	630	224/524	636
<i>Coarse aggregate</i>	1175	1014/1183	1275

In these tests the fire resistance and the critical temperature of steel of the CFCH-PC columns were from 7min to 32min and from 434°C to 564°C, respectively (Figure 2.3). Other results for the ones with square and rectangular cross-sections besides the circular cross-section are given in Table 2.4.

These fire resistances are much smaller than those reported in the NRCC tests cited above. However, differences in the experimental method (*e.g.* the failure criterion adopted) and the parameters tested (*e.g.* load level) may justify these divergences.

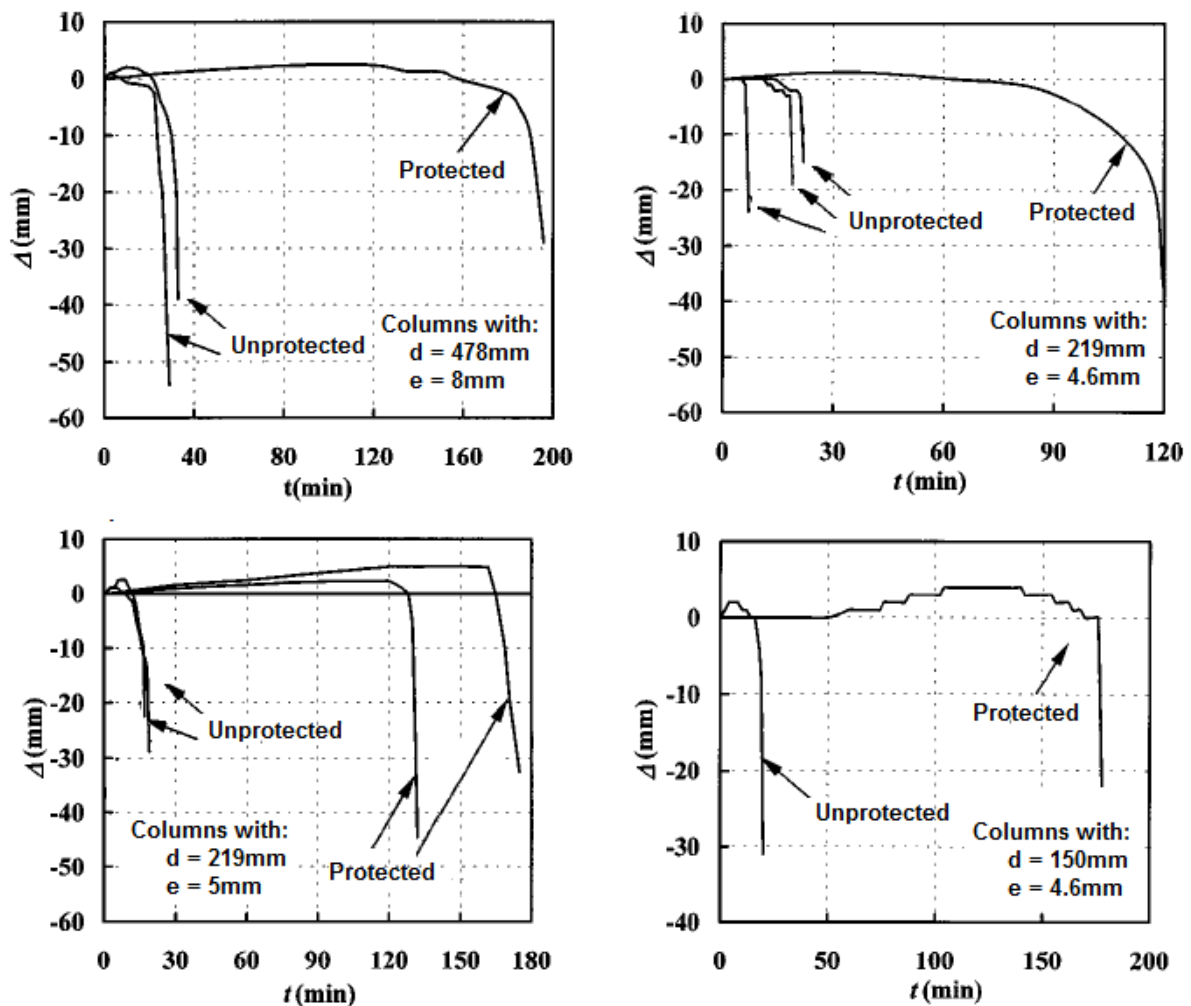


Figure 2.3 – Axial deformation of tested CFCH-PC columns (Adapted from Han *et al.* 2003b).

The main conclusions of these studies are not so different from those previously drawn. Again the authors ratified that the section size of the column and the thickness of the fire protection have a significant influence on the fire resistance of the column. If one of them is increased, the fire resistance will increase too. The effect of load eccentricity on fire resistance is insignificant when the column has a constant load ratio.

Also the authors recommended that the fire resistance of these columns should be enhanced by using a fire protection coating if a high load ratio was applied. According to the authors, it frequently happens that CFH columns in tall buildings subjected to high loads and filled only with PC cannot reach the required fire resistance.

The failure modes observed were by compression and global buckling. The latter was the predominant failure mode (Figure 2.4).

Table 2.4 – Fire resistance and steel critical temperature of the CFH-PC columns tested in Han *et al.* (2003a and 2003b)

<i>CFH columns</i>	<i>Rectangular cross-section</i>	<i>Circular cross-section</i>	<i>Square cross-section</i>
<b>Without fire protection</b>			
Fire resistance (min)	16 - 24	7 - 32	-
Critical temperature of steel (°C)	636 - 786	434 - 564	-
<b>Fire protected</b>			
Fire resistance (min)	78 - 146	120 - 196	109 - 169
Critical temperature of steel (°C)	500 - 530	533 - 829	504 - 668

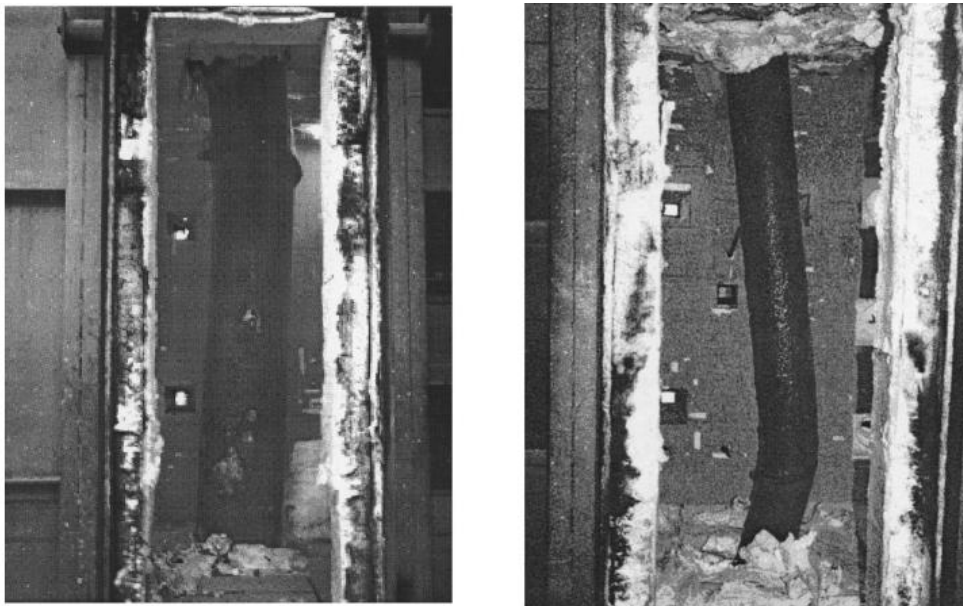


Figure 2.4 – Typical failure mode of CFH-PC columns (Han *et al.*, 2003b).

In addition Han *et al.* (2003a) explained the composite action between the steel tube and concrete core that enhanced the structural behaviour of the CFH columns during a fire. According to them, first the steel tube expands at the early stage of heating, thus reducing the

load on the concrete core. Next, the steel tube buckles locally due to the high temperatures reached in the steel tube and the load is transmitted to the concrete core. Finally, the steel tube can no longer confine the concrete core and it fails in a brittle manner.

As in their previous studies, the authors suggested formulae to calculate the fire resistance and fire protection of CFH columns. They concluded that the accuracy of their results is reasonable when compared with the numerical model presented in Han, 2001 and the experimental tests. In general, the results calculated are conservative if compared with the experimental tests (Figure 2.5).

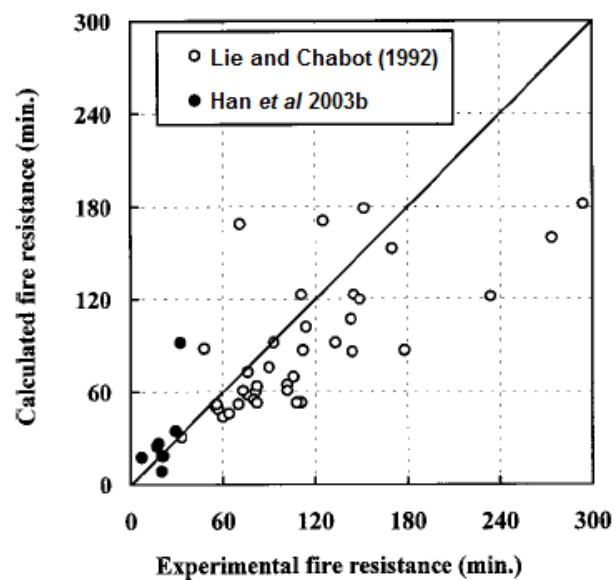


Figure 2.5 – A comparison of fire resistance calculated by Han's *et al.* formula and test results (Adapted from Han *et al.*, 2003b).

In 2005, Han *et al.* presented a further series of residual fire tests with CFH columns but this time focused on the flexural behaviour besides the compression performance. Eight specimens were tested, namely four stub columns under compression and four beams under bending. They reconfirmed the accurate prediction of their numerical model cited above and expanded the formulae to calculate the residual axial strength of post-fire damaged columns to calculate the residual bending moment for beams.

In 2007 Tan *et al.* presented a series of 15 fire resistance tests on rectangular hollow sections columns (*i.e.* steel columns) axially restrained. The effective length of the columns was 1.74m (real length of 1.50m), the end conditions were pinned-pinned and the load applied was 50%



of the ambient column load bearing capacity, which was determined experimentally. Parameters such as slenderness (45, 55, 81 and 97) and 4 levels of axial restraint ratio increasing from zero to around 0.16 were tested. The heating rate was 8°C/min. The main conclusions were that axial restraints as well as initial imperfections significantly reduce the failure times of axially-loaded steel columns.

Lu *et al.* (2010) presented a study on the fire performance of 6 self-consolidating concrete filled double skin tubular columns. The main parameters tested were the load level which varied from 31% to 65%, the eccentricity of the applied load of 0mm and 74mm, the cavity ratio which varied from 43% to 78% and the shape of steel tube. Combinations of double circular, double square and square-circular steel hollow tubes were tested with a width of 280mm and external diameter of 300mm. The diameter of the inner tubes was 125 or 225mm for circular tubes and the width of the square tubes was 140mm. The length of the columns was 3810mm and the thickness of wall tube was 5mm in all cases. The heating and failure criteria of the columns were as laid down in ISO834 and a pinned-fixed end condition was adopted. The yield strength of the tubes was 320MPa, the concrete had a 28-day cube strength of 26 MPa and 17.7 GPa of elastic modulus.

The main conclusions were that the self-consolidating double skin tubular columns have higher limiting temperatures on outer steel tubes than unfilled and CFH columns and consequently better endurance in the event of fire; there is a composite action between the steel tube and concrete in composite columns during a fire. The authors stated that there was no slipping between the outer steel tube and the concrete; the cavity ratio affected the fire endurance of the composite columns. This claim of there being no evidence of slipping is contrary to the findings of other authors such as Espinos *et al.* 2010.

In 2011 Romero *et al.* presented 16 fire resistance tests conducted on slender CFCH columns. The columns were filled with normal and high strength concrete. The main parameters tested were the strength of concrete (30 and 80MPa), the type of infill (PC, RC and FRC), and the load level (20% and 40%). The relative slenderness of all columns was greater than 0.5 and they were tested under fixed-pinned end conditions. The lengths of the columns were 3810mm, their external diameter was 159mm and the steel tube wall was 6mm thick. S275JR grade steel was used although the real yield strength was around 337MPa and the steel modulus of elasticity was 210GPa. The columns were tested as per the ISO834 (1980) fire curve and with unrestrained column elongation. Finally in the CFCH-RC columns, 4 longitudinal reinforcing bars, each 12mm in diameter, and 6mm stirrups are located every 30cm. Thus, the reinforcement ratio was close to 2.5%. As to the columns reinforced with steel fibre, a ratio of 40kg/m<sup>3</sup> of high strength Dramix 40/60 steel fibres was used.

The main conclusions of this study were: there was no spalling in the columns filled with high strength concrete probably due to their external diameters being small and the short duration of the fire tests; using filling with reinforcing bars was more advantageous in columns filled with high strength concrete than in those filled with normal concrete (*i.e.* for the same fire resistance level, the axial load may be increased in the first columns); high second order effects induced by the curvature of a steel tube cannot be transferred to a fragile material like an unreinforced concrete core and consequently it is not effective in very slender columns; the EN1994-1-2 (2005) simple calculation method has limitations and should be revised; the fire resistance of columns filled with high strength concrete and with a higher contribution of the concrete core was less than in those filled with normal concrete due to spalling. However the filling with high strength concrete is interesting because this enables the load level to be increased and a moderate fire resistance to be obtained; finally, the filling with FRC was not so advantageous when compared with PC.

Table 2.5 shows the fire resistance of the CFCH columns tested in this research. These fire resistances are smaller than those obtained in the NRCC fire tests already presented in this chapter. Another difference in these tests was the fire behaviour of the CFCH-FRC columns, the fire resistance of which are not higher than the columns filled with PC.

Table 2.5 – Fire resistance of the CFCH columns tested in Romero *et al.* (2011)

<i>CFH columns</i>	<i>PC filled</i>	<i>RC filled</i>	<i>FRC filled</i>
<b>Normal concrete (30MPa)</b>			
Load level of 20%	42	43	37
Load level of 40%	25	30	22
Load level of 60%	14	13	-
<b>High Strength concrete (80MPa)</b>			
Load level of 20%	38	65	36
Load level of 40%	11	19	16

Also two fire tests on pinned-pinned CFCH-PC columns were presented. The fire resistance of the columns was 13min and 18min respectively for load levels of 20% and 40%. The columns were filled with normal concrete (30MPa). These results suggest that if the end-conditions are changed from pinned to fixed, the fire resistance will be increased. However, there are few tests that enable major conclusions to be drawn.

### 2.3 Numerical and analytical researches

In numerical approach, one of the first researches was presented by Lie in 1994. The author presented a mathematical model to evaluate the fire resistance of CFCH-RC columns. The column temperature was calculated by a finite difference method and the heating rate followed the ASTM E119 (1990) or CAN/ULC-S101 (1989) standard curves. The model considered the retard in the development of temperature caused by the evaporation of moisture but did not consider the migration of moisture toward the centre of the column. The strength of the column (*i.e.* the maximum load that the column can bear) was calculated by a method based on a load-deflection or stability analysis (Allen and Lie, 1974 *apud* Lie 1994).

In the calculation of column strength some assumptions were made: (a) the properties of steel and concrete follow the model proposed in Lie (1994); (b) concrete has no tensile strength; (c) plane sections remain plane; (d) there is no slip between steel and concrete; (e) there is no composite action between the steel and concrete; (f) the reduction in column length before exposure to fire is negligible.

The model was validated in a comparison with two specimens tested and presented in Chabot and Lie (1992). The columns were 3810mm long, had an external diameter of 273mm, the tube wall was 6.35mm thick and the bar reinforcement ratio was 2.3%. The strength of concrete on the test day was around 47MPa and the yield strength specified for the steel tube was of 350MPa. Two load levels were applied: 37% (in column 1) and 67% (in column 2) of the compression resistance of the CFCH column as per CAN3-S16.1-M89 (1989). Figure 2.6 shows a comparison for temperatures and axial deformation between those that were theoretically calculated in Lie's model and those that were measured in test in column 1. Figure 2.7 shows this comparison for column 2.

Lie also concluded that the development of temperature showed good agreement between that measured and that calculated except at an early stage due to the migration of moisture toward the centre of the column. According to him the slow rises in temperature around 100°C may be because this migration of moisture is being induced.

There was reasonably good agreement for axial deformation between the calculated and measured results. According to Lie, there were some differences, however, due to several factors that influence axial deformation such as load, thermal expansion, bending, and creep that cannot be completely taken into account in the theoretical calculations.

Lie stated that a difference of 10% in the coefficients of thermal expansion of steel may cause a difference of approximately 5mm in axial deformation. The effect of creep that is more pronounced at the later stages of fire exposure may be even greater.

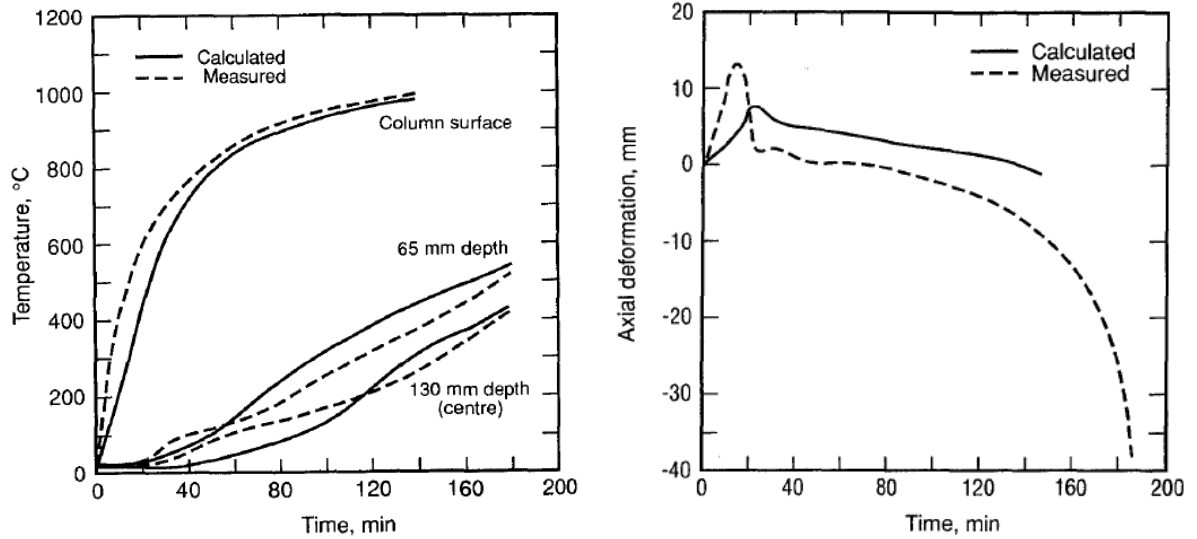


Figure 2.6 – A comparison of results between those that were calculated using Lie’s model and tests results for column 1 (Lie, 1994).

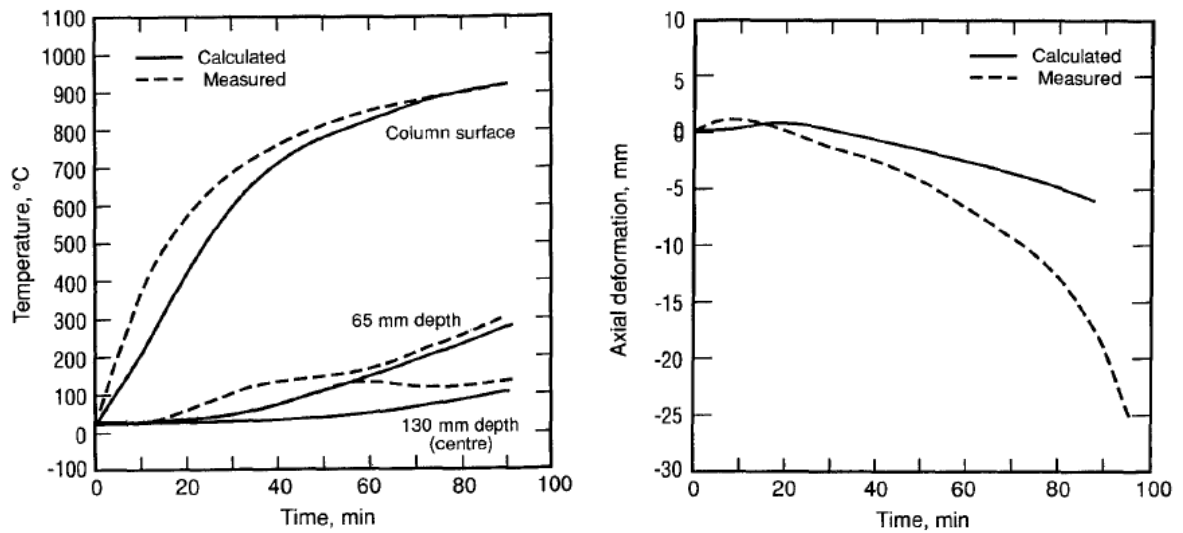


Figure 2.7 – A comparison of results between those that were calculated using Lie’s model and tests results for column 2 (Lie, 1994).

Also he pointed out that the calculated fire resistance results were 20% lower for column 1 and 10% for column 2 than the test results. According to him the differences were probably due the considerable contraction of the columns which the model cannot totally take into account but in general the results indicated that the model is conservative in its predictions.

In the following year Lie and Irwin (1995) presented a mathematical model similar to the one shown in Lie (1994). However, it is able to predict the fire resistance of CFH-RC columns with rectangular cross-sections. Again the model was validated by comparison with tests presented in Chabot and Lie (1992). This time, three columns were used with different cross-section sizes (203, 250 and 305mm). Again the columns were 3810mm tall and the thickness of the steel tube was 25mm.

In 1996 Lie and Kodur presented a parametric study based on numerical models presented in (Lie, 1994 and Lie and Irwin, 1995). In their paper, Lie and Kodur analyzed the behaviour of CFH-RC columns with circular and square cross-sections, the external cross-sectional dimension ranged from 178 to 305mm for square columns and from 168 to 406mm for circular columns. The effective lengths varied from 2500 to 4500mm, the bar reinforcement ratio were 1.5%, 3% and 5% and the compression strength of the concrete was 20, 35 and 50MPa using axis distance of reinforcing bars  $u_s$  of 20 and 50mm. Siliceous and carbonate aggregates were studied.

They showed that the external diameter/dimension (Figure 2.8), effective length (Figure 2.9), and the load on the column (Figure 2.10) have the greatest influence on the fire resistance of CFH-RC columns. The first is directly proportional to the fire resistance and the others are inversely proportional to it. The strength of the concrete as well as the type of aggregate has moderate influence on fire resistance. The resistance of the carbonate aggregates was 10% higher than that of the siliceous aggregates and the higher the concrete strength, the higher the fire resistance is. The influence of the thickness of the steel tube, bar reinforcement ratio and axis distance of reinforcing bars  $u_s$  on fire resistance is small.

In addition they proposed simple equations for calculating the fire resistance of CFH-RC columns with square and circular cross-sections. There are slight differences between the results calculated using the equations and those predicted by the numerical model (Figure 2.11) or measured experimentally (Figure 2.12). But according to the authors, the expressions are able to predict the fire resistance reasonably accurately.

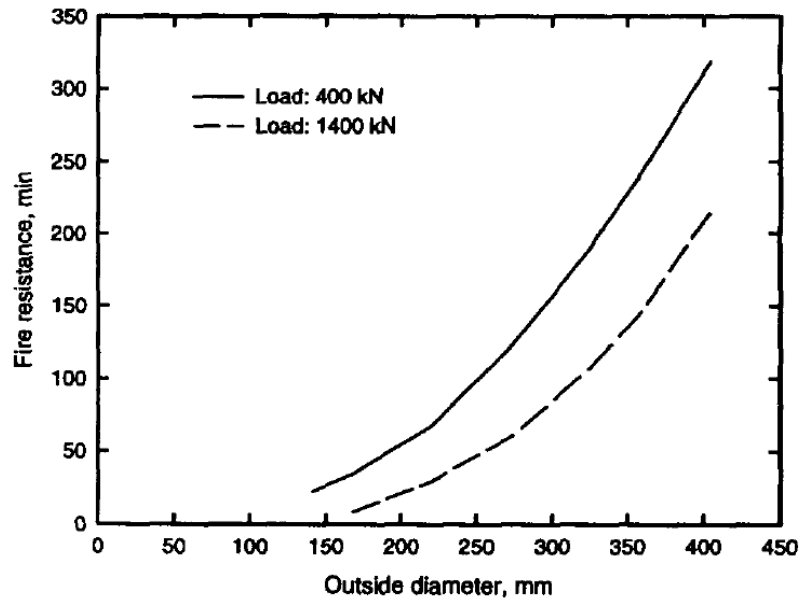


Figure 2.8 – Influence of the external diameter of a column on fire resistance (Lie and Kodur, 1996).

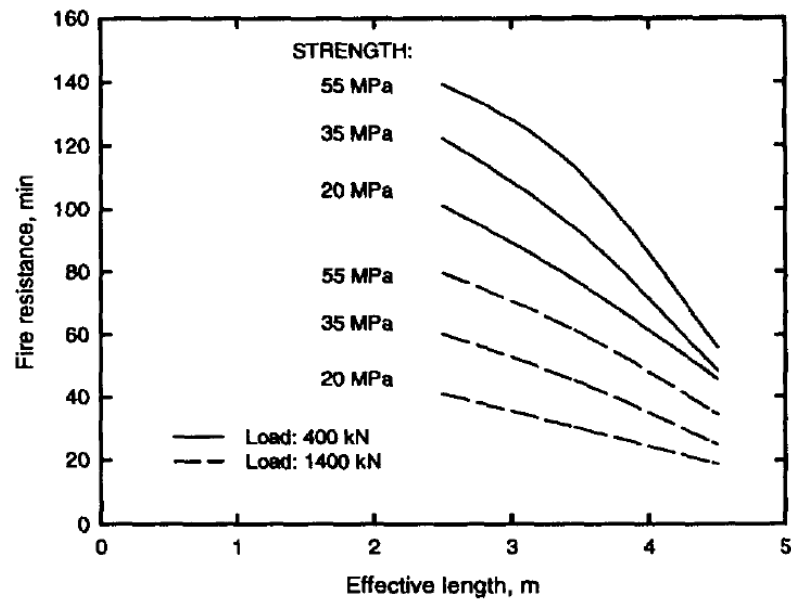


Figure 2.9 – Influence of the effective length of a column on fire resistance (Lie and Kodur, 1996).

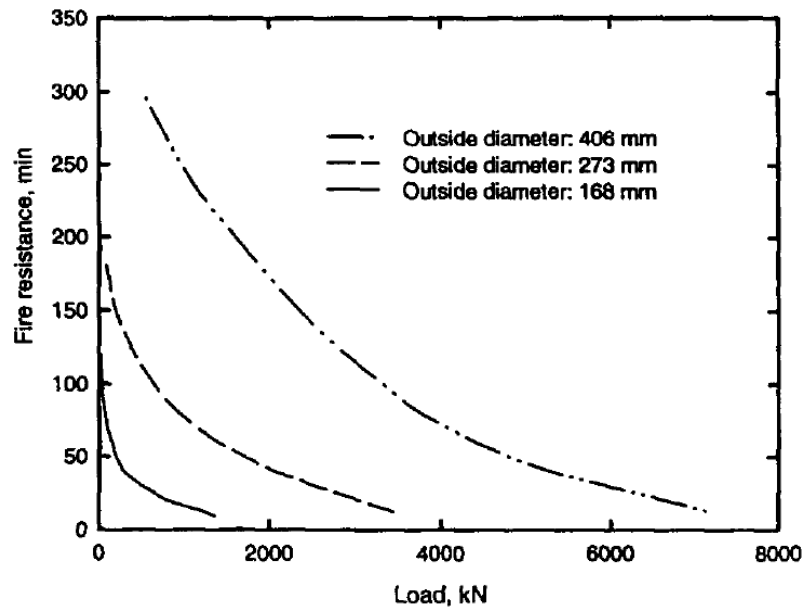


Figure 2.10 – Influence of load applied on fire resistance (Lie and Kodur, 1996).

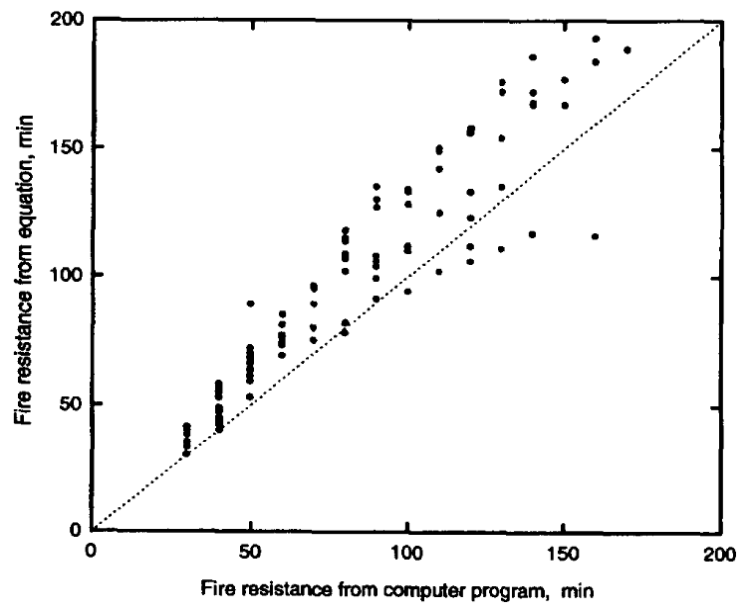


Figure 2.11 – Fire resistance calculated by Lie and Kodur's equation and numerical predictions (Lie and Kodur, 1996).

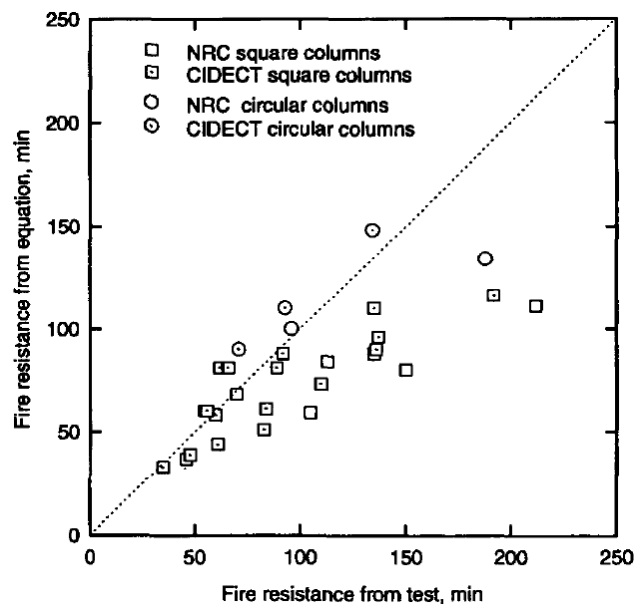


Figure 2.12 – Fire resistance calculated by Lie and Kodur’s equation and test results (Lie and Kodur, 1996).

In another paper (Kodur and Lie, 1996b), they presented a similar mathematical model for evaluating the fire resistance of CFCH-FRC columns. As in their other studies, the model was validated by making a comparison with two tested columns. The lengths of the columns were 3810mm, their walls were 6.35mm thick and their external diameters 324 and 356mm. Both columns were made of tube with steel grade 350, the concrete strength on the day of the test was 57MPa and the steel fibre ratio was 1.77% by mass.

Following year Wang (1997) concluded that the ENV1994-1-2 (1994) calculation method is conservative and suggested that “curve a” should be adopted instead of “curve c” when designing for elevated temperatures, thus giving less conservative results. Moreover, Wang proposed a simple method to implement the general calculation method of ENV1994-1-2 (1994) and concluded that the equivalent time concept from ENV1991-2-2 (1994) is applicable to CFH columns but the equation should be modified to consider the inter dependence between load and the ventilation factor. These conclusions were based in a comparison between 43 CFH-PC columns (36 columns with circular and 7 with square cross-sections) presented in NRCC tests and its predicted fire resistance as per as the calculation method proposed by ENV1994-1-2 (1994).



Later, Kodur (1998) presented a parametric study using the numerical model already presented above. The main conclusions were: the external diameter, the effective length, and the load applied had a great influence on the fire resistance of CFH-FRC columns; however, the strength of concrete and the type of aggregates have only a moderate influence; and the influence of the steel tube wall on fire resistance is insignificant.

Also two simple equations to evaluate the fire resistance of these types of columns were presented. The equations take into account parameters such as load applied, cross-section dimensions of the column and the strength of the concrete.

Still based on these parametric studies, Kodur (1999) summarized a unique simplified design equation to evaluate the fire resistance of CFH-PC, CFH-RC, CFH-FRC columns.

The equation is a function of the following parameters: compression strength of concrete after 28 days, dimension and shape of the cross-section of the column, applied load, effective length of buckling length, infill material (*i.e.* PC, RC or FRC), reinforcement ratio and axis distance of reinforcing bars  $u_s$ . The values obtained by the equation are generally 10-15% more conservative than those results observed in the experimental tests with which they were compared.

He ratified that the infill material, cross-section dimension, effective length and applied load have a great influence on the fire resistance of the CFH columns. The influence of the compression strength of concrete and aggregate type is only moderate and the thickness of the tube wall had no effect on the fire resistance.

Finally, Kodur concluded that the use of CFH columns is a good solution for improving resistance to fire. For this to be greater than 120 min, he suggested the use of CFH-RC and CFH-FRC columns. Such CFH columns should also be used for slender columns and for columns with eccentric loads because the behaviour of CFH-PC columns is unpredictable under these conditions. For high axial compression loads, RC filling should be considered. Moreover, according to Kodur, using circular cross-sections and carbonate aggregate in concrete filling provides higher fire resistance than square cross-sections and siliceous aggregate respectively.

In addition he gave guidelines for the construction such as the use of FRC rather than RC filling for cross-section diameters smaller than 200mm, a minimum axis distance of reinforcing bars  $u_s$  of 20mm, stirrups over the full length of the column and pairs of small vent holes (*i.e.* minimum diameter of 12.7mm) on each floor level to avoid the columns bursting under steam pressure due to heat from the fire.

In 1999, Valente and Neves presented the results of a numerical study on H profile steel columns with axial and rotational restraining. The parameters studied were the slenderness of the column (40, 80 and 120), the eccentricity of the applied load (0,  $h/2$  and  $h$ ), the axial restraint level (0, 5, 50 and 5000 kN/cm) and the rotational restraint level of the surrounding structure (0,  $9.3 \cdot 10^2$ ,  $9.3 \cdot 10^3$ ,  $9.3 \cdot 10^4$  kN m and  $\infty$ ). The constant load applied was 70% of the design value of the buckling resistance of a hinged column at ambient temperature as per ENV1993-1-1 (1992). It was concluded that increasing axial restraining led to a reduction in the critical temperatures while rotational restraining has the opposite effect.

In the same year Wang (1999) presented a numerical research using finite-elements on the effects of structural continuity on the fire resistance of CFH columns. A parametric study was carried on CFH-PC and CFH-RC columns and tested parameters such as column lengths, cross-section sizes and load ratios. The main conclusions were: the recommendation of ENV1994-1-2 (1994) on the effective length of columns at the fire limit state is correct; the additional axial loads in columns due to restrained thermal elongation are very small; and the column bending moments in a fire become much lower than those at ambient temperature. Therefore, he said that to calculate the column fire resistance it may be considered as pure axially loaded equal to its ambient temperature value. Also he reported for slender columns a complex double curvature bending mode but this did not reduce the fire resistance of the column.

Han (2001) presented an analytical method to predict the fire resistance of CFH columns and beam-columns with circular or square cross-sections. A finite element method was applied to determine the temperature in the cross-section. One of the greatest innovations of this model was to consider the composite action between the steel tube and the concrete core, which is often neglected by other researchers. This effect was considered introducing a constraining factor into the stress-strain relationship of the concrete. These relationships were defined based on test results of short CFH columns under constant temperature conducted by Han.

Figure 2.13 presents a comparison between the fire resistances calculated and the experimental tests undertaken by the NRCC and by Han.

Other conclusions of this research were that if the dimension is increased (Figure 2.14) or the slenderness is reduced (Figure 2.15), the fire resistance of the columns is higher. However, the influence of other parameters such as steel reinforcement ratio, load eccentricity, strength of concrete and steel on fire resistance is small.

Yin et al. (2006) presented a numerical nonlinear analysis model for predicting the fire resistance of CFH-PC columns with circular and square cross-sections. By comparing

different sizes of cross-sections and thickness of the steel tube, they showed that circular columns have a slightly higher fire resistance than square columns. They emphasized too that the calculation of stress in concrete is more difficult than in steel because concrete is influenced not only by the temperature dependent on material properties but also by thermal strain and other strains such as transient and stress-induced strains.

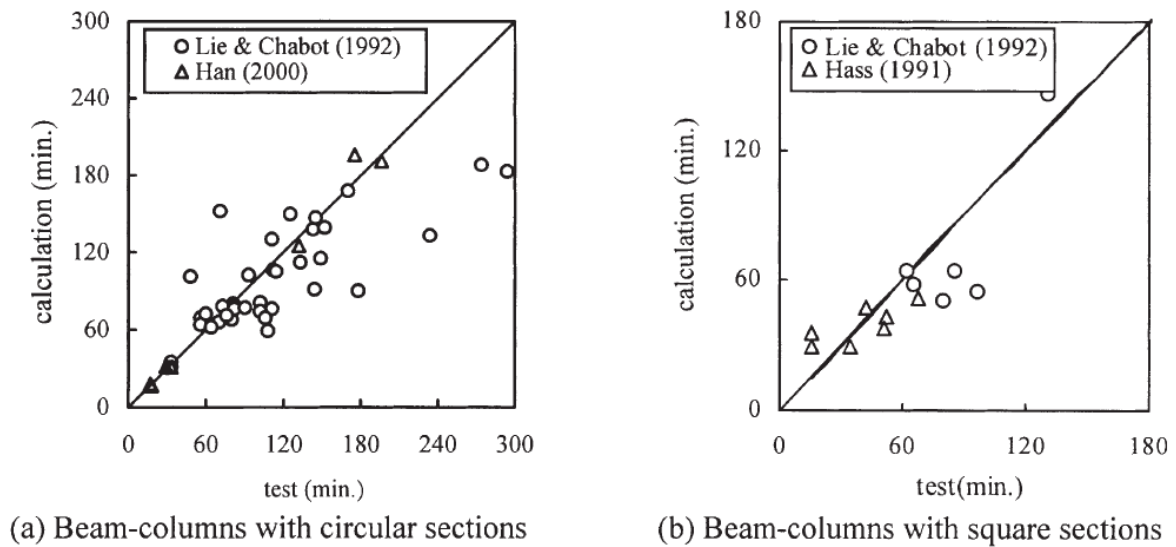


Figure 2.13 – Fire resistance calculated by Han’s model and test results (Han, 2001).

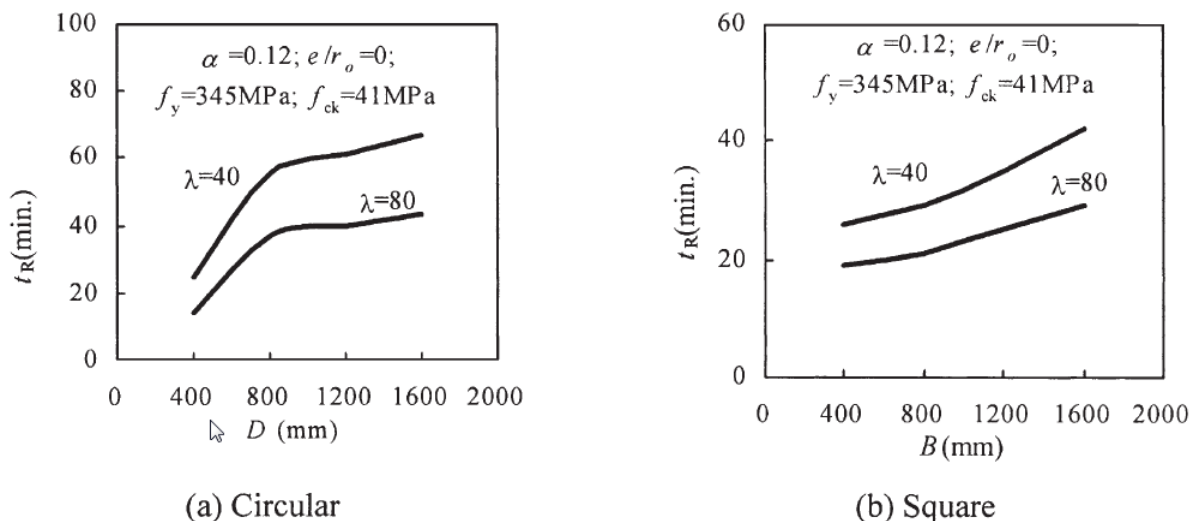


Figure 2.14 – Influence of the dimension on fire resistance (Han, 2001).

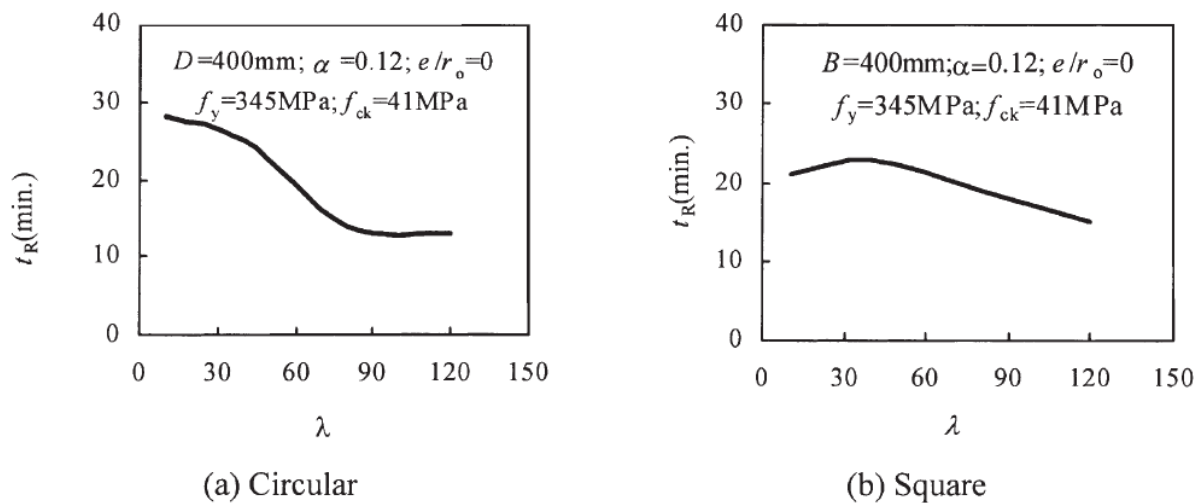


Figure 2.15 – Influence of the slenderness on fire resistance (Han, 2001).

In 2008, Ding and Wang (2008) presented a numerical model developed in the commercial finite element package ANSYS to assess the behaviour in the event of fire of CFH columns with circular and rectangular columns.

Assuming uniform heating along the length of columns and due to the symmetry of the geometry and boundary conditions, they simulated thermal analysis with a 2D model and modelled only one quadrant of the cross-section. The fire resistance (*i.e.* structural analysis) was calculated using a 3D finite element model and due to the symmetry, only half of the columns were analysed. The type of elements applied for the thermal analysis were PLANE55 (the 2-D solid thermal element) for the cross-section and SURF151 (the 2-D thermal surface element) for the external layer exposed to the fire. For the structural analysis, SOLID145 (the 3-D structural solid element) was applied.

The model was validated by making a comparison with calculated and measured tests on 34 CFH columns conducted by the NRCC as cited above and by CIDECT (*Comité international pour le développement et l'étude de la construction tubulaire*) and presented in CIDEC Report C1/C2 apud Ding and Wang (2008).

Important features often neglected by other researchers were addressed in this study such as the influence of an interface air gap and slip between the steel tube and concrete core, the concrete tensile behaviour and the initial imperfection of a column on the fire behaviour of CFH columns.

They justified the air gap at the interface between the steel tube and concrete core as being due to the differences in the thermal expansion coefficients of the two materials. Steel has a higher radial expansion than concrete does and also these differences in thermal expansion and strain in longitudinal direction may overcome the bond at this interface. Figure 2.16 presents the effect of the different gap values between the steel tube and concrete core in the numerical simulations and makes a comparison with a CFH-RC column with square cross-sections which had a 200mm external side and a 6.3mm thick tube wall.

Also they point out that it is difficult to determine the thermal properties of concrete due to its complexity. Therefore it is difficult to obtain accurate predictions of concrete temperature in, for example, the inner concrete core (Figure 2.16 “b” and “c”). However they stated it is possible to improve predictions of temperature simply by introducing an air gap.

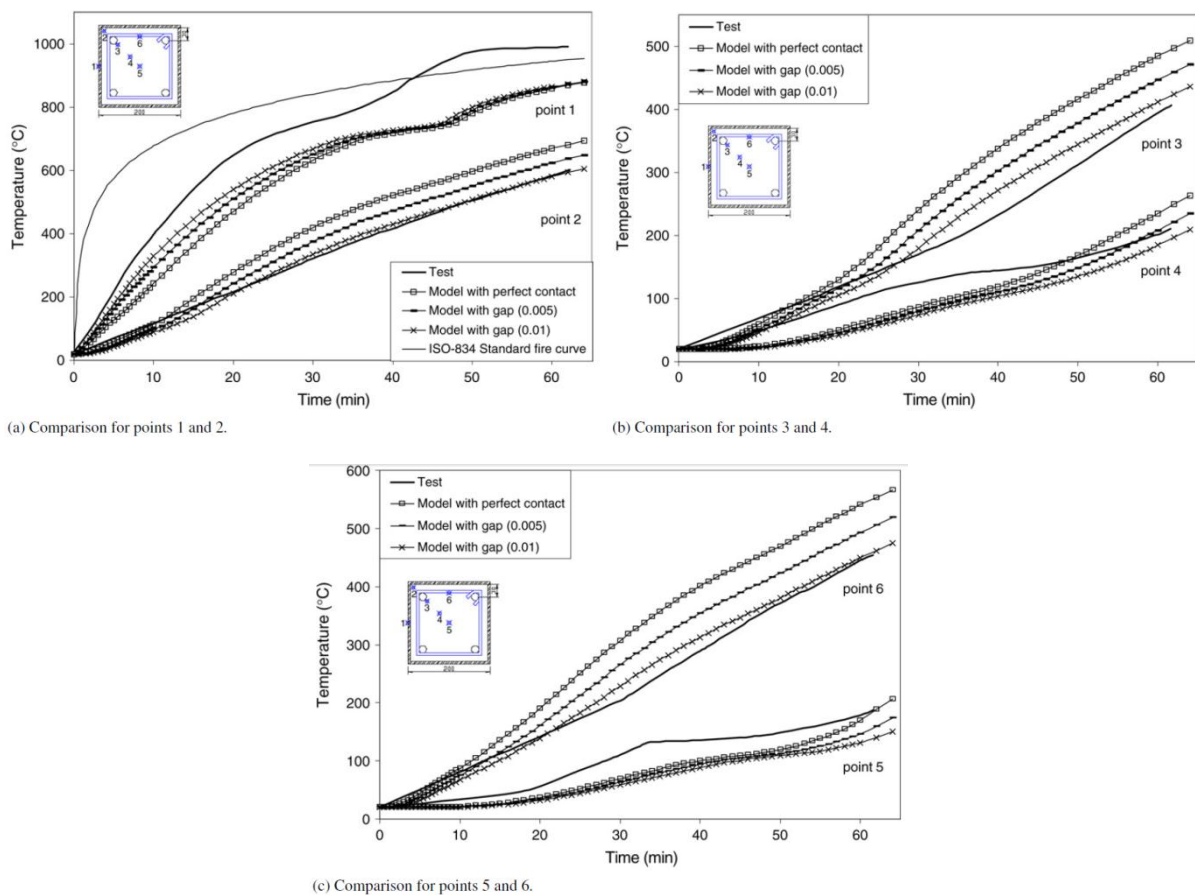


Figure 2.16 – Temperature calculated using Ding and Wang’s model and test results (Ding and Wang, 2008).

Figure 2.17 presents a comparison between the results calculated by the model proposed by Ding and Wang (2008) and the test results in (a) the vertical displacement at the top of a 200mm CFH-RC column which has a 6.3mm thick tube wall and in (b) a general comparison of all fire resistances. The difference in general does not exceed 15% according to the authors.

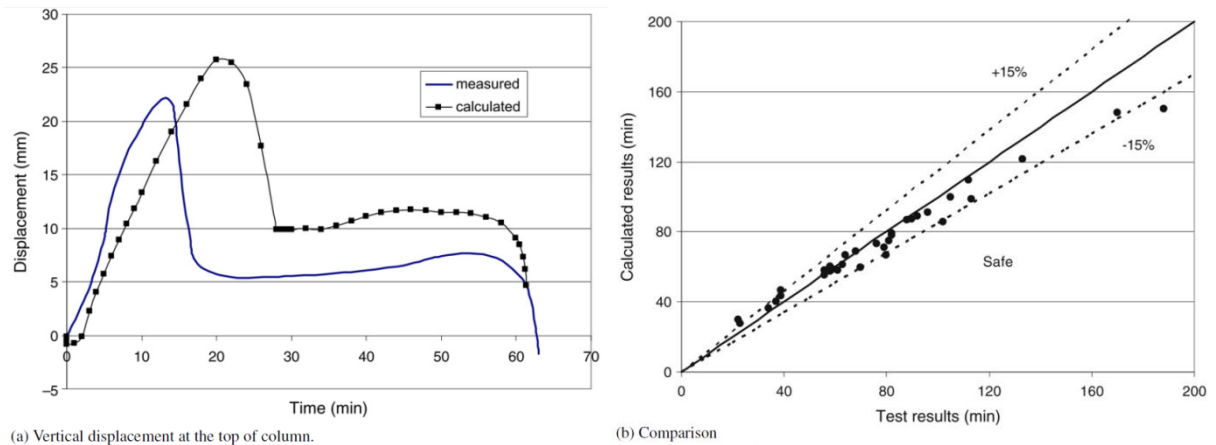


Figure 2.17 – Results calculated using Ding and Wang’s model and test results (Ding and Wang, 2008)

A parametric study was conducted using this model and the main conclusions were: whether or not slipping between the steel tube and concrete core is included, this has a minor influence on the calculated fire resistance but including the slip gives a better prediction of column deflections; the influence of tensile strength and tangential stiffness of concrete on fire resistance is small; making use of the air gap for calculations improves the accuracy of predictions for temperatures and structural behaviour; and the influence of the initial deflection of the column on fire resistance is small. They suggest a maximum initial imperfection of  $L/1000$ .

Hong and Varma (2009) proposed a three sequentially coupled analysis to predict the fire behaviour of CFH columns. The first step is a fire dynamics analysis conducted on a Fire Dynamics Simulator (FDS) to simulate the heat transfer from the fire source to the outermost surface of the column. The second is a heat transfer analysis to calculate the temperatures along the cross-section and column length and finally the third step is a stress analysis to simulate the structural response. The latter two steps are developed in the finite element program ABAQUS. The model was validated by making a comparison with 15 CFH columns with and without fire protection tested by other authors including the NRCC tests and those reported in Han *et al.* (2003a).

The heat transfer and stress analysis were conducted respectively with a DC3D8 and a C3D8R 3-D finite element type eight node continuum for the concrete core and a DS4 and S4R four node shell for the steel tube. The model did not consider any movement and transmigration of water vapour within the concrete core. In addition the steel and concrete temperatures in the interface were assumed to be equal. The reinforcement was modelled using a T3D2 two node truss element embedded in the concrete elements. The isotropic multi-axial plasticity model with Von Mises yield was used for the steel elements and the concrete damage plasticity model for concrete.

A detailed sensitivity analysis was conducted and the main parameters were identified, thus giving recommendations for the simulation of CFH columns. The suggestions were: (a) the steel tube should be modelled using the stress-strain-temperature model proposed by Poh (2001) *apud* Hong and Varma (2009), (b) the concrete using the stress-strain-temperature model proposed by Lie and Irwin (1995), (c) the linear thermal expansion models for steel and concrete may be used and (d) the full composite action with no local buckling may be used to model the columns.

A comparison between the temperatures predicted with the Hong and Varma (2009) model and those measured in tests is presented in Figure 2.18. Two CFH-RC columns with square cross-sections were presented: in (a) a column with an external side of 203mm, four reinforcing bars with 16mm of diameter, and 16% of load level; and in (b) a column with an external side of 305mm, four reinforcing bars with 25mm of diameter, and 33% load level. The length of both columns was 3810mm, the steel tube was 6.35mm thick and had fixed end conditions.

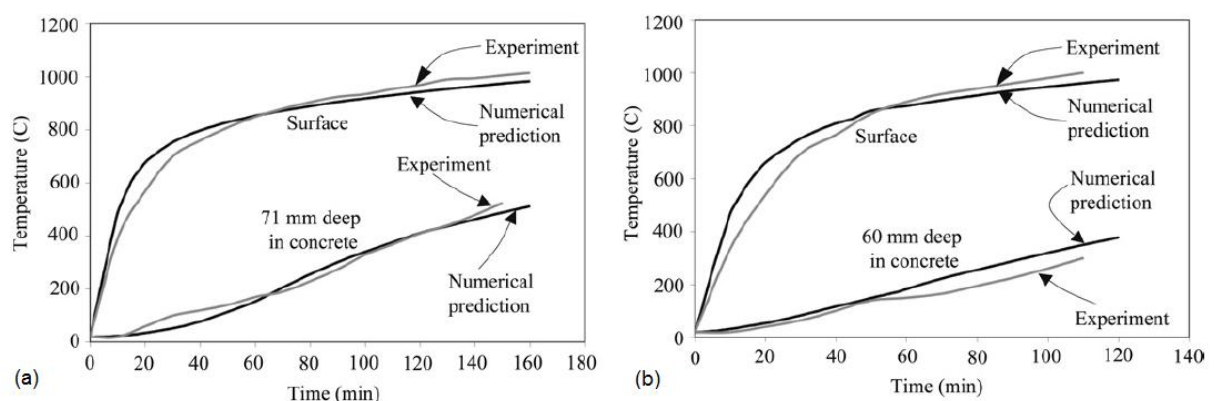


Figure 2.18 – Temperature calculated using Hong and Varma’s model and test results (Hong and Varma, 2009).

Some differences were observed in the temperatures and the authors justified these due to the variations in the thermal properties of the material and the approach used to model the moisture content of the concrete infill.

Figure 2.19 shows the comparison between the axial deformations predicted using Hong and Varma's (2009) model and those measured in fire tests. In (a) and (b), the same columns as described above are used. In (c), a CFH-RC column with external dimension of 254mm, four reinforcing bars with 16mm of diameter is presented. The steel tube is 3.25mm thick, 3810mm in length, has a 32% load level and fixed end conditions. In (d), an CFH-PC is presented. Its external dimension is 300mm, the steel tube is 9mm thick, 3500mm in length, has a 75% load level and pin ended conditions. The failure time is indicated by solid black circles in the Figures.

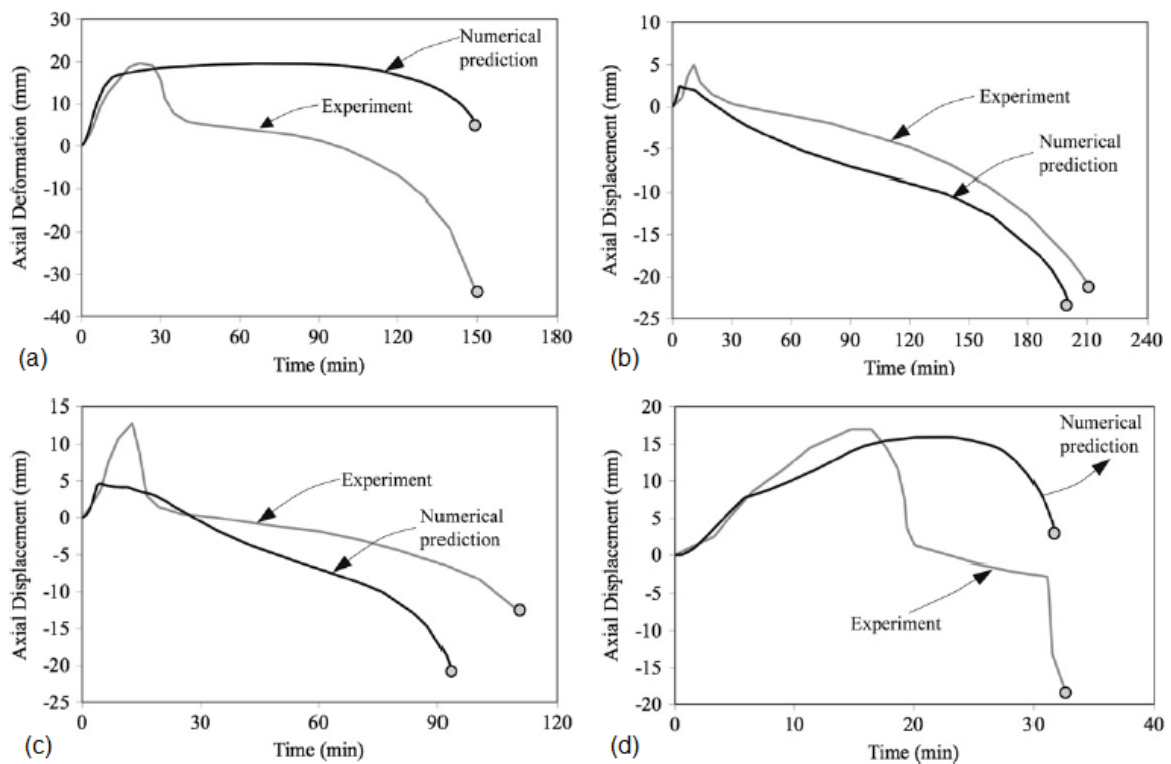


Figure 2.19 – Axial deformation calculated by Hong Varma's model and test results (Hong and Varma, 2009)



The failure times predicted with Hong and Varma's (2009) model and measured in fire tests are presented in Table 2.6. According to the authors, the numerical predictions with pin ended conditions neither reproduced the failure times nor the axial deformation accurately. Therefore columns 13 and 14 were recalculated with fix ended conditions and these produced better results.

Table 2.6 – Failure times calculated using Hong Varma's model and test results (Adapted from Hong and Varma, 2009)

<i>Column</i>	<i>Experimental failure time (min)</i>	<i>Numerical failure time (min)</i>	$ Exp - Num $ <i>(min)</i>	$\frac{Exp. fail time}{Num. fail time}$
<b>1</b>	150	149	1	1.01
<b>2</b>	110	93	17	1.18
<b>3</b>	212	201	11	1.06
<b>4</b>	33	32	1	1.03
<b>5</b>	180	197	17	0.92
<b>6</b>	165	180	15	0.92
<b>7</b>	148	161	13	0.92
<b>8</b>	98	108	10	0.91
<b>9</b>	188	183	5	1.03
<b>10</b>	135	112	23	1.20
<b>11</b>	194	112	82	1.73
<b>12</b>	87	71	16	1.22
<b>13</b>	169	59 – pin	110	-
		120 – fix	49	1.41
<b>14</b>	143	98 – pin	45	-
		146 – fix	3	0.99
<b>15</b>	110	85	25	1.29

The authors justified the discrepancies between numerical and experimental results due to the assumptions and limitations of the numerical models and potential errors while conducting the fire tests. The variability and uncertainty of the behaviour of the materials at elevated temperatures; the limitation of the element type (i.e. continuum C3D8R and the S4R shell) on modelling bending and flexural behaviour; the fact of the model not taking into account accurately the tension cracking behaviour of concrete; the complexity of fire tests in columns

with few experimental tests for comparison; and the unintentional errors during the experimental measuring were pointed out as main limitations.

According to the authors despite these assumptions, limitations and potential errors, the model predicted the fire behaviour of the columns with reasonable accuracy and it is able to conduct parametric studies to design guidelines.

In 2009 Schaumann *et al.* presented a 2D numerical research focused on the fire behaviour of CFH-PC, CFH-RC and CFH-FRC columns. High strength concrete was used to fill the columns and they compared the results obtained using the North American code provisions CSA A23.3-M04 (1994) and CSA S16.1 (2001) and those obtained from European Union material properties as per EN1992-1-2 (2004) and EN1994-1-2 (2005) – Figure 2.20.

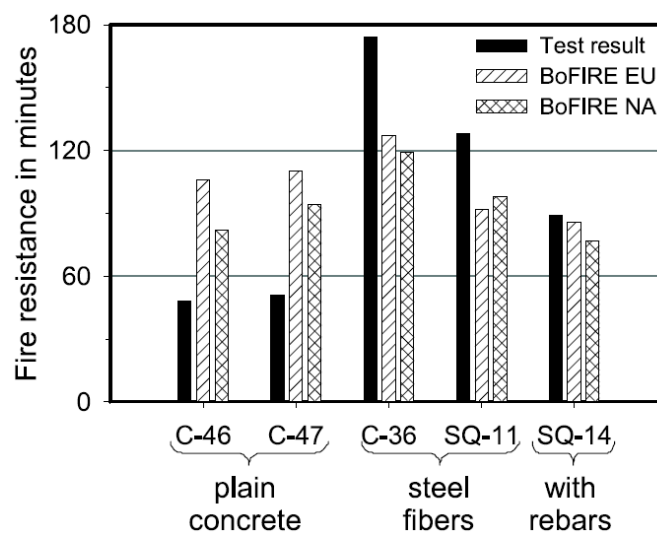


Figure 2.20 – Fire resistances calculated using the Schaumann *et al.* model and test results (Schaumann *et al.*, 2009).

The variables considered in this research were different types of concrete filling, moisture content, section size, cross-sectional shape, column slenderness, load eccentricities and the compression strength of concrete. A parametric study was carried out in the transient, nonlinear, incremental computer code BoFire. First, the model evaluates the temperatures of the cross-section (thermal response) then determines the deformation and remaining strength of the members (mechanical response). The failure criterion was when the resistance of the member was less than the initial applied load.

The authors concluded that there are major differences in material properties of high strength concrete proposed by the North American and European codes at high temperatures. The same was not verified for normal concrete which has a different behaviour in these conditions. For steel, the material properties are well-established in these codes and do not have major differences but for concrete the fire resistance results using the North American properties are more conservative with regard to increasing concrete strengths and decreasing cross-sectional dimensions.

Other conclusions were the possibility of the model overestimating results due to local effects such as gaping cracks and local plastic buckling that are not considered by most conventional simulation tools and might occur in CFH-PC columns. Also high strength concrete filling is beneficial for massive columns with a low A/V section factor rather than in leaner columns and in non-slender columns with moderate load eccentricity; CFH columns with circular cross-sections provide a higher fire resistance than the ones with square cross-sections of similar cross-sectional area besides which by adding reinforcement (*i.e.* reinforcing steel bars or steel fibres) to the concrete, the fire resistance may be enhanced.

An advanced three-dimensional nonlinear finite element model developed in ABAQUS for evaluating the fire behaviour of axially loaded CFCH columns was presented by Espinos *et al.* (2010). In an extensive research study, including important features such as the thermal conductance and friction model of the steel-concrete interface, the thermal expansion coefficients of steel and concrete and the type of finite element used in the simulation of the reinforcing bars, they validated the model by comparing results from it with experimental tests undertaken by the NRCC already presented in this chapter and by CIDECT in research reports 15B and 15C1/C2 *apud* Espinos *et al.* (2010).

The model was meshed with three-dimensional eight-node solid elements for both the steel tube and the concrete core and two-node elements for the reinforcing bars. The mesh density was controlled so that the maximum size of an element size was 20mm. The mechanical model for concrete was that proposed by Lie (1994) and the thermal properties at elevated temperatures were extracted from EN1992-1-2 (2004). For the steel tube both the thermal and mechanical properties followed the recommendations of EN1993-1-2 (2005). As to the reinforcing steel, the thermal and mechanical properties were the same as those for the steel tube. However the strength and deformation were reduced using the factors recommended by EN1992-1-2 (2004).

In addition the thermal expansion coefficient for concrete was replaced by the value proposed by Hong and Varma (2009). The moisture content of concrete in the column was taken into account through a peak value in specific heat. According to the authors, the best results were

obtained with 3% moisture for the siliceous aggregate (peak value in specific heat of 2020J/kg °C) and 10% for the calcareous aggregate (peak value in specific heat of 5600J/kg °C).

An initial geometrical imperfection of the column was considered following the first buckling mode shape of the hinged column multiplied by a factor of  $L/1000$ . According to the authors, a sequentially coupled thermal-stress analysis was designed instead of a fully coupled one due to the latter requiring a high amount of computational time and convergence problems may occur.

The values of the governing parameters to solve the heat transfer problem recommended by EN1991-1-2 (2002) were adopted. The thermal resistance at the boundary between the steel tube and the concrete core was modelled by applying a constant value of  $200\text{W/m}^2\text{ °C}$  for the gap conductance. A radioactive heat transfer was also modelled in the steel tube-concrete core interface with emissivity of both steel and concrete surfaces of 0.7 and a configuration factor of 1. The tangent behaviour was modelled using the Coulomb friction model with a constant friction coefficient of 0.3.

The authors explained the structural behaviour of CFCH columns in 4 stages. The first occurs when heating begins where the steel tube heats and expands more quickly due to its higher thermal conductivity than the concrete core and the fact of its being directly exposed to fire. Therefore, a slip occurs in the steel tube-concrete core interface and the concrete core loses its contact with the top plate. Consequently the entire applied load starts to be transferred to the steel tube. The second stage starts after the steel tube reaches the critical temperature of the steel, buckling locally and starts to shorten. The third stage starts when the top plate of the columns enters in contact again with the concrete core due to the steel tube shortening, and thus a transfer of the applied load to the concrete core starts. Because of its low thermal conductivity the concrete core degrades more slowly than the steel tube but finally when the concrete loses its strength and stiffness, the column fails and the last stage occurs (Figure 2.1).

Figure 2.21 presents a comparison of the axial displacement at the top between those calculated using the model by Espinos *et al.* (2010) and those measured in the fire tests. The columns are 3810mm tall, 319.1mm in external diameter, the thickness of the steel tube is 4.78mm (in “a”) and 8.18mm (in “b”), they have fixed- fixed end conditions and a load level of around 25%.

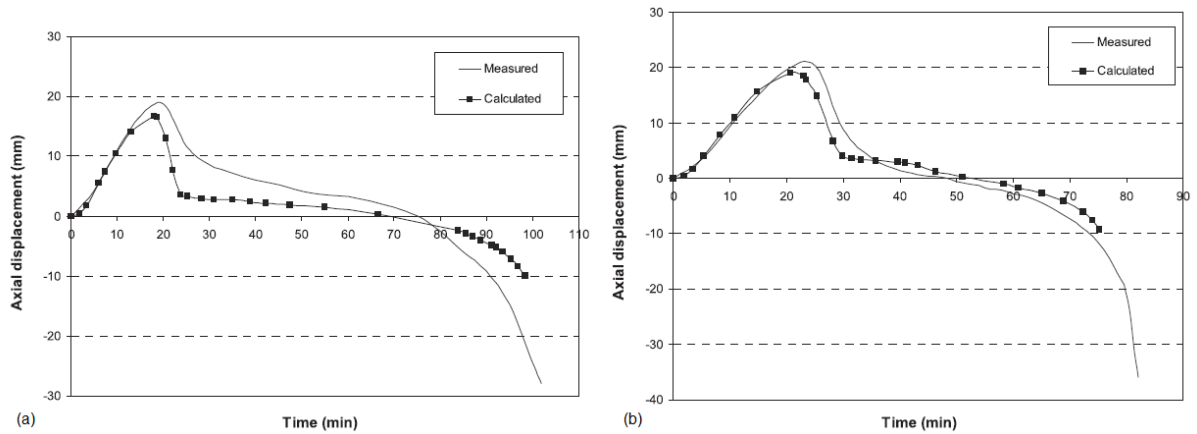


Figure 2.21 – Axial deformation calculated using the model by Espinos *et al.* and test results (Espinos *et al.*, 2010).

According to the authors, for the CFCH columns with normal concrete (*i.e.* resistance under 40MPa), there was good agreement between the numerical and experimental results. Most of the fire resistance results calculated were in the range of 15% error (Figure 2.22 “a”). However for medium or high strength concrete filling, the occurrence of spalling may cause divergence in results and a more advanced thermo-hydro-mechanical model is required to predict spalling (Figure 2.22 “b”).

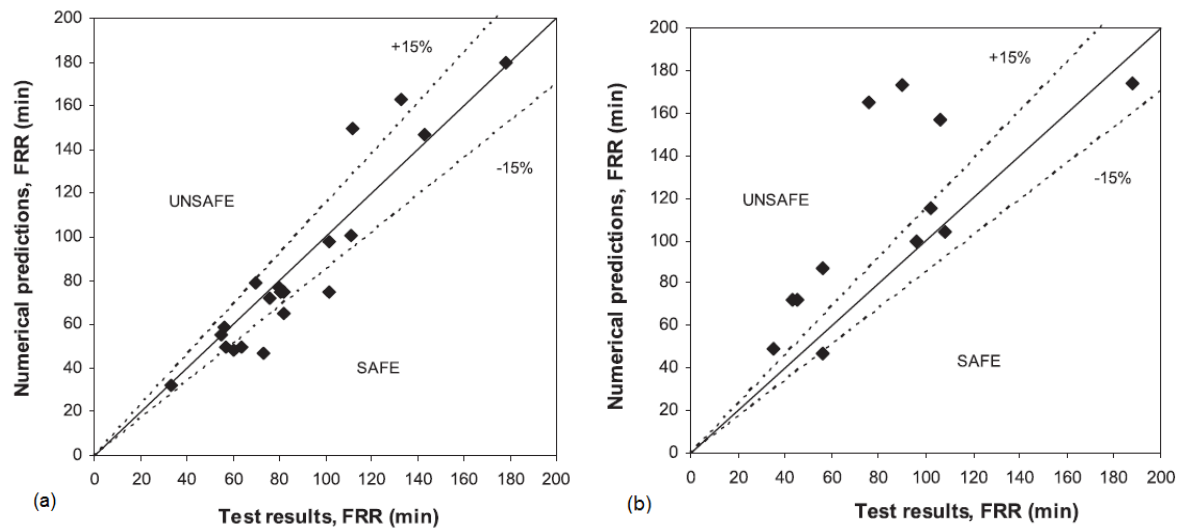


Figure 2.22 – Fire resistances calculated using the model by Espinos *et al.* and tests results (Espinos *et al.*, 2010).

Also the authors pointed out that the best results were observed in columns with the smallest external diameters. While the introduction of a concrete core in massive columns is a major contribution, this also leads to more errors due to the complex failure mechanism of concrete. In addition, better results were observed when pinned-fixed end conditions were simulated even when the real end condition was pinned-pinned columns.

As to the thermal model, the temperatures showed a good agreement with test results except for the concrete core layers in the range between 100°C and 200°C where the evaporation of moisture occurs and the model cannot realistically predict moisture movement and evaporation (Figure 2.23).

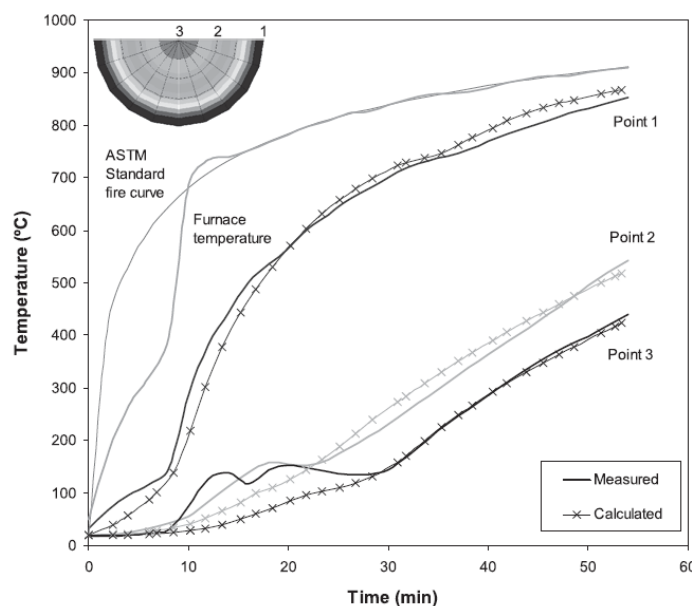


Figure 2.23 – Temperatures calculated by Espinos *et al.* and test results (Espinos *et al.*, 2010).

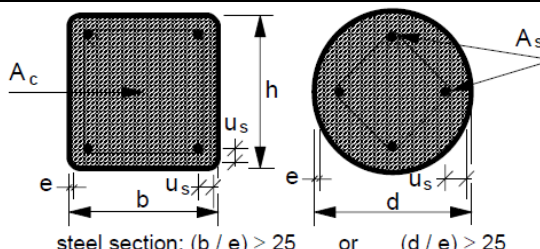
## 2.4 EN1994-1-2 – Tabulated data and simple calculation method

Besides the approach of using advanced calculation models to assess the structural behaviour of composite columns in the event of a fire, EN1994-1-2 (2005) offers two other approaches that are easier to apply: tabulated data and simple calculation models.

The first is extremely easy to apply and gives the fire resistance based on recognized design solutions for specific types of structural members exposed to the ISO834 (1999) standard for fire. For CFCH columns, a table sets out the minimum cross-sectional dimensions, minimum

reinforcement ratios and minimum axial distance of the reinforcing bars for a specified load level (*i.e.* 28%, 47% and 66%) in order to reach a standard fire resistance (Table 2.7).

Table 2.7 Standard fire resistance and minimum requirements for CFH columns (EN1994-1-2, 2005)

	<i>Standard Fire Resistance</i>				
	R30	R60	R90	R120	R180
<b>1. Minimum cross-sectional dimensions for load level <math>\eta_{fi,t} \leq 0.28</math>:</b> 1.1 Minimum dimensions h and b or minimum diameter d (mm) 1.2 Minimum ratio of reinforcement $A_s/(A_c+A_s)$ in (%) 1.3 Minimum axis distance of reinforcing bars $u_s$ (mm)	160	200	220	260	400
<b>2. Minimum cross-sectional dimensions for load level <math>\eta_{fi,t} \leq 0.47</math>:</b> 2.1 Minimum dimensions h and b or minimum diameter d (mm) 2.2 Minimum ratio of reinforcement $A_s/(A_c+A_s)$ in (%) 2.3 Minimum axis distance of reinforcing bars $u_s$ (mm)	260	260	400	450	500
<b>3. Minimum cross-sectional dimensions for load level <math>\eta_{fi,t} \leq 0.66</math>:</b> 3.1 Minimum dimensions h and b or minimum diameter d (mm) 3.2 Minimum ratio of reinforcement $A_s/(A_c+A_s)$ in (%) 3.3 Minimum axis distance of reinforcing bars $u_s$ (mm)	260	450	550	-	-
	3.0	6.0	6.0	-	-
	25	30	40	-	-

However this method limits the user to a few solutions presented in the code. In addition this method was based on test results which as shown above do not consider important parameters that may influence fire resistance such as restraining thermal elongation although the same code states that this method should give conservative results.

The other method (*i.e.* simple calculation method – SCM) presents in annex H of EN1994-1-2 (2005) a way to access the fire resistance of CFH columns with circular and rectangular cross-sections exposed to the ISO834 (1999) standard fire curve on all sides. The method is divided into two steps which are described below.

The first step is to determine the temperature distribution on the CFH column cross-section based on the acknowledged principles and assumptions of the theory of heat transfer. EN1994-1-2 (2005) does not give an explicit formulation to obtain the temperatures; it only gives recommendations. As shown above, the non-uniform distribution of temperature in the concrete core is a complex problem to solve.

In the second step, the design of the axial buckling load at elevated temperature  $N_{fi,rd}$  may be obtained by Equations 2.1 to 2.3 presented in EN1994-1-2 (2005). The design axial buckling load  $N_{fi,rd}$  is defined when the elastic critical load  $N_{fi,cr}$  becomes equal to the design value of the plastic resistance to axial compression of the total cross-section  $N_{fi,pl,rd}$ . The recommendation of the code is to increase the strain in steps until Equation 2.1 is satisfied. On the other hand, due to the non-uniform temperatures and consequently a non-uniform distribution of material strength and stiffness, the terms of Equations 2.2 and 2.3 ( $E_{i,\theta,\sigma} I_i$  and  $A_i \sigma_{i,\theta}$  respectively) should be calculated as a summation of all elementary elements  $dy dz$  having temperature  $\theta$  after a fire duration  $t$ . Thus, a numerical aid is needed to solve the equations and users usually find the method is not easy to apply.

$$N_{fi,Rd} = N_{fi,cr} = N_{fi,pl,rd} \quad (2.1)$$

$$N_{fi,cr} = \frac{\pi^2 (E_{a,\theta,\sigma} I_a + E_{c,\theta,\sigma} I_c + E_{s,\theta,\sigma} I_s)}{l_\theta^2} \quad (2.2)$$

$$N_{fi,pl,rd} = \frac{A_a \sigma_{a,\theta}}{\gamma_{M,fi,a}} + \frac{A_c \sigma_{c,\theta}}{\gamma_{M,fi,c}} + \frac{A_s \sigma_{s,\theta}}{\gamma_{M,fi,s}} \quad (2.3)$$

Wang (2000) highlighted this difficult that users have in implementing the method and proposed an alternative simple method to access the fire resistance of unprotected and protected CFH columns where it is no longer necessary to evaluate the non-uniform temperature distribution in the column and only a few linear interpolations are required to obtain the column squash load and rigidity. According to the author the method is sufficient



for evaluating the load bearing capacity of a column under fire conditions reasonably accurately.

Kodur (1999) and Han *et al.* (2003b) also proposed alternative simple methods as already cited above.

## 2.5 Chapter remarks

This chapter presented an overview of the main experimental and numerical research studies carried out in the last 20 or so years, principally those focused on CFCH columns subjected to fire. In addition, other studies and a brief overview of the simple methods presented in EN1994-1-2 (2005) were presented to complement the state of the art. This research was fundamental to define the main way of the steps of this thesis which will be presented in the following chapters. The main conclusions of this chapter were:

- There are few experimental data from tests conducted with CFH columns subjected to fire;
- The influence of the stiffness of the surrounding structure on the behaviour of these columns subjected to fire had been little studied and is not very clear. Some research studies pointed out that the higher the axial restraining is, the lower the fire resistance is. Rotational restraining has the opposite effect: increasing one increases the other;
- Slenderness of the column, cross-sectional dimensions, effective length, load level and type of concrete filling (PC, RC or FRC) have a great influence on the fire resistance of CFH columns. Other parameters such as the strength of the concrete and steel, the type of aggregates and the eccentricity of the loading have a moderate influence and the ratio of steel reinforcement, the thickness of the steel tube wall and the axis distance of reinforcing bars us only have a minor influence on the fire resistance of these columns;
- There are great differences in the experimental methods applied (*e.g.* differences in failure criterion, heating rate and test procedure) or in important parameters (*e.g.* load level, restraining level and end conditions). This fact hampers comparisons and induces differences in the test results;
- The numerical models also presented some important differences such as the numerical model applied, the finite element mesh, the thermal and mechanical properties of steel and concrete adopted and the thermo-mechanical behaviour in the

interface between the steel tube and concrete core. The modelling of the concrete behaviour in high temperatures such as the migration of humidity inside concrete are difficult problems to solve;

- Few numerical models simulate the restraints on thermal elongation imposed by the surrounding structure and validate them with experimental tests probably due to few fire tests having restrained CFH columns;
- Most experimental research studies were performed in CFH columns with low load level and smaller external diameters. Consequently several numerical models were validated based in this situation;
- CFH-PC columns cannot reach high fire resistances since a high load level is applied (Kodur, 1999; Han *et al.* 2003a and 2003b). The load level should be reduced or a fire protection should be designed. This column is not recommended in slender situations according to Romero *et al.* (2011).
- CFH columns with circular cross-sections have a slightly higher fire resistance than the ones with square cross-sections (Yin *et al.* 2006; Schaumann *et al.* 2009);
- There is a need to improve the simple methods presented in EN1994-1-2 (2005) so that they are easier to apply and still give accurate results and consider the most important parameters that influence the behaviour of CFH columns in the event of a fire.

### 3. FIRE RESISTANCE TESTS ON CONCRETE FILLED CIRCULAR HOLLOW COLUMNS

#### 3.1 Introduction

This chapter presents the fire resistance tests on Concrete Filled Circular Hollow (CFCH) columns with axial and rotational restraining to thermal elongation performed at the Laboratory of Testing Materials and Structures of the University of Coimbra, in Portugal.

The columns were filled with plain concrete (CFCH-PC columns) and reinforced concrete (CFCH-RC columns). The parameters considered on the series of tests carried out included the slenderness, cross-sectional diameter (168.3 and 219.1mm), loading level (30% and 70%  $N_{ed}$ ), stiffness of surrounding structure (a lower level with  $K_{as}$  of 13 kN/mm and  $K_{rs}$  of 4091 and 1992 kN m/rad and a higher level with  $K_{as}$  of 128 kN/mm and  $K_{rs}$  of 5079 and 2536 kN m/rad), steel reinforcement ratio (0% and around 2.5%) and degree of concrete filling inside the steel tube (completely filled or with a ring around the internal surface of the steel tube wall). Also Circular Hollow Sections (CHS) columns (*i.e.* steel columns) were tested for comparison.

The results obtained showed that the critical time of the columns was less than 46 min. The use of a concrete ring around the internal surface of the column wall is not offering advantage in terms of its behaviour under fire conditions because this concrete ring suffers extensive spalling and cracking due to the overheating of the steel tube. The main failure mode of the columns was global buckling. However in several cases local buckling also occurred. Details of tests conducted and results of development of temperatures in furnace and columns, restraining forces, axial deformations, critical times and temperatures, and failure modes are presented and discussed in the following sections.

#### 3.2 Experimental programme

##### 3.2.1 Test set-up

An experimental system was mounted at the Laboratory of Testing Materials and Structures of the University of Coimbra, in Portugal for fire resistance tests on building columns with restrained thermal elongation (Correia and Rodrigues, 2011 and 2012 and Pires *et al.*, 2012a). The following figures show steps of the system assembly.



Figure 3.1 – Restraining steel beams and M27 threaded rods



Figure 3.3 – Upper restraining frame assembly



Figure 3.2 – Upper restraining steel beams



Figure 3.4 – Furnace modules



Figure 3.5 – Furnace assembly



Figure 3.7 – 3D restraining frame assembly



Figure 3.6 – 2D reaction frame assembly



Figure 3.8 – Final configuration of test apparatus

Below is given a detailed description of each component of the test apparatus and its location is indicated in the general view (Figure 3.9) and in the scheme (Figure 3.10) of the testing set up.



A 3D restraining steel frame (1), consisting of four columns, two upper and two lower beams, arranged orthogonally, simulates the stiffness of the structure surrounding the column subjected to fire. Different positions for the columns of this restraining frame allowed different values for the stiffness of the surrounding structure to the column in test. Values of axial stiffness ( $K_{as}$ ) between 13 and 128kN/mm and of rotational stiffness ( $K_{rs}$ ) between 4091 and 5079kN·m/rad in direction X1 and between 1992 and 2536kN·m/rad in direction X2 may be achieved by this restraining frame. M24 bolts, grade 8.8, were used for the connections of the restraining frame, except the ones between its peripheral columns and the upper beams, where M27 threaded rods (2), steel grade 8.8, were used.

During all tests, a constant compressive load was applied to the test column in order to simulate its serviceability load when in a real building structure. This load was applied using a hydraulic jack with a total capacity of 3 MN (3). The applied load was controlled by a load cell (4), placed between the upper beam of the 3D restraining frame and the head of the piston of the hydraulic jack. The hydraulic jack was fixed in a 2D reaction frame (5), in which a safety structure (6) was also mounted to prevent damage to the experimental setup in case of sudden collapse of the column.

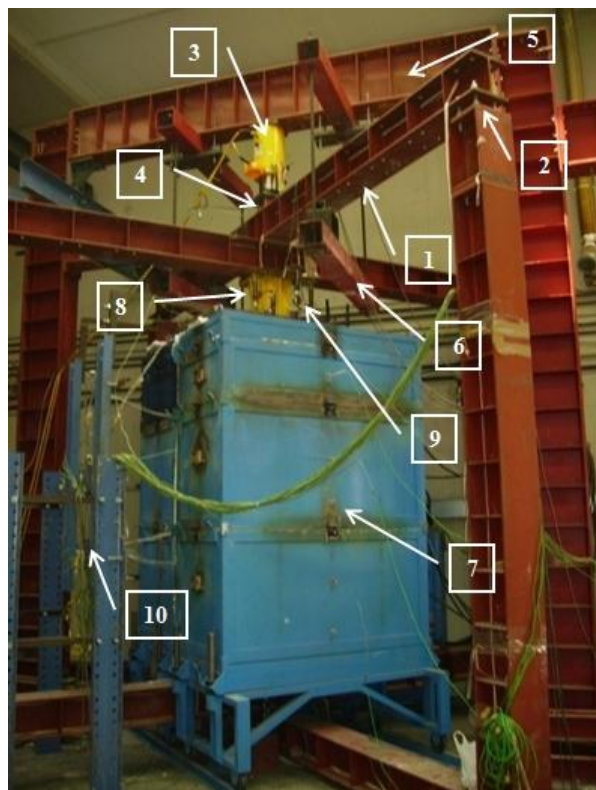


Figure 3.9 – General view of testing set up.

The thermal action was applied by a modular electric furnace (7) comprising two modules of 1.5 m x 1.5 m x 1.0 m and one module of 1.5 m x 1.5 m x 0.5 m, placed on top of each other, thus forming a 2.5 m high chamber around the column.

A special device was built to measure the restraining forces generated in the columns tested during the fire resistance tests (8). It consists of a hollow and stiff cylinder of high strength steel, rigidly connected to the upper beams of the 3D restraining frame, into which a massive steel cylinder, rigidly connected on the top of the test column, was placed. The lateral surface of the massive cylinder was Teflon (PTFE) lined in order to prevent friction with the external hollow steel cylinder. The restraining forces were measured by a 3MN load cell, placed inside the hollow steel cylinder, which was compressed by the massive steel cylinder due to the column having been thermally elongated during the fire resistance test.

To measure the axial displacements of the columns, linear variable displacement transducers (LVDT) were used. Three were placed three on the top and four on the bottom of the test columns (9) orthogonally arranged for also measuring the rotations. The lateral deflections of the columns were also measured by cable LVDT placed at different levels (10). However, due to the fact that there were not any well-defined bending plan in the test columns, it was difficult to determine these displacements.

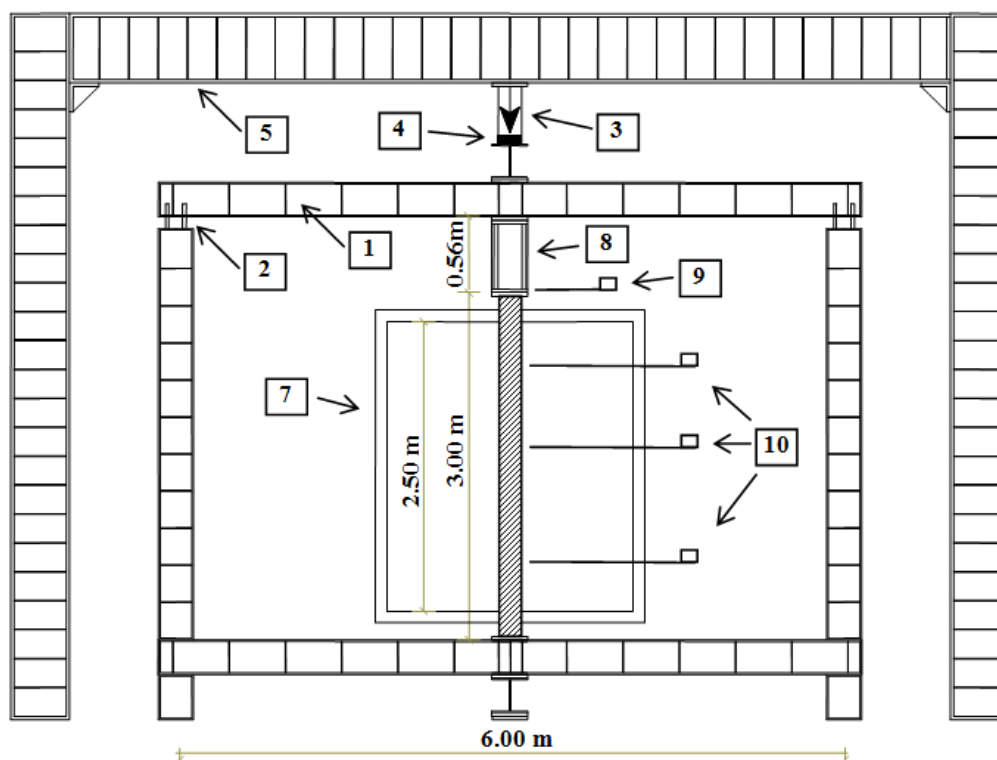


Figure 3.10 – Scheme of testing set up.

To determine the axial stiffness of the 3D restraining frame ( $K_{as}$ ) a specific test at ambient temperature was conducted and measurements taken of this parameter in the two frame positions used in the fire tests, *viz.*, the lower restraining level ( $K_{low}$ ) and the higher restraining level ( $K_{high}$ ). To test the reliability of these measurements, the restraining stiffness was also calculated with the values of the restraining forces and axial displacements measured in the fire resistance tests. Figure 3.11 shows the axial stiffness measured for the lower and higher restraining level (stiffness test 1 and 2 respectively). Also the axial stiffness obtained in fire resistance tests A20 and A40 were plotted for comparative purposes.

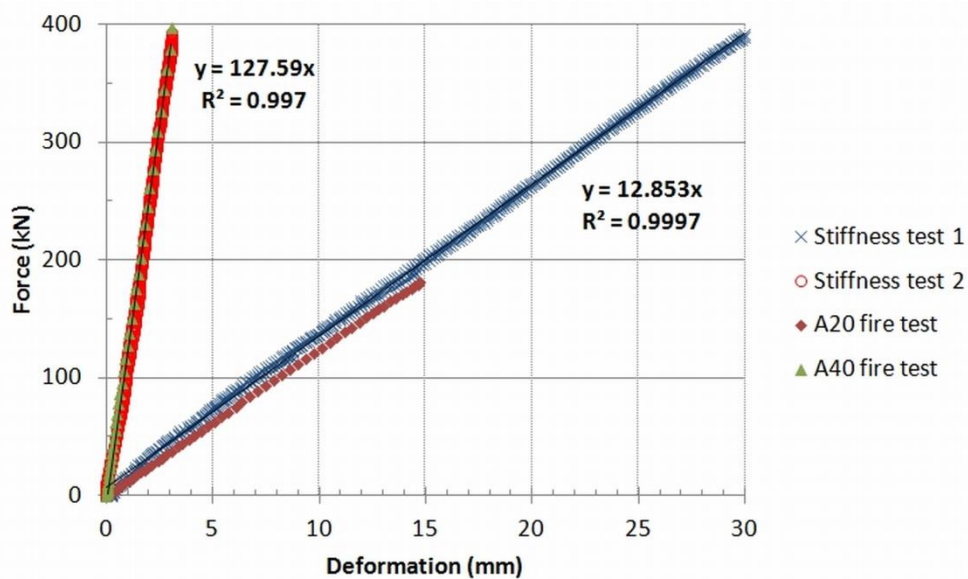


Figure 3.11 – Axial stiffness of the 3D restraining frame.

The rotational stiffness of the 3D restraining frame ( $K_{rs}$ ) was numerically calculated with ABAQUS (2011) program. For each restraining level there are two different values of rotational stiffness: one in direction X1 and the other in the perpendicular direction X2. Figure 3.12 shows the rotational stiffness in direction X1 and X2 for the lower and higher restraining level (stiffness test 1 and 2 respectively).

The test starts by applying the serviceability load to the test column. Prior to the fire resistance test, in order to transfer the applied load to the test column, the nuts of the M27 threaded rods (see 2 Figure 3.9) were loosened. When the loading in the test column reached the serviceability load, the nuts of the threaded rods were tightened and the surrounding structure started to exert axial restraining on the column being tested. Having done so, the fire resistance test was fit to start.



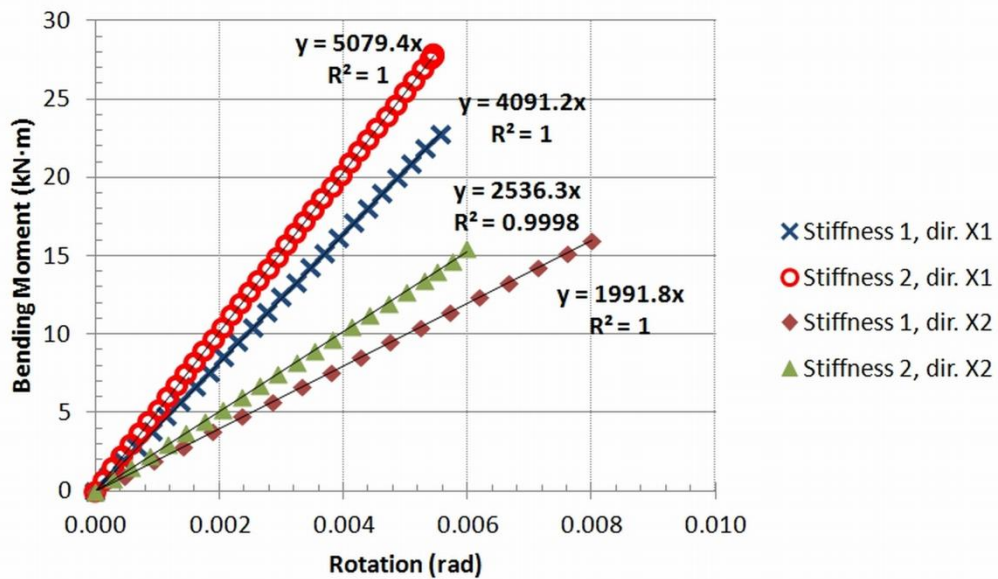


Figure 3.12 – Rotational stiffness of the 3D restraining frame.

### 3.2.2 Test columns

All the test columns were made from CHS tubes, steel grade S355, with two different external diameters, 219.1 mm and 168.3 mm, both 6 mm thick walls. Concrete C25/30 class (EN 206-1, 2007) was used in the fabrication of the test columns. The concrete completely filled or covered, in a ring, the internal wall surface of the steel tube. The concrete ring was 50 and 40 mm thick for the 219.1 mm and 168.3 mm diameter columns, respectively.

Some of the columns were filled with steel reinforced concrete and others no. The steel reinforcement used being 6 steel bars with diameter of 10mm for the columns with external diameter of 168.3 mm and 6 steel bars with diameter of 12mm for the ones of 219.1 mm diameter (see Table 3.3). The steel grade of the reinforcing bars was A500 (EN 10080, 2005). In all these cases, 6 mm diameter stirrups, spaced 200 mm apart, were adopted. The axis distance for reinforcing bars to the inner surface of the column wall ( $u_s$ ) was 30 mm in all the cases (Figure 3.13).

All the columns length were 3 m, but only 2.5 m of specimen length was directly exposed to the furnace heating.

The internal ring on the CFCH column was made with a Styrofoam cylinder placed in the steel tube before casting (Figure 3.14). After the casting this cylinder was dissolved by propanone (acetone –  $C_3H_6O$ ).

At the bottom of the columns 4 stiffeners were welded in the connection of the steel tube with the steel plate (Figure 3.16). The same was done at the top of the columns. Also 4 small vent holes were done at the steel tube wall, two at the bottom and two at the top of the column for water vapour releasing during the heating.



Figure 3.13 – Reinforcing steel bars and stirrups (steel reinforcement).



Figure 3.15 – Steel reinforcement with Styrofoam cylinder.



Figure 3.14 – CFCH-RC column with concrete ring before casting.



Figure 3.16 – Stiffeners welded at the base/top of a CFCH column.

The curing of the concrete in all specimens took place under laboratory ambient conditions for a minimum period of 90 days after concrete casting (Figure 3.18). The concrete mixed used in the fabrication of the test columns is presented in Table 3.1. The mechanical properties at ambient temperature of the materials as well as the humidity and density of concrete were tested (Appendix A). The Table 3.1 summarizes the results for concrete and Table 3.2 for steel.



Figure 3.17 – Columns before the casting



Figure 3.18 – Curing of the CFCH columns

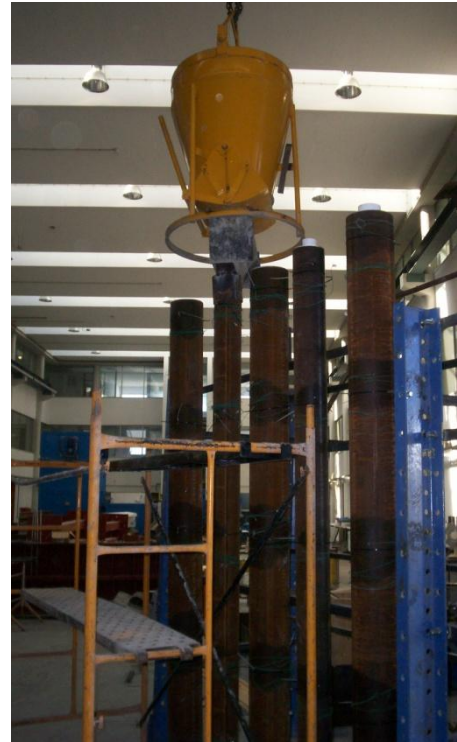


Figure 3.19 – Casting of the CFCH columns.

Table 3.1 – Mechanical properties of the concrete at ambient temperature

<i>Reference</i>	<i>Quantity</i>	<i>Unit</i>
<b>Concrete compositions:</b>		
Calcareous aggregate	900	Kg/m <sup>3</sup>
Fine siliceous sand	320	Kg/m <sup>3</sup>
Medium siliceous sand	550	Kg/m <sup>3</sup>
Cement II/A-L 42.5 R (EN197-1, 2001)	330	Kg/m <sup>3</sup>
Super - plasticizer Mira 44S	3.3	Kg/m <sup>3</sup>
Water	195	Kg/m <sup>3</sup>
<b>Compressive strength at 28 days (<math>f_{cu,28}</math>)</b>	33.2	MPa
<b>Compressive strength at the age of the first test</b>	34.2	MPa
<b>Compressive strength at the age of the last test</b>	35.8	MPa
<b>Humidity rate</b>	4.25	%
<b>Dry density</b>	2186	Kg/m <sup>3</sup>

Table 3.2 – Mechanical properties of the steel at ambient temperature

<i>Reference</i>	<i>Quantity (MPa)</i>
<b>Steel tube 168.3mm:</b>	
Yield strength ( $f_{ay}$ )	430.5
Ultimate strength ( $f_{au}$ )	510.7
<b>Steel tube 219.1mm:</b>	
Yield strength ( $f_{ay}$ )	529.0
Ultimate strength ( $f_{au}$ )	591.7
<b>Reinforcing steel bars:</b>	
Yield strength ( $f_{sy}$ )	505.7
Ultimate strength ( $f_{su}$ )	624.3

The temperatures in the specimens were measured with type K thermocouples, placed at five cross-sections (S1 to S5) of the specimen column, as shown in Figure 3.20.

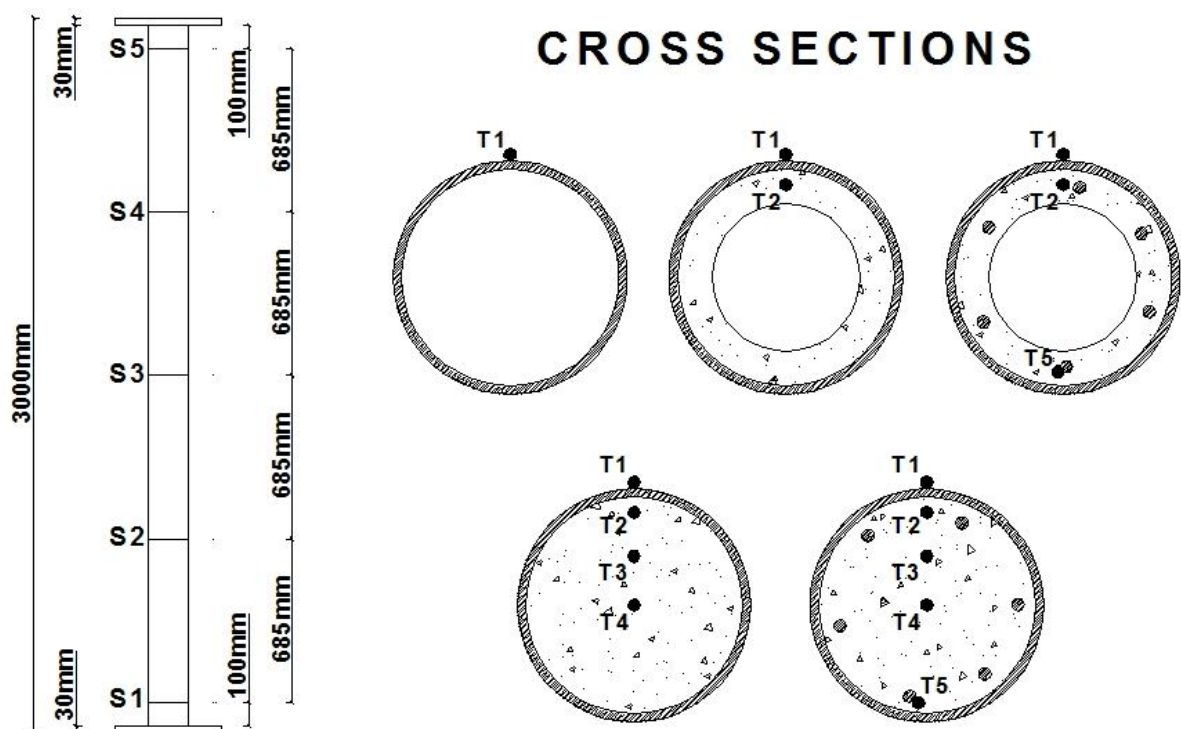


Figure 3.20 – Position of thermocouples on the columns by height and cross-section

### 3.2.3 Test plan

The values of the serviceability load applied to the columns were 70% and 30% of the design value of the buckling load at room temperature ( $N_{ed}$ ) calculated according to the methods of EN1994-1-1 (2005). The heating curve adopted was the ISO 834 fire curve (ISO834-1, 1999).

Two values of stiffness of the surrounding structure were applied to the tests, that corresponded to 13kN/mm of axial stiffness and 4091 and 1992kN·m/rad of rotational stiffness in directions X1 and X2 respectively, for lower stiffness ( $K_{low}$ ) and 128kN/mm of axial stiffness and 5079 and 2536kN·m/rad of rotational stiffness in directions X1 and X2 respectively, for higher stiffness ( $K_{high}$ ).

Table 3.3 presents the parameters of all the 40 test columns. Table column 1 indicates the specimen reference, column 2 the external diameter of the steel tube, column 3 the degree of concrete filling, column 4 the relative slenderness  $\bar{\lambda}$  (Eq. 3.1) according to EN1994-1-1 (2005), column 5 the steel reinforcement used, column 6 the serviceability load applied to the columns, column 7 the degree of axial restraint  $\alpha$  (Eq. 3.2), columns 8 and 9 the degree of rotational restraint  $\beta_1$  (direction X1) and  $\beta_2$  (direction X2) (Eq. 3.4), column 10 the critical times and column 11 the failure mode of the test columns.

$$\bar{\lambda} = \sqrt{\frac{N_{pl,Rk}}{N_{cr}}} \quad (3.1)$$

$$\alpha = \frac{K_{as}}{K_{as,c}} \quad (3.2)$$

$$K_{as,c} = \frac{(EA)_{eff}}{L_e} \quad (3.3)$$

$$\beta_i = \frac{K_{rs,i}}{K_{rs,c}} \quad (3.4)$$

$$K_{rs,c} = \frac{4(EI)_{eff}}{L_e} \quad (3.5)$$

The test columns can be identified as follow: AXX (XX is the reference code presented in Table 3.3) followed in subscript by the external diameter of the column (168 or 219), by the degree of concrete filling (RING or TOT), by the type of concrete filling (PC or RC), by the loading level (30% or 70%) and by the stiffness of the surrounding structure ( $K_{low}$  or  $K_{high}$ ) (e.g. A01<sub>168-TOT-PC-70%-Klow</sub>).

Table 3.3 – Test plan, critical times and failure modes.

Ref.	Diameter (mm)	Degree of concrete filling	Relative slenderness $\bar{\lambda}$	Reinforcement	Serviceability load (kN) (% Ned)	Axial restraint $\alpha$	Rotational restraint		Critical time (min)	Failure mode
							$\beta_1$	$\beta_2$		
A01	168.3	Total	0.883	--	816 (70%)	0.038	1.388	0.676	16	global buckling
A02	168.3	Total	0.911	6 $\phi$ 10mm	874 (70%)	0.035	1.345	0.655	13	global+local buckling
A03	168.3	Ring (40 mm)	0.855	--	775 (70%)	0.043	1.404	0.684	15	global+local buckling
A04	168.3	Ring (40 mm)	0.885	6 $\phi$ 10mm	753 (70%)	0.040	1.360	0.662	12	global+local buckling
A05	168.3	--	0.826	--	593 (70%)	0.073	1.751	0.852	8	global+local buckling
A06	219.1	Total	0.682	--	1359 (70%)	0.025	0.570	0.278	16	global buckling
A07	219.1	Total	0.698	6 $\phi$ 12mm	1478 (70%)	0.023	0.546	0.266	19	global+local buckling
A08	219.1	Ring (50 mm)	0.653	--	1242 (70%)	0.029	0.581	0.283	19	global+local buckling
A09	219.1	Ring (50 mm)	0.672	6 $\phi$ 12mm	1363 (70%)	0.027	0.556	0.271	14	global+local buckling
A10	219.1	--	0.629	--	877 (70%)	0.056	0.774	0.377	11	global+local buckling
A11	168.3	Total	0.883	--	350 (30%)	0.038	1.388	0.676	27	global buckling
A12	168.3	Total	0.911	6 $\phi$ 10mm	375 (30%)	0.035	1.345	0.655	30	global buckling
A13	168.3	Ring (40 mm)	0.855	--	332 (30%)	0.043	1.404	0.684	26	global+local buckling
A14	168.3	Ring (40 mm)	0.885	6 $\phi$ 10mm	323 (30%)	0.040	1.360	0.662	15	global buckling
A15	168.3	--	0.826	--	254 (30%)	0.073	1.751	0.852	14	global buckling
A16	219.1	Total	0.682	--	583 (30%)	0.025	0.570	0.278	27	global buckling
A17	219.1	Total	0.698	6 $\phi$ 12mm	633 (30%)	0.023	0.546	0.266	43	global buckling
A18	219.1	Ring (50 mm)	0.653	--	532 (30%)	0.029	0.581	0.283	29	global buckling
A19	219.1	Ring (50 mm)	0.672	6 $\phi$ 12mm	584 (30%)	0.027	0.556	0.271	23	global+local buckling
A20	219.1	--	0.629	--	376 (30%)	0.056	0.774	0.377	14	global+local buckling



Table 3.3 – Test plan, critical times and failure modes (cont.).

Ref.	Diameter (mm)	Degree of concrete filling	Relative slenderness $\bar{\lambda}$	Reinforcement	Serviceability load (kN) (% Ned)	Axial restraint $\alpha$	Rotational restraint		Critical time (min)	Failure mode
							$\beta_1$	$\beta_2$		
A21	168.3	Total	0.883	--	816 (70%)	0.372	1.723	0.860	15	global buckling
A22	168.3	Total	0.911	6 $\phi$ 10mm	874 (70%)	0.349	1.670	0.834	17	global+local buckling
A23	168.3	Ring (40 mm)	0.855	--	775 (70%)	0.421	1.743	0.870	14	global buckling
A24	168.3	Ring (40 mm)	0.885	6 $\phi$ 10mm	753 (70%)	0.391	1.689	0.843	12	global buckling
A25	168.3	--	0.826	--	593 (70%)	0.722	2.173	1.085	10	global buckling
A26	219.1	Total	0.682	--	1359 (70%)	0.244	0.708	0.354	16	global buckling
A27	219.1	Total	0.698	6 $\phi$ 12mm	1478 (70%)	0.229	0.677	0.338	19	global buckling
A28	219.1	Ring (50 mm)	0.653	--	1242 (70%)	0.286	0.722	0.360	17	global buckling
A29	219.1	Ring (50 mm)	0.672	6 $\phi$ 12mm	1363 (70%)	0.266	0.690	0.344	13	global+local buckling
A30	219.1	--	0.629	--	877 (70%)	0.550	0.960	0.480	14	global+local buckling
A31	168.3	Total	0.883	--	350 (30%)	0.372	1.723	0.860	26	global buckling
A32	168.3	Total	0.911	6 $\phi$ 10mm	375 (30%)	0.349	1.670	0.834	31	global buckling
A33	168.3	Ring (40 mm)	0.855	--	332 (30%)	0.421	1.743	0.870	21	global buckling
A34	168.3	Ring (40 mm)	0.885	6 $\phi$ 10mm	323 (30%)	0.391	1.689	0.843	14	global buckling
A35	168.3	--	0.826	--	254 (30%)	0.722	2.173	1.085	12	global buckling
A36	219.1	Total	0.682	--	583 (30%)	0.244	0.708	0.354	21	global buckling
A37	219.1	Total	0.698	6 $\phi$ 12mm	633 (30%)	0.229	0.677	0.338	46	global buckling
A38	219.1	Ring (50 mm)	0.653	--	532 (30%)	0.286	0.722	0.360	26	global buckling
A39	219.1	Ring (50 mm)	0.672	6 $\phi$ 12mm	584 (30%)	0.266	0.690	0.344	28	global buckling
A40	219.1	--	0.629	--	376 (30%)	0.550	0.960	0.480	13	global+local buckling

### 3.3 Results

#### 3.3.1 Evolution of temperatures

The mean temperature in the furnace was similar in all the tests. Figure 3.21 shows a comparison between the evolution of the mean temperature in the furnace for all the fire resistance tests and the ISO834 (1999) fire curve. A difference between them was observed in the first 8 min of heating due to the furnace thermal inertia that the electric system did not have enough power to eliminate.

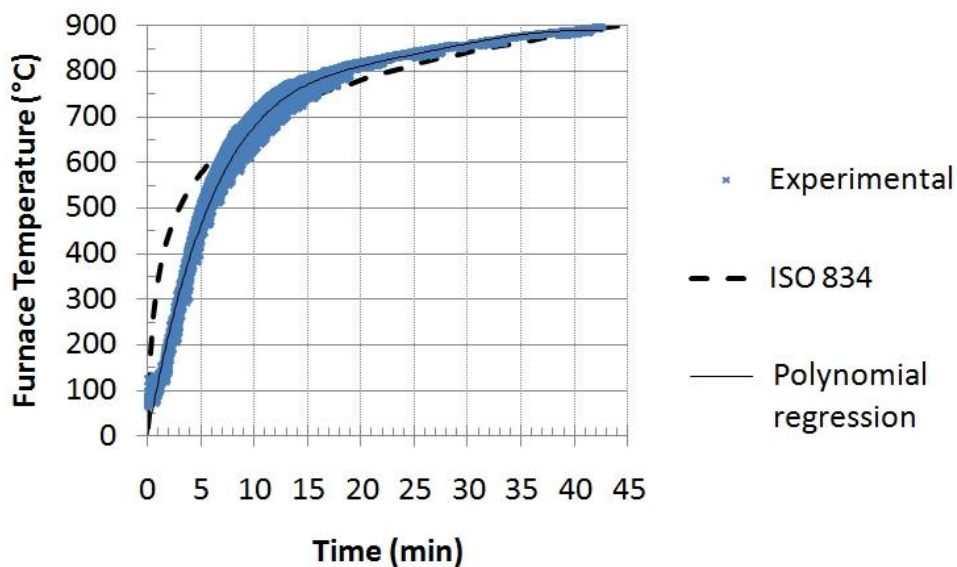


Figure 3.21 – Evolution of furnace temperature as a function of time for all the tests

Figure 3.22 shows the evolution of temperature at cross-section S3 corresponding to the mid-height of the column. As can be observed in all the tests, the temperature in the steel tube increased much faster than in the concrete and tends to follow the furnace temperatures (Figure 3.22). The concrete core remains colder than the steel tube and the rise in its temperature varies linearly with time. Hence, there was a huge thermal gradient at the steel concrete interface (Figure 3.22).

Figure 3.23 shows the evolution of temperature in a cross-section of a column with an internal ring of concrete. The evolution of temperature in this case was similar to Figure 3.22. The evolution of temperatures in all 5 cross-sections (S1 up to S5) of all tested columns is presented in Appendix B.



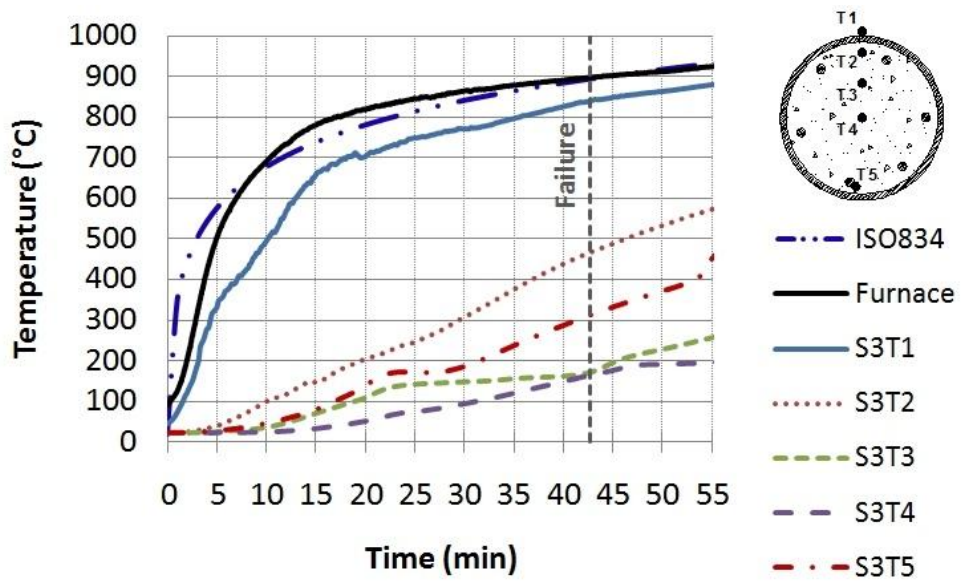


Figure 3.22 – Distribution of temperature in cross-section S3 for test column A17<sub>219-TOT-RC-30%-Klow</sub>.

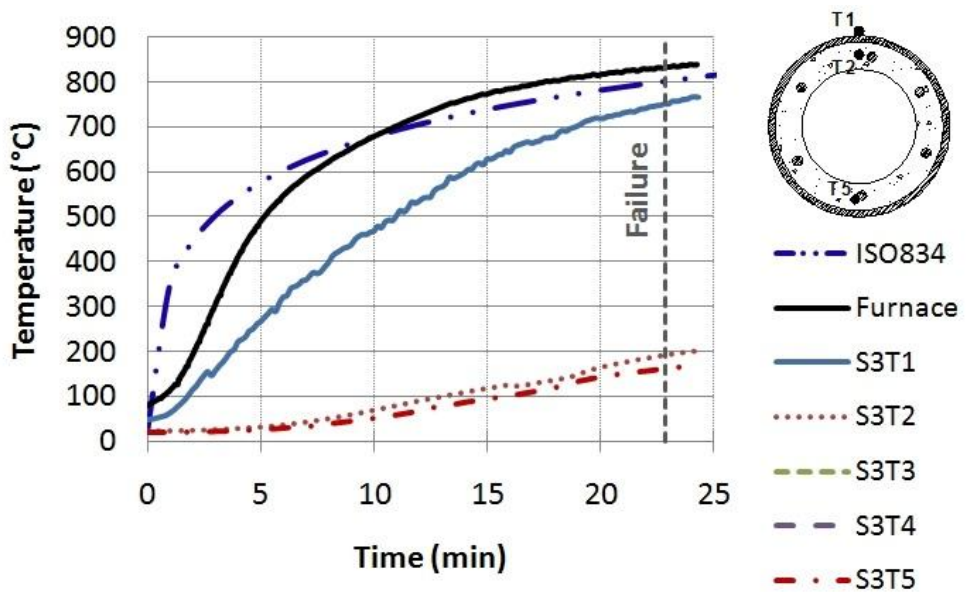


Figure 3.23 – Distribution of temperature in cross-section S3 for test column A19<sub>219-RING-RC-30%-Klow</sub>.

A slightly reduction in the increase of temperatures in the steel tube was observed in the CFCH columns as pointed out by other authors such as Romero *et al.* 2011.

The Figure 3.24 presents the mean evolution of temperatures in the steel tube at cross-section S3 for the columns with external diameter of 168.3mm. As the load level and the stiffness of the surrounding structure do not influence the evolution of temperature, there are 4 similar tests for each type of CFCH column: total filled with PC, total filled with RC, ring filled with PC and ring filled with RC beyond the CHS column (*i.e.* steel column).

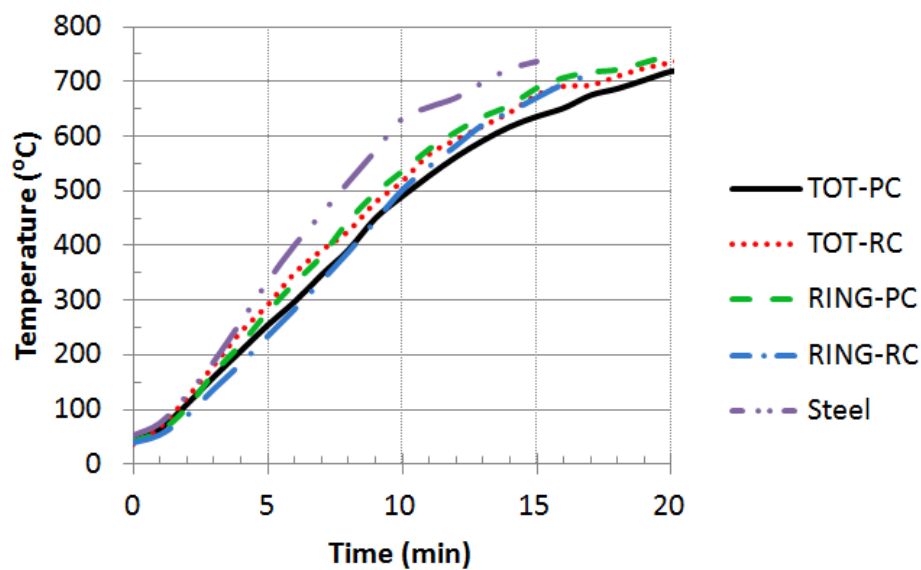


Figure 3.24 – Effect of filling in steel tube temperature of CFCH columns with  $d = 168.3\text{mm}$  at cross-section S3.

Figure 3.25 presents the same results for the columns with 219.1mm. The major reduction in steel tube temperature was observed in the CFCH-PC columns total filled. This demonstrates the influence of the filling reducing the temperatures in the steel tube due to the smaller thermal conductivity of the concrete than steel.

Figure 3.26 shows the distribution of temperature in the different thermocouples by specimen height at the instant of failure. The temperatures were quite uniform in the central part of the column and reduced in the direction of the column end supports, which were outside the furnace.

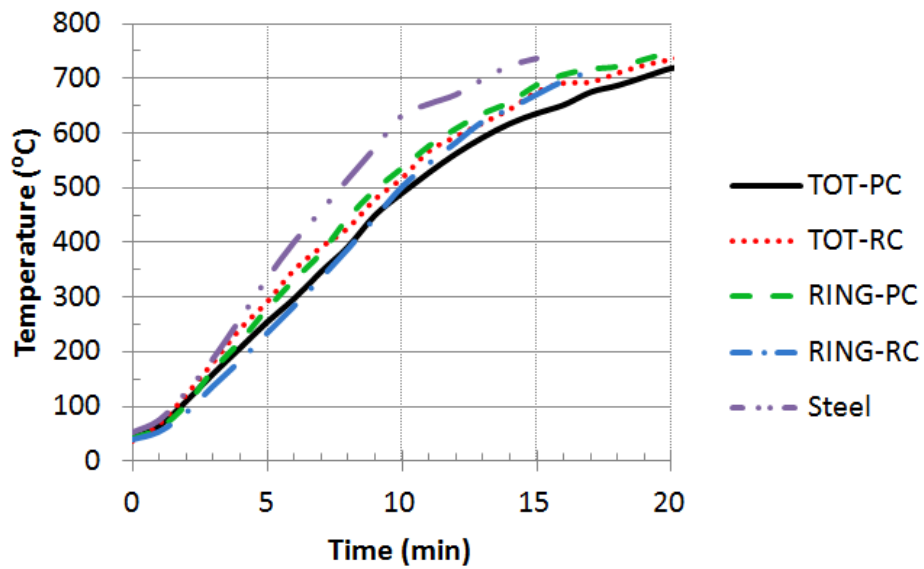


Figure 3.25 – Effect of filling in steel tube temperature of CFCH columns with  $d = 219.1\text{mm}$  at cross-section S3.

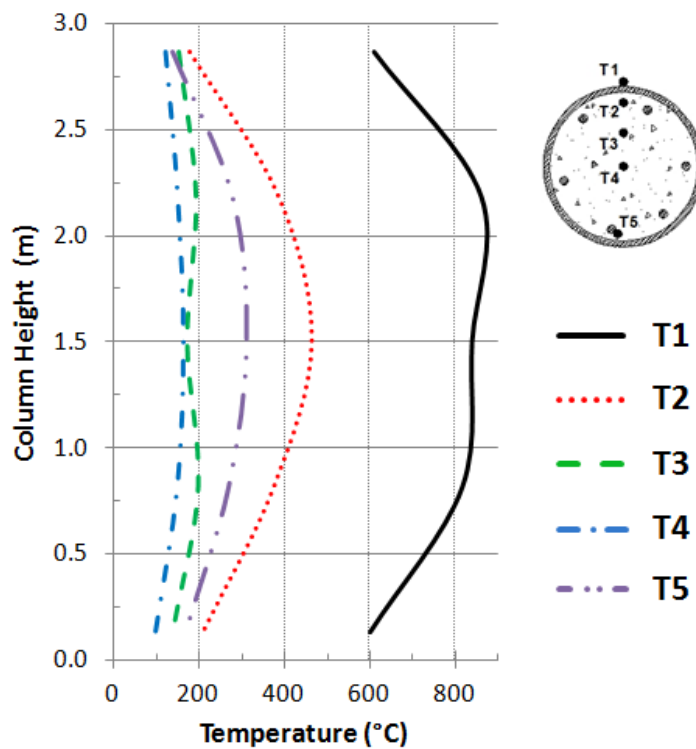


Figure 3.26 – Distribution of temperature over height at the moment of failure for column A17<sub>219-TOT-RC-30%-Klow</sub>.

A high thermal gradient was observed along the cross-section of the CFCH columns due the filling with concrete. The Figure 3.27 presents the temperature distribution along the cross-section at the moment of failure for column A17<sub>219-TOT-RC-30%-Klow</sub>.

The ends of the columns were outside of the furnace and remained colder than the rest of the column (*i.e.* central part of the column) during the heating. This is the reason of the lower temperatures in sections S1 and S5 in Figure 3.27.

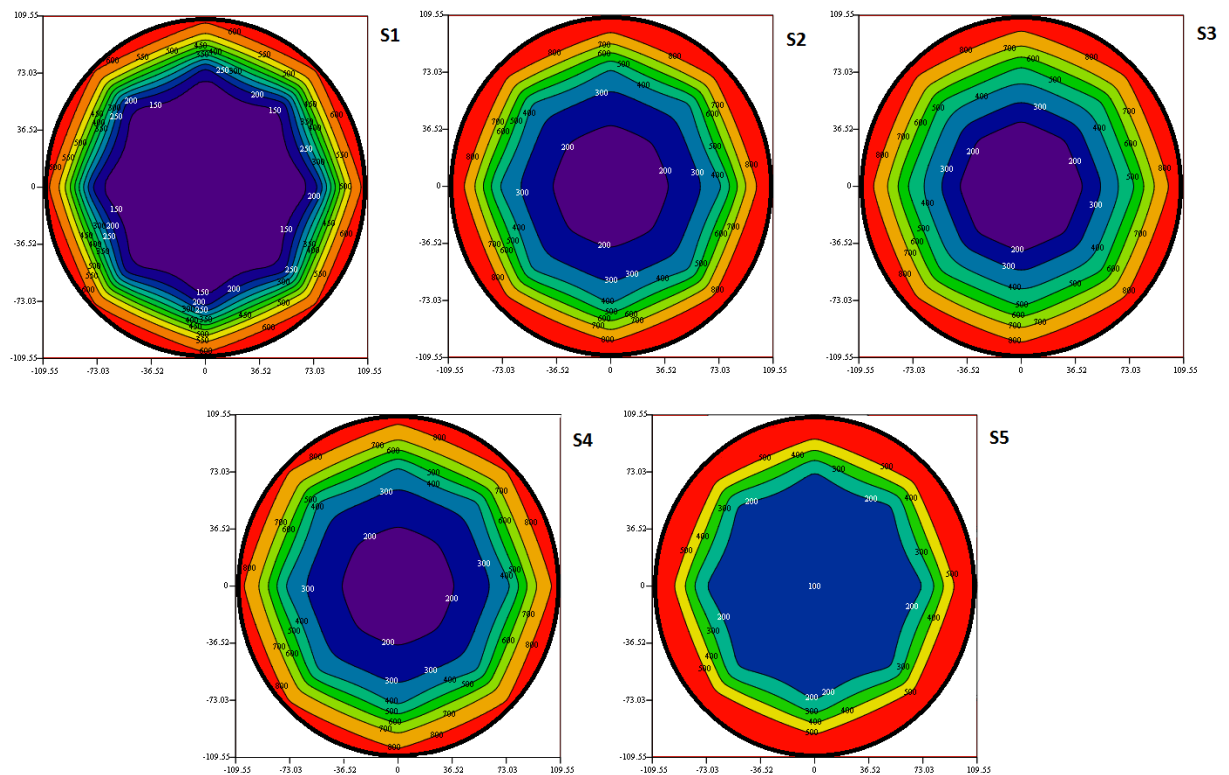


Figure 3.27 – Distribution of temperature along the cross-section at the moment of failure for column A17<sub>219-TOT-RC-30%-Klow</sub>.

### 3.3.2 Restraining forces

The restraining forces as a function of time are represented from Figure 3.28 to Figure 3.35. They are represented in a non-dimensional way, dividing the absolute load by the initial applied load ( $P/P_0$ ). The initial applied load is a percentage of the design value of the buckling load at room temperature ( $N_{ed}$ ) calculated according to the methods of EN1994-1-1 (2005).

These relative restraining forces increase up to a maximum value then decrease due to the degradation of the mechanical properties of the materials (steel and concrete) until they again reach the initial applied load.

As can be observed, the stiffness of the restraining frame did not influence the critical time of the columns. Nevertheless higher restraining forces were observed in columns of the same type of cross-section and load level in which the stiffness of the restraining frame was higher.

In addition the results showed that an increase in load level reduces the critical time of the columns and the relative restraining forces (*e.g.* see Figure 3.28 and Figure 3.32 or Figure 3.29 and Figure 3.33). The CFCH columns with 70%  $N_{ed}$  presented the smallest relative restraining forces and critical times (*e.g.* Figure 3.28 to Figure 3.31).

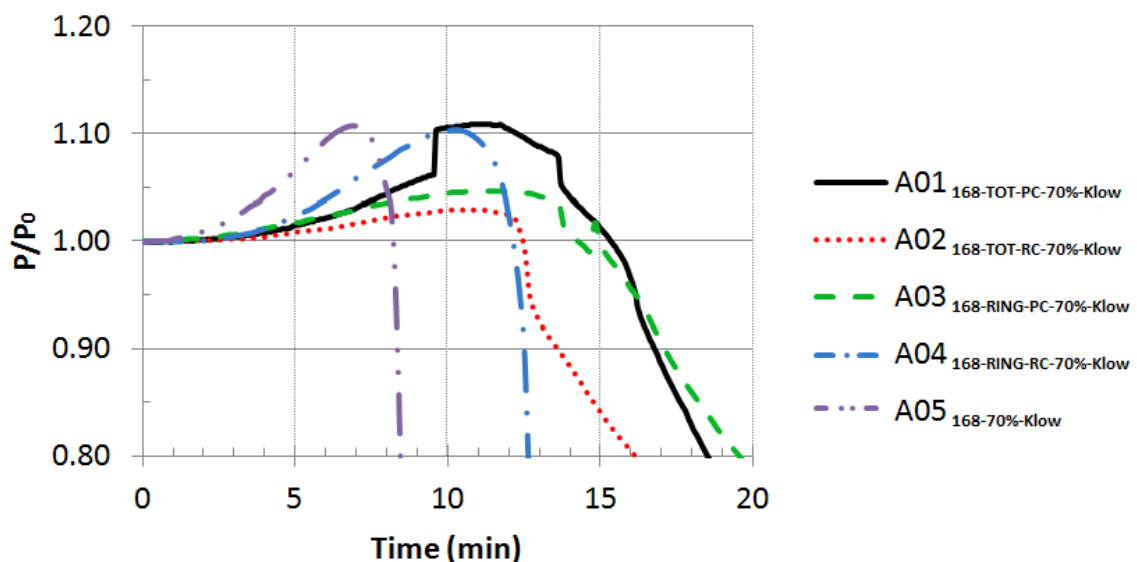


Figure 3.28 – Restraining forces for a load level of 70%, column diameter of 168.3 mm and axial stiffness of the surrounding structure of 13 kN/mm.

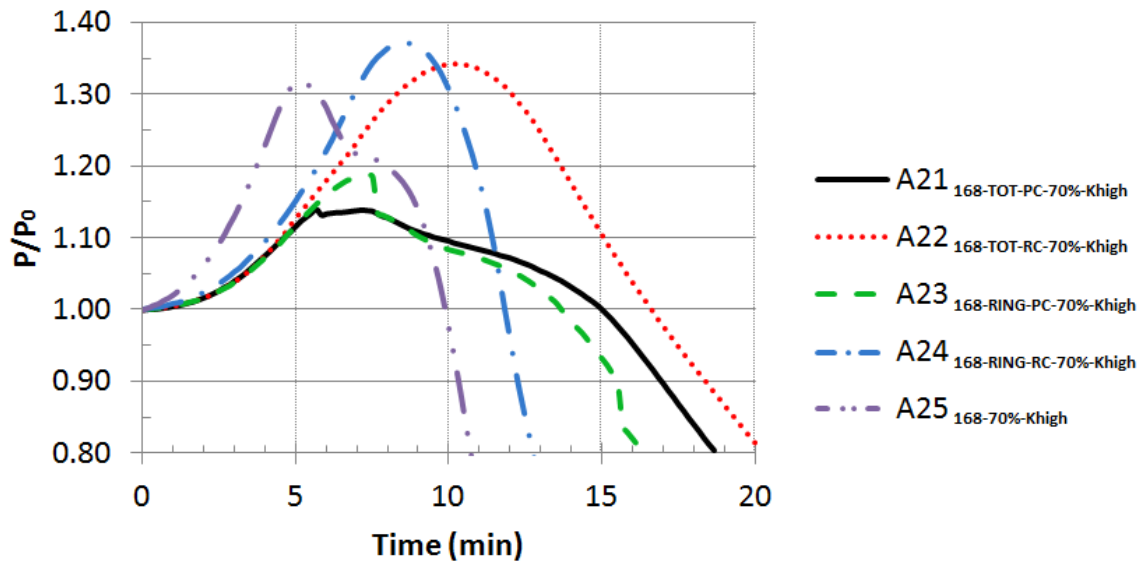


Figure 3.29 – Restraining forces for a load level of 70%, column diameter of 168.3 mm and axial stiffness of the surrounding structure of 128 kN/mm.

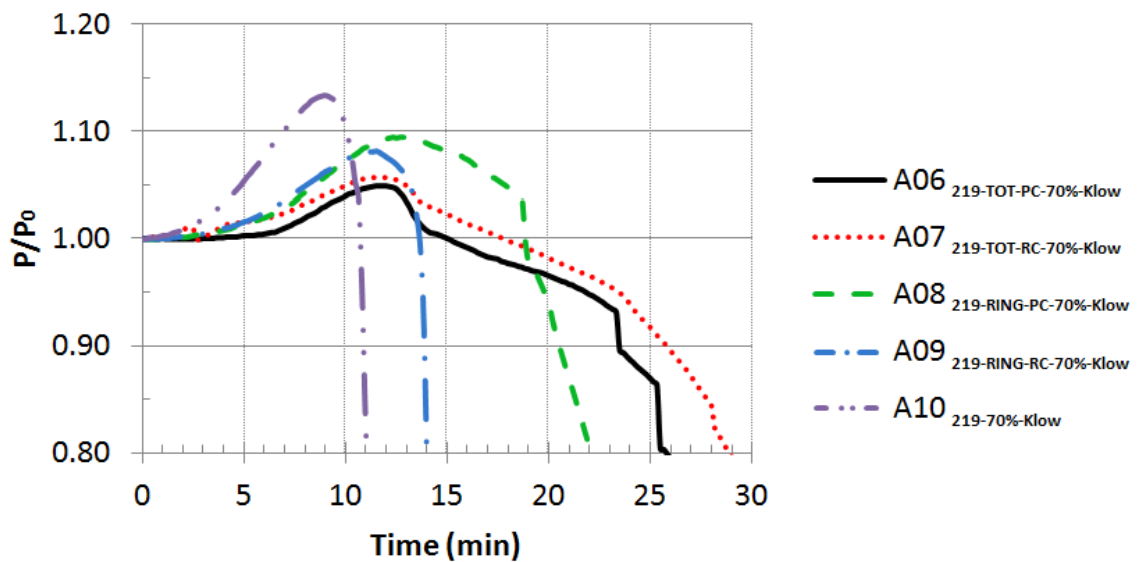


Figure 3.30 – Restraining forces for a load level of 70%, column diameter of 219.1 mm and axial stiffness of the surrounding structure of 13 kN/mm.

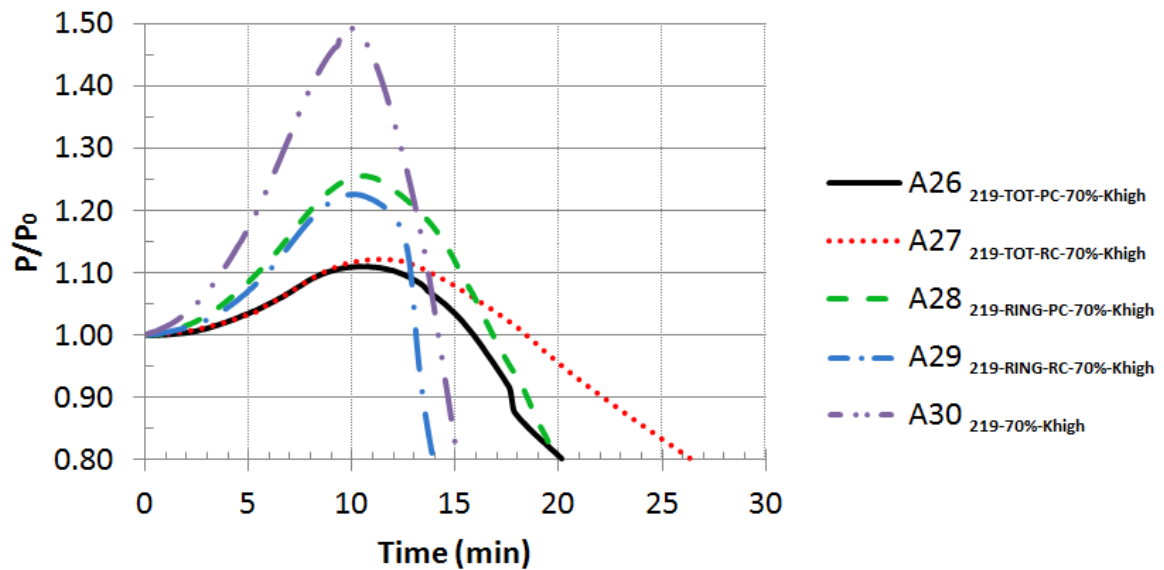


Figure 3.31 – Restraining forces for a load level of 70%, column diameter of 219.1 mm and axial stiffness of the surrounding structure of 128 kN/mm.

When the slenderness of the columns was changed by increasing the diameter of the cross-section, an increase in the critical times of the columns was observed but the effect on the relative restraining forces was not so clear. Sometimes this increased them (*e.g.* A34<sub>168-RING-RC-30%-Khigh</sub> and A39<sub>219-RING-RC-30%-Khigh</sub> in Figure 3.33 and Figure 3.35 respectively) and sometimes it reduced them (*e.g.* A14<sub>168-RING-RC-30%-Klow</sub> and A19<sub>219-RING-RC-30%-Klow</sub> in Figure 3.32 and Figure 3.34 respectively). Therefore, major conclusions cannot be drawn about the influence of the slenderness of a column on the restraining forces.

The concrete filling increases the critical times of the columns and reduces the relative restraining forces (*e.g.* Figure 3.34). In general, the CHS columns (*i.e.* steel columns) presented the smallest critical times and the largest relative restraining forces that after reaching the maximum value drop quite suddenly. In the CFCH columns, probably due to the concrete core inside the steel tube, the relative restraining forces diminished more gradually (*e.g.* Figure 3.35).

Sometimes the contribution of concrete core was not so evident in the restraining forces graphs (*e.g.* A36<sub>219-TOT-PC-30%-Khigh</sub> and A37<sub>219-TOT-RC-30%-Khigh</sub> in Figure 3.35). The reason may be that CFCH-PC columns may not transfer the load to concrete core and the failure occurs by buckling of the steel tube as pointed out by Romero *et al.* (2011).

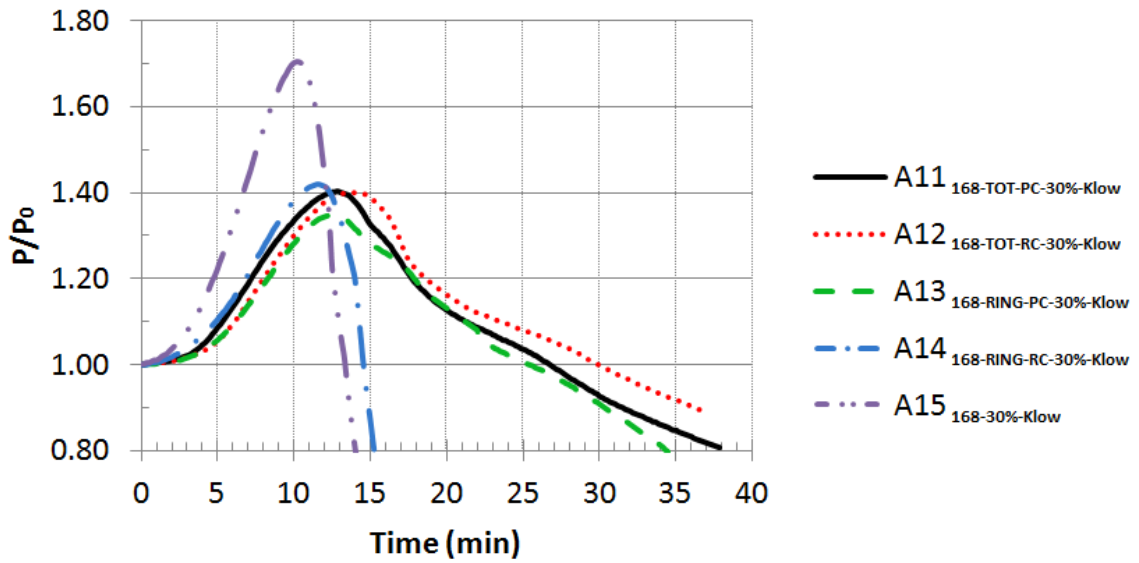


Figure 3.32 – Restraining forces for a load level of 30%, column diameter of 168.3 mm and axial stiffness of the surrounding structure of 13 kN/mm.

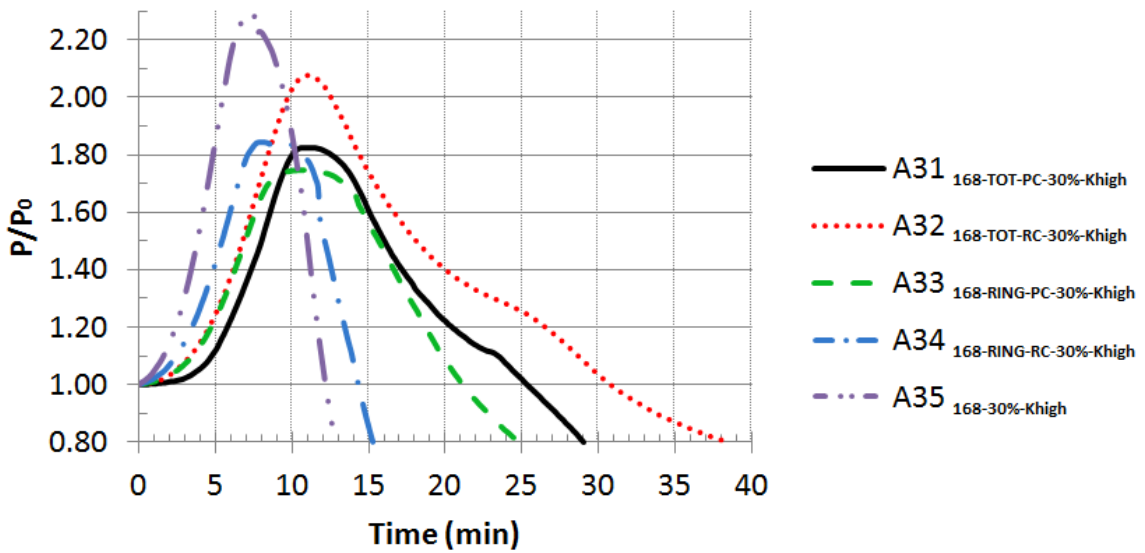


Figure 3.33 – Restraining forces for a load level of 30%, column diameter of 168.3 mm and axial stiffness of the surrounding structure of 128 kN/mm.



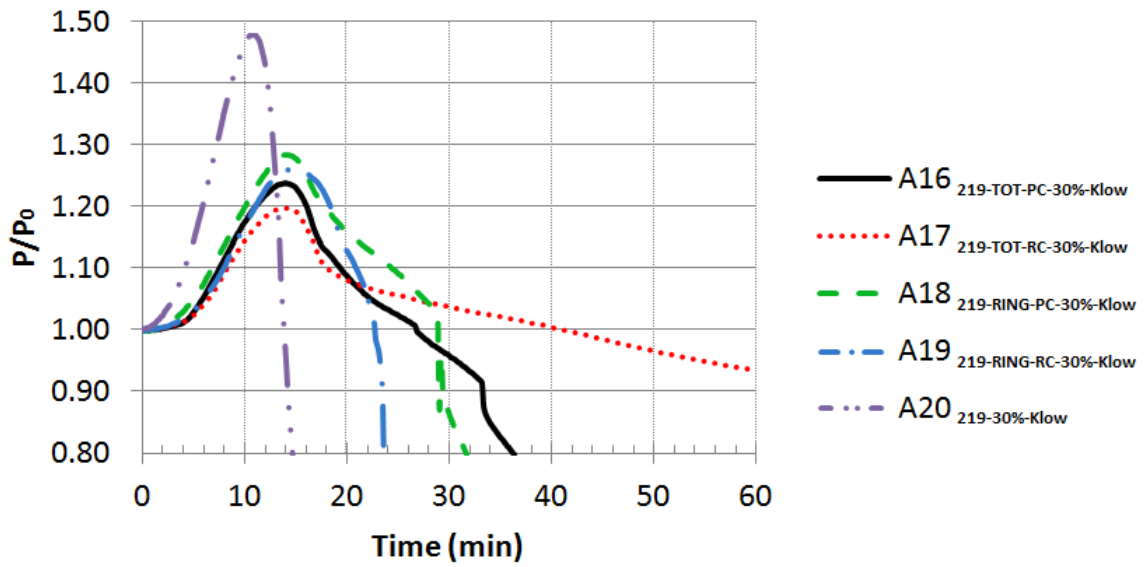


Figure 3.34 – Restraining forces for a load level of 30%, column diameter of 219.1 mm and axial stiffness of the surrounding structure of 13 kN/mm.

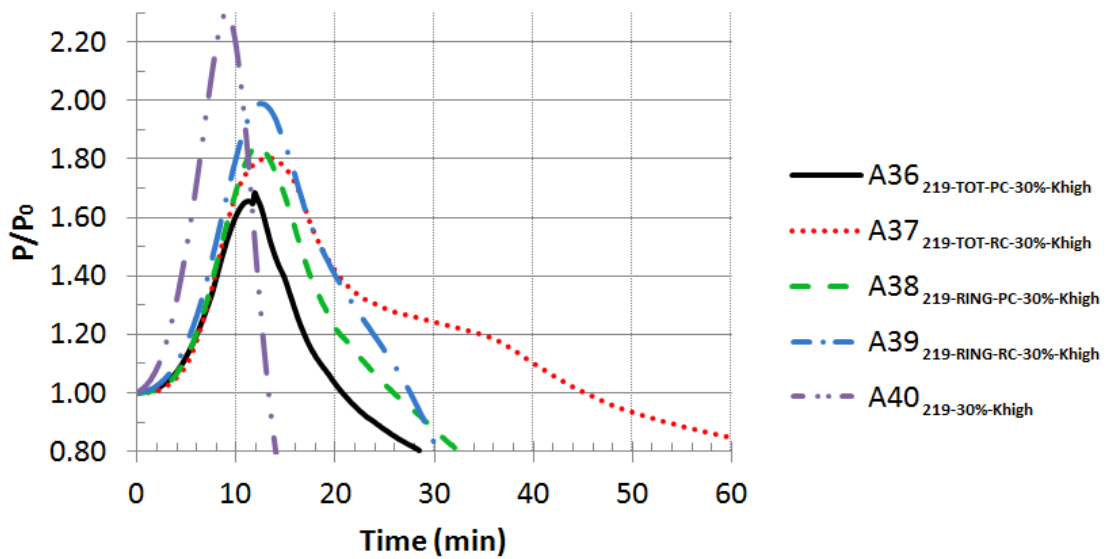


Figure 3.35 – Restraining forces for a load level of 30%, column diameter of 219.1 mm and axial stiffness of the surrounding structure of 128 kN/mm.

### 3.3.3 Axial deformations

The axial deformations of the column as a function of time are represented from Figure 3.36 to Figure 3.43. The axial deformations developed in a very similar way to the restraining forces, they increased up to a maximum value after which they declined until reaching the initial value.

The results indicate that the stiffness of the surrounding structure influences the development of axial deformation. In general an increase in this parameter reduces the axial deformation (e.g. Figure 3.36 and Figure 3.37).

Also an increase in the load level reduces the axial deformation of the columns (e.g. Figure 3.36 and Figure 3.40).

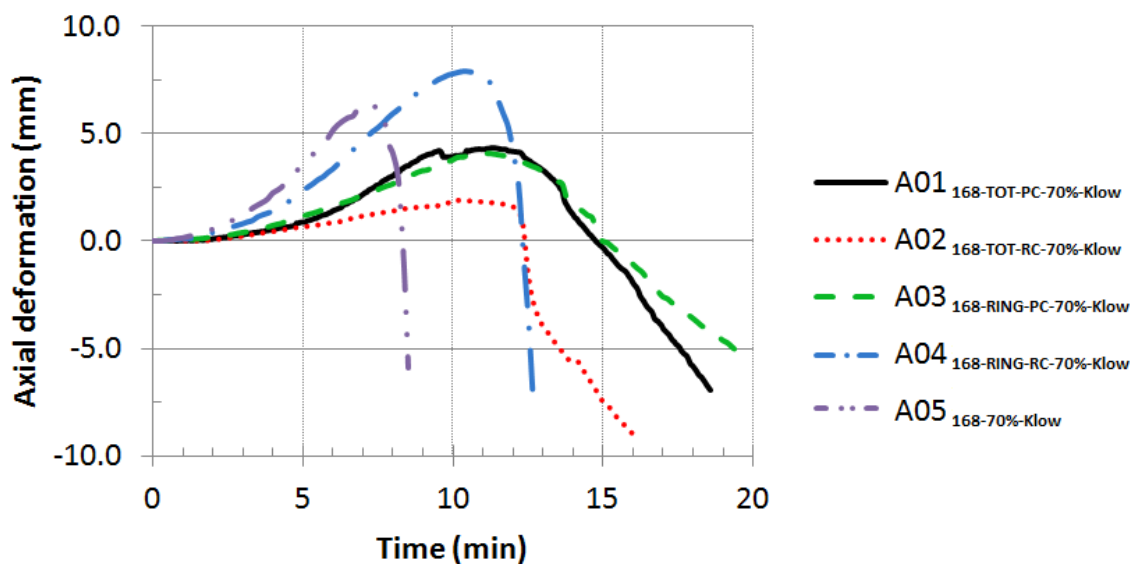


Figure 3.36 – Axial deformations for a load level of 70%, column diameter of 168.3 mm and axial stiffness of the surrounding structure of 13 kN/mm.

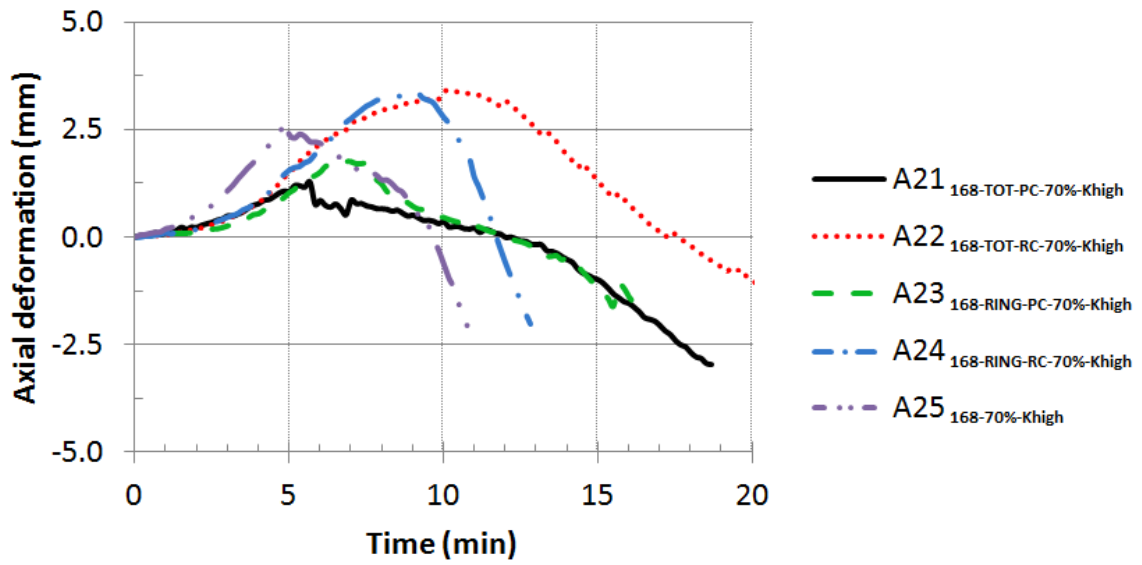


Figure 3.37 – Axial deformations for a load level of 70%, column diameter of 168.3 mm and axial stiffness of the surrounding structure of 128 kN/mm.

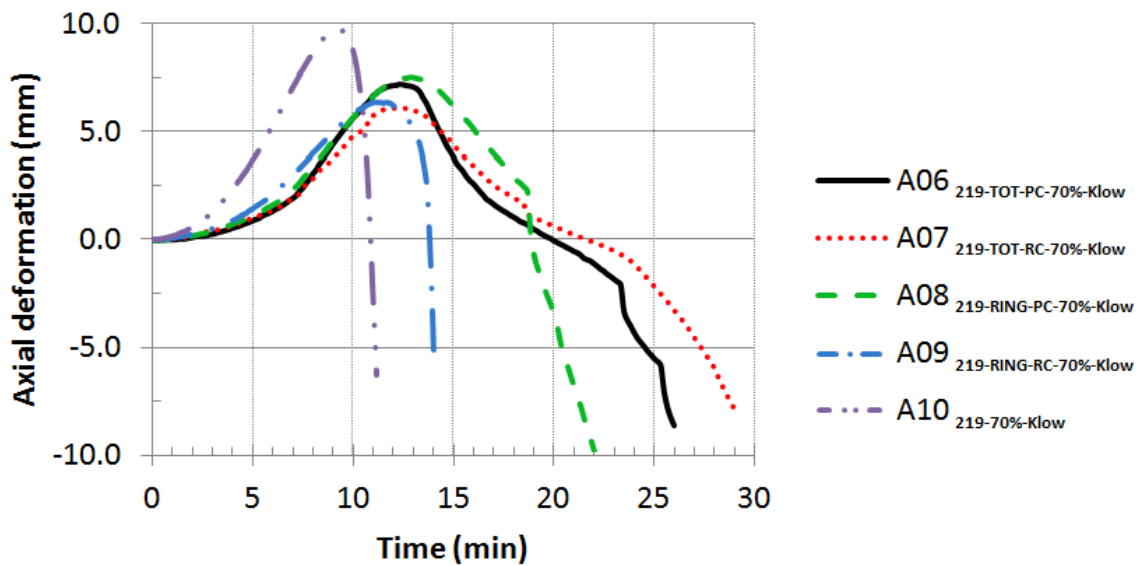


Figure 3.38 – Axial deformations for a load level of 70%, column diameter of 219.1 mm and axial stiffness of the surrounding structure of 13 kN/mm.

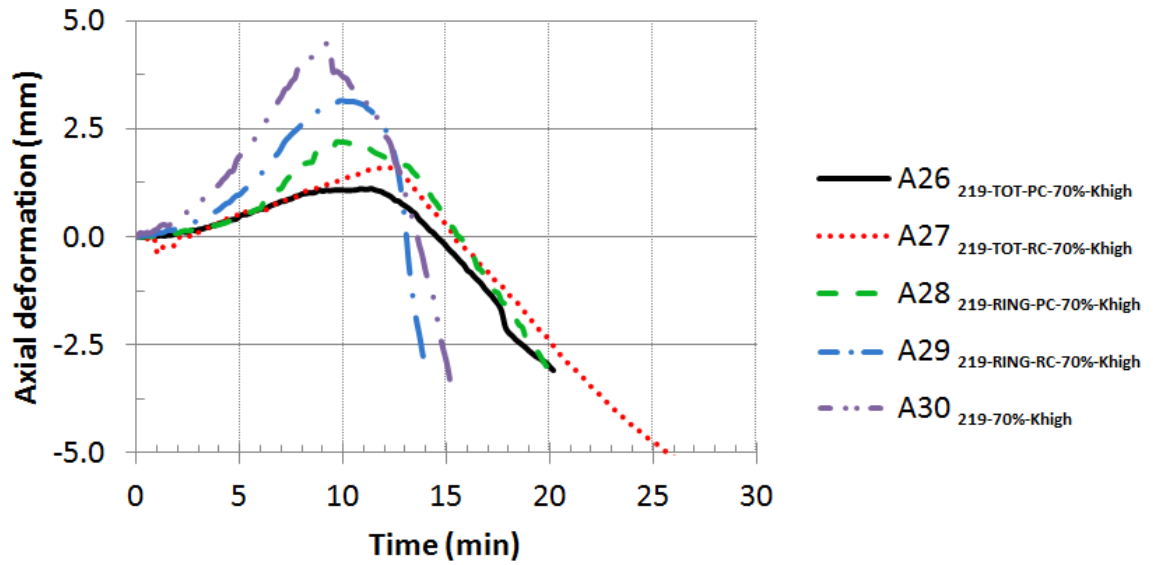


Figure 3.39 – Axial deformations for a load level of 70%, column diameter of 219.1 mm and axial stiffness of the surrounding structure of 128 kN/mm.

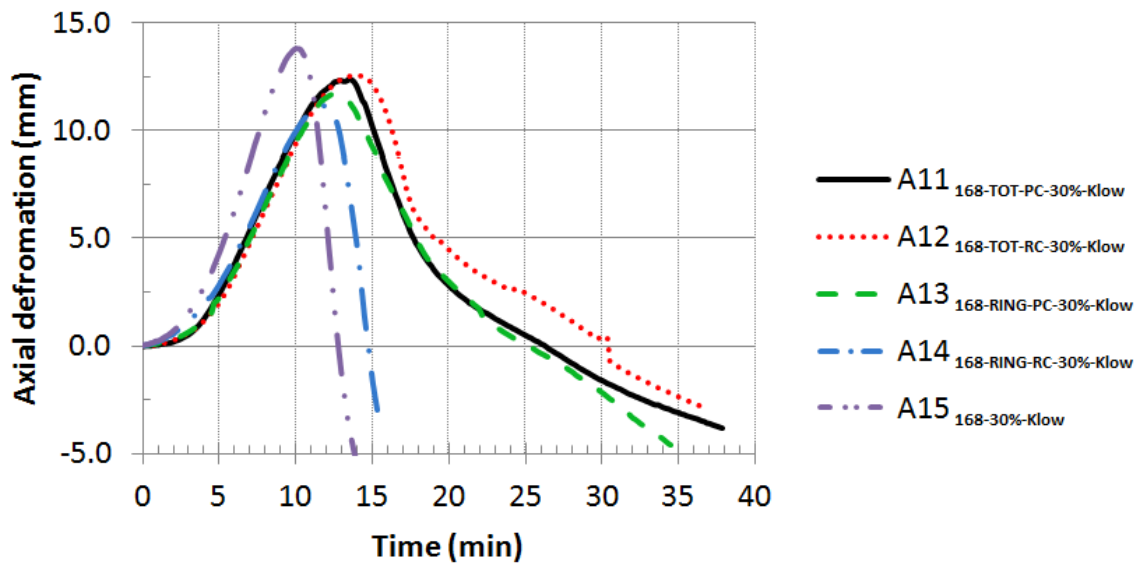


Figure 3.40 – Axial deformations for a load level of 30%, column diameter of 168.3 mm and axial stiffness of the surrounding structure of 13 kN/mm.

In general the column axial deformation was very small when the axial stiffness of the surrounding structure was 128 kN/mm (*e.g.* Figure 3.41).

In general, as the results obtained show, the axial deformation was higher in CHS columns – steel columns (which also presented greater restraining forces) than in CFCH ones. This result is coherent given that the concrete filling reduces restraining forces and consequently it reduces the axial deformation (*e.g.* Figure 3.42).

As in the restraining forces, no visible influence of the slenderness of the columns on the axial deformation was registered. Sometimes an increase in the diameter reduces the axial deformation and sometimes the reverse was observed (*e.g.* Figure 3.41 and Figure 3.43).

There were not any well defined bending plan in the test columns, it hampered the measurements of lateral deflections and may introduce a bias in results. Thereby these results were not presented in the main text of this thesis. Anyway the lateral deflections of the CFCH columns are presented in Appendix C.

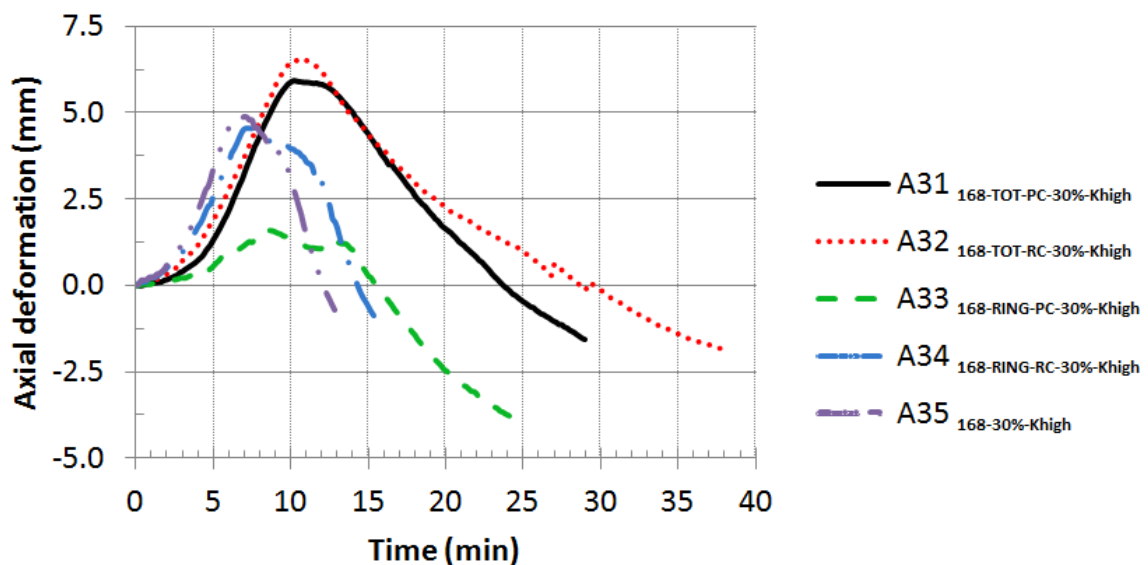


Figure 3.41 – Axial deformations for a load level of 30%, column diameter of 168.3 mm and axial stiffness of the surrounding structure of 128 kN/mm.

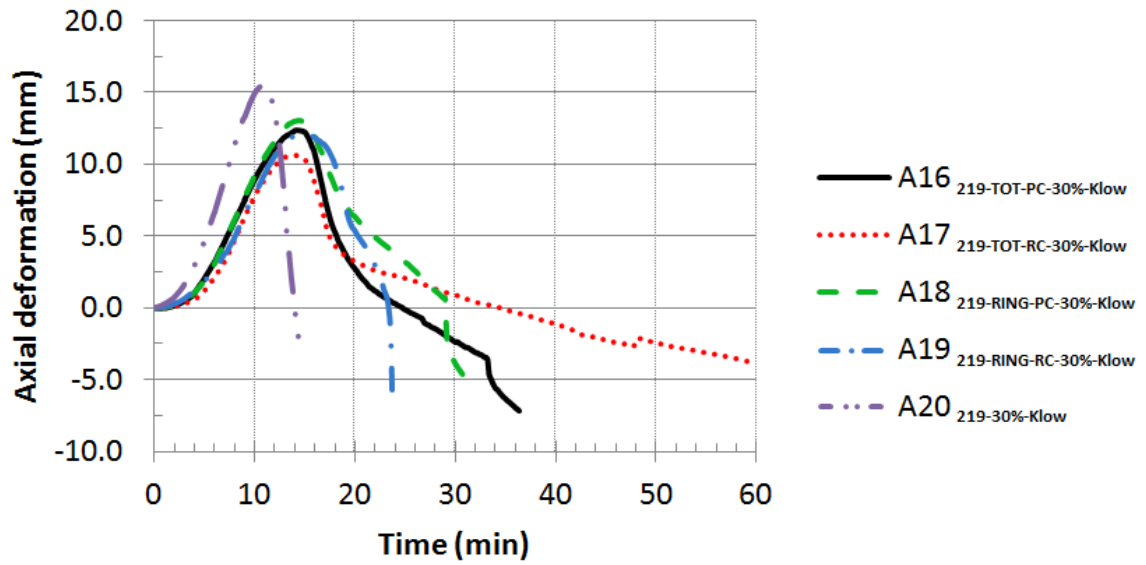


Figure 3.42 – Axial deformations for a load level of 30%, column diameter of 219.1 mm and axial stiffness of the surrounding structure of 13 kN/mm.

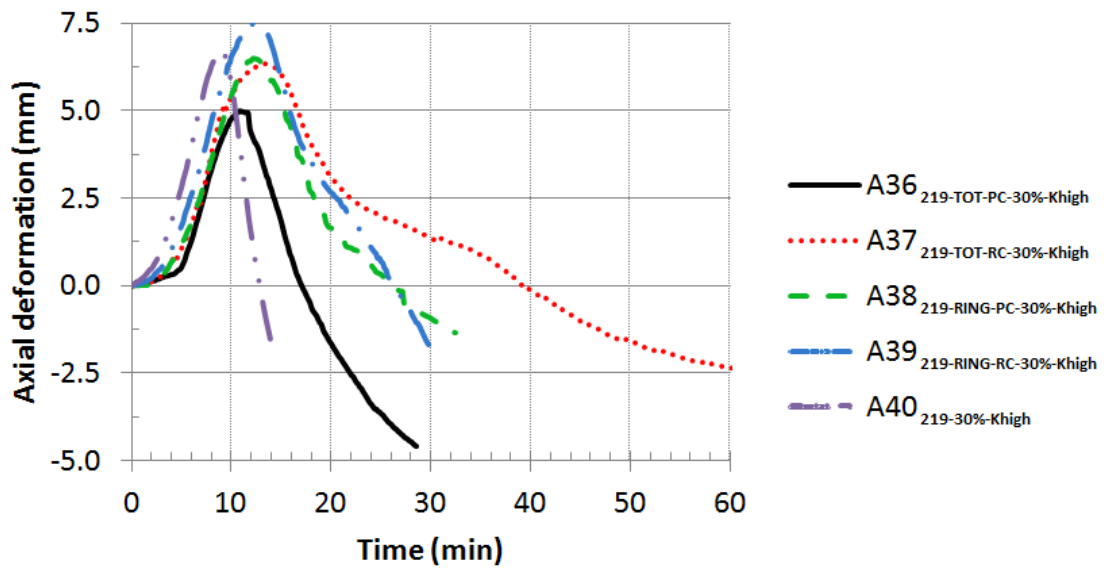


Figure 3.43 – Axial deformations for a load level of 30%, column diameter of 219.1 mm and axial stiffness of the surrounding structure of 128 kN/mm.

### 3.3.4 Critical times

As the tests conducted in this research were not standard fire resistance tests, it was deemed to be more appropriate to use the concept of critical time instead of fire resistance (EN1994-1-2, 2005). Critical time is here defined as the instant when the restraining forces return to the value of the initial applied load, after increasing due to column restraining thermal elongation and decreasing due to the degradation of the mechanical properties with the temperature. The critical times obtained in these tests are presented in Table 3.3.

In these tests, the maximum critical time was 14 min for CHS columns (*i.e.* steel columns *e.g.* A30<sub>219-70%-Khigh</sub>). For the CFCH-PC columns the maximum critical time was 27 min for those that were completely filled (*e.g.* A16<sub>219-TOT-PC-30%-Klow</sub>) and 29 min for those filled with a ring (*e.g.* A18<sub>219-RING-PC-30%-Klow</sub>). In the CFCH-RC columns the maximum critical time was 46 min for those completely filled (*e.g.* A37<sub>219-TOT-RC-30%-Khigh</sub>) and 28 min for those filled with a ring (*e.g.* A39<sub>219-RING-RC-30%-Khigh</sub>).

These critical times are in general smaller than those registered by the National Research Council of Canada (NRCC) researchers except for the CHS columns (*i.e.* steel columns). However, it should be highlighted that these tests were carried out without restraining to thermal elongation of the column and the failure criterion adopted was different to the one of this study.

The critical times obtained in this study as a function of the parameters tested are presented from Figure 3.44 to Figure 3.48. A 5% error margin was considered.

This study also set out to study the influence of the stiffness of the surrounding structure on the critical times of the columns. Therefore, tests employing two different surrounding structure stiffness were conducted:  $K_{low}$  ( $K_{as}= 13\text{kN/mm}$ ,  $K_{rs,X1}= 4091$  and  $K_{rs,X2}= 1992\text{kN}\cdot\text{m/rad}$ ) and  $K_{high}$  ( $K_{as}= 128\text{kN/mm}$ ,  $K_{rs,X1}= 5079$  and  $K_{rs,X2}= 2536\text{kN}\cdot\text{m/rad}$ ). The results obtained show that changing the stiffness of the surrounding structure, between the values mentioned, did not lead to great changes in the critical times of the columns (Figure 3.44).

This phenomenon may occur because usually associated with an increase on axial restraining is an increase on rotational restraining. The increasing of both restraining is common in real structures but in fact an increasing on axial restraining does not mean an increasing on rotational restraining. As it is known an increasing on axial restraining leads to a reduction on the critical time and temperature of the columns while an increasing on the rotational restraining has the opposite effect (Correia and Rodrigues, 2011).

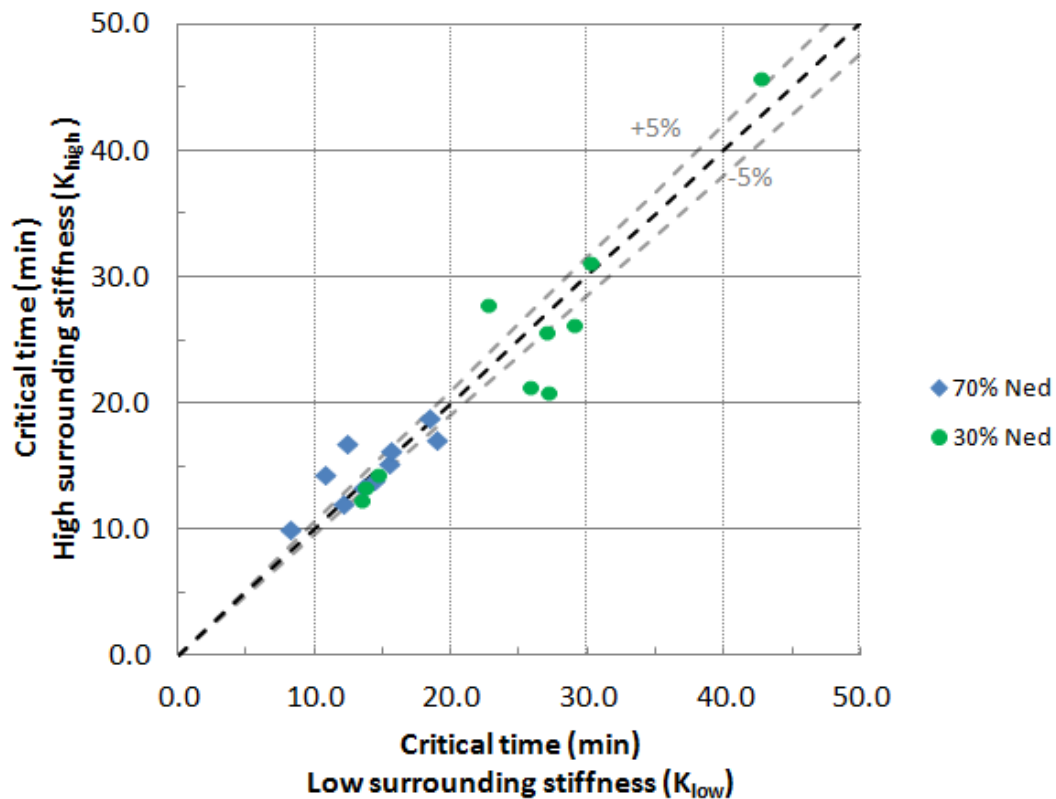


Figure 3.44 – Comparison of the critical times of columns obtained for the lower surrounding structure stiffness with the critical times of other columns for the higher stiffness.

As it is expected, the load level has a significant influence on the critical times of the CFCH columns. It was noticed, in all tests that for CFCH columns with a load level of 30%  $N_{ed}$ , the critical times were higher than those obtained for those with a load level of 70%  $N_{ed}$  (Figure 3.45). In other words, the increasing in the column load level reduces its critical time. Similar results were also obtained for CHS columns (*i.e.* steel columns).

The maximum critical time registered in this experimental study was 46 min for a load level of 30%  $N_{ed}$  (*e.g.* A37<sub>219</sub>-TOT-RC-30%-K<sub>high</sub>). For the load level of 70%  $N_{ed}$  the maximum critical time obtained was 19 min (*e.g.* A08<sub>219</sub>-RING-PC-70%-K<sub>low</sub>). This suggests that this load level is probably too high for the fire design of these columns.



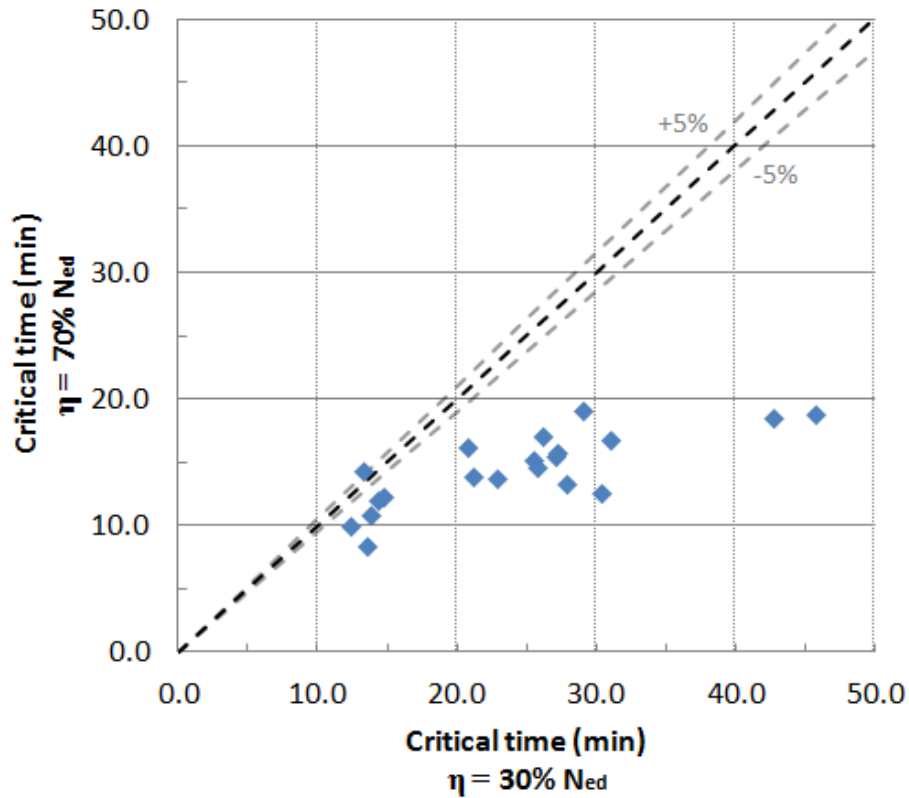


Figure 3.45 – Comparison of the critical times of columns obtained for the load level of 30% with columns bearing a load level of 70%.

Figure 3.46 shows the critical times of the tested columns comparing the influence of the external diameter (219.1 mm and 168.3 mm). It is observed that the critical times of columns with 219.1 mm were higher the ones of columns with 168.3 mm diameter.

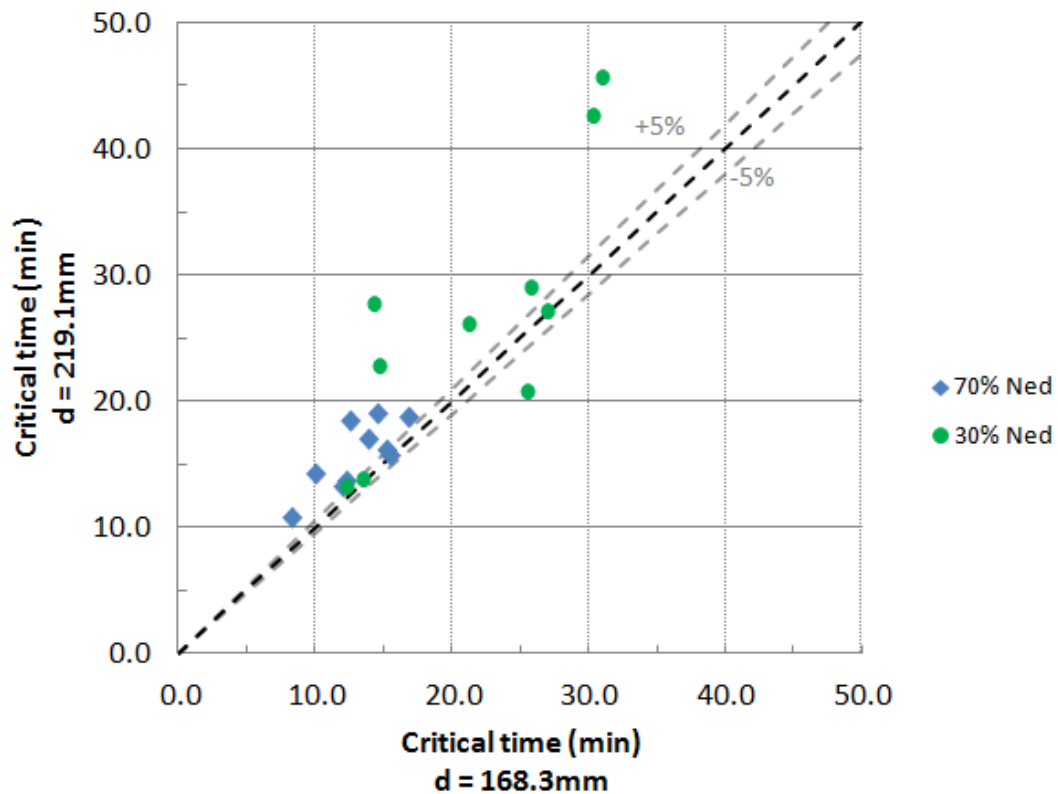


Figure 3.46 – Comparison of the critical times obtained for columns with diameter of 219.1 mm with columns that have a diameter of 168.3 mm

In general, the CFCH columns that were completely filled presented higher critical times than the ones with a concrete ring inside (Figure 3.47). Thus, partially filling of CFCH columns does not seem to be an appropriate solution for fire resistance. Despite the concrete ring increases the critical time of the columns, the unconfined internal concrete face may contribute to the occurrence of concrete spalling. In fact, sounds of spalling could be “heard” during the tests in the CFCH columns with concrete ring.

On comparing CFCH columns completely filled, it was also noticed that adding reinforcing steel bars increases their critical time, as shown in Figure 3.48. This result was especially noticed in cases where the load level was 30%  $N_{ed}$ .

The critical times of CFCH-RC columns loaded with 30%  $N_{ed}$  varied from 36 to 46 min. These results were the highest ones obtained in this series of tests with CFCH columns.

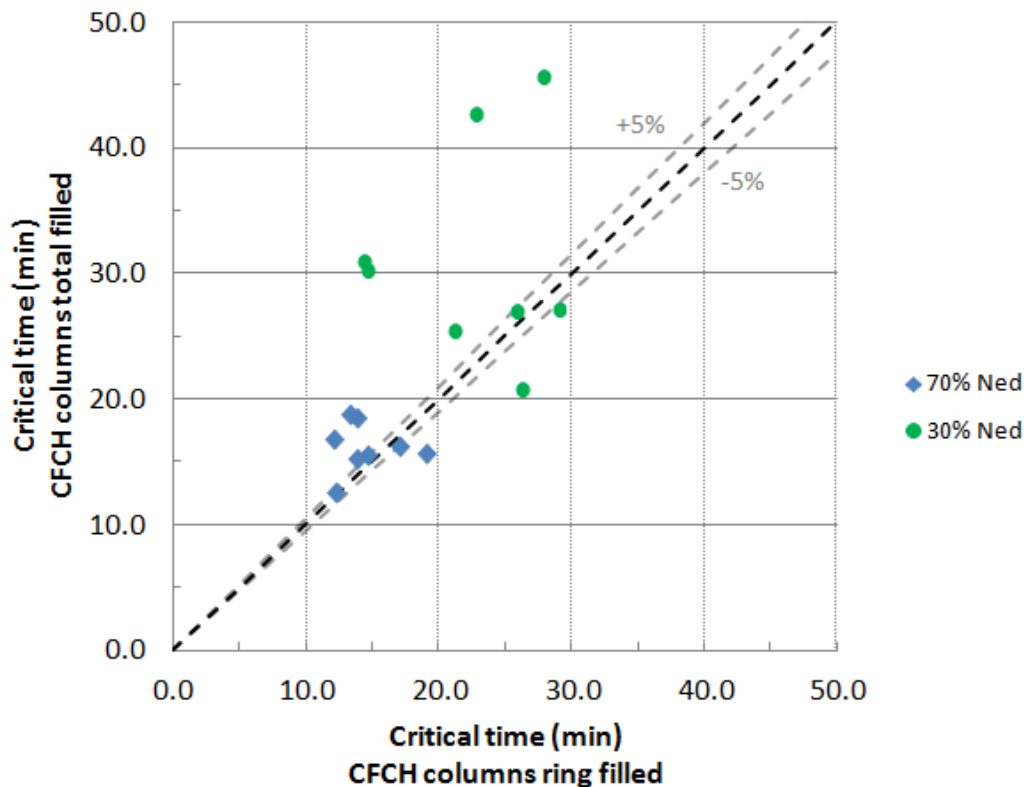


Figure 3.47 – Comparison of the critical times of CFCH columns obtained for the completely filled columns with the critical times for partially filled columns (concrete ring).

### 3.3.5 Failure mode

The failure mode in most of the columns was global buckling (Figure 3.49). Global buckling with double curvature (similar to a slight “s”) in some cases (e.g. A01<sub>168-TOT-PC-70%-Klow</sub> and A14<sub>168-RING-RC-30%-Klow</sub> in Figure 3.49) was also observed. Wang (1999) observed similar deformed shapes.

The EN1994-1-1 (2005) states that the effects of local buckling may be neglected when the  $d/e$  ratio is less than 59 for these types of CFCH columns. All the columns presented here had a smaller ratio diameter thickness  $d/e$  (i.e. 28 in 168.3 mm and 37 in 219.1 mm columns). Nevertheless several cases of local buckling were observed (Figure 3.50).

Figure 3.51 shows the percentage of columns tested that presented local buckling as a function of the stiffness of the surrounding structure, the load level, the column diameter and the degree of concrete filling.

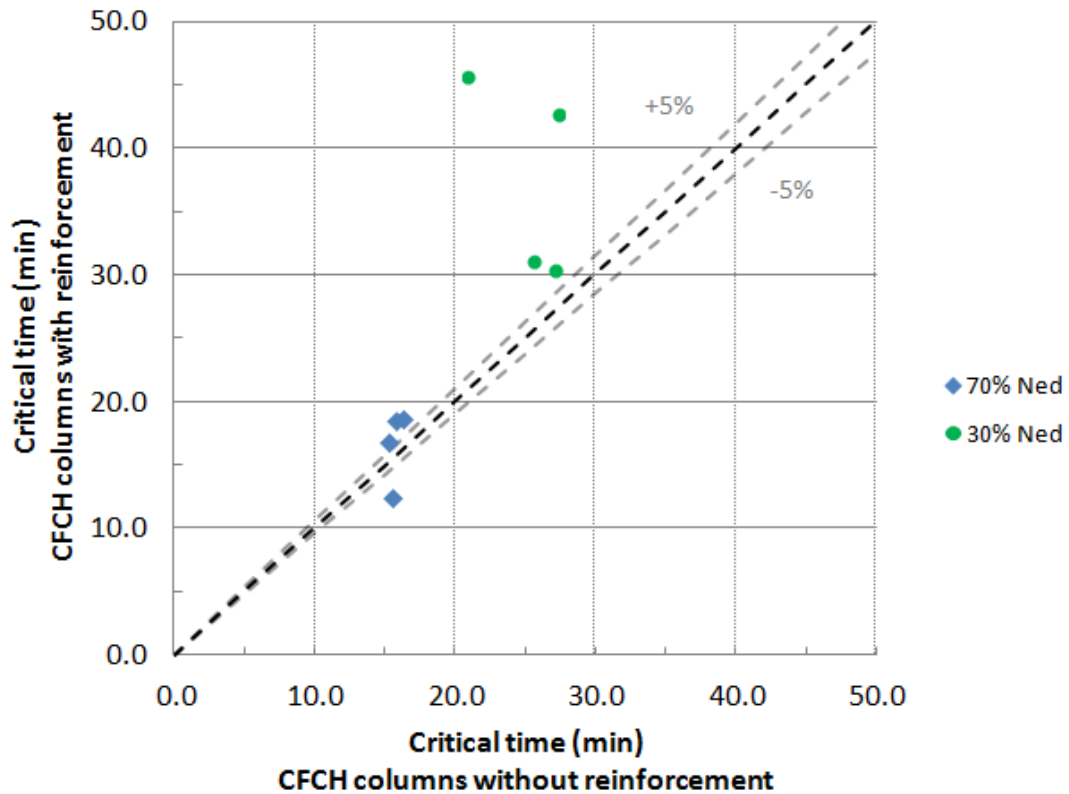


Figure 3.48 – Comparison of the critical times obtained for the CFCH columns with steel bars reinforcement with those without.

On comparing all the results obtained, it is seen that local buckling occurred more often in the following cases:

- Lower stiffness of surrounding structure ( $K_{low}$  i.e.  $K_{as} = 13\text{kN/mm}$ ,  $K_{rs,X1} = 4091$  and  $K_{rs,X2} = 1992\text{kN}\cdot\text{m/rad}$ );
- Load of 70%  $N_{ed}$ ;
- A cross-section diameter equal to 219.1 mm (these cross-sections have higher diameter-thickness –  $d/e$  ratio than those with a diameter equal to 168.3 mm);
- CHS columns (i.e. steel columns);

- CFCH columns partially filled with concrete (concrete ring), compared to those that are completely filled. The concrete filling avoids local buckling. However, a concrete ring was not effective enough to prevent local buckling.



Figure 3.49 – Deformed shape of tested columns.

The largest number of local buckling cases was observed in columns tested with low stiffness of the surrounding structure that may be justified by a higher transmission of the applied loading to the columns in the failure phase. It is important to point out that the failure modes could only be observed after the tests (*i.e.* after the opening of the furnace). This fact hampers determining the principal failure mode of the columns and when it occurs. However certainly it occurs in the later stages of the test.

The Appendix D presents figures of deformed shapes of all tested columns. Finally the Appendix E presents the results for two CFCH-FRC (steel + polypropylene fibre reinforced concrete) columns tested in addition.



Figure 3.50 – Local buckling in tested columns.

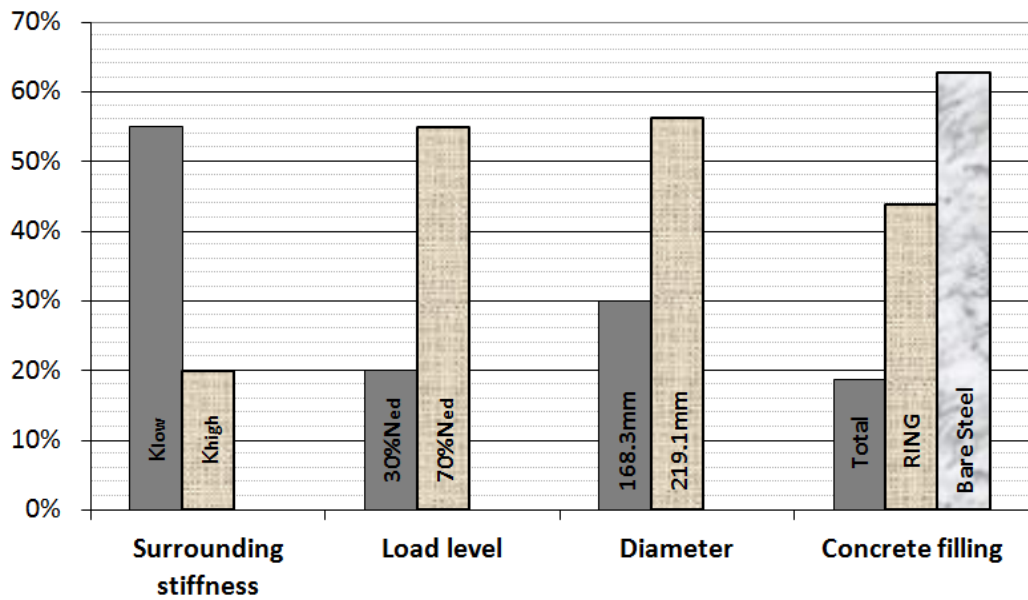


Figure 3.51 – Percentage of columns tested that presented local buckling.

### 3.4 Chapter remarks

This chapter reported the results of an experimental study carried out on the behaviour of CFCH columns with restraining thermal elongation and subjected to fire. The following conclusions may be drawn from the results of this research:

#### *Critical times*

- The critical times of the CFCH columns tested in this research were smaller than those registered by the NRCC researchers for similar experimental tests however without restraining to their thermal elongation;
- Increasing the stiffness of the surrounding structure from  $K_{low}$  ( $K_{as}= 13\text{kN/mm}$ ,  $K_{rs,X1}= 4091$  and  $K_{rs,X2}= 1992\text{kN}\cdot\text{m/rad}$ ) to  $K_{high}$  ( $K_{as}= 128\text{kN/mm}$ ,  $K_{rs,X1}= 5079$  and  $K_{rs,X2}= 2536\text{kN}\cdot\text{m/rad}$ ) did not lead to major changes in the critical times of the columns;
- The load level and slenderness of the columns had a great influence on the critical time of the columns. Reducing these parameters contributes to enhancing the performance of the columns in fire;
- Concrete filling improves the behaviour of CFCH columns when there is a fire. However the use of a concrete ring does not seem to be a good solution. The critical times of the CFCH columns filled with a concrete ring were lower than those of the ones completely filled;
- The use of RC increase the critical time of a column, especially in columns with a load level of 30%;
- CFCH-RC columns completely filled and with a load level of 30% presented the highest critical times (between 30 min and 46 min);

#### *Restraining forces*

- Increasing the axial stiffness of the surrounding structure leads to an increase in the restraining forces of the columns although this did not influence the critical time;
- Relative restraining forces were higher for the small load level (30%);

- Relative restraining forces were also higher in CHS columns (*i.e.* steel columns) than in CFCH columns;
- A higher degree of concrete filling reduces the relative restraining forces of the columns.

#### ***Axial deformation***

- Increasing the stiffness of the surrounding structure or the load level reduces the axial deformation of the columns;
- A higher degree of concrete filling also reduces the axial deformation of the columns. CHS columns (*i.e.* steel columns) presented a greater axial deformation than CFCH columns.

#### ***Failure mode***

- The main failure mode of the columns was global buckling, however in several cases local buckling also occurred, although the columns presented a diameter-thickness ratio ( $d/e$ ) smaller than 59;
- In general, the probability of local buckling occurs increases with the reduction of the stiffness of the surrounding structure, the increasing of the load level or the increasing of the cross-section diameter;
- Concrete filling avoids local buckling, but concrete ring was not enough effective to prevent the occurrence of this phenomenon.



## **4. NUMERICAL ANALYSIS OF CONCRETE FILLED CIRCULAR HOLLOW COLUMNS SUBJECTED TO FIRE**

### **4.1 Introduction**

This Chapter presents a three-dimensional nonlinear finite element model developed in ABAQUS (2011) to predict the behaviour of Concrete Filled Circular Hollow (CFCH) columns in a fire situation, after verifying their most relevant parameters, and considering the restraints of columns to their thermal elongation. This adds a rather difficult step to the problem analysis.

Validation of the proposed model is investigated by comparing numerical results and experimental data obtained in fire tests, presented in Chapter 3, conducted with thermal elongation restrained CFCH columns.

The model considers these parameters have an influence on the fire resistance of the columns used in the fire tests. These parameters include slenderness, cross-sectional diameter, loading level, stiffness of surrounding structure, steel reinforcement ratio and degree of concrete filling inside the steel tube (which may be completely filled or with a ring around the internal surface of the steel tube wall).

Continuing the research on this area, this model makes use of the main suggestions proposed by the authors presented in Chapter 2 of this thesis, such as the friction and thermal model for the steel tube-concrete core interface.

The model shows a good agreement between the numerical and experimental results and is able to assess the fire performance of CFCH columns.

### **4.2 Numerical model**

#### **4.2.1 Geometry**

Basically the numerical model is divided into three parts: the steel tube including the steel plates (top and bottom of columns); the concrete core; and the steel bar reinforcement. Obviously some of these parts may be suppressed according to the type of column simulated. For example, bare steel columns do not have bar reinforcement nor does the concrete core.

As commonly adopted in numerical analysis of columns, an initial geometric imperfection is imposed on the columns (due to the manufacturing process, for instance). A large range of different values for maximum imperfection along the length of columns can be found in the literature reviewed (L/7500 is suggested by Hong and Varma, 2009 while L/1000 up to L/2000 is proposed by Espinos *et al.*, 2010). In this thesis, the value of L/1000 is adopted, as this seems to be the value recommended by most authors.

#### 4.2.2 Thermal and mechanical properties

##### *Steel*

The steel model follows the temperature dependent formulation for thermal and mechanical properties presented in EN1993-1-2 (2005), as suggested by EN1994-1-2 (2005), and the isotropic classical metal plasticity model was adopted.

A small reduction of 10% in the thermal expansion coefficient of steel led to a reduction of maximum axial deformations ( $u_{max}$ ), as also observed by Lie (1994), and a better agreement with the measured values of this parameter. However, problems with convergence and major divergences in critical times were noted for results with this reduced coefficient. Therefore, the thermal elongation of steel recommended by EN1993-1-2 (2005) was adopted in the model and this still led to acceptable results.

##### *Concrete*

A wide variety of concrete models has been presented in the international literature presented in Chapter 2, especially for mechanical properties at elevated temperatures. The numerical model presented in this research follows the mechanical and thermal properties presented in EN1992-1-2 (2004) while minor changes will be pointed out in what follows. The concrete damaged plasticity model was adopted. A thermal dependent formulation was used to simulate the effects of heating due to fire, except for the thermal expansion coefficient and the density of concrete.

The EN1992-1-2 (2004) mechanical model for concrete presented very similar results when compared to the model proposed by Lie (1994). Thus, the EN1992-1-2 (2004) mechanical model was adopted in this work. Hong and Varma (2009) and Espinos *et al.* (2010) followed Lie's model.

A constant value of  $6 \times 10^{-6} \text{ } ^\circ\text{C}^{-1}$  for the thermal expansion coefficient of concrete, a simplification suggested by Hong and Varma (2009), is adopted as well as a constant value of  $2300 \text{ kg/m}^3$  for concrete density, as suggested by most researches instead of the temperature dependent formulation proposed in EN1992-1-2 (2004).

The EN1994-1-2 (2005) takes into account the effect of moisture in concrete by using a peak value in the specific heat. The values of  $2020 \text{ J/kg K}$  for moisture content of 3% of concrete weight and  $5600 \text{ J/kg K}$  for moisture of 10% are recommended. The numerical model adopts a peak value of  $2659 \text{ J/kg K}$  corresponding to moisture of 4.25% determined in the experimental tests (Chapter 3), obtained from linear interpolation.

### 4.2.3 Analysis procedure

Sequentially, coupled thermal-stress analysis was carried out instead of fully coupled thermal-stress analysis, because the former is less time-consuming and leads to fewer problems of convergence than the latter, as suggested by Espinos *et al.* (2010).

In fact, the first approach simplifies the problem because the stress/strain solution is dependent on the temperature, but the inverse relation is not. In a fully coupled thermal-stress analysis, the conductance thermal gap decreases when the steel tube and concrete core surfaces are detached, due to the different thermal expansion of these materials. Therefore, the thermal and structural solutions affect each other and this approach seems to better represent a real situation than a sequentially coupled thermal-stress analysis.

However, as indicated in Section 4.3, results obtained with sequentially coupled thermal-stress analysis showed good agreement with experimental tests and thus it can be concluded that a more complex analysis does not seem to be necessary. Given this, the numerical analysis runs as follows: the nodal temperatures (output), obtained from thermal analysis of CFCH columns, are the input data for stress analysis. In the following, details of each analysis models will be further discussed.

#### *Thermal model*

The thermal model corresponds to a pure heat transfer analysis. The surfaces of the CFCH columns were submitted to the furnace temperature curve measured in experimental tests (Chapter 3) and two mechanisms of heat transfer were considered: convection and radiation. In the inner part of the CFCH columns, conduction was the heat transfer mechanism. The

values suggested in EN1991-1-2 (2002) were used and the main parameters are presented in Table 4.1.

Table 4.1 – Parameters for the thermal model

<i>Parameter</i>	<i>Value</i>	<i>Unit</i>
<b>Convective heat transfer coefficient (<math>h_c</math>)</b>	25	W/m <sup>2</sup> K
<b>Radiation configuration factor (<math>\phi_r</math>)</b>	1	--
<b>Stephan-Boltzmann constant (<math>\sigma</math>)</b>	$5.67 \times 10^{-8}$	W/m <sup>2</sup> K <sup>4</sup>
<b>Absolute zero temperature</b>	-273	°C
<b>Emissivity of the material (<math>\varepsilon_m</math>)</b>	0.7	--
<b>Emissivity of fire (<math>\varepsilon_f</math>)</b>	1	--
<b>Initial temperature (<math>\theta_0</math>)</b>	20	°C

The heat transfer mechanism in the steel tube-concrete core interface and concrete core-steel bar reinforcement will be detailed in Section 4.2.4.

### ***Structural analysis***

The structural model corresponds to non-linear thermal-mechanical stress analysis. The nodal temperatures at the inner and outer surfaces of the CFCH column, obtained from heat transfer analysis, are the input data for the structural model. The meshes are the same for all simulations. The structural analysis is divided into two steps.

In the first step all the load is applied on the top plate of the CFCH columns. The plate distributes the load to the steel tube and to the concrete core. In the second step, the restraint to thermal elongation is active and heating starts.

#### **4.2.4 Interaction**

##### ***Steel tube – concrete core interface***

Espinos *et al.* (2010) commented that the thermal interface between the wall of the steel tube and the surface of the concrete core had been traditionally ignored and recommended a constant gap conductance of 200 W/m<sup>2</sup> K, as suggested by Ding and Wang (2008), and a

radiation heat transfer for this interface. The recommended emissivity ( $\varepsilon_m$ ) for both materials (steel and concrete) is 0.7 and the radiation configuration factor ( $\phi_r$ ) is 1.0.

In ABAQUS software, the mechanical interface may be modeled with normal and tangential behavior. The normal behavior considers the “hard” contact formulation that uses the classical Lagrange multiplier method and allows any pressure value when the surfaces are in contact while no pressure is allowed when the surfaces are not in contact. The tangential behavior considers the penalty method of the friction model which permits some relative motion between the surfaces (an “elastic slip”) when they should be sticking to each other. The hard contact option and the friction coefficient equal to 0.3 were adopted in this thesis, following Espinos *et al.* (2010). On the other hand, these authors commented that no difference was observed when employing different values of friction coefficient due to the separation of the steel tube from the concrete core in a fire situation. The same behavior was also observed in this research study.

### ***Steel bars - concrete core interface***

To define the interface between the reinforcement steel bars and the concrete core, a tie constraint was used, namely each node of the steel bar element was tied to the corresponding node of the concrete core element. This constraint ties two separate surfaces together so that there is no relative motion between them.

### ***Thermal elongation restraint***

A basic axial flexion wire feature connector was applied on the top plate of the CFCH columns to simulate the restraint of the surrounding structure to thermal elongation. An axial-rotational spring was set-up at the top plate with the respective value for the stiffness of the surrounding structure.

## **4.2.5 Load and boundary conditions**

The load was considered as uniformly distributed over a central square area on the top plate of the CFCH columns to avoid a high concentrated load at a specific point. Gravity was also considered in the entire column.

The bottom plate was fixed, simulating the action of the floor where the columns were supported. Then, the initial load is applied and afterwards, the top plate is submitted to an axial-rotational spring that imposes stiffness to axial deformation and rotation on the top of the columns.

These load conditions are coherent for the load conditions used in the experiments presented in Chapter 3.

The initial temperature in the columns for the numerical thermal model was 20°C. The final temperatures obtained with this modelling were then applied as the thermal load (input data) for the structural numerical modelling.

#### 4.2.6 Mesh

All parts of the model (except the reinforced bars) were meshed with three-dimensional twenty node solid elements: a DC3D20 element for the thermal model and a C3D20R element for the structural model. The bars were meshed with one-dimensional three node truss elements (T3D3 element) for the structural model and with a three node heat transfer link (DC1D3 element) for the thermal model. An approximate global size of 2cm for the element was defined and was sufficient for the accuracy of the numerical results to be good (see Section 4.3). Figure 4.1 presents an example of the finite element mesh applied.

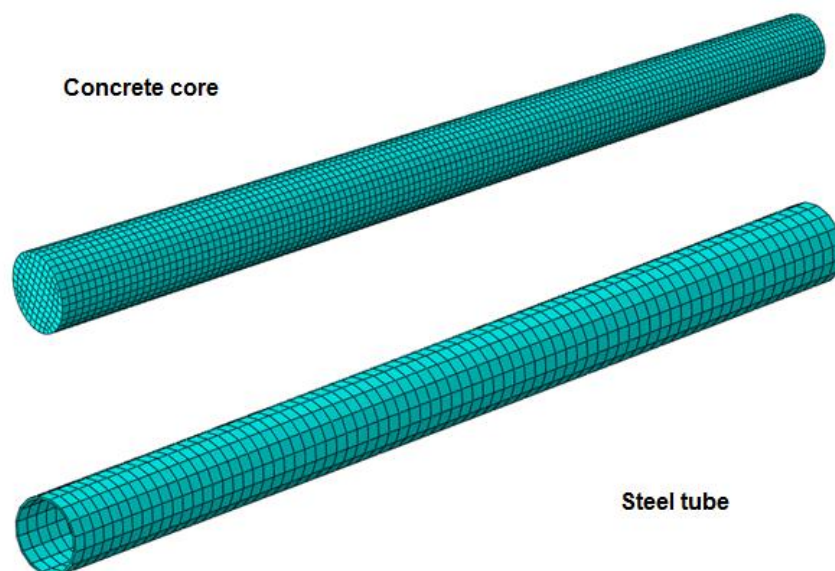


Figure 4.1 – Three-dimensional finite element model for CFCH columns

Some studies use solid linear elements in order to save computing time. This thesis employs quadratic geometric order elements, instead. Despite the increase in computing time (computer time was not a variable to be studied in this thesis), this was preferred so as to try to avoid any possible approximation error due to discretization and to make all computer runs uniform. In fact, sometimes different and refined mesh was employed in order to verify if the results converged. In the end, with the mesh adopted, the convergence of the results was considered acceptable, and no further refinement was justified. Table 4.2 resumes details of the mesh used in each simulation.

Table 4.2 – Mesh details for the numerical models

<i>Model</i>	<i>Columns</i>	<i>Diameter (mm)</i>	<i>Element type</i>		<i>N° of elements</i>	<i>N° of nodes</i>
			thermal	mechanical		
<b>1</b>	CHS columns	168.3			1728	9538
<b>2</b>	( <i>i.e.</i> without filling)	219.1	DC3D20	C3D20R	2062	11898
<b>3</b>	CHS columns total	168.3			10542	50609
<b>4</b>	filled with PC	219.1	DC3D20	C3D20R	16174	76017
<b>5</b>	CHS columns total	168.3	DC3D20/	C3D20R/	8484	38787
<b>6</b>	filled with RC	219.1	DC1D3*	T3D3*	26464	115611

\* In reinforced steel bars

### 4.3 Validation of the model

The numerical model was validated by a comparison with the fire resistance tests on the CFCH columns previously summarized in Chapter 3.

The numerical results show a good agreement with the experimental tests. Figure 4.2 to Figure 4.5 show the development of the relative restraining forces and axial deformation over time by making a comparison between the numerical and experimental results for some CFCH columns.

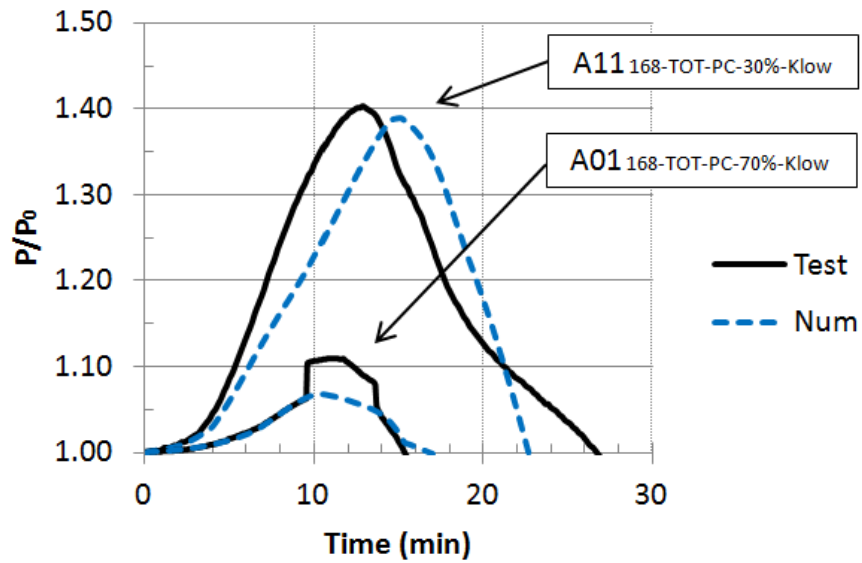


Figure 4.2 – Experimental vs. numerical restraining forces for a load level of 30% and 70%, a column diameter of 168.3mm and axial stiffness of the surrounding structure of 13 kN/mm

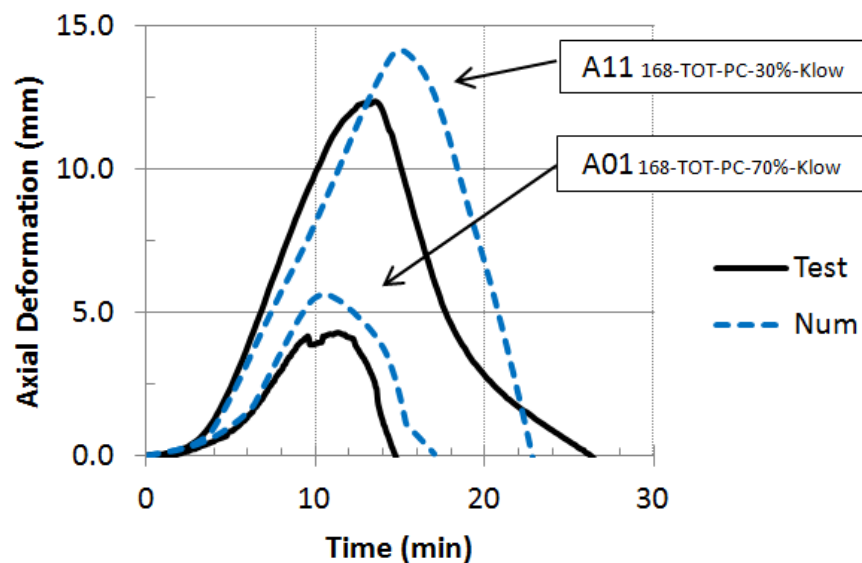


Figure 4.3 – Experimental vs. numerical axial deformations for a load level of 30% and 70%, a column diameter of 168.3mm and axial stiffness of the surrounding structure of 13 kN/mm



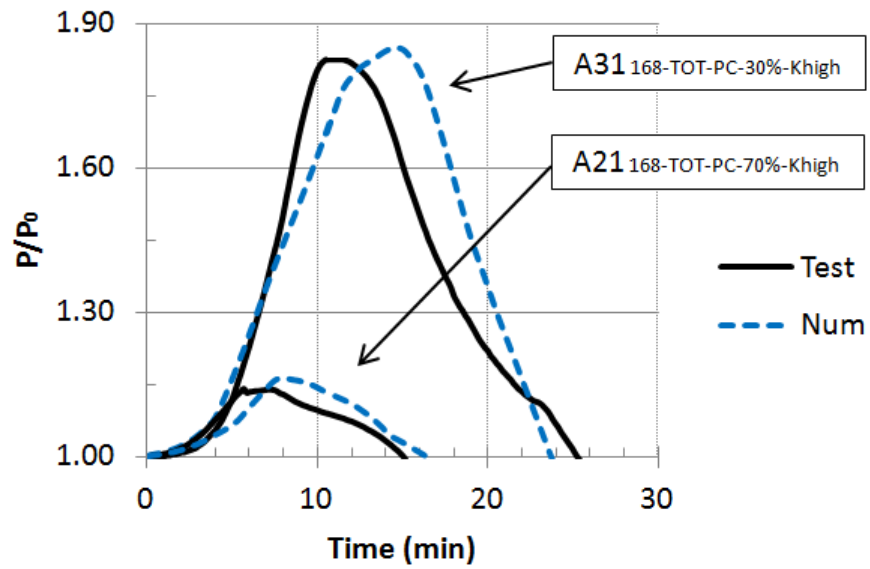


Figure 4.4 – Experimental vs. numerical restraining forces for a load level of 30% and 70%, a column diameter of 168.3mm and axial stiffness of the surrounding structure of 128 kN/mm

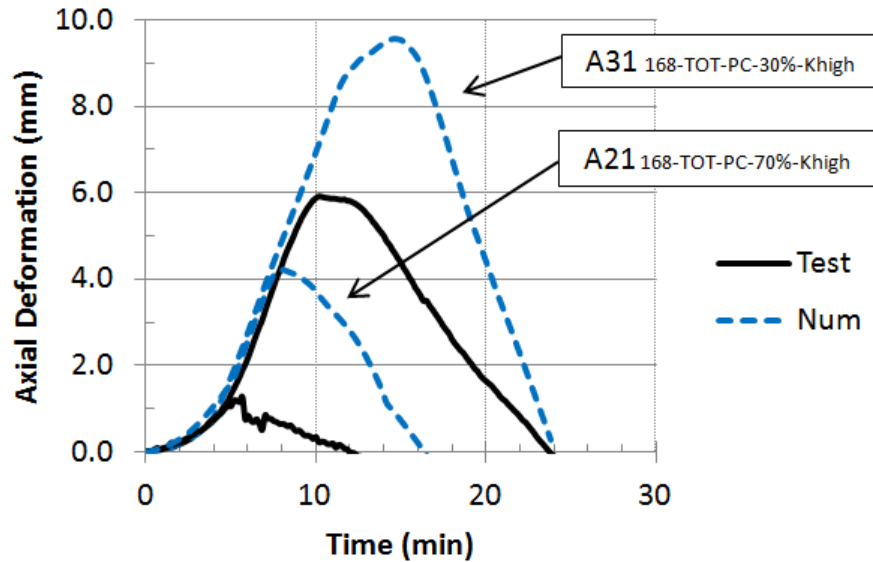


Figure 4.5 – Experimental vs. numerical axial deformations for a load level of 30% and 70%, a column diameter of 168.3mm and axial stiffness of the surrounding structure of 128 kN/mm

The axial deformation presents greater differences between the experimental and numerical results than the relative restraining force does. However this difference is small if compared with the total length of the columns (3000mm) – see Figure 4.5.

The following sections present a generalized comparison between the numerical and experimental results of CFCH columns, for which three key-points were chosen: the critical time ( $t_{cr}$ ), the maximum relative restraining forces ( $P/P_{0máx}$ ) and the maximum axial deformation ( $u_{máx}$ ). Comments on each of these results are presented in what follows.

In addition a comparison between the failure mode of the CFCH columns simulated by the numerical model and the ones registered in the tests is presented.

#### 4.3.1 Critical times

The critical time defined in this research is the instant when the restraining forces return to the initial value (*i.e.* the value of the initial load applied). The choice of this definition rather than fire resistance is because these tests are not standard fire tests (EN 1994-1-2: 2005).

Figure 4.6 presents a comparison between the critical times obtained with the numerical model and the experimental results measured in the tests. Two 5-minute error lines were plotted to aid the analysis.

In general, the numerical critical times are slightly higher than the experimental ones. In 75% of the cases, the difference between the numerical and experimental critical time was less than 5 minutes as can be observed in Figure 4.7 which plots the absolute frequency of this difference in a histogram graph and its cumulative frequency in a line graph.

One of the reasons that may explain the critical times in the numerical results being higher than in the experimental tests is that the temperatures calculated with the numerical model were slightly lower than those measured in the experimental tests such as in column A01<sub>168-TOT-PC-70%-Klow</sub> (Figure 4.8). Consequently the critical time of the column will be greater.

Ding and Wang (2008), and Hong and Varma (2009) pointed out similar differences in temperature values numerically calculated and measured in their tests, especially in the concrete core. Hong and Varma (2009) justify the divergence due to variations in the thermal properties of the material and the approach used to model the moisture content of the concrete infill.

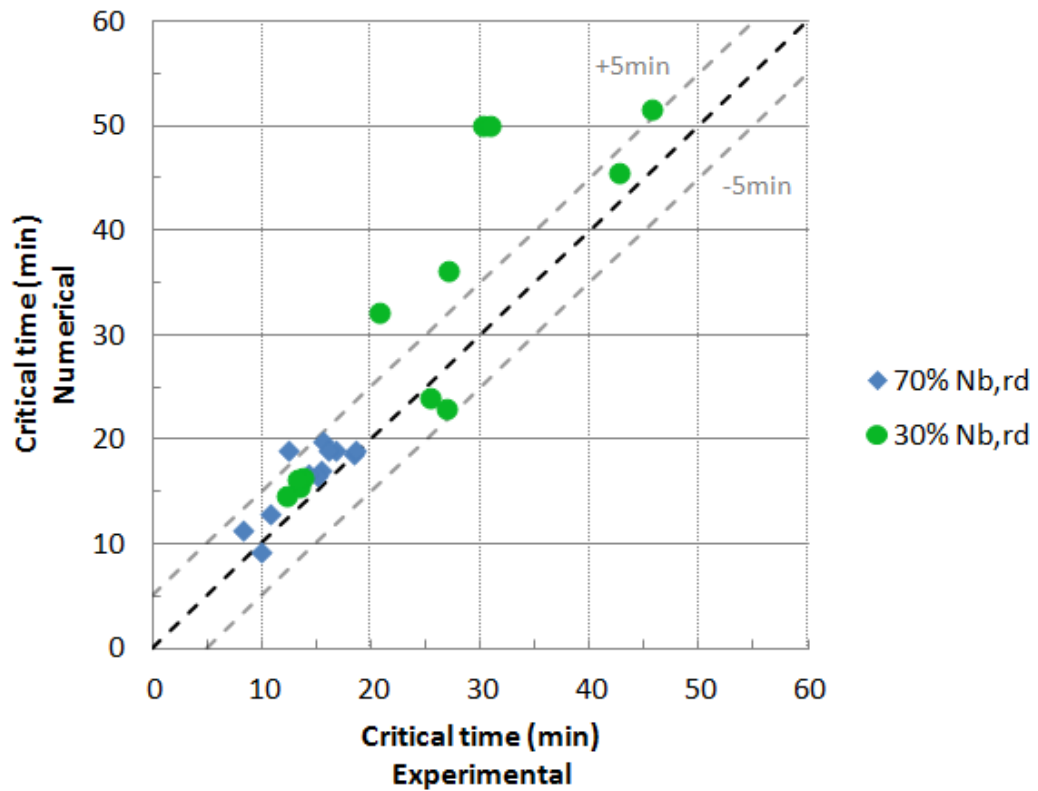


Figure 4.6 – Numerical vs. experimental critical times

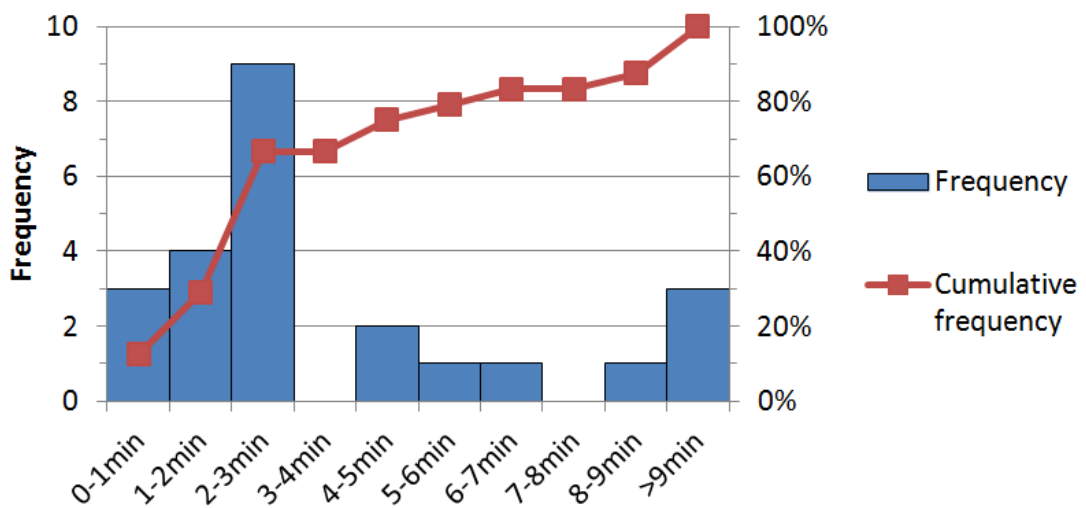


Figure 4.7 – Frequency of the num-exp critical time difference

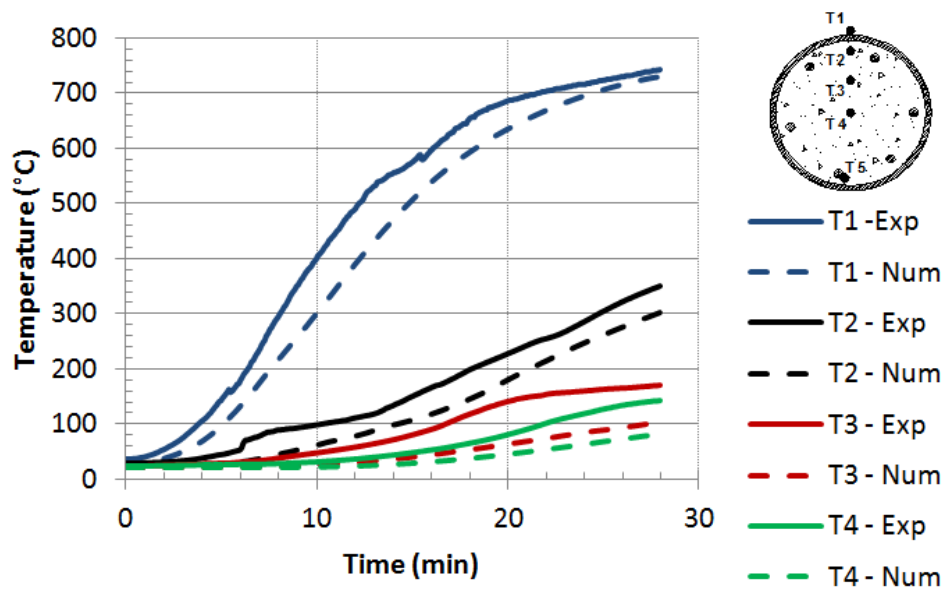


Figure 4.8 – Temperatures in the middle height cross-section of column A01<sub>168-TOT-PC-70%-Klow</sub>

In fact, as the numerical model considers the effect of the moisture in the concrete core simply as an increase in the specific heat peak, this may justify the deviation in temperatures principally at the earlier stages (between 100 and 200°C), as also suggested by Lie (1994). A better mathematical modelling of the behaviour of the migration of moisture along the concrete core leads to an improvement in the results.

After the first few minutes of exposure to fire, the temperatures calculated with the model and measured in tests present a tendency of convergence, principally in the steel tube.

Columns A12<sub>168-TOT-RC-30%-Klow</sub>, A16<sub>219-TOT-PC-30%-Klow</sub>, A32<sub>168-TOT-RC-30%-Khigh</sub> and A36<sub>219-TOT-PC-30%-Khigh</sub> present the greatest differences between the numerical and experimental critical times (*i.e.* greater than 7 minutes – see Table 4.3). All of them shared the same load level (30%  $N_{ed}$ ).

However the frequency of these results was very low (*i.e.* just 16.7% of total – see Figure 4.7) and further studies are necessary.

For larger columns, those with the largest concrete cores (*i.e.* an external diameter of 219.1mm), the model has presented a reasonable agreement with tests. Espinos *et al.* (2010) report some problems with simulations of massive columns. According to these authors, the

errors observed in massive columns are due to the higher contribution of the concrete core and its more complex failure mechanisms. Other authors also presented similar comments (Lie, 1994; Ding and Wang 2008; Schaumann *et al.*, 2009; Hong and Varma, 2009).

This numerical validation addressed CFCH columns with a maximum diameter of 219.1mm. There are columns with larger diameters in practical situations. Therefore and in agreement with the above comments, further studies should be conducted so as to better represent the behaviour of concrete at elevated temperatures in numerical models.

Finally the average error between the numerical and experimental critical times was 4.2min with a standard deviation of 4.6min (Table 4.3).

Table 4.3 – Exp vs. Num - Critical times and Maximum axial deformation

<i>Column</i>	<i>Critical times (min)</i>			<i>Maximum axial deformation (mm)</i>		
	<i>Exp.</i>	<i>Num.</i>	<i> Exp – Num </i>	<i>Exp.</i>	<i>Num.</i>	<i> Exp – Num </i>
<b>A01</b> <sub>168-TOT-PC-70%-Klow</sub>	15.5	17	1.5	4.3	5.6	1.3
<b>A02</b> <sub>168-TOT-RC-70%-Klow</sub>	12.5	18.8	6.3	1.9	4.4	2.5
<b>A03</b> <sub>168-RING-PC-70%-Klow</sub>	14.5			4.1		
<b>A04</b> <sub>168-RING-RC-70%-Klow</sub>	12.2					
<b>A05</b> <sub>168-70%-Klow</sub>	8.3	11.3	3.0	6.3	10.5	4.1
<b>A06</b> <sub>219-TOT-PC-70%-Klow</sub>	15.7	19.8	4.1	7.2	4.2	3.0
<b>A07</b> <sub>219-TOT-RC-70%-Klow</sub>	18.5	18.5	0.0	6.1	3.2	2.9
<b>A08</b> <sub>219-RING-PC-70%-Klow</sub>	19.0					
<b>A09</b> <sub>219-RING-RC-70%-Klow</sub>	13.7					
<b>A10</b> <sub>219-70%-Klow</sub>	10.8	12.8	2.0	9.7	11.4	1.7
<b>A11</b> <sub>168-TOT-PC-30%-Klow</sub>	27.0	22.8	4.2	12.4	14.1	1.8
<b>A12</b> <sub>168-TOT-RC-30%-Klow</sub>	30.3	40.0	9.7	12.6	11.5	1.1
<b>A13</b> <sub>168-RING-PC-30%-Klow</sub>	25.8			11.6		
<b>A14</b> <sub>168-RING-RC-30%-Klow</sub>	14.7					
<b>A15</b> <sub>168-30%-Klow</sub>	13.5	15.4	1.9	13.8	16.0	2.2
<b>A16</b> <sub>219-TOT-PC-30%-Klow</sub>	27.2	36.0	8.8	12.4	14.2	1.8
<b>A17</b> <sub>219-TOT-RC-30%-Klow</sub>	42.7	45.5	2.8	10.6	13.4	2.8
<b>A18</b> <sub>219-RING-PC-30%-Klow</sub>	29.0					
<b>A19</b> <sub>219-RING-RC-30%-Klow</sub>	22.8					
<b>A20</b> <sub>219-30%-Klow</sub>	13.8	16.3	2.5	15.5	16.7	1.2
<b>A21</b> <sub>168-TOT-PC-70%-Khigh</sub>	15.2	16.5	1.3	1.3	4.2	2.9
<b>A22</b> <sub>168-TOT-RC-70%-Khigh</sub>	16.8	18.8	2.0	3.4	3.3	0.1
<b>A23</b> <sub>168-RING-PC-70%-Khigh</sub>	13.8			1.7		
<b>A24</b> <sub>168-RING-RC-70%-Khigh</sub>	12.0					

Table 4.3 – Exp vs. Num - Critical times and Maximum axial deformation (cont.)

<i>Column</i>	<i>Critical times (min)</i>			<i>Maximum axial deformation (mm)</i>		
	<i>Exp.</i>	<i>Num.</i>	<i> Exp – Num </i>	<i>Exp.</i>	<i>Num.</i>	<i> Exp – Num </i>
<b>A25</b> <sub>168-70%-Khigh</sub>	10.0	9.2	0.8	2.7	7.4	4.8
<b>A26</b> <sub>219-TOT-PC-70%-Khigh</sub>	16.2	18.8	2.6	1.1	3.5	2.4
<b>A27</b> <sub>219-TOT-RC-70%-Khigh</sub>	18.7	18.8	0.1	1.6	2.9	1.3
<b>A28</b> <sub>219-RING-PC-70%-Khigh</sub>	17.0					
<b>A29</b> <sub>219-RING-RC-70%-Khigh</sub>	13.2					
<b>A30</b> <sub>219-70%-Khigh</sub>	14.3	16.7	2.4	4.5	8.1	3.6
<b>A31</b> <sub>168-TOT-PC-30%-Khigh</sub>	25.5	23.8	1.7	5.9	9.6	3.7
<b>A32</b> <sub>168-TOT-RC-30%-Khigh</sub>	31.0	50.0	19.0	6.6	8.4	1.9
<b>A33</b> <sub>168-RING-PC-30%-Khigh</sub>	21.2			1.6		
<b>A34</b> <sub>168-RING-RC-30%-Khigh</sub>	14.3					
<b>A35</b> <sub>168-30%-Khigh</sub>	12.3	14.5	2.2	4.9	11.4	6.5
<b>A36</b> <sub>219-TOT-PC-30%-Khigh</sub>	20.8	35.0	14.2	5.0	10.6	5.6
<b>A37</b> <sub>219-TOT-RC-30%-Khigh</sub>	45.7	51.5	5.8	6.4	9.9	3.5
<b>A38</b> <sub>219-RING-PC-30%-Khigh</sub>	26.2					
<b>A39</b> <sub>219-RING-RC-30%-Khigh</sub>	27.8					
<b>A40</b> <sub>219-30%-Khigh</sub>	13.3	16.1	2.8	6.7	13.5	6.7
<i>Average error</i>			<b>4.2</b>			<b>2.9</b>
<i>Standard deviation</i>			<b>4.6</b>			<b>6.7</b>

#### 4.3.2 Maximum relative restraining forces

Figure 4.9 indicates the numerical and experimental results of the maximum relative restraining forces. A difference with an order of magnitude of around 10%, between calculated and measured internal forces, is acceptable for practical design purposes. Thus, a 10% error line is also plotted on the graph.

The numerical model shows a very good agreement with the test results measured for the maximum restraining forces. The error between the numerical and experimental results was less than 10% for 83.3% of the cases tested (Figure 4.10). Just four columns (A22<sub>168-TOT-RC-70%-Khigh</sub>, A30<sub>219-70%-Khigh</sub>, A32<sub>168-TOT-RC-30%-Khigh</sub> and A37<sub>219-TOT-RC-30%-Khigh</sub>) present errors greater than 10%, all of them being columns tested with the higher stiffness of the surrounding structure ( $k_{high}$ ).

Figure 4.10 plots the absolute frequency of the difference in maximum relative restraining forces in a histogram graph and its cumulative frequency in a line graph.

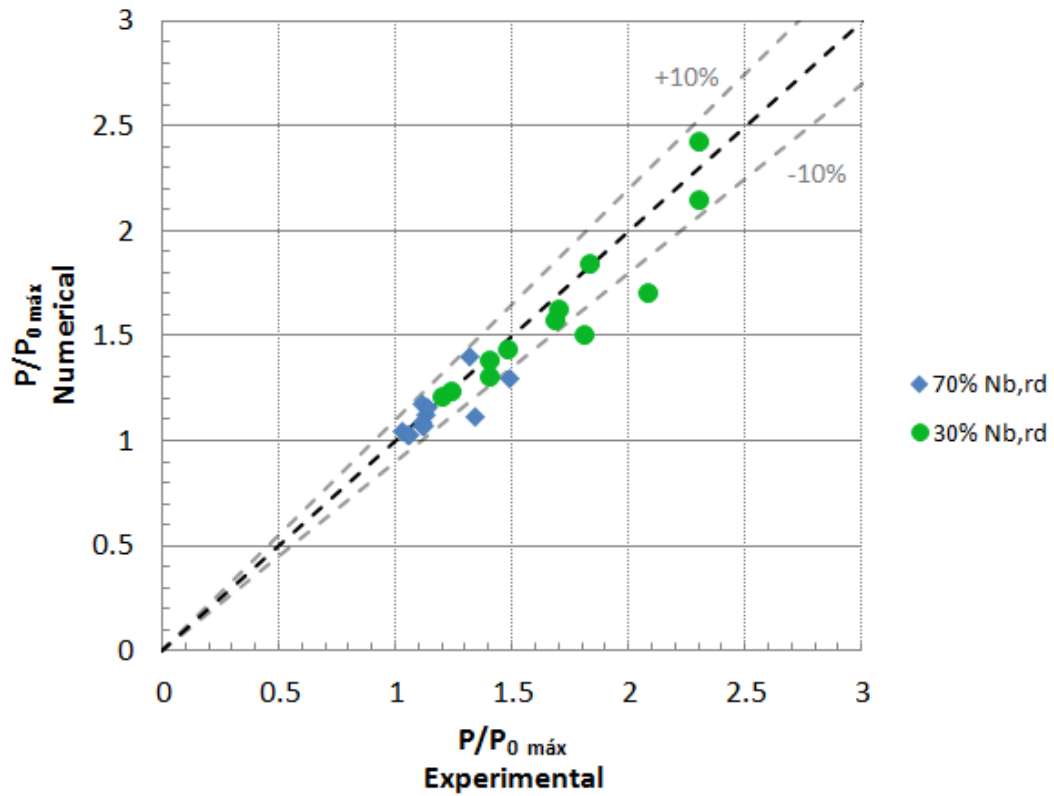


Figure 4.9 – Numerical vs. experimental maximum relative restraining forces

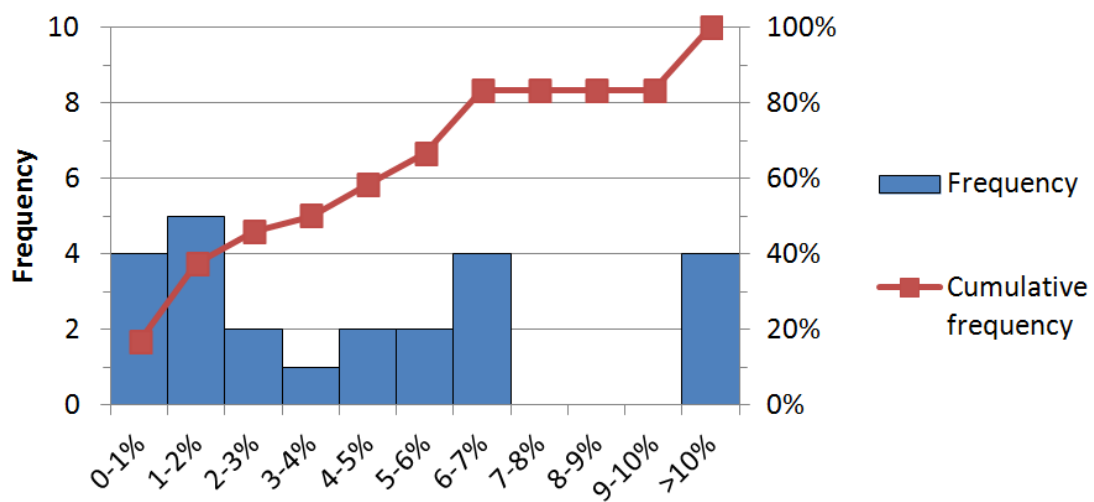


Figure 4.10 – Frequency of the difference in num-exp maximum relative restraining forces

### 4.3.3 Maximum axial deformation

The axial deformation presents some differences between the numerical and experimental results but in general the differences are acceptable (Figure 4.11).

Figure 4.11 compares the numerical and experimental results for the maximum axial deformation and note that in general the numerical results are higher than the experimental ones. Error lines of 5mm (1.7% of columns length) were plotted.

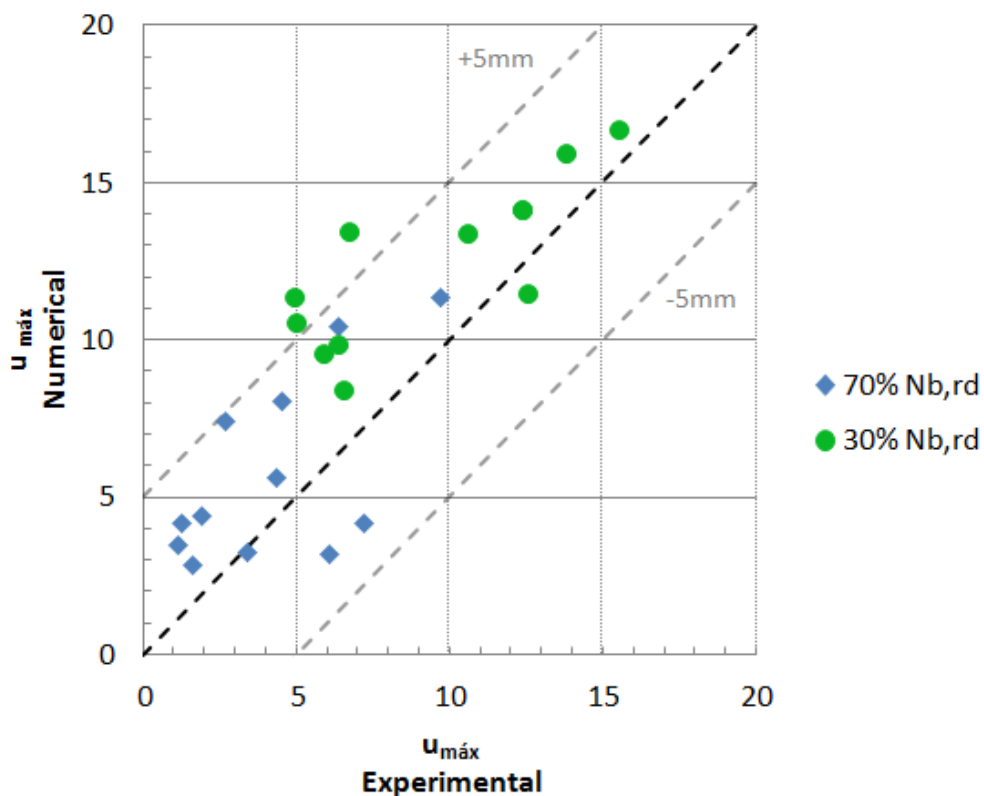


Figure 4.11 – Numerical vs. experimental maximum axial deformation

In most cases (87.5%), the difference between the numerical and experimental maximum axial deformation was up to 5mm (Figure 4.12). This difference was greater than 5mm in only three columns (A35<sub>168-30%-Khigh</sub>, A36<sub>219-TOT-PC-30%-Khigh</sub> and A40<sub>219-30%-Khigh</sub>) (Table 4.3).

The average error between the numerical and experimental maximum axial deformation was 2.9mm with a standard deviation of 6.7mm (Table 4.3).



The axial deformation (less than 20mm) is too small if compared with the column length (3000mm). Moreover, as suggested by Lie (1994), several factors influence axial deformation such as load, the thermal expansion coefficient, bending, creep and these cannot be completely taken into account in software simulations. Due to the influence of these factors, the differences between calculated and measured axial deformations obtained here are irrelevant.

Figure 4.12 plots the absolute frequency of the maximum axial deformation differences in a histogram graph and its cumulative frequency in a line graph.

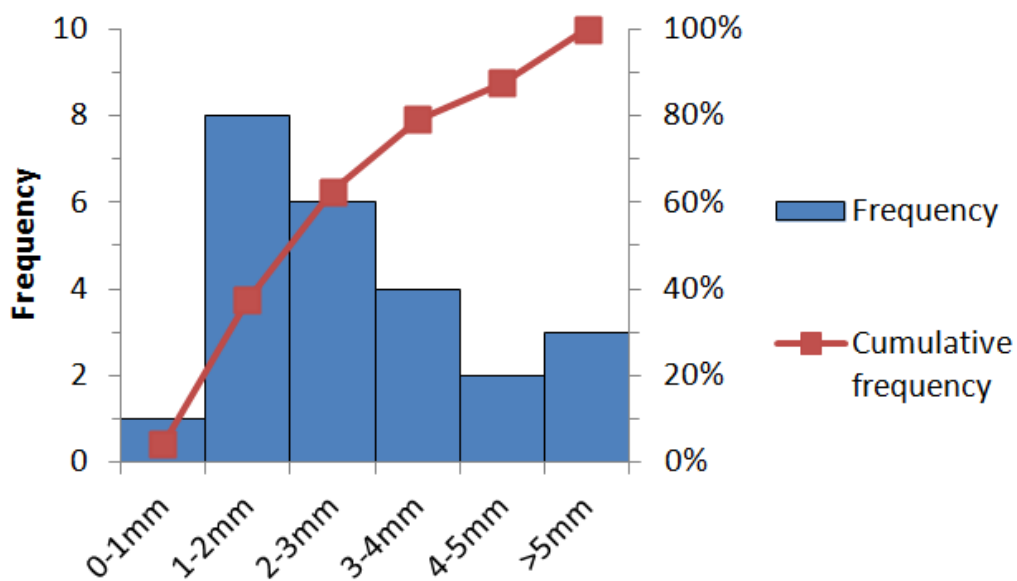


Figure 4.12 – Frequency of num-exp maximum axial deformation differences

#### 4.3.4 Failure mode

Figure 4.13 presents a comparison between numerical and experimental deformed shapes of some the columns studied from which the following comments can be drawn.

First, the deformed shapes simulated with the numerical model were very similar to those observed in the experimental tests. In most cases, the failure mode was global buckling but local buckling of the steel tube also occurred.

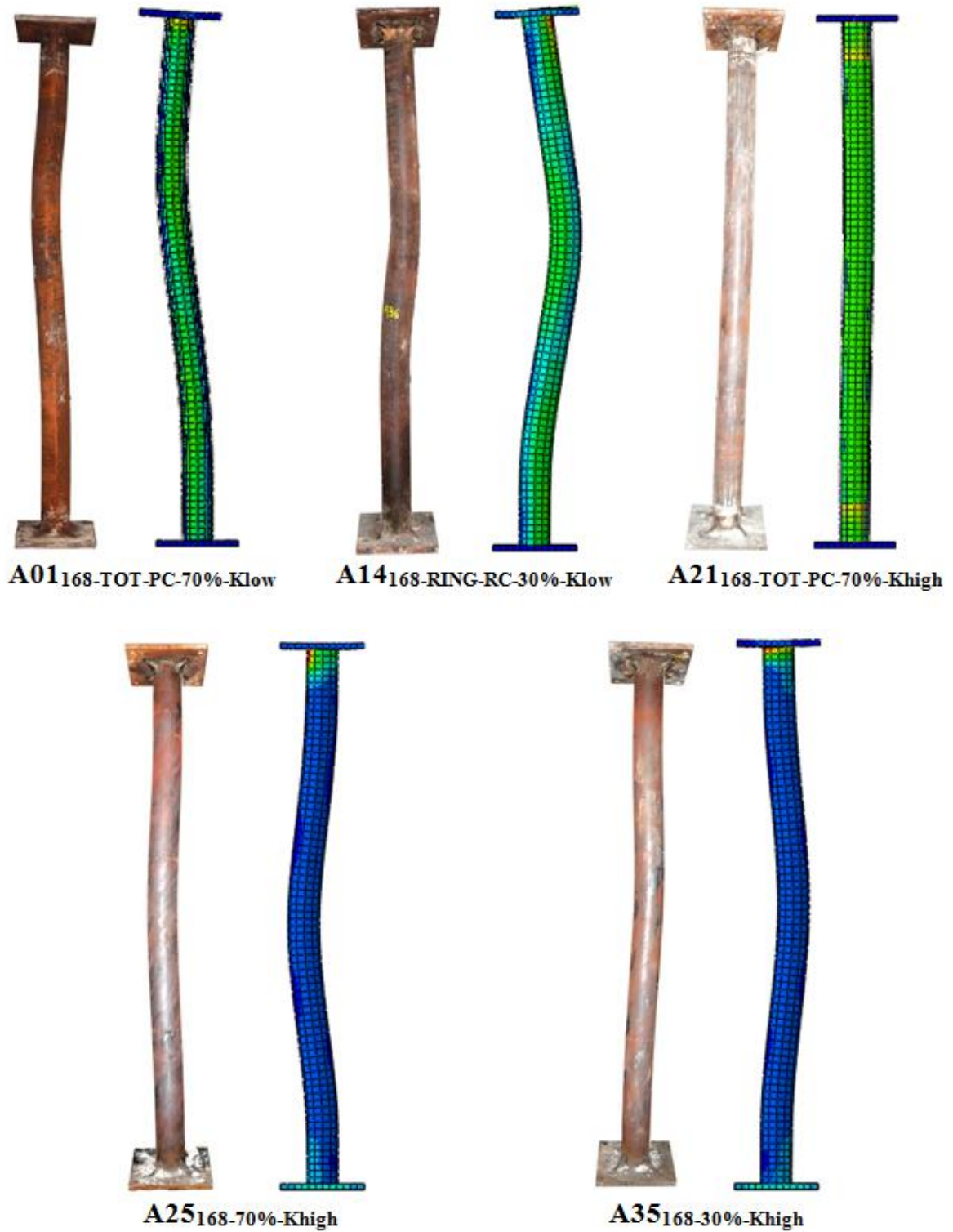


Figure 4.13 – Num-exp deformed shapes of CFCH columns

Second, it is visually clear that the CFCH columns subjected to the lower stiffness of the surrounding structure ( $k_{low}$ ) presented a deformed shape, suggesting a pinned-fixed end-condition (A01<sub>168-TOT-PC-70%-Klow</sub> and A14<sub>168-RING-RC-30%-Klow</sub>). However, those with the highest stiffness in the surrounding structure ( $k_{high}$ ) suggested there is a fixed-fixed end-condition shape (A25<sub>168-70%-Khigh</sub> and A35<sub>168-30%-Khigh</sub>).

Lastly, even in cases where it was difficult to identify the failure mode (A21<sub>168-TOT-PC-70%-Khigh</sub>), in general, the columns presented an agreement with the deformed shape registered in tests and with the results (*i.e.* critical time, maximum relative restraining forces and maximum axial deformation).

Future research studies might well focus on the failure mode of CFCH columns and its influence in fire resistance.

#### 4.4 Chapter remarks

This chapter proposed a three-dimensional nonlinear finite element model to predict the behaviour of CFCH columns in a fire situation. The model also takes into account the restraint of columns to thermal elongation, a novelty that has not so far been widely discussed in the literature.

How to determine the most relevant parameters is discussed and the values used for these parameters widen the analysis, given that restraint of columns to thermal elongation is not commonly addressed (experimentally and numerically) and very few data have been reported in the literature.

The proposed model was validated with the support of a set of fire experiments realized with thermal elongation restrained CFCH columns and presented in Chapter 3. As shown, the numerical results obtained are in close agreement with the experimental ones. It is important to stress, however, that it is quite difficult for any numerical model to represent all imperfections of experimental tests accurately.

The following remarks about the results obtained sum up the performance of the numerical approach:

- The proposed numerical approach presented results in close agreement with the experimental tests and therefore can be considered as an option to assess the fire performance of CFHS columns;

- The numerical critical times obtained were slightly higher than the experimental ones. However, in most cases, this difference was not large, i.e. less than 5 minutes;
- The temperatures calculated with the numerical model were slightly lower than those measured in the experimental tests;
- The numerical relative restraining forces obtained were in close agreement with those measured in the experimental test. In general, the error was less than 10%;
- In general, the numerical axial deformations were higher than those in the experimental results. However, in most cases, this difference was less than 5mm, which is negligible given the length of the columns.
- The deformed shapes of the columns subjected to the lowest stiffness of the surrounding structure ( $k_{low}$ ) suggested a pinned-fixed end-condition failure. However, those subjected to the highest stiffness of the surrounding structure ( $k_{high}$ ) suggested they were of a fixed-fixed end-condition shape.

## 5. AN ANALYSIS BASED ON NUMERICAL DATA OF CONCRETE FILLED CIRCULAR HOLLOW COLUMNS SUBJECTED TO FIRE

### 5.1 Introduction

This chapter presents simplified equations to represent the fire performance of Concrete Filled Circular Hollow (CFCH) Columns based on experimental and numerical results. The behaviour of CFCH columns when there is a fire was simulated with a three-dimensional nonlinear finite element model developed in ABAQUS (2011). The numerical simulations make use of the suggestions already presented in Chapter 4 for column discretization.

A series of results was then obtained using ABAQUS (2011), employing the numerical modelling already tested, in order to discuss the response of CFCH Columns on fire, based on the numerical data. The parameters chosen for this study were: load level (10%, 20%, 30%, 50%, 70% and 90%  $N_{ed}$ ), the diameter of the column (168.3mm, 219.1mm, 323.9mm and 457mm) and the ratio of reinforcement with reinforcing steel bars (0% – without reinforcement, 3% and 6%). These ranges include typical values for CFCH columns, especially for load level and steel reinforcement bars. Values outside these ranges have no meaning for practical cases.

All the columns were simulated with grade S355 steel tubes, which had a wall that was 6 mm thick, C30/37 class concrete (EN 206-1, 2007) that filled the entire cross section and grade A500 reinforcing steel bars. The distance from the central axis of the longitudinal bar to the inner surface of the column wall was 30 mm in all cases. All the columns were 3 m long and the whole length was exposed to an ISO834 curve (ISO834-1, 1999).

Based on the numerical data obtained, simplified equations for the design of CFCH columns are studied using standard regression analysis. As the regression functions for the numerical data obtained showed acceptable approximation, a set of simplified equations is thus developed to predict the critical times of CFCH columns.

In addition, a comparison with the simple calculation methods given in EN1994-1-2 (2005) is presented. This comparison showed that the tabulated method can be unsafe for some cases and the simple calculation method may be conservative, when compared to the results obtained from the simplified equations developed or by the tests (Chapter 3).

It should be emphasized that issues such as the lack of experimental results, especially for more massive CFCH columns, the difficulty in standardizing tests in order to compare results,

the use of different criteria to define the fire resistance, the limitation on representing the experiments numerically, and the accuracy of mathematical models that describe the mechanical behaviour of materials raise challenges as to completely understanding the behaviour of CFCH columns subjected to fire. Nevertheless, the proposal of simplified equations prompts discussion on some of these key points, and seeks to contribute towards future studies that will be undertaken in this field.

## 5.2 Numerical data – discussion and simplified equations

Figure 5.1 to Figure 5.3 show the calculated critical times arising from the load level for different CFCH columns with reinforcement ratios of 0%, 3% and 6% respectively.

The results ratify the great influence of the load level on the critical times of the columns, as previously shown in Chapter 3. The higher the load level, the lower the critical time is. However, in general, the simulated columns present low critical times (*i.e.* under 30min) for load levels above 50%  $N_{ed}$ , especially for reinforcement ratios of 0% and 3%.

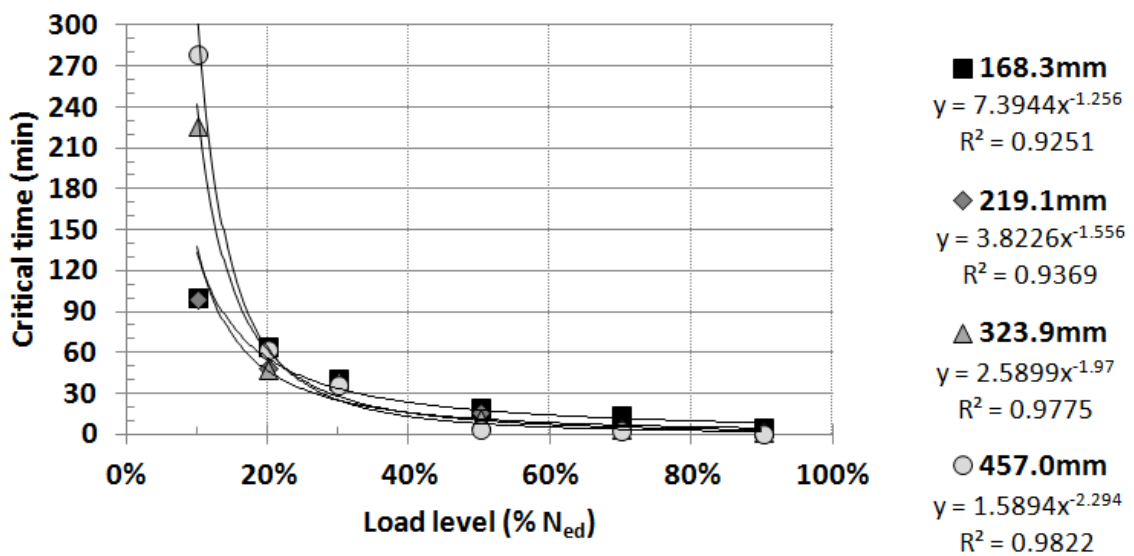


Figure 5.1 – Critical times arising from a load level of CFCH columns with a reinforcement ratio of 0%

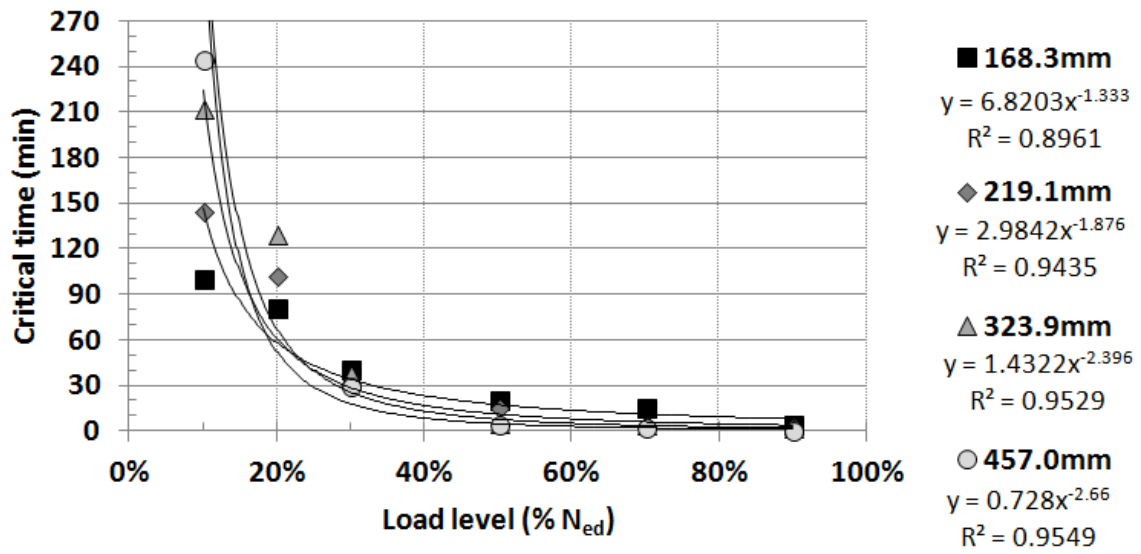


Figure 5.2 – Critical times arising from a load level of CFCH columns with a reinforcement ratio of 3%

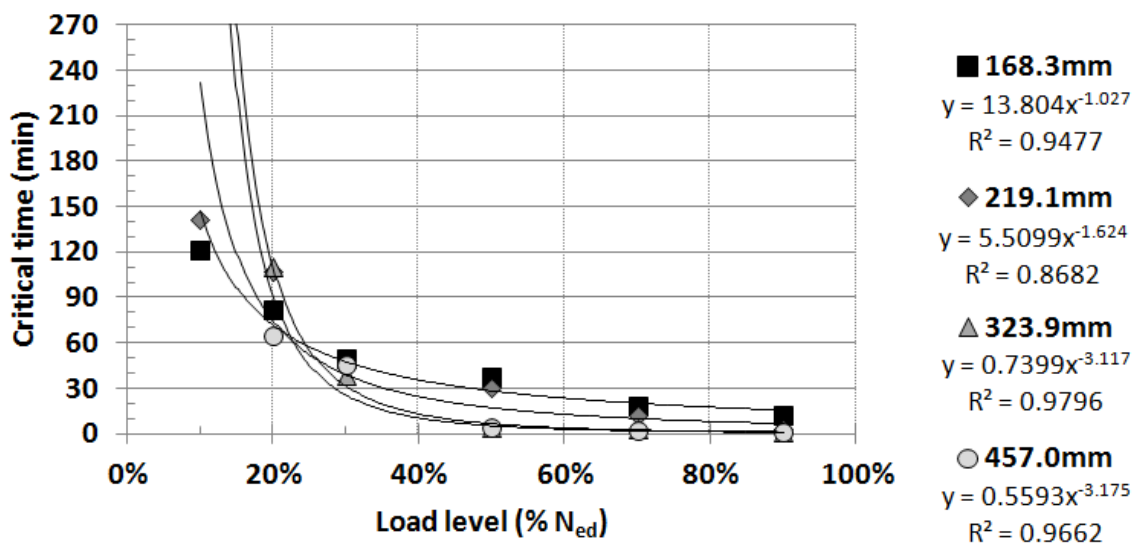


Figure 5.3 – Critical times arising from a load level of CFCH columns with a reinforcement ratio of 6%

A regression analysis was carried out and a relationship between the independent variables (*i.e.* load level  $\eta$ , column diameter  $d$  and reinforcement ratio  $\rho$ ) and the dependent variable (*i.e.* critical time) was defined. Figure 5.1 to Figure 5.3 also present the regression functions.

The regression functions presented an acceptable approximation with the numerical data. The choice of regression function was the coefficient of determination  $R^2$  above 0.9.

Therefore, the critical times of CFCH columns may be expressed by Equations 5.1, 5.2 and 5.3, as shown below.

*For the reinforcement ratio  $\rho = 0\%$*

$$t_{cr} = \begin{array}{ll} 7.3944 \eta^{-1.256} & \text{if } d = 168.3\text{mm} \\ 3.8226 \eta^{-1.556} & \text{if } d = 219.1\text{mm} \\ 2.5899 \eta^{-1.970} & \text{if } d = 323.9\text{mm} \\ 1.5894 \eta^{-2.294} & \text{if } d = 457.0\text{mm} \end{array} \quad (5.1)$$

*For the reinforcement ratio  $\rho = 3\%$*

$$t_{cr} = \begin{array}{ll} 6.8203 \eta^{-1.330} & \text{if } d = 168.3\text{mm} \\ 2.9842 \eta^{-1.876} & \text{if } d = 219.1\text{mm} \\ 1.4324 \eta^{-2.396} & \text{if } d = 323.9\text{mm} \\ 0.7280 \eta^{-2.660} & \text{if } d = 457.0\text{mm} \end{array} \quad (5.2)$$

*For the reinforcement ratio  $\rho = 6\%$*

$$t_{cr} = \begin{array}{ll} 13.804 \eta^{-1.027} & \text{if } d = 168.3\text{mm} \\ 5.5099 \eta^{-1.624} & \text{if } d = 219.1\text{mm} \\ 0.7399 \eta^{-3.117} & \text{if } d = 323.9\text{mm} \\ 0.5593 \eta^{-3.175} & \text{if } d = 457.0\text{mm} \end{array} \quad (5.3)$$

The numerical results also showed that for load levels of 10% and 20% the greater the diameter of the columns is, the greater the calculated critical times are. For a load level of 30% the critical time does not change and, finally, for load levels above 50% a slight



reduction in critical times is observed (see Figure 5.4). The same tendency was observed for columns with reinforcement ratios of 0% and 6%.

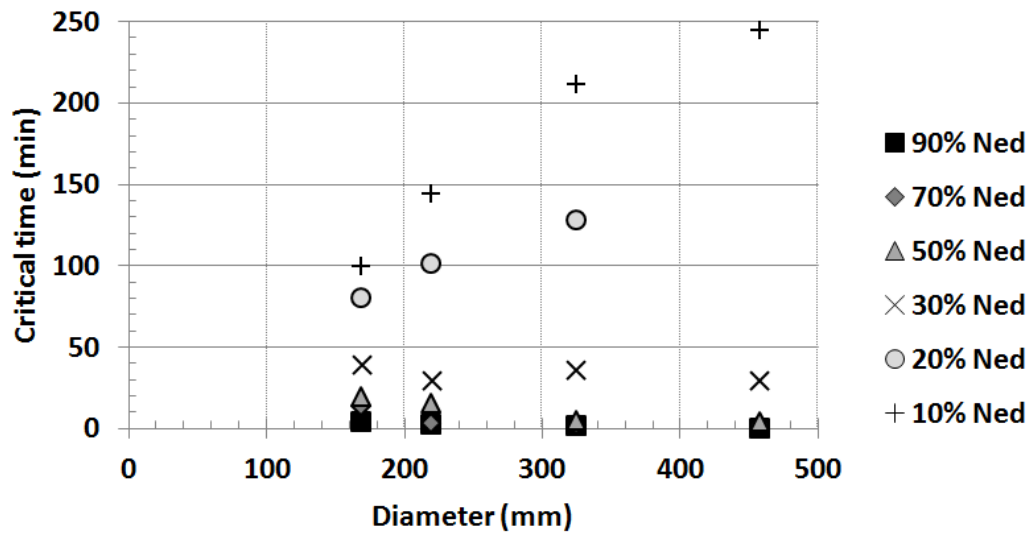


Figure 5.4 – Critical times arising from CFCH column diameters with 3% steel reinforcement

On applying the concept of fire resistance as employed by some authors and presented in Chapter 2, it is expected that this resistance will increase for CFCH columns with the highest diameters. This same tendency was identified when applying the critical time criteria, as used in this thesis (Chapter 3). As mentioned in Chapter 4, the same numerical and experimental data were used to compare these models, and showed good agreement. In this chapter, the discretization and boundary conditions of the columns followed the modelling described in Chapter 4, for all computer runs. On the other hand, in order to study the standard behaviour of CFCH columns the data used for the mechanical properties of materials correspond to the theoretical standard values given in the literature while for the fire curve, ISO834 (ISO834-1, 1999) was adopted.

However, in this case, for columns with the highest diameters, as mentioned above, an increase in the critical time was not observed for the highest load levels (Figure 5.4). Several comments may be made about these results.

It has been commented in the literature, as for instance by Espinos *et al.* (2010), that the agreement between experimental and numerical results is better for less massive columns than for massive ones. According to these authors, the error observed in these larger columns may

be justified by the higher contribution of the concrete core and its more complex failure mechanisms. However, further studies are still necessary before this conclusion can be drawn.

There are two others key questions that arise from this issue. First, how large can the column diameter be with regard to applying the numerical techniques available? Second, what is, in fact, the influence of the load level on the behaviour of the largest columns?

It is important to observe that in their interesting paper Espinos *et al.* (2010) analysed columns with diameters of up to 273.1mm and load levels up to 45%. The NRCC (National Research Council of Canada) experimental tests, presented in Chapter 2, also worked for load levels of up to 45%. The numerical results obtained here tend to show similar behaviour for load levels of up to 30% and diameters of 168.3mm and 219.1mm. Comparisons between experimental and numerical results for columns with larger diameters are scarce due to the inherent difficulty of the tests. However, far from proposing a final conclusion, these values should be taken as a reference for future research. It is also important to comment that the fire resistance adopted in the studies mentioned above differs from the critical time considered here.

Furthermore, all the experimental and numerical analyses carried out in this study have taken into account the axial and rotational restriction to thermal elongation, thus simulating the effect of the surrounding structure.

This consideration has not yet been taken into account in research about CFCH columns in a fire situation.

Another key point: the failure mode also may justify the column behaviour shown by the numerical results. The thickness was kept constant when the diameter of the columns was increased. On analysing the deformed shapes of the columns (ABAQUS, 2001 output), local buckling is more frequent for higher diameters (Figure 5.5). This may suggest the failure is sooner of CFCH columns with a steel tube thickness of 6.3mm, a higher load level, and diameters of 323.9 and 457mm.

Previously, the experimental (Chapter 3) and numerical analyses (Chapter 4) showed that the higher the diameter of the columns, the higher the volume of local buckling is. This same tendency is observed when using numerical data. The number of cases of local buckling increases in columns with diameters of 323.9 and 457mm. In addition, local buckling in columns with a reinforcement ratio of 6% (Figure 5.6) is less frequent.

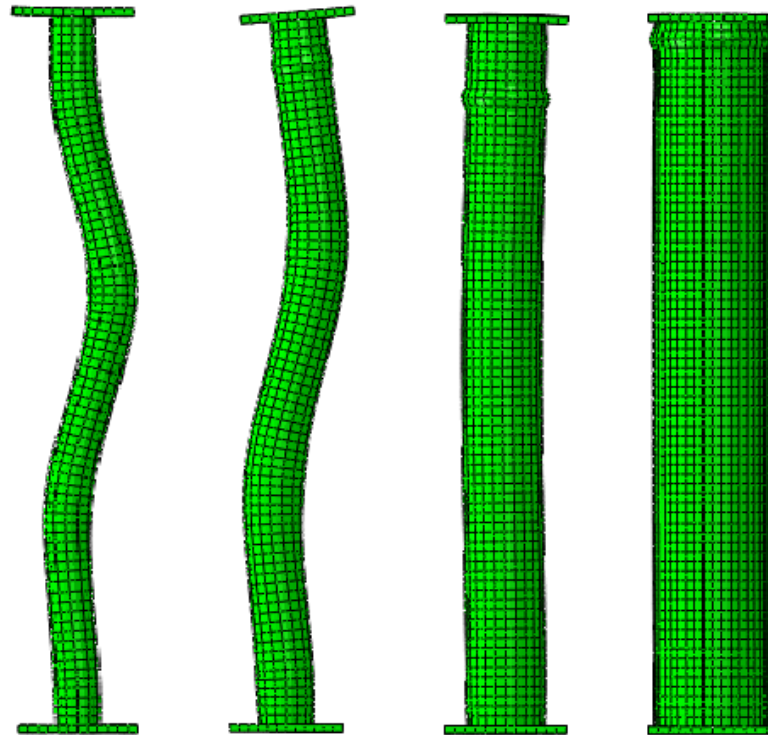


Figure 5.5 – Influence of diameter on the failure mode of the CFCH column

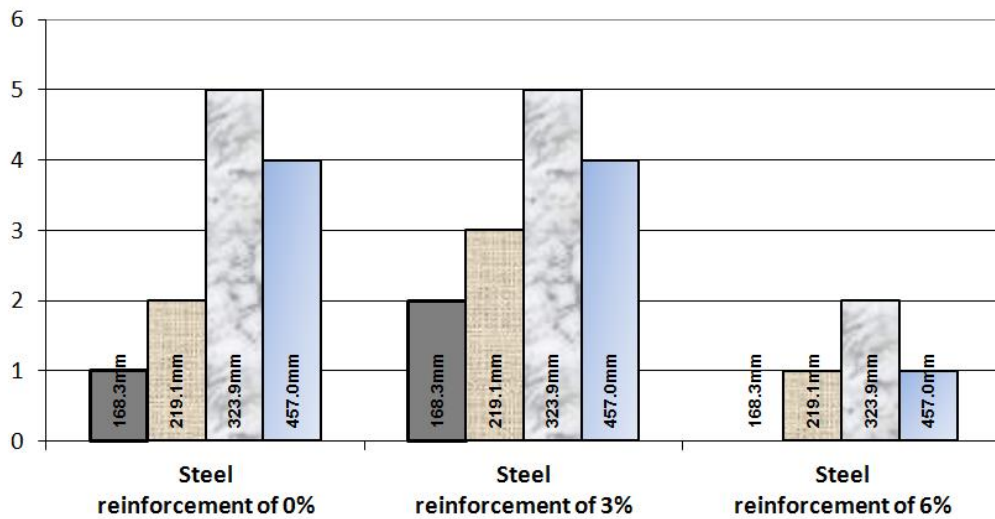


Figure 5.6 – Number of CFCH columns that presented local buckling

Steel reinforcement and the increase in its ratio in CFCH columns slightly increase the critical time of the columns calculated, especially for those with a reinforcement ratio of 6% (Figure 5.7). However, this small increase does not justify great changes in the critical time of the CFCH columns due to there having been an increase in the reinforcement ratio.

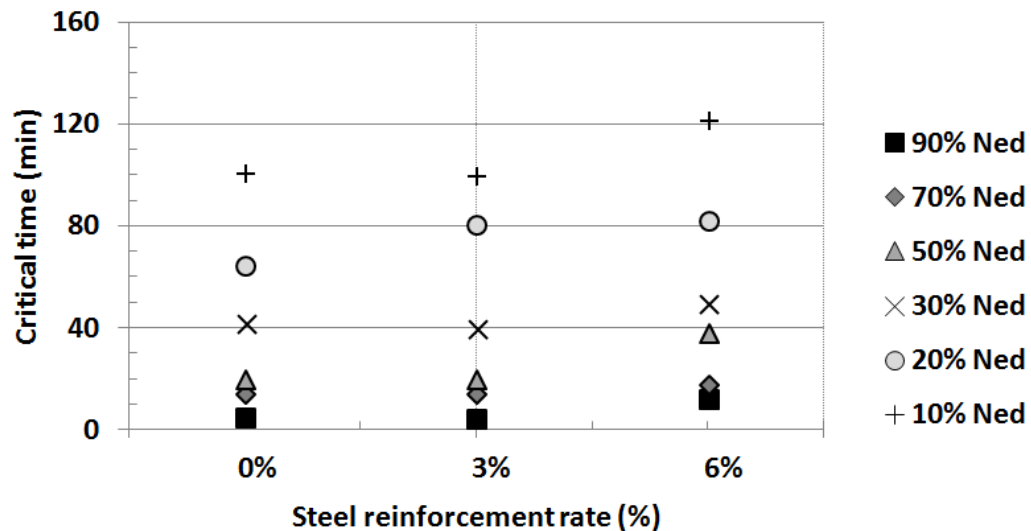


Figure 5.7 – Critical times arising from a reinforcement ratio for CFCH columns with a diameter of 168.3mm

Considering the above conclusions, a simpler equation (Equation 5.4) independent of the reinforcement ratio may be addressed for CFCH columns and provides good agreement with numerical data. Figure 5.8 presents the regression function for this situation and its coefficient of determination  $R^2$ .

Equations (5.1 to 5.4) may be a reference for future studies. It seems that further research should be carried out including into other parameters such as the thickness of the steel tube, the compressive resistance of concrete, the yield strength of the steel tube and the support boundary conditions, principally for massive CFCH columns. A wider database would probably provide a non-linear multivariate regression analysis and, consequently, a more general equation would be proposed (perhaps with greater reliability) to predict the critical time of CFCH columns. However, it is not known to the author whether or not a similar study has already been addressed for CFCH columns with restrained thermal elongation, and therefore, the simplified equations presented here are the first attempt to approach a parametric study for this purpose.

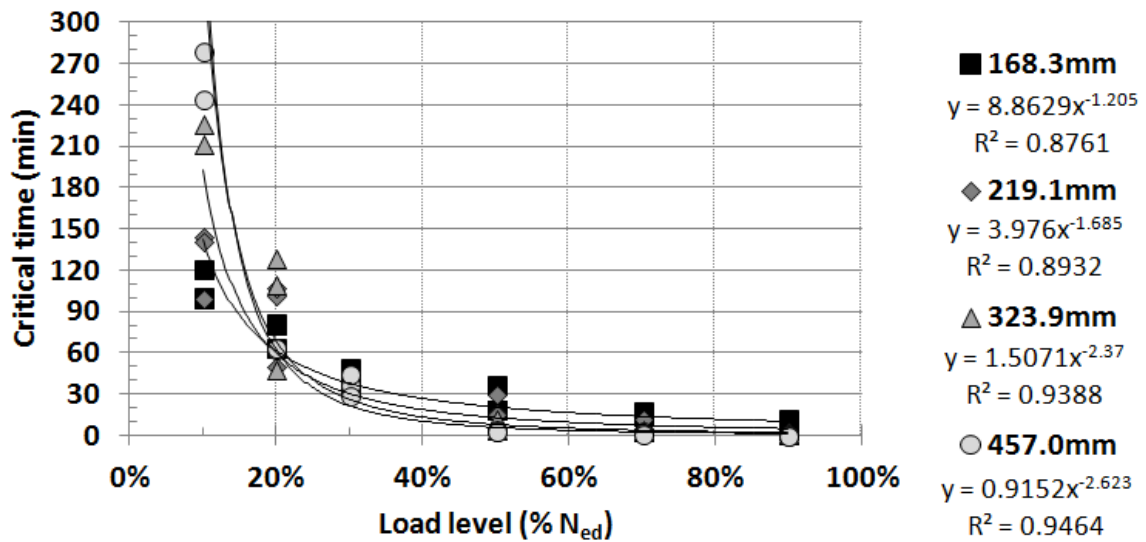


Figure 5.8 – Critical times arising from the CFCH load level

$$t_{cr} = \begin{cases} 8.8629 \eta^{-1.205} & \text{if } d = 168.3\text{mm} \\ 3.9760 \eta^{-1.685} & \text{if } d = 219.1\text{mm} \\ 1.5071 \eta^{-2.370} & \text{if } d = 323.9\text{mm} \\ 0.9152 \eta^{-2.623} & \text{if } d = 457.0\text{mm} \end{cases} \quad (5.4)$$

### 5.3 Comparison with simple methods of EN1994-1-2 (2005)

In Chapter 2 two simple methods for assessing the structural behaviour of CFCH columns under fire were presented. They are: the tabulated data method and the simple calculation model (SCM) both presented in EN1994-1-2 (2005). A comparison of both methods with the experimental and numerical results obtained for similar columns will be presented in what follows.

#### 5.3.1 Tabulated data method

Table 4.7 of EN1994-1-2 (2005) prescribes minimum cross-sectional dimensions, minimum reinforcement ratios and minimum axis distance for reinforcing bars of CFCH columns to reach a standard fire resistance according to their load levels  $\eta$ .

Table 5.1 presents the standard fire resistance, according to Table 4.7 of EN1994-1-2 (2005), and the experimental critical time of eight CFCH columns presented in Chapter 3. Figure 5.9 plots these values. The other tested columns could not be classified in accordance with the standard fire resistance (*i.e.* they have fire resistance under 30min) and thus a comparison was not possible for these cases. In fact, the load level applied in the tests was slightly higher than the limits prescribed by the code and a 2% tolerance was considered to enable comparison.

Table 5.1 – Standard fire resistance and critical times for CFCH columns

<i>CFCH columns</i>	<i>Standard Fire resistance</i>	<i>Critical Time <math>t_{cr}</math> (min)</i>
<b>Cross-section diameter: <math>d = 168.3\text{mm}</math> Reinforcement ratio: <math>\rho = 0.0\%</math> Distance of reinforcing axis bars: <math>u_s = 30\text{mm}</math></b>	R30	26 – 27
<b>Cross-section diameter: <math>d = 219.1\text{mm}</math> Reinforcement ratio: <math>\rho = 0.0\%</math> Distance of reinforcing axis bars: <math>u_s = 30\text{mm}</math></b>	R30	21 – 27
<b>Cross-section diameter: <math>d = 168.3\text{mm}</math> Reinforcement ratio: <math>\rho = 2.5\%</math> Distance of reinforcing axis bars: <math>u_s = 30\text{mm}</math></b>	R30	30 – 31
<b>Cross-section diameter: <math>d = 219.1\text{mm}</math> Reinforcement ratio: <math>\rho = 2.2\%</math> Distance of reinforcing axis bars: <math>u_s = 30\text{mm}</math></b>	R60	43 – 46

Three columns with a diameter of 219.1mm are in the unsafe zone (*i.e.* they have critical times lower than the standard fire resistance) and lie outside the 5min tolerance line. Two columns with a diameter of 168.3 mm are in the unsafe zone and the other two columns are close to the limit of the safe zone.

Figure 5.10 plots the standard fire resistance of the columns versus their critical time as evaluated in numerical simulations. Some columns, especially the larger columns with diameters of 323.9 and 457.0mm, presented critical times lower than the tabulated standard fire resistance, so they are positioned in the unsafe zone.

These results suggest that the tabulated data method may be slightly unsafe especially for larger columns.

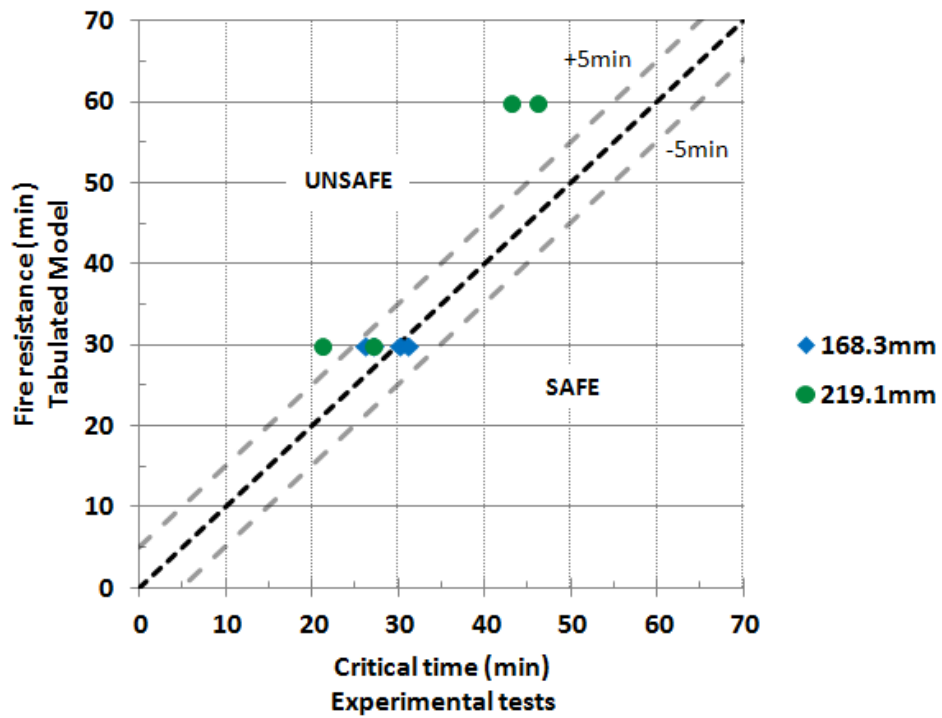


Figure 5.9 – Tabulated method vs. experimental critical time of CFCH columns

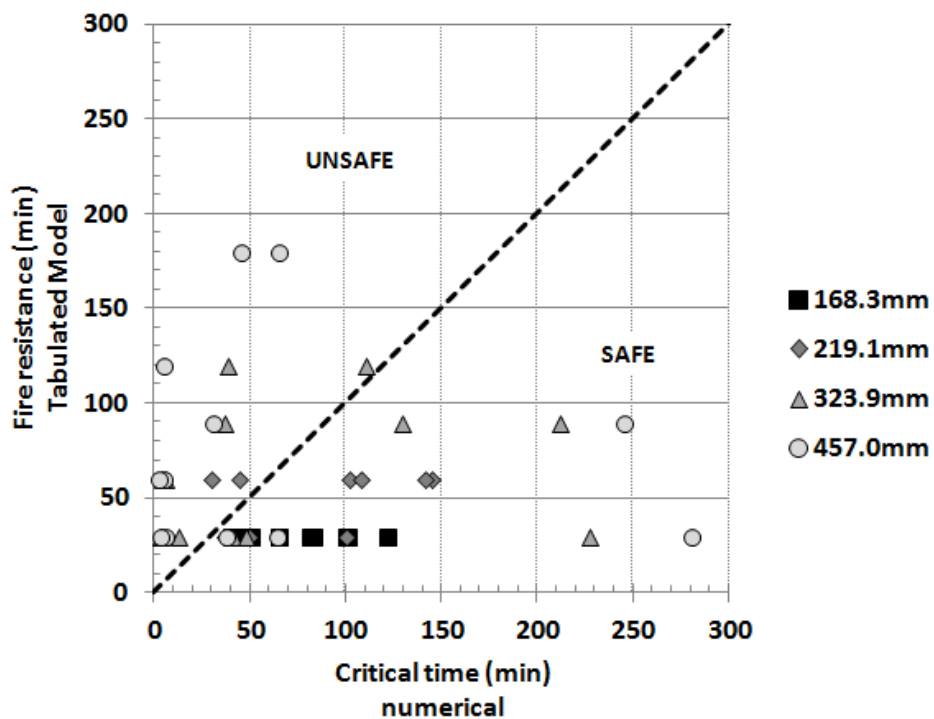


Figure 5.10 – Tabulated method vs. numerical study of the critical time of the CFCH columns

Figure 5.11 plots the results obtained by the simplified equations versus the experimental tests. The columns approximated to the safe zone. The columns with a diameter of 168.3mm and one with a diameter of 219.1 are slightly within the unsafe zone but on the 5min tolerance line.

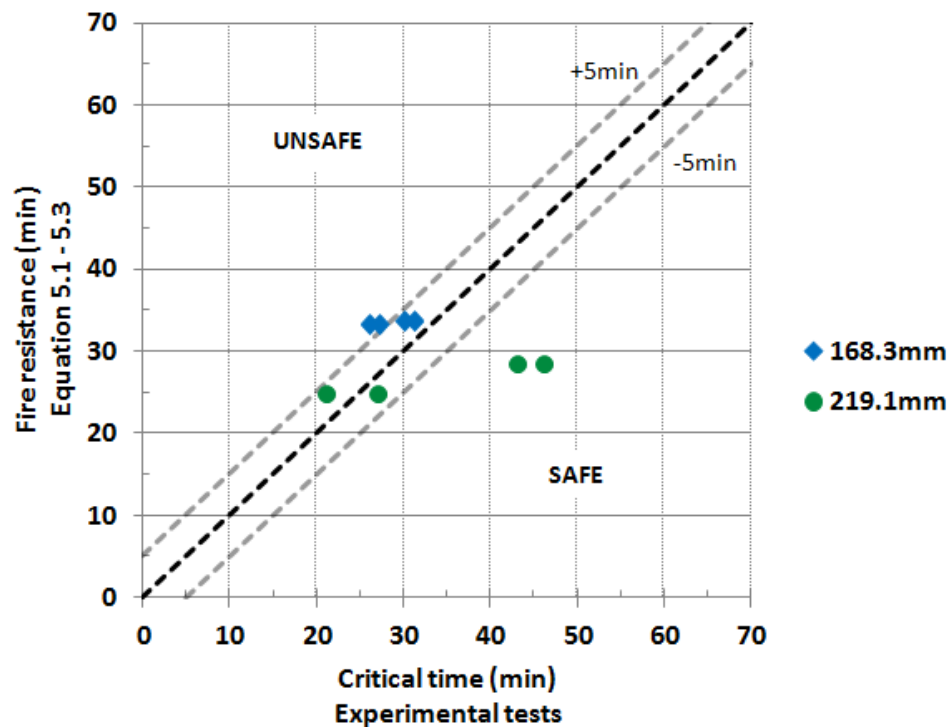


Figure 5.11 – Simplified equations vs. experimental critical time of the CFCH columns

### 5.3.2 Simple Calculation Model

EN1994-1-2 (2005) presents a simple calculation model (SCM) to determine the design value of the resistance of a CFCH column in axial compression and in the fire situation. This method was discussed in Chapter 2.

Figure 5.12 to Figure 5.15 show the critical times obtained by the SCM, in experimental tests (load level of 30% and 70%) and in simplified equations (load level between 10% and 90%) for similar CFCH columns.

The temperatures measured of the columns in experimental tests were used as the first step of the simple calculation model (SMC). In the second step, the design axial buckling load  $N_{fi,Rd}$  was normalized by the design value of the buckling load at room temperature  $N_{b,Rd}$  in order to



make the comparison for each load level  $\eta$  possible. The partial material safety factor in fire design was 1.0.

Figure 5.12 to Figure 5.15 also show that the simple calculation model for fire resistance gives smaller results for critical times than those obtained with experimental tests and numerical simulations. This suggests that the simple calculation model is conservative when evaluating the design value of the resistance of a CFCH column in a fire situation

The implementation of the SCM is not a straightforward task. In addition to not proposing a simple mathematical model for heat transfer problem, it requires an incremental solution for the mechanical problem. It can be concluded that the simplified equations proposed can be a viable alternative to determine critical times instead of using SCM as shown by Figure 5.12 to Figure 5.15.

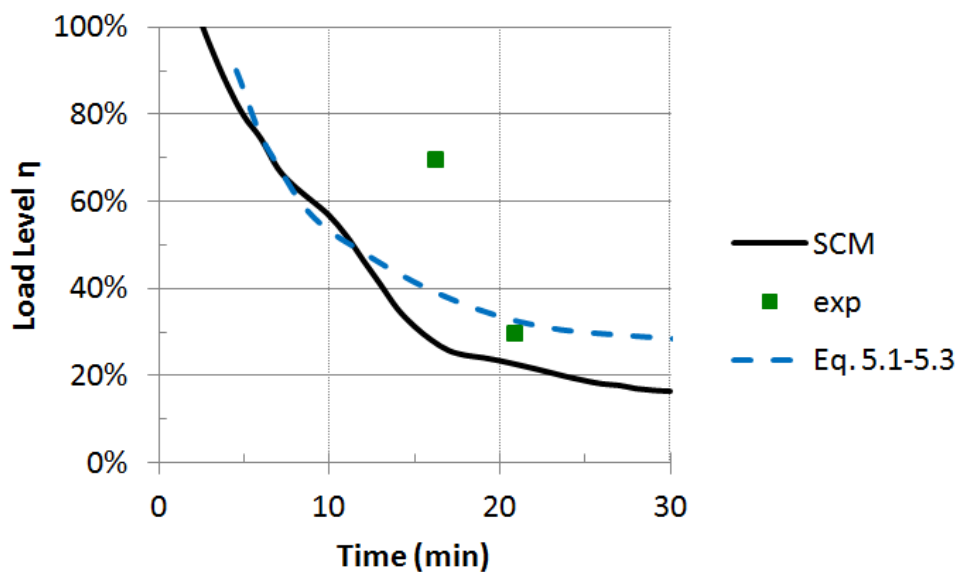


Figure 5.12 – Critical times for SMC, experimental tests and simplified equation for a CFCH-PC column total filled which has a diameter of 219.1mm

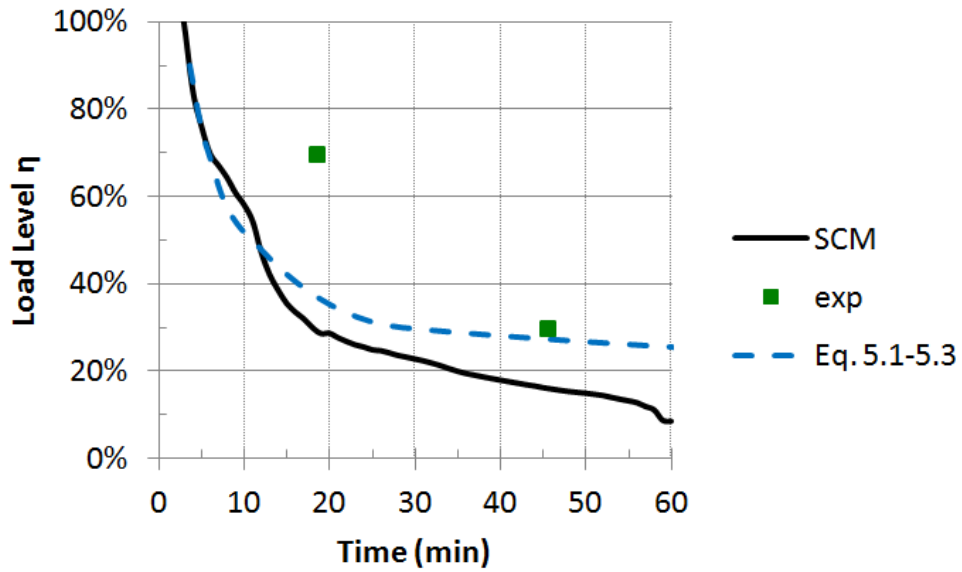


Figure 5.13 – Critical times for SMC, experimental tests and simplified equation for a CFCH-RC column total filled which has a diameter of 219.1mm

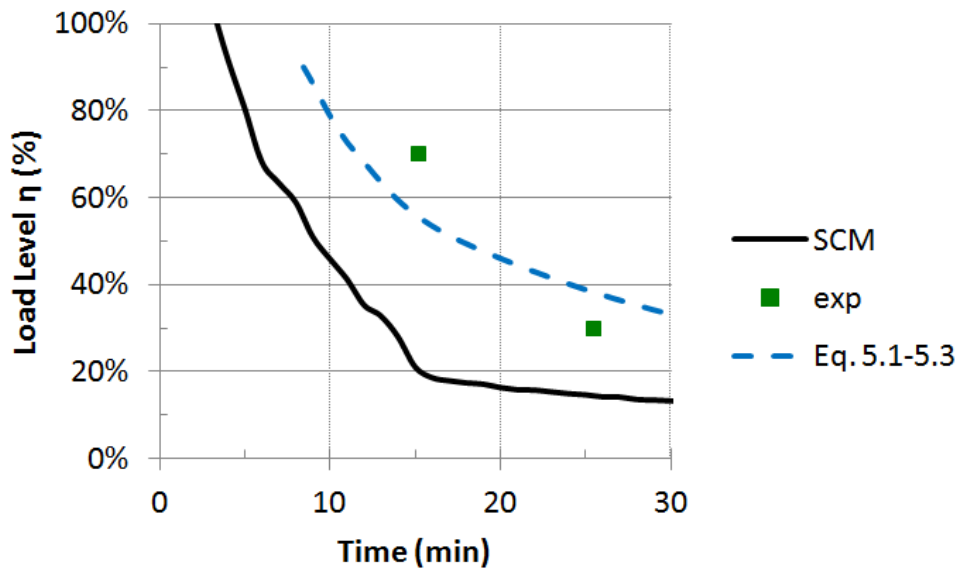


Figure 5.14 – Critical times for SMC, experimental tests and simplified equation for a CFCH-PC column total filled which has a diameter of 168.3mm

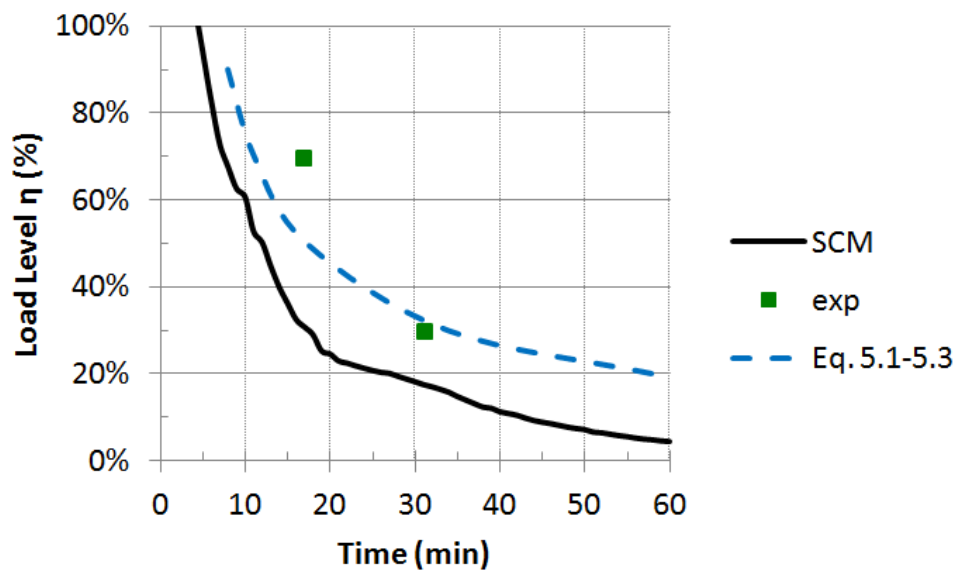


Figure 5.15 – Critical times for SMC, experimental tests and simplified equation for a CFCH-RC column total filled which has a diameter of 168.3mm

#### 5.4 Chapter remarks

This chapter presented a numerical study about the fire performance of CFCH columns. The numerical simulations were carried out in a three-dimensional nonlinear finite element model developed in ABAQUS (2011). The parameters studied were: load level (10%, 20%, 30%, 50%, 70% and 90%  $N_{ed}$ ), column diameter (168.3mm, 219.1mm, 323.9mm and 457mm) and reinforcement ratio with reinforcing steel bars (0% – without reinforcement, 3% and 6%). Ranges outside these values have less practical meaning.

Based on numerical data, simplified equations were proposed for design of CFCH columns. In addition, a comparison with the simple calculation methods from EN1994-1-2 (2005) was presented.

In accordance with the numerical results it can be said:

- The higher the load level, the lower the critical time is;
- The larger the diameter of the columns, the greater its critical time for low load levels. For higher load levels the same was not observed;

- Increasing the in diameter of the columns, while keeping the thickness of the tube wall constant, increases the number of cases of local buckling;
- The ratio of steel reinforcement does not justify great increases in critical times;

The following remarks may be also addressed:

- The tabulated data method was shown to be slightly unsafe when compared to the results obtained in experimental and numerical simulations, especially for larger columns;
- The SCM leads to safe results in comparison with the numerical simulations and experimental tests;
- The simplified equations proposed can be a viable alternative to determine critical times instead of using SCM and principally the tabulated method.

---

## 6. CONCLUSIONS

In the last ten years or so Concrete Filled Circular Hollow (CFCH) columns have become popular principally in high-rise and industrial buildings as a proper solution for fire situations. Advantages such as their having a higher load-bearing capacity and seismic resistance; an attractive appearance; being slender; and the construction process being less time-consuming and at reduced cost justify this choice.

Despite several studies on fire resistance of CFCH columns (*e.g.* the NRCC tests – summarized in Kodur, 1999, Han *et al.*, 2003a and 2003b, Ding and Wang, 2008, Hong and Varma, 2009, Schaumann *et al.*, 2009, and Espinos *et al.*, 2010) their mechanical behaviour in a fire situation is not completely understood. Most of these studies did not consider columns with restrained thermal elongation, which is an important parameter for the columns' response to fire especially when considering the stiffness of the surrounding structure connected to the columns (Ali *et al.*, 1998, Valente and Neves, 1999, Rodrigues *et al.*, 2000, and Neves *et al.*, 2002).

This thesis presented the results of a series of forty fire resistance tests conducted on circular CFCH columns with restrained axial and rotational thermal displacements. The columns were filled with plain concrete (CFCH-PC) and reinforced concrete (CFCH-RC). Relevant parameters that have considerable influence on the fire resistance of the columns were tested. They are: the slenderness and cross-sectional external diameter of the column; its load level; the stiffness of the surrounding structure which imposes restraints on the thermal elongation of the column; the ratio of steel bar reinforcement; and the degree of concrete filling inside the column. Circular Hollow Sections (CHS) columns (*i.e.* steel columns) were also tested for comparison.

A three-dimensional non-linear finite element model developed in ABAQUS (2011) to predict the behaviour of these columns was studied in order to verify its most relevant parameters, and took the restraints of columns to their thermal elongation into account. This adds a rather difficult step to the analysis of the problem. The numerical model was validated in a comparison with the results of the experimental fire tests.

The study of the behaviour, in a fire, of CFCH columns with restrained thermal elongation was complemented with the development of a parametric study. A range of practical values of the load level, the diameter of the column and the ratio of reinforcement was studied. Based on numerical data, simplified equations to evaluate the critical time of CFCH columns with restrained thermal elongation were proposed.

In addition, a comparison between experimental results and the set of simplified equations proposed is presented using the tabulated and the simple calculation methods proposed by EN1994-1-2 (2005). This is done in order to verify the ability of these methods to assess the structural behaviour in a fire of the CFCH columns with axial and rotational restraints to thermal elongation.

The main conclusions from this research are commented on in what follows.

### ***State of the art***

- Few experimental results from tests conducted with CFH columns subjected to fire can be found in the literature, especially those with massive columns. There is much less data available on taking into account the influence of the stiffness of the surrounding structure;
- Significant differences can be identified in general experimental procedures (*e.g.* failure criterion, heating rate) and in important test parameters (*e.g.* load level, restraint level and end conditions). This fact hampers comparisons and induces differences in the test results;
- Numerical models also presented some important differences (*e.g.* the thermal and mechanical properties of steel and concrete, and the thermo-mechanical behaviour in the steel tube-concrete core interface). The numerical modelling of the behaviour of concrete at high temperatures still requires further experiments for massive CFH columns;
- Few numerical models simulate the restraints on thermal elongation imposed by the surrounding structure;
- Most experimental research studies were performed on CFH columns with low load levels and smaller external diameters. Consequently, several numerical models were validated based on these situations;

### ***Experimental tests***

- The critical times of the CFCH columns tested in this research were smaller than those registered by the NRCC researchers for similar experimental tests – however without restraining their thermal elongation;
- Increasing the stiffness of the surrounding structure did not lead to major changes in the critical times of the columns;

- 
- The load level and slenderness of the columns had a great influence on the critical time of the columns. If one of them is reduced, the column critical time increases;
  - Concrete filling improves the behaviour of CFCH columns when subjected to fire, but the use of a concrete ring does not seem to be a good solution;
  - Increasing the stiffness of the surrounding structure leads to an increase in the restraining forces of the columns, although this did not influence the critical time;
  - Increasing the stiffness of the surrounding structure or the load level reduces the axial deformation of the columns;
  - CHS columns (*i.e.* steel columns) presented a greater axial deformation than CFCH columns.
  - The main failure mode of the columns was global buckling. However in several cases local buckling also occurred, although the columns presented a diameter-thickness ratio ( $d/e$ ) smaller than 59;

#### ***Numerical model***

- The proposed numerical model presented results in close agreement with those obtained in fire experiments conducted with thermal elongation restrained CFCH columns. Therefore, numerical modelling can be considered as an option to assess the fire performance of CFHS columns;
- The numerical critical times obtained were slightly higher than the experimental ones. However, in most cases, this difference was not large, less than 5 minutes;
- The temperatures calculated with the numerical model were slightly lower than those measured in experimental tests;
- The numerical relative restraining forces obtained were in close agreement with those measured in the experiments. In general, the error was less than 10%;
- In general, the numerical axial deformations were higher than the experimental results. However, in most cases this difference was less than 5mm, which is negligible given the length of the columns.

#### ***Numerical analysis***

- The ratio of steel reinforcement does not justify great increases in critical times;

- The set of simplified equations proposed is a viable alternative for assessing the critical times of CFCH columns;
- The tabulated data method was shown to be slightly unsafe when compared to the results obtained in experimental and numerical simulations especially for larger columns;
- The SCM leads to safe results in comparison with the numerical simulations and experimental tests;

#### ***Future studies***

- Experimental tests may include other parameters such as end conditions (pinned-pinned, pinned-fixed and fixed-fixed) and thickness of the steel tube wall;
- Experimental tests should be conducted with CFH columns including other variables, such as: larger diameters, higher slenderness, other cross-section shapes (square, rectangular and elliptical) and eccentricity of applied load. Always considering the restraint to thermal elongation;
- Advances in the mathematical model to represent the concrete behaviour at high temperatures should be addressed, considering, for example, the migration of water during the heating (*i.e.* thermo-chemo-hydro-mechanical models);
- Parametric studies should be conducted, thus widening the numerical database. Therefore, a non-linear multivariate regression analysis should be planned to obtain approximated equations to evaluate the critical times of CFH columns of greater reliability, including also other parameters that influence the fire resistance of the columns;
- Further research studies are still required to focus on the failure mode (buckling of the columns) and its influence on fire performance.



---

## REFERENCES

- ABAQUS/standard version 6.11 user's manual*. (2011). Vol. I-III. Pawtucket, Rhode Island: Hibbit, Karlsson & Srenson, Inc., USA.
- Ali, F.A., Shepherd, A., Randall, M., Simms, I.W., O'Connor, D.J. and Burgess I. (1998). "The effect of axial restraint on the fire resistance of steel columns". *Journal of Constructional Steel Research*, vol. 46, n° 1-3, pp. 305-306.
- ASTM E119 (2012). "Standard test methods for fire tests of building construction and materials". American Society for Testing and Materials International, West Conshohocken, PA, USA.
- Buchanan, A.H. (2001). "*Structural design for fire safety*". John Wiley & Sons Ltd, University of Canterbury, New Zealand.
- Chabot, M. and Lie, T.T. (1992). "Experimental Studies on the fire resistance of hollow steel columns filled with bar-reinforced concrete". *Internal Report N° 628, Institute for Research in Construction, National Research Council of Canada, Ottawa*.
- Correia, A.M., Pires, T.A.C., Rodrigues, J.P.C., (2010) "Behaviour of Steel Columns Subjected to Fire". *In: Sixth International Seminar on Fire and Explosion Hazards*. pp. 879-890, United Kingdom.
- Correia, A.J.P.M. and Rodrigues, J.P.C. (2011). "Fire resistance of partially encased steel columns with restrained thermal elongation". *Journal of Constructional Steel Research*, vol. 67, pp. 593-601.
- Correia, A.M., Pires, T.A.C., Rodrigues, J.P.C., (2011) "Análise Experimental do comportamento ao Fogo de Pilares Mistos de Aço e Betão". *In: VIII Congresso de Construção Metálica e Mista*. V. 1. p. II-77-II-86, Portugal.
- Correia, A.J.P.M. and Rodrigues, J.P.C. (2012). "Fire resistance of steel columns with restrained thermal elongation". *Fire Safety Journal*, vol. 50, pp. 1-11.
- Cox, G. (1996). "*Combustion Fundamentals of Fire*". Academic Press Inc, San Diego, USA.
- CAN/ULC-S101 (1989). "Standard Methods of Fire Endurance Tests of Building Construction and Materials". Underwriters' Laboratories of Canada, Canada.
- CSA A23.3-M04 (1994). "Code for the design of Concrete Structures for Buildings". Canadian Standards Association, Canada.
- CSA S16.1 (2001). "Limit States Design of Steel Structures". Canadian Standards Association, Canada.
- Department for Communities and Local Government (2012). "*Fire Statistics – Great Britain – 2011 to 2012*", London, UK.

- Ding, J. and Wang, Y.C. (2008). "Realistic modeling of thermal and structural behavior of unprotected concrete filled tubular columns in fire". *Journal of Constructional Steel Research*, vol. 64, pp.1086-1102.
- Drysdale, D. (1998). "An introduction to fire dynamics". 2nd ed. John Wiley & Sons Ltd., University of Edinburgh, UK.
- EN 1991-1-2 (2002). "EUROCODE 1: Actions on Structures. Part 1-2: General Actions – Actions on Structures Exposed to Fire". European Committee for Standardization, Belgium.
- EN 197-1 (2001). "Cement. Part 1: Composition, specifications and conformity criteria for common cements". European Committee for Standardization, Belgium.
- EN 10080 (2005). "Steel for the reinforcement of concrete - Weldable reinforcing steel - General". European Committee for Standardization, Belgium.
- EN 1992-1-2 (2004). "EUROCODE 2: Design of Concrete Structures. Part 1-2: General Rules – structural fire design European Committee for Standardization, Belgium.
- EN 1993-1-2 (2005). "EUROCODE 3: Design of Steel Structures. Part 1-2: General Rules – Structural Fire Design". European Committee for Standardization, Belgium.
- EN 1994-1-1 (2005). "EUROCODE 4: Design of composite steel and concrete structures. Part 1-1: general rules and rules for buildings". European Committee for Standardization, Belgium.
- EN 1994-1-2 (2005). "EUROCODE 4: Design of composite steel and concrete structures. Part 1-2: general rules – structural fire design". European Committee for Standardization, Belgium.
- EN 206-1 (2007). "Concrete. Part 1: Specification, performance, production and conformity". European Committee for Standardization, Belgium.
- EN 1995-1-2 (2004). "EUROCODE 5: Design of Timber Structures. Part 1.2: General Rules – Structural Fire Design". European Committee for Standardization, Belgium.
- EN 1996-1-2 (2005). "EUROCODE 6: Design of Masonry Structures. Part 1.2: General Rules – Structural Fire Design". European Committee for Standardization, Belgium.
- EN 1999-1-2 (2007). "EUROCODE 9: Design of Aluminium Alloy Structures. Part 1.2: General Rules – Structural Fire Design". European Committee for Standardization, Belgium.
- Espinos, A., Romero, M.L. and Hospitaler, A. (2010). "Advanced model for predicting the fire response of concrete filled tubular columns". *Journal of Constructional Steel Research*, vol. 66, pp.1030-1046.
- Fitzgerald, R. W. (2003). "Building fire performance analysis – a way of thinking". Vol. 3. Center for fire safety studies, Worcester Polytechnic, USA.

- Hall Jr., J.R. (2005). “*The total cost of fire in the United States*”. National Fire Protection Association, Quincy, MA, USA.
- Han, L.H. (2001). “Fire performance of concrete filled steel tubular beam-columns”. *Journal of Constructional Steel Research*, vol. 57, pp. 695-709.
- Han, L.H., Yang, Y.F., Yang, H. and Huo, J.S. (2002). “Residual strength of concrete-filled RHS columns after exposure to the ISO834 standard fire”. *Thin-Walled Structures*, vol. 40, pp. 991-1012.
- Han, L.H. and Huo, J.S. (2003). “Concrete-filled hollow structural steel columns after exposure to ISO-834 fire standard”. *Journal of Structural Engineering*, vol.129, n°1, pp. 68-78.
- Han, L.H., Yang, Y.F. and Xu, L. (2003a). “An experimental study and calculation on the fire resistance of concrete-filled SHS and RHS columns”. *Journal of Constructional Steel Research*, vol. 59, pp. 427-452.
- Han, L.H., Zhao, X.L., Yang, Y.F., and Feng, J.B. (2003b). “Experimental study and calculation of fire resistance of concrete-filled hollow steel columns”. *Journal of Structural Engineering*, vol. 129, n° 3, pp.346-356.
- Han, L.H., Huo, J.S. and Wang, Y.C. (2005). “Compressive and flexural behavior of concrete filled steel tubes after exposure to standard fire”. *Journal of Constructional Steel Research*, vol. 61, pp.882-901.
- Hong, S. and Varma, A.H. (2009). “Analytical modeling of the standard fire behavior of loaded CFT columns”. *Journal of Constructional Steel Research*, vol. 65, pp.54-69.
- ISO834-1 (1999). “Fire resistance tests-elements – elements of building construction – Part 1 General requirements.” International Organization for Standardization, Switzerland.
- Kodur, V.K.R. and Lie, T.T. (1995). “Experimental studies on the fire resistance of circular hollow steel columns filled with steel-fibre-reinforced concrete”. *Internal Report N° 691, Institute for Research in Construction, National Research Council of Canada, Ottawa.*
- Kodur, V.K.R. and Lie, T.T. (1996). “Experimental studies on the fire resistance of square hollow steel columns filled with steel-fibre-reinforced concrete”. *Internal Report N° 662, Institute for Research in Construction, National Research Council of Canada, Ottawa.*
- Kodur, V.K.R. and Lie, T.T. (1996-b). “Fire resistance of circular steel columns filled with fiber-reinforced concrete”. *Journal of Structural Engineering*, vol. 122, n° 7, pp. 776-782.
- Kodur, V.K.R. (1998). “Design equations for evaluating fire resistance of SFRC-filled HSS columns”. *Journal of Structural Engineering*, vol. 124, N° 6, pp. 671-677.

- Kodur, V.K.R. (1999). "Performance-based fire resistance design of concrete-filled steel columns". *Journal of Constructional Steel Research*, vol. 51, pp. 21-36.
- Lie, T.T. and Chabot, M. (1990). "A method to predict the fire resistance of circular concrete filled hollow steel columns". *Journal of Fire Protection Engineering*, 2 (4), pp. 111-126.
- Lie, T.T., Chabot, M. and Irwin, R.J. (1992). "Fire resistance of circular hollow steel sections filled with bar-reinforced concrete". *Internal Report N° 636, Institute for Research in Construction, National Research Council of Canada, Ottawa.*
- Lie, T.T. and Irwin R.J. (1992). "Fire resistance of rectangular hollow steel sections filled with bar-reinforced concrete". *Internal report N° 631, Institute for Research in Construction, National Research Council of Canada, Ottawa.*
- Lie, T.T. and Chabot, M. (1992). "Experimental Studies on the Fire Resistance of Hollow Steel Columns Filled with Plain Concrete". *Internal Report N° 611, Institute for Research in Construction, National Research Council of Canada, Ottawa.*
- Lie, T.T. (1994) "Fire resistance of circular steel columns filled with bar-reinforced concrete", *Journal of Structural Engineering*, vol. 120, n° 05, pp. 1489-1509.
- Lie, T.T. and Irwin, R.J. (1995) "Fire resistance of rectangular steel columns filled with bar-reinforced concrete", *Journal of Structural Engineering*, vol. 121, n° 05, pp. 797-805.
- Lie, T.T. and Kodur, V.K.R. (1996). "Fire resistance of steel columns filled with bar-reinforced concrete". *Journal of Structural Engineering*, vol. 122, n° 1, pp. 30-36.
- Lu, H., Zhao, X. and Han, L. (2009). "Fire behavior of high strength self-consolidating concrete filled steel tubular stub columns". *Journal of Constructional Steel Research*, 65 (10-11), pp. 1995-2010.
- Lu, H., Han, L. and Zhao, X.L. (2010). "Fire performance of self-consolidating concrete filled double skin steel tubular columns: Experiments". *Fire Safety Journal*, 45, pp. 106-115.
- Moller, K. (2001). "*The socio-economic costs of fire in Denmark*". Emergency Management Agency, Bikerod, Denmark.
- Neves, I.C., Valente, J.C. and Rodrigues, J.P.C. (2002). "Thermal restraint and fire resistance of columns". *Fire Safety Journal*, vol. 37, pp. 753-771.
- Pires, T.A.C, Rodrigues, J.P.C., Rêgo Silva, J.J., (2010) "Buckling of concrete filled steel hollow columns in case of fire". In: *International Colloquium on Stability and Ductility of Steel Structures*, V. 1., pp 481-488, Brazil.
- Pires, T.A.C, Rodrigues, J.P.C., Rêgo Silva, J.J., Correia, A.M., (2010). "Concrete filled steel hollow columns subjected to fire". In: *International Symposium Steel Structures: Culture & Sustainability*, pp 427-436, Turkey.

- Pires, T.A.C, Duarte, D.C., Rêgo Silva, J.J., Rodrigues, J.P.C. (2010) “Resistência Mecânica Residual de Vigas em Concreto Armado Após Incêndio”. *In: Encontro Nacional sobre Conservação e Reabilitação de Estruturas*.
- Pires, T.A.C, Rodrigues, J.P.C., Rêgo Silva, J.J., Correia, A.M., (2011) “Flambagem de Pilares Tubulares preenchidos com Concreto em Situação de Incêndio”. *In: 2as Jornadas de Segurança aos Incêndios Urbanos. Vol. 1. pp. 147-155, Portugal*.
- Pires, T.A.C, Rodrigues, J.P.C., Rêgo Silva, J.J., Correia, A.M., (2011) “Pilares Circulares em Aço preenchidos por Concreto sujeito à Incêndio”. *In: 1º Congresso Ibero-Latino-Americano em Segurança Contra Incêndio, Brazil*.
- Pires, T.A.C, Rodrigues, J.P.C., Rêgo Silva, J.J., Correia, A.M., (2011) “CHS and Partially Encased Columns Subjected to Fire”. *In: 6th European Conference on Steel and Composite Structures, Vol. B. pp. 1569-1574, Hungary*.
- Pires, T.A.C, Rodrigues, J.P.C., Rêgo Silva, J.J. (2012a). “Fire resistance of concrete filled circular hollow columns with restrained thermal elongation”. *Journal of Constructional Steel Research*, vol. 77, pp. 82-94.
- Pires, T.A.C, Rodrigues, J.P.C., Rêgo Silva, J.J., Correia A.M. (2012b). “Fire resistance tests on concrete filled hollow columns”. *In: 15th International Conference on Experimental Mechanics - ICEM15, Portugal*.
- Pires, T.A.C, Rodrigues, J.P.C., Rêgo Silva, J.J.(2013) “Numerical Assessment of the Fire Resistance of Tubular Steel Columns Filled with Concrete”. *In: Design Fabrication and Economy of Metal Structures, Hungary*.
- Pires, T.A.C, Rodrigues, J.P.C., Rêgo Silva, J.J. (2013). “Numerical and experimental analysis of concrete filled steel hollow columns subjected to fire”. *In: 13th International Conference and Exhibition on Fire Science and Engineering - INTERFLAM2013, pp. 606-610, United Kingdom*.
- Pires, T.A.C, Rodrigues, J.P.C., Rêgo Silva, J.J. (2013) “Simulação Numérica de Pilares Tubulares em Aço preenchidos por Concreto Sujeito à Incêndios”. *In: Congresso Ibero-Latino-Americano sobre Segurança contra Incêndio - 2º CILASCI, pp.169-176, Portugal*.
- Pires, T.A.C, Duarte, D.C., Rêgo Silva, J.J., Rodrigues, J.P.C. (2013) “Resistência Residual de Vigas em Concreto Armado Após Incêndio”. *In: Congresso Ibero-Latino-Americano sobre Segurança contra Incêndio - 2º CILASCI, pp. 311-322, Portugal*.
- Pires, T.A.C, Rodrigues, J.P.C., Rêgo Silva, J.J., Garcia, I. (2013) “Estudo Paramétrico em Colunas Tubulares de Aço preenchidas com Betão em Situação de Incêndio”. *In: IX Congresso de Construção Metálica e Mista, Portugal*.
- Quintiere, J.G.(1998). “*Principles of fire behavior*”. Delmar Publishers, USA.
- Ramachandran, G. (1998). “*The Economics of Fire Protection*”. Routledge, London, UK.

- Rodrigues, J.P.C., Laím, L. and Correia, A.C. (2010). "Behaviour of fiber reinforced concrete columns in fire". *Composite structures*, vol. 92, pp.1263-1268.
- Rodrigues, J.P.C., Neves, I.C. and Valente, J.C. (2000). "Experimental research on the critical temperature of compressed steel elements with restrained thermal elongation". *Fire Safety Journal*, vol. 35, pp. 77-98.
- Rodrigues, J.P.C. (2000). "Fire resistance of steel columns with restrained thermal elongation". PhD thesis, Department of Civil Engineering of Technical University of Lisbon – Instituto Superior Técnico, Lisbon, 1 vol..
- Romero, M.L., Moliner, V., Espinos, A., Ibañez, C. and Hospitaler, A. (2011). "Fire behavior of axially loaded slender high strength concrete-filled tubular columns". *Journal of Constructional Steel Research*, vol. 67, pp.1953-1965.
- Santos, C.C., Rodrigues, J.P.C., Pires, T.A.C. (2012) "Fire resistance tests on concrete columns". In: *15th International Conference on Experimental Mechanics - ICEM15*, Portugal.
- Segurancaonline@ (2012). <http://www.segurancaonline.com/gca/?id=880>. Portal Segurança Online – Associação Portuguesa de Segurança - APSEI (homepage), Portugal.
- Schaunman, P.; Stern, J. & Bush. R. (1995). "*Total Cost of Fire in Canada: An Initial Estimate*". National of Research Council of Canada, Canada.
- Schaumann, P., Kodur, V. and Bahr, O. (2009). "Fire behaviour of hollow structural section steel columns filled with high strength concrete". *Journal of Constructional Steel Research*, vol. 65, pp.1794-1802.
- Seito, A.I., et al (2008). "*A Segurança Contra Incêndio no Brasil*". Projeto Editora, São Paulo, Brasil (in Portuguese).
- Tan, K.H. and Tang, C.Y. (2004). "Interaction model for unprotected concrete filled steel columns under standard fire conditions", *Journal of structural engineering*, 130, nº 09, pp. 1405-1413.
- Tan, K.H., Toh, W.S., Huang, Z.F. and Phng G.H. (2007). "Structural responses of restrained steel columns at elevated temperatures. Part 1: Experiments", *Engineering Structures*, 29, pp. 1641-1652.
- Technical Note N° 30 (1996). "European Recommendations for the Fire Safety of Steel Structures". Technical Committee 3 – Fire Safety of Steel Structures. European Convention for Constructional Steelwork. Elsevier Scientific Publishing Co., Netherlands.
- Teixeira, C.J.M., Rodrigues, J.P.C., Barata, P., Pires, T.A.C., (2012) "Experimental and Numerical Simulations of a natural Fire in a Compartment". In: *15th International Conference on Experimental Mechanics - ICEM15*, Portugal.

- Valente, J.C. and Neves, I.C. (1999). "Fire resistance of steel columns with elastically restrained axial elongation and bending", *Journal of Constructional Steel Research*, 52, pp. 319-331.
- Wang, Y.C. (1997). "Some considerations in the design of unprotected concrete-filled steel tubular columns under fire conditions". *Journal of Constructional Steel Research*, vol. 44, n°3, pp. 203-223.
- Wang, Y.C. (1999). "The effects of structural continuity on the fire resistance of concrete filled columns in non-sway frames". *Journal of Constructional Steel Research*, vol. 50, pp. 177-197.
- Wang, Y.C. (2000). "A simple method for calculating the fire resistance of concrete-filled CHS columns". *Journal of Constructional Steel Research*, vol. 54, pp. 365-386.
- Yin, J., Zha, X.X. and Li, L.Y. (2006). "Fire resistance of axially loaded concrete filled steel tube columns". *Journal of Constructional Steel Research*, vol. 62, pp. 723-729.

## APPENDIX A – Mechanical properties of concrete and steel at ambient temperature and other tests

### A.1 Mechanical properties of concrete at room temperature

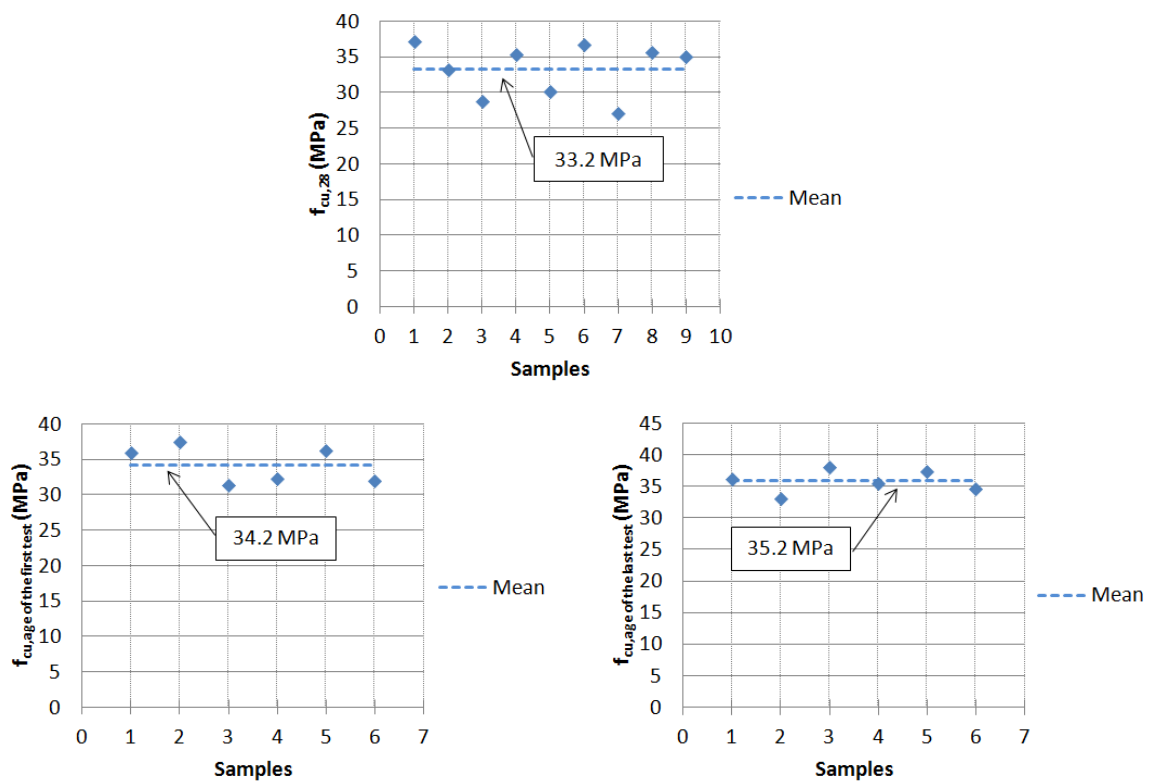


Figure A.1 – Cubic compressive strength of concrete at 28 days, in the age of the first test and in the age of the last test.



### A.2 Mechanical properties of steel at room temperature

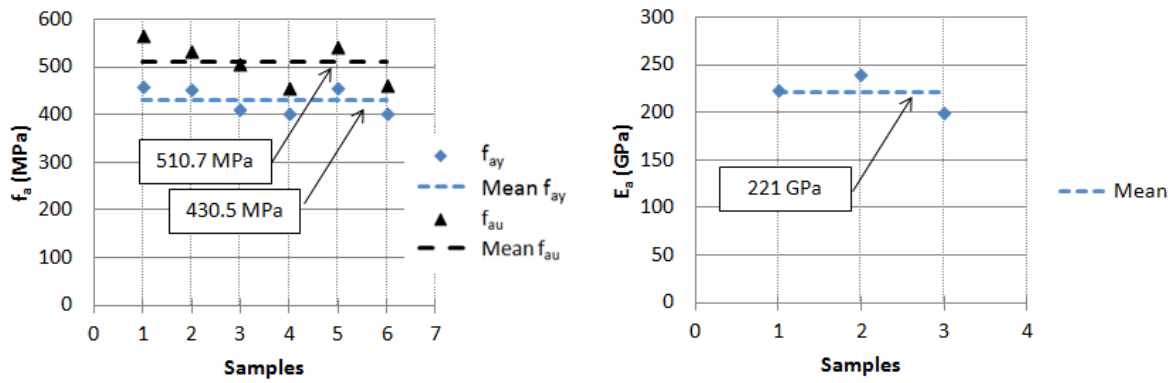


Figure A.2 – Yield strength ( $f_{ay}$ ), Ultimate strength ( $f_{au}$ ), and Modulus of Elasticity ( $E_a$ ) for the CHS steel tube with 168.9mm of diameter.

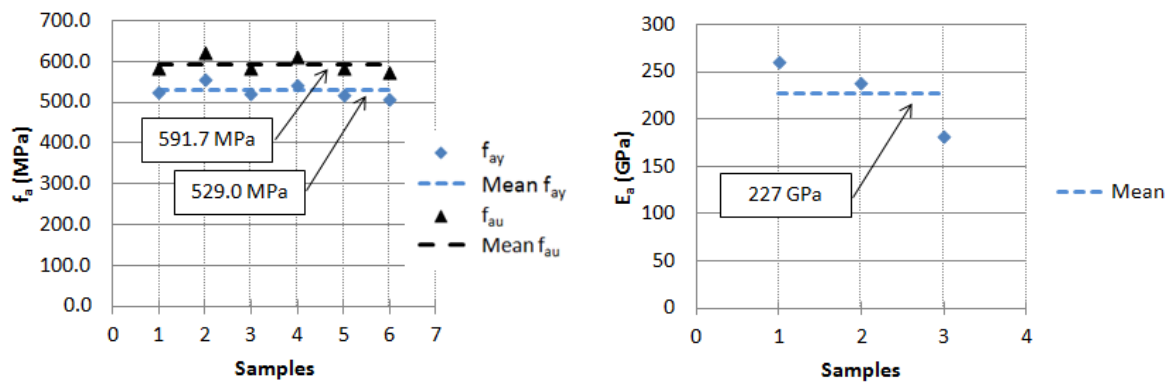


Figure A.3 – Yield strength ( $f_{ay}$ ), Ultimate strength ( $f_{au}$ ), and Modulus of Elasticity ( $E_a$ ) for the CHS steel tube with 219.1 mm of diameter.

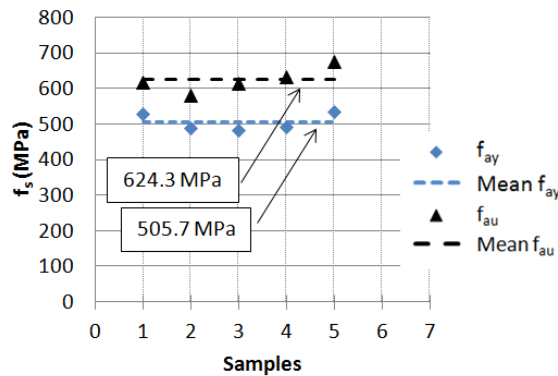


Figure A.4 – Yield strength ( $f_{sy}$ ) and Ultimate strength ( $f_{su}$ ) for the reinforcing steel bars.

### A.3 Humidity rate and density of concrete

Table A.1 – Mass variation of concrete samples along the days in the kilns.

Meas.	Sample 01		Sample 02		Sample 03		Sample 04		Sample 05		Date
	Mass (g)	$\Delta m$ (%)	Mass (g)	$\Delta m$ (%)	Mass (g)	$\Delta m$ (%)	Mass (g)	$\Delta m$ (%)	Mass (g)	$\Delta m$ (%)	
$m_0$	3642.6	-	1169.6	-	1272.4	-	145.7	-	135.0	-	-
$m_1$	3514.7	3.64	1128.7	3.62	1218.4	4.43	139.2	4.67	129.1	4.57	1st day
$m_2$	3511.7	0.09	1128.0	0.06	1217.7	0.06	139.2	0.00	129.1	0.00	4 <sup>th</sup> day
$m_3$	3509.8	0.05	1127.6	0.04	1217.3	0.03	139.2	0.00	129.1	0.00	12 <sup>th</sup> day

\*Average temperature in the kilns of 115°C

Table A.2 – Humidity and density of concrete samples.

Meas.	Sample 01	Sample 02	Sample 03	Sample 04	Sample 05	Mean
<b>Dimensions (mm)*</b>	150x150x68	150x80x45	152x74x48	75x50x17	75x51x16	-
<b>Dry mass (g)</b>	3509.8	1127.6	1217.3	139.2	129.1	-
<b>Density (kg/m<sup>3</sup>)</b>	2294.0	2088.1	2254.7	2183.5	2109.5	2186.0
<b>Humidity (%)</b>	3.78	3.72	4.53	4.67	4.57	4.25

\*Prismatic samples

### APPENDIX B – Evolution of temperatures in the tests

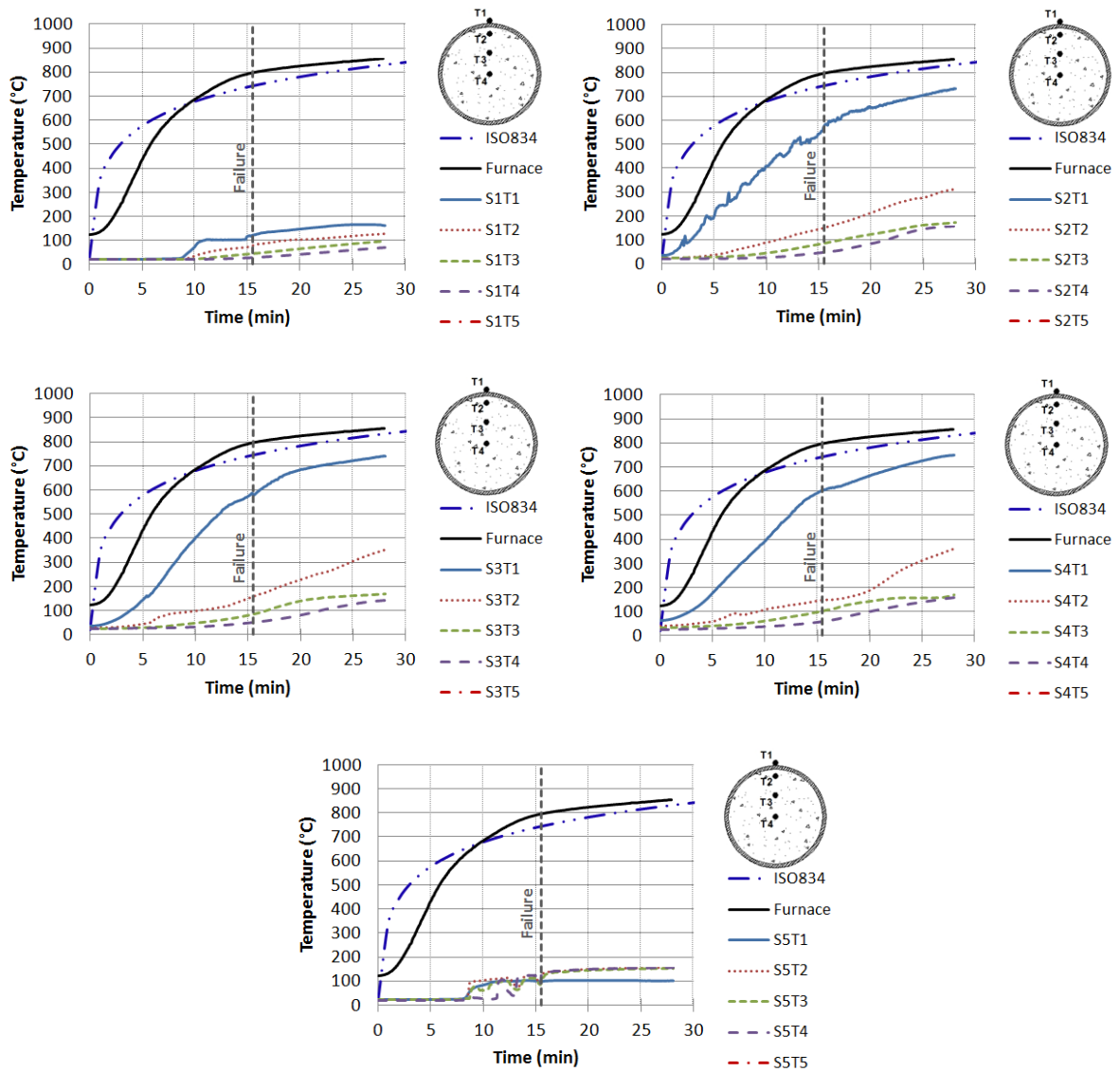


Figure B.1 – Distribution of temperature in cross-sections S1 to S5 for test column A01<sub>168-TOT-PC-70%-Klow</sub>.

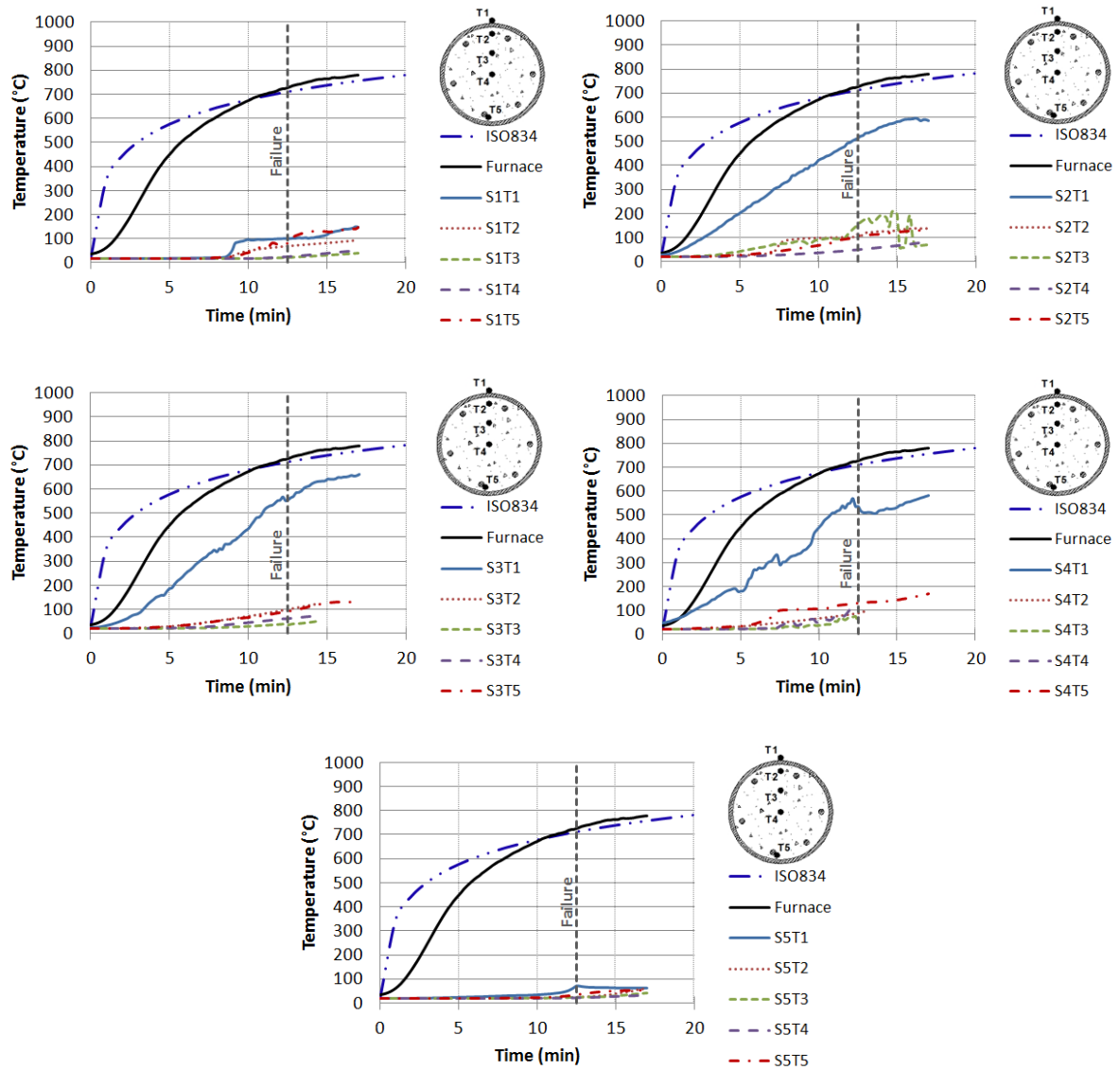


Figure B.2 – Distribution of temperature in cross-sections S1 to S5 for test column A02 168-TOT-RC-70%-Klow.

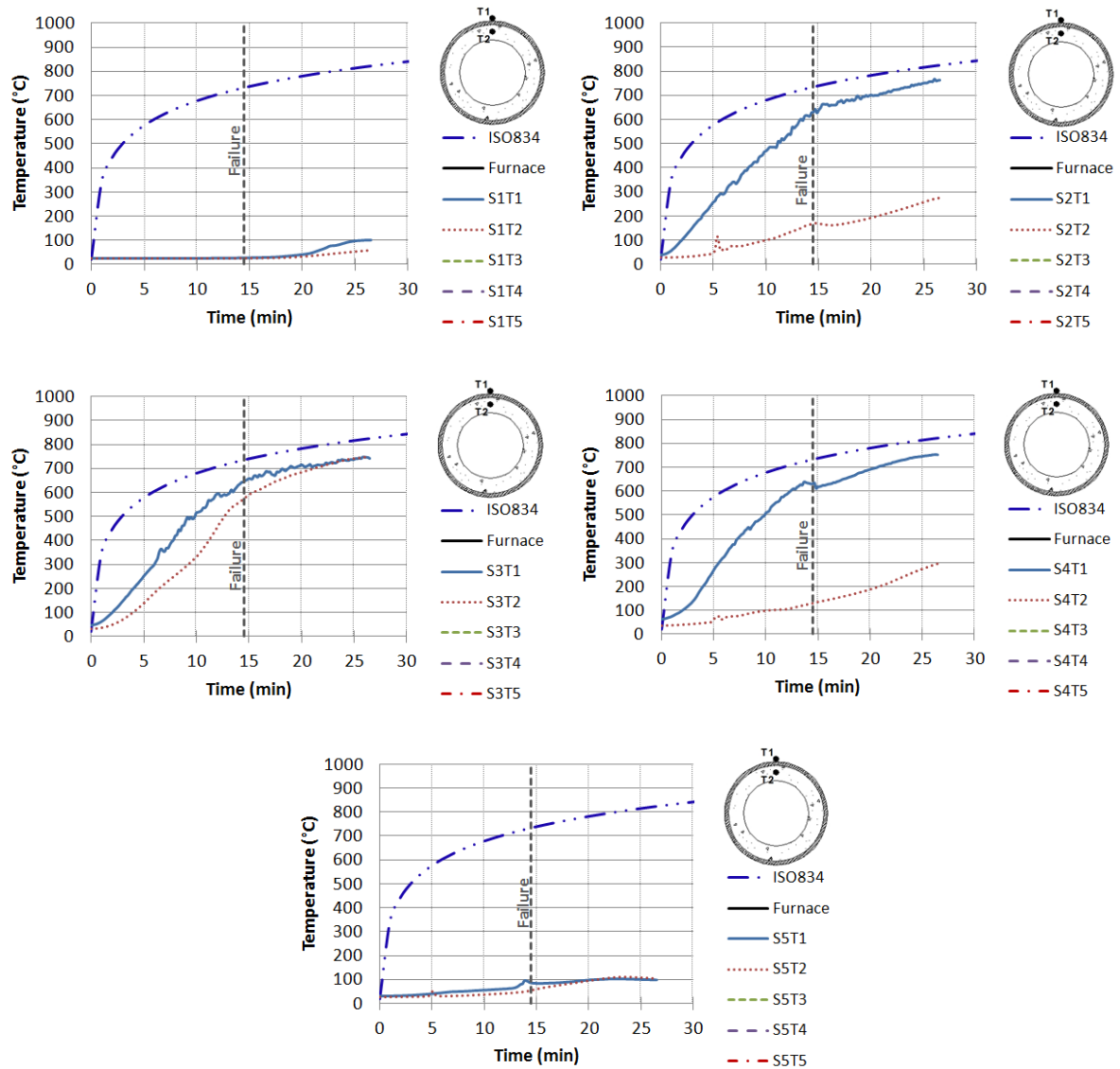


Figure B.3 – Distribution of temperature in cross-sections S1 to S5 for test column A03 168-RING-PC-70%-Klow.

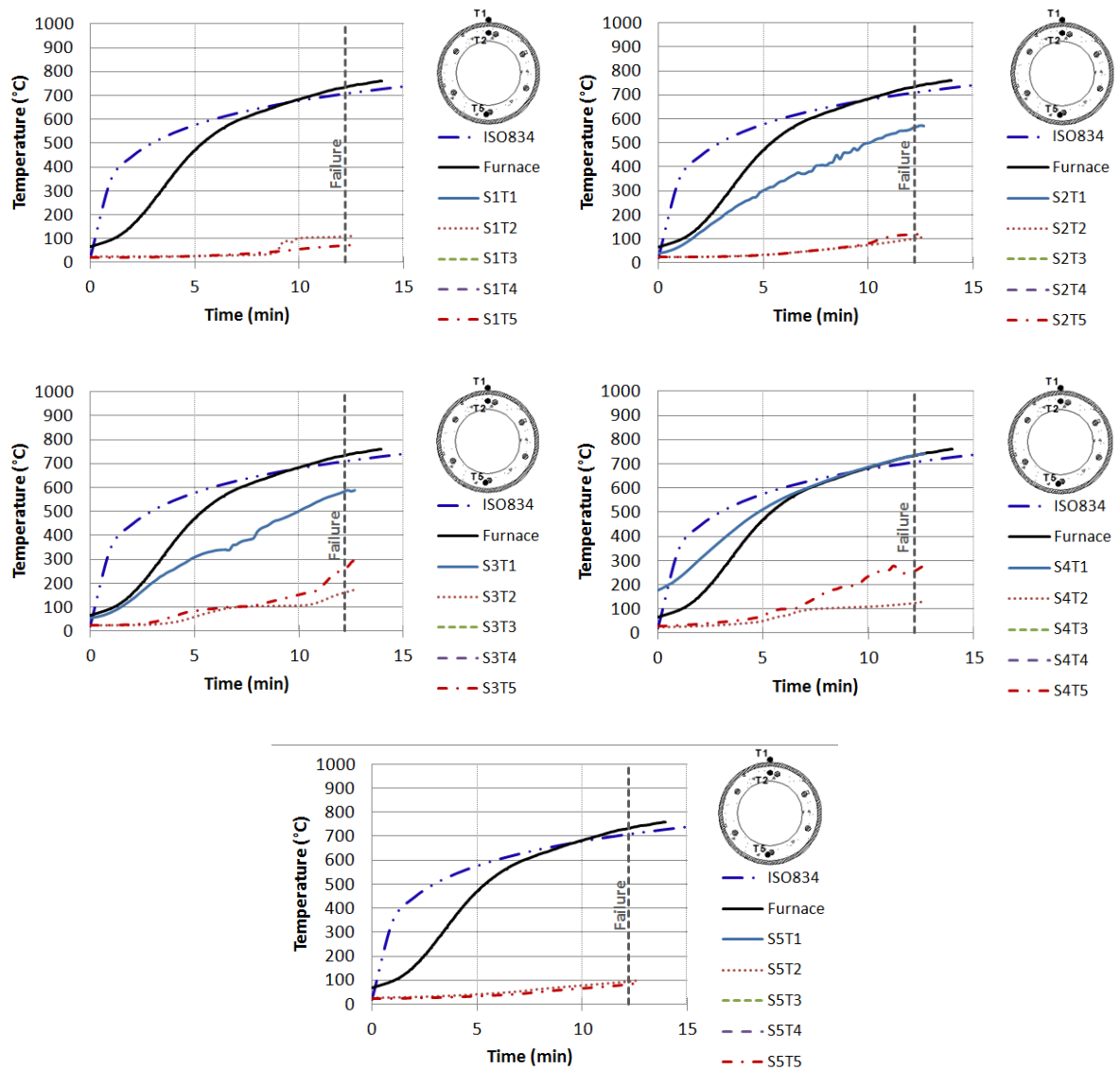


Figure B.4 – Distribution of temperature in cross-sections S1 to S5 for test column A04<sub>168-RING-RC-70%-Klow</sub>.

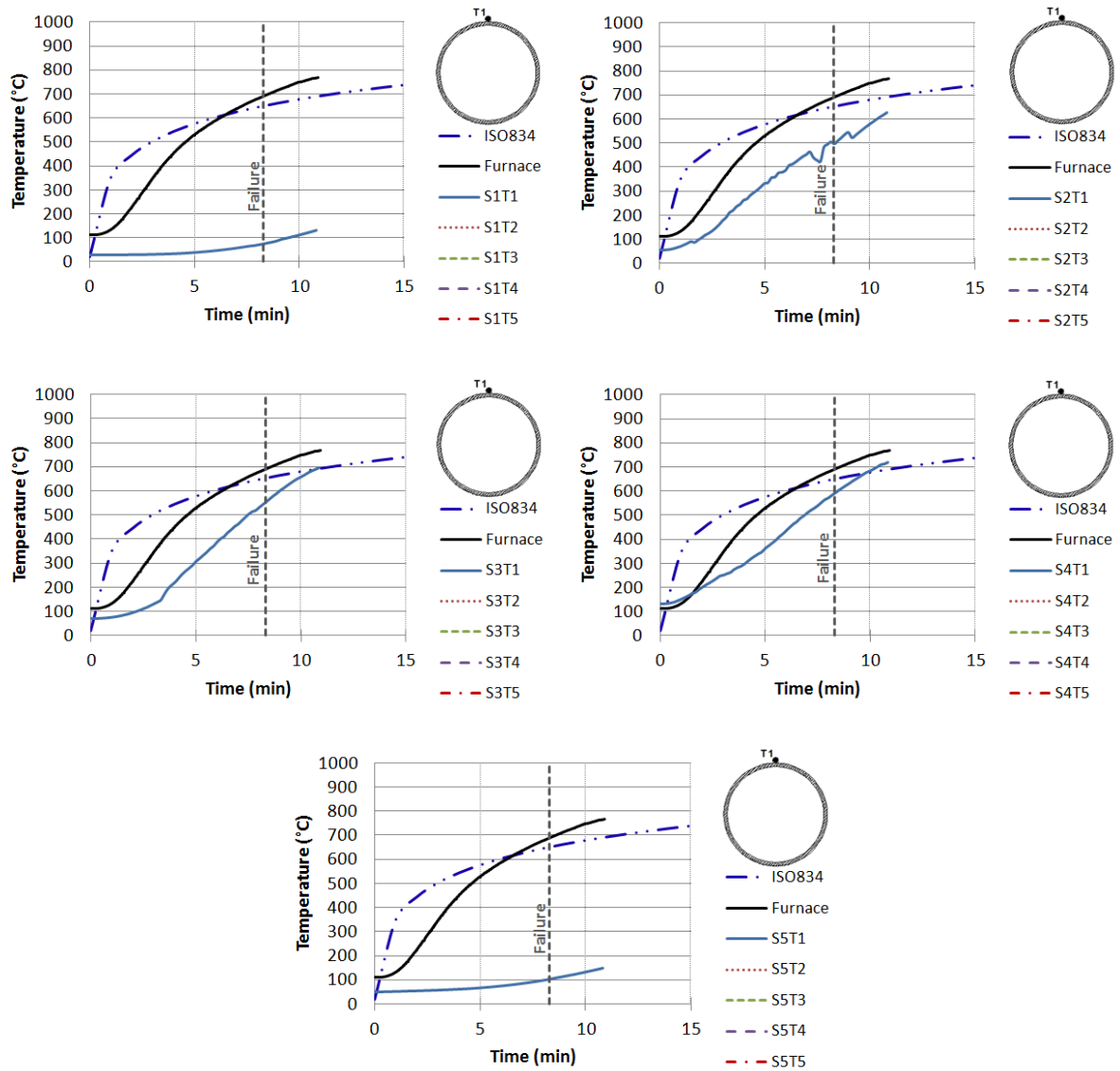


Figure B.5 – Distribution of temperature in cross-sections S1 to S5 for test column A05<sub>168-70%-Klow</sub>.

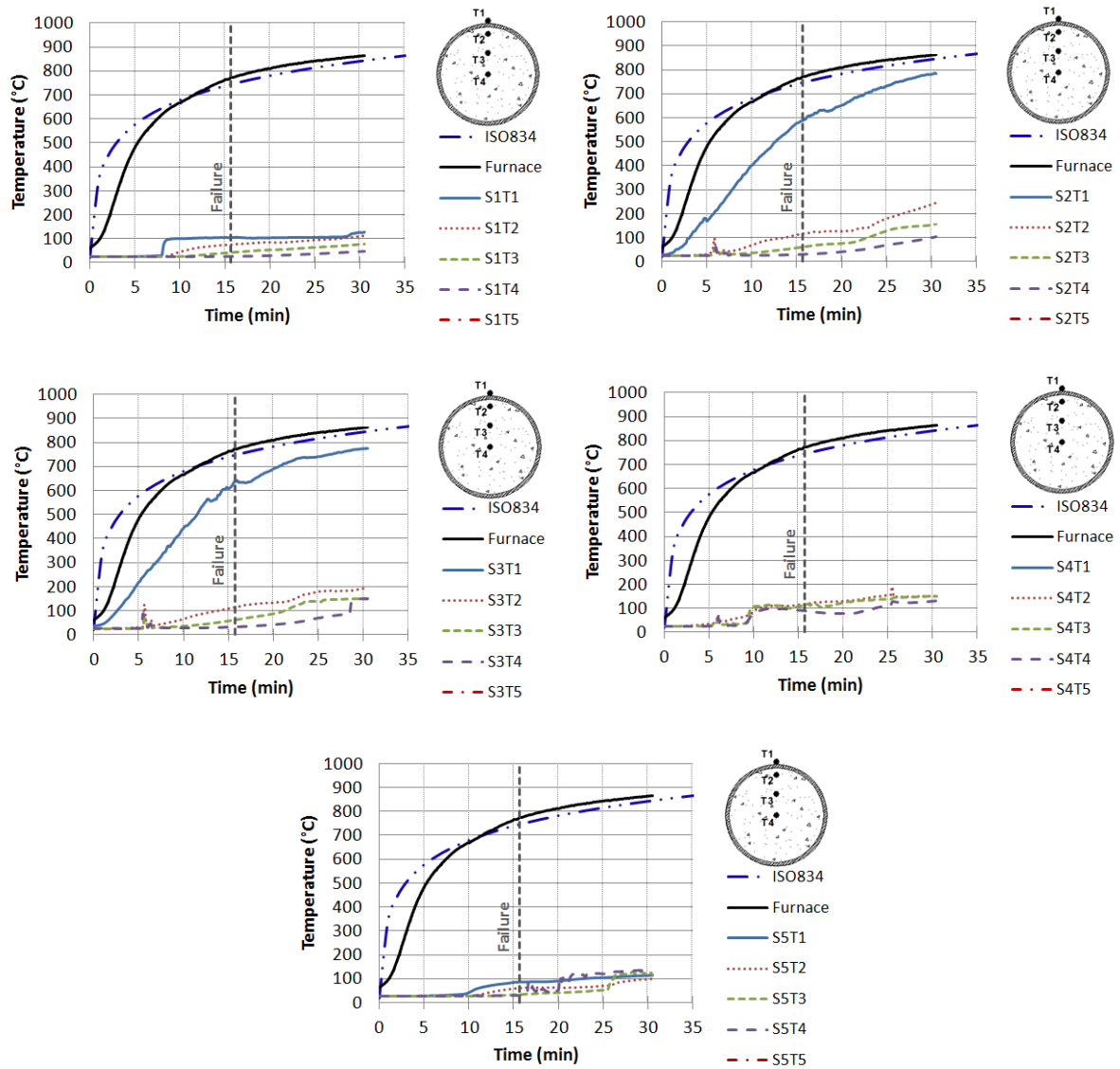


Figure B.6 – Distribution of temperature in cross-sections S1 to S5 for test column A06<sub>219-TOT-PC-70%-Klow</sub>.



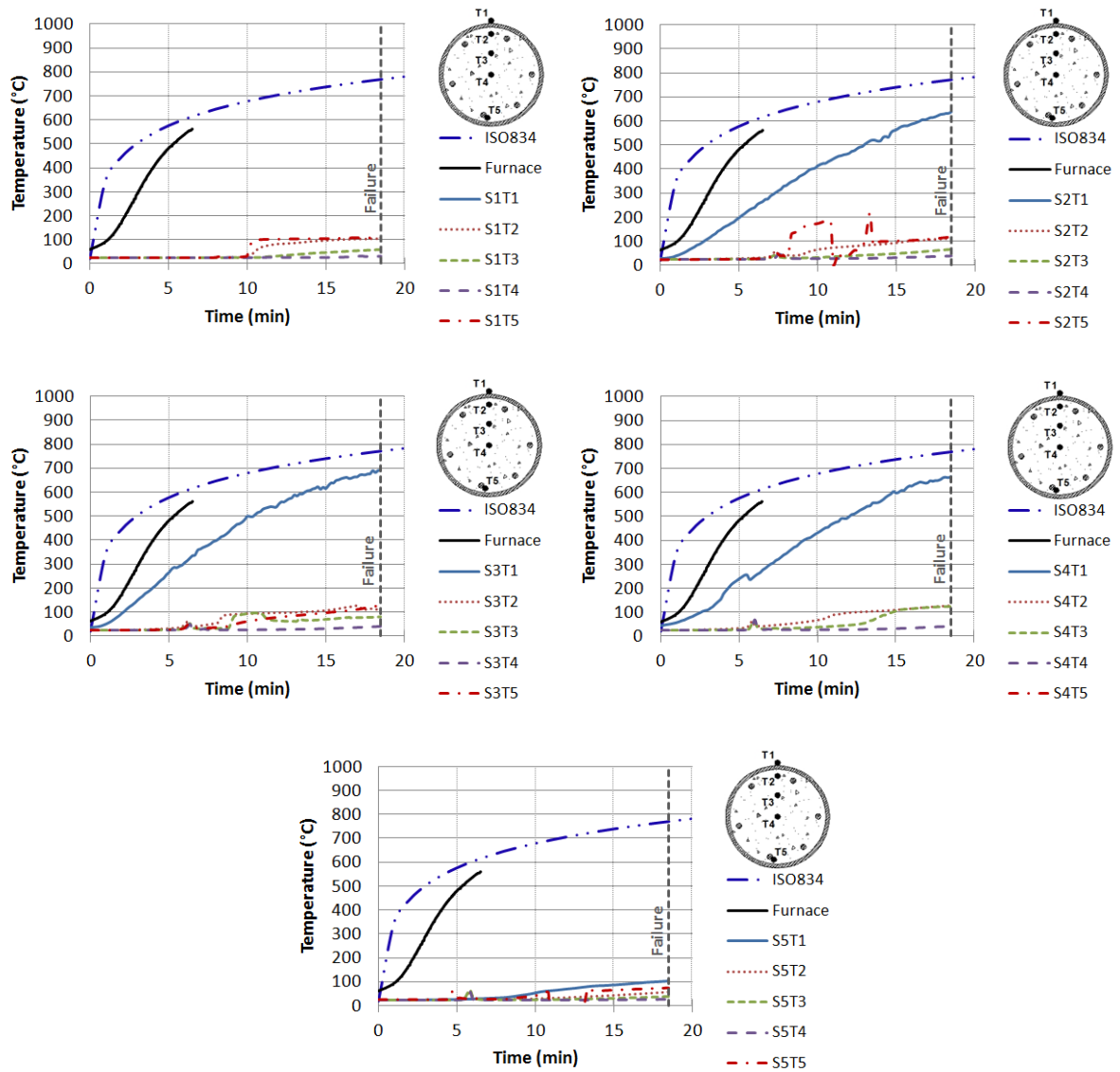


Figure B.7 – Distribution of temperature in cross-sections S1 to S5 for test column A07<sub>219-TOT-RC-70%-Klow</sub>.

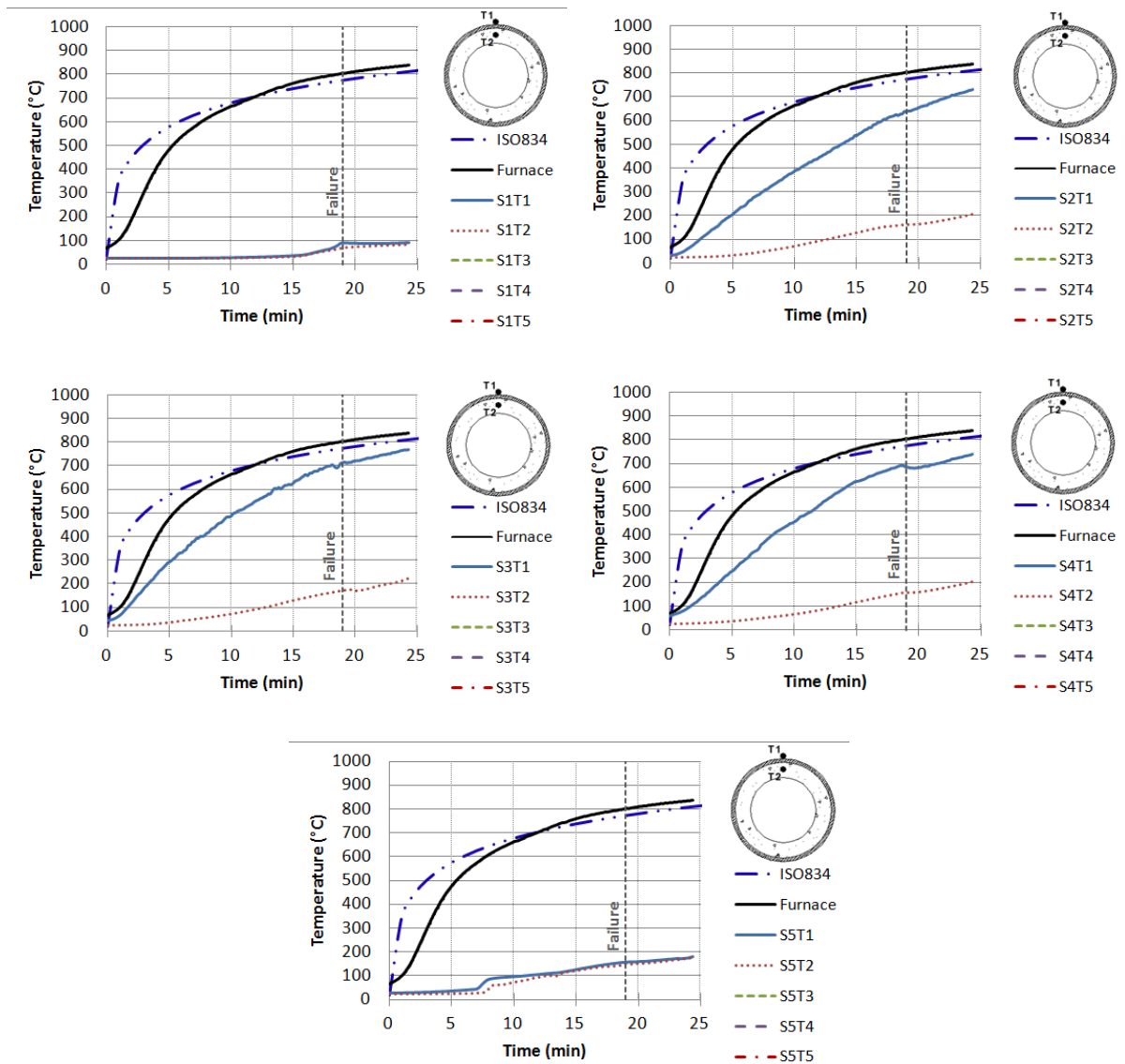


Figure B.8 – Distribution of temperature in cross-sections S1 to S5 for test column A08<sub>219-RING-PC-70%-Klow</sub>.

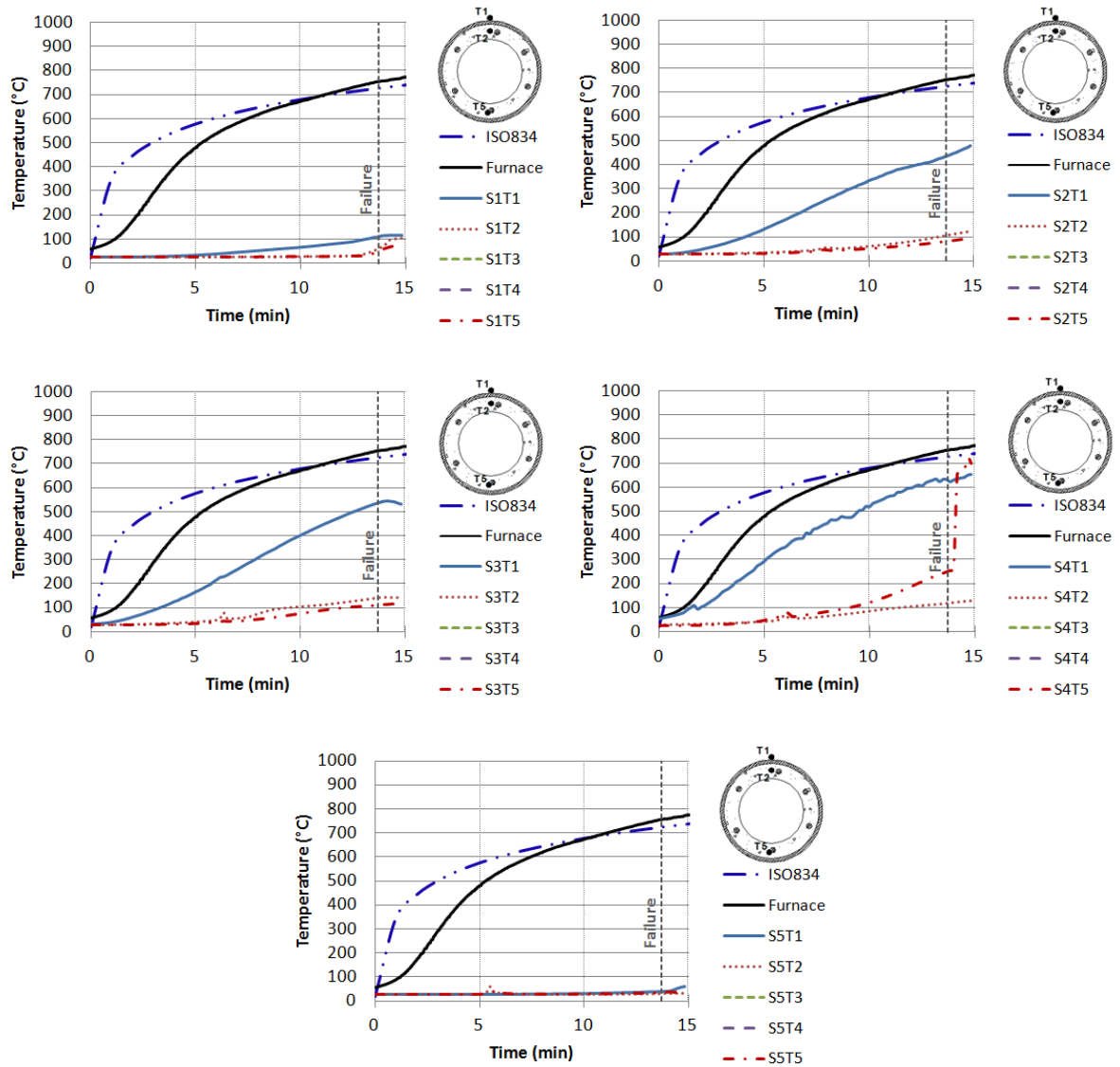


Figure B.9 – Distribution of temperature in cross-sections S1 to S5 for test column A09<sub>219-RING-RC-70%-Klow</sub>.

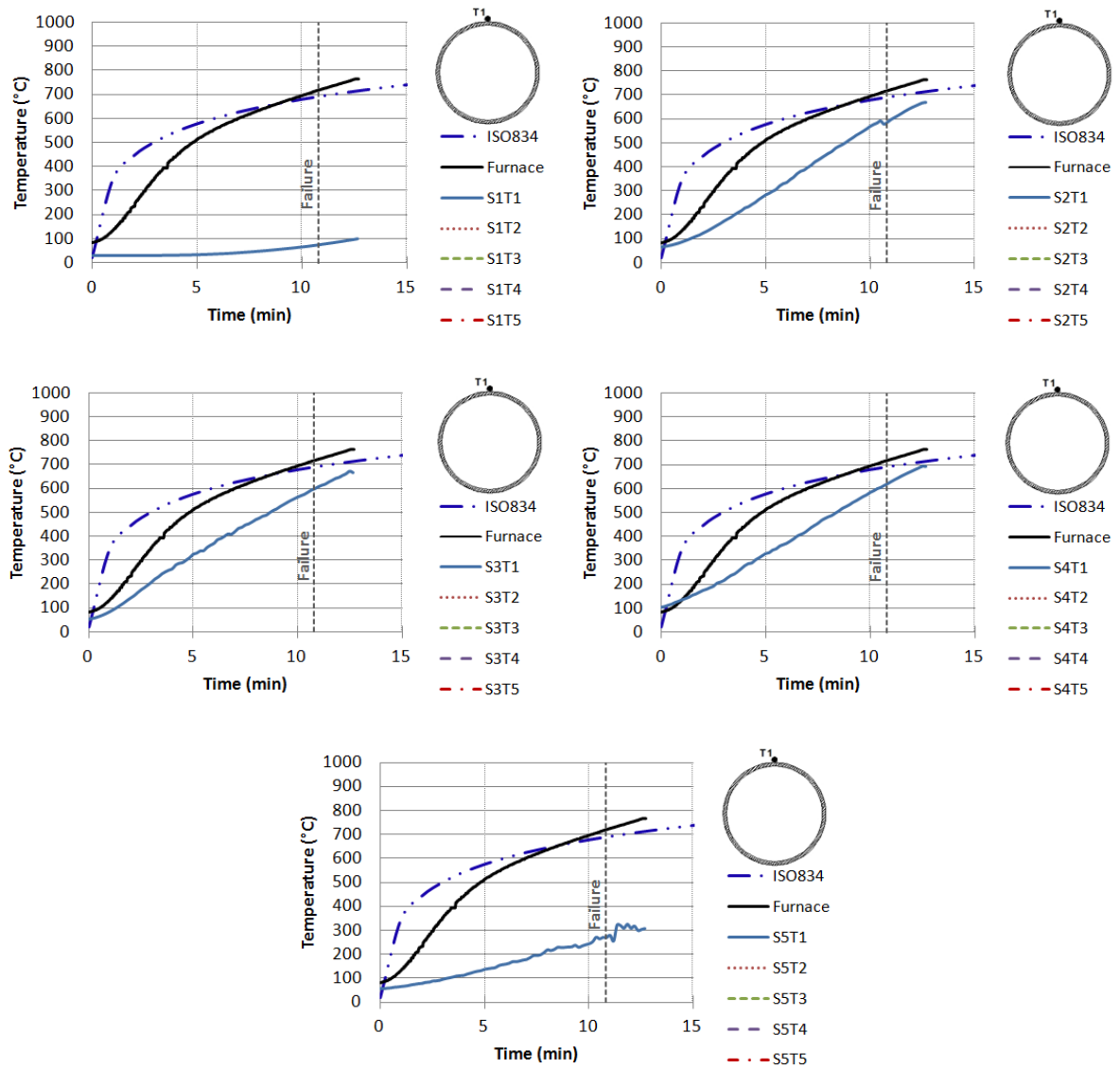


Figure B.10 – Distribution of temperature in cross-sections S1 to S5 for test column A10<sub>219-70%-Klow</sub>.

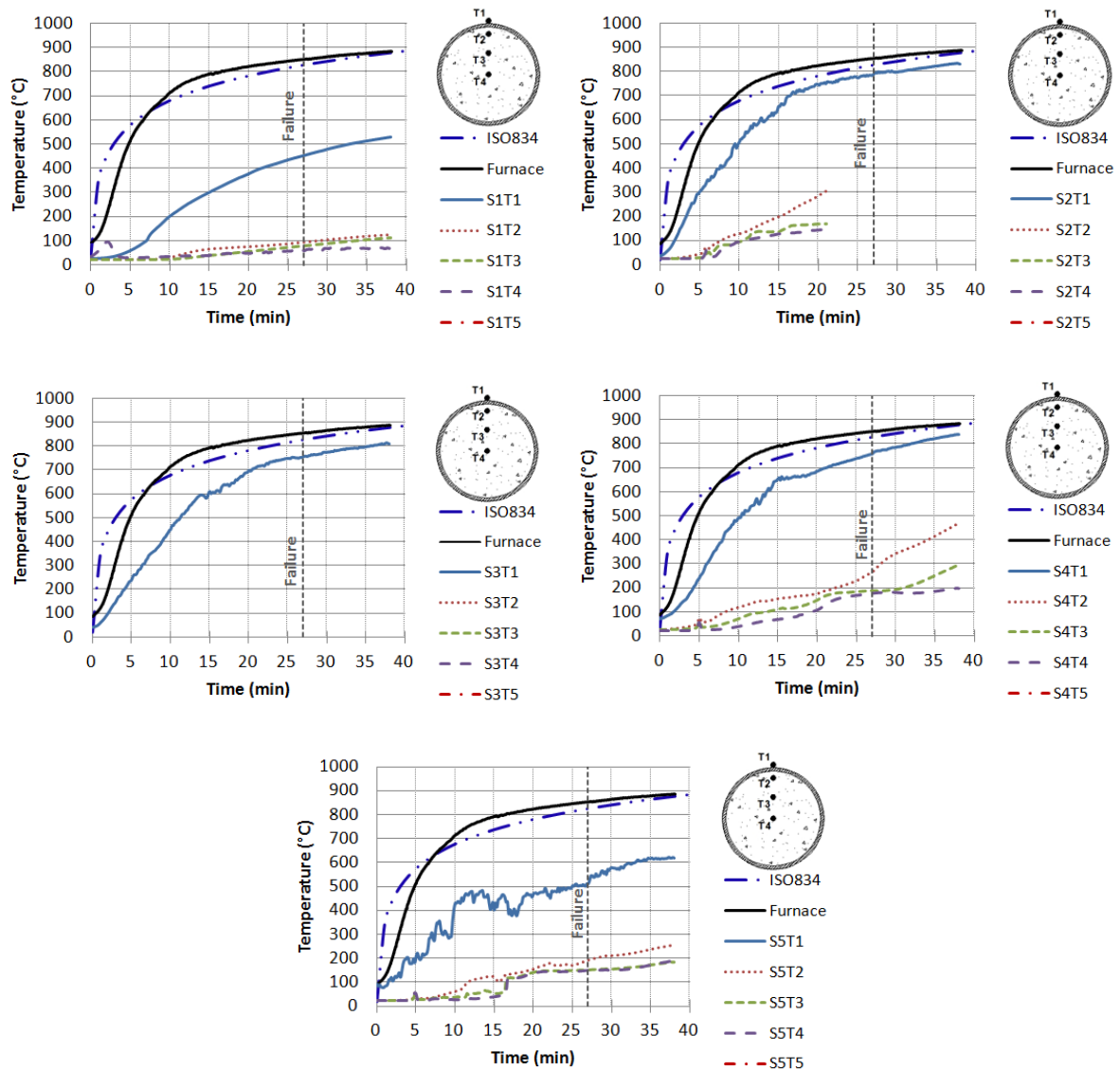


Figure B.11 – Distribution of temperature in cross-sections S1 to S5 for test column A11<sub>168-TOT-PC-30%-Klow</sub>.

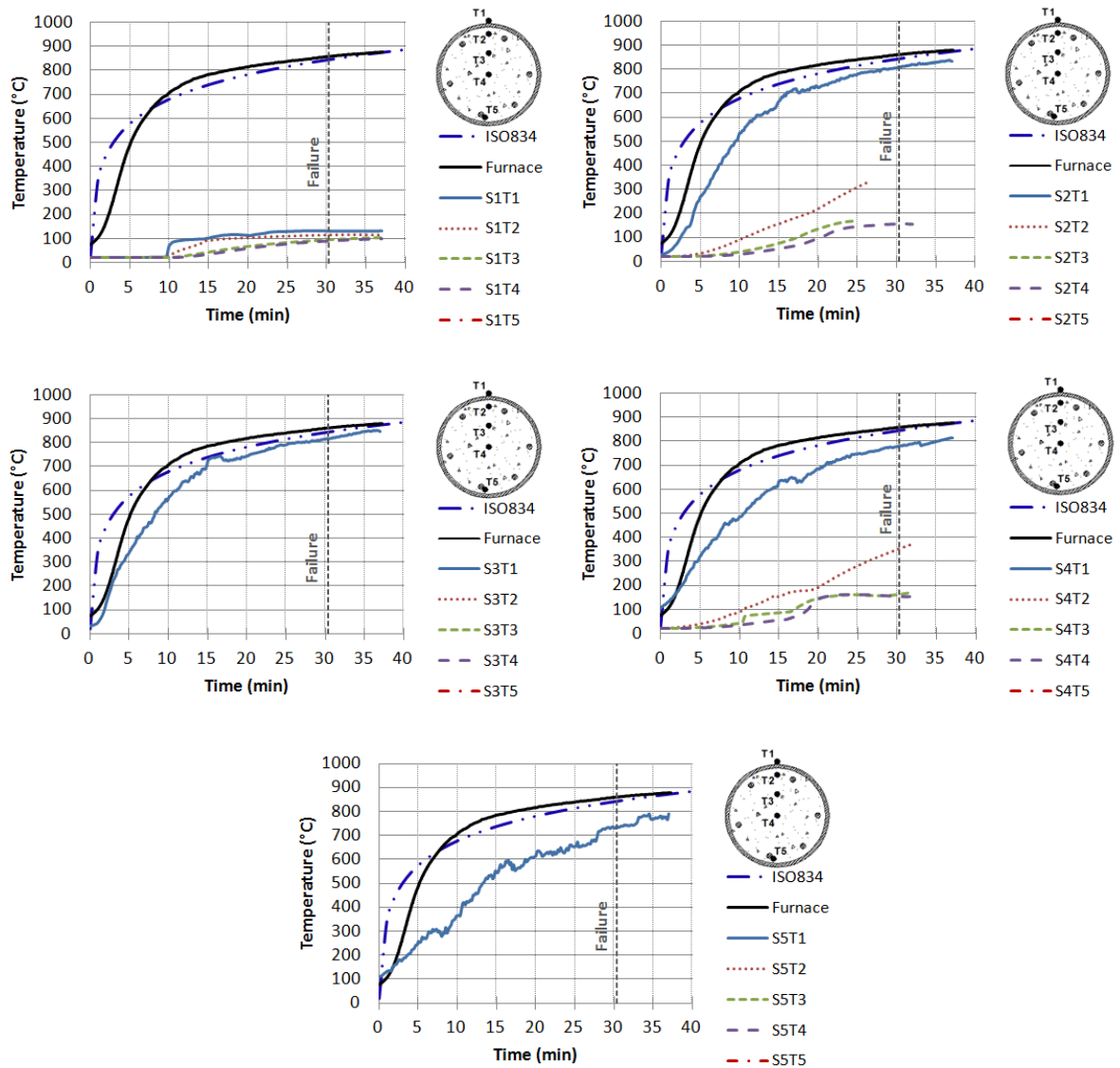


Figure B.12 – Distribution of temperature in cross-sections S1 to S5 for test column A12<sub>168-TOT-RC-30%-Klow</sub>.

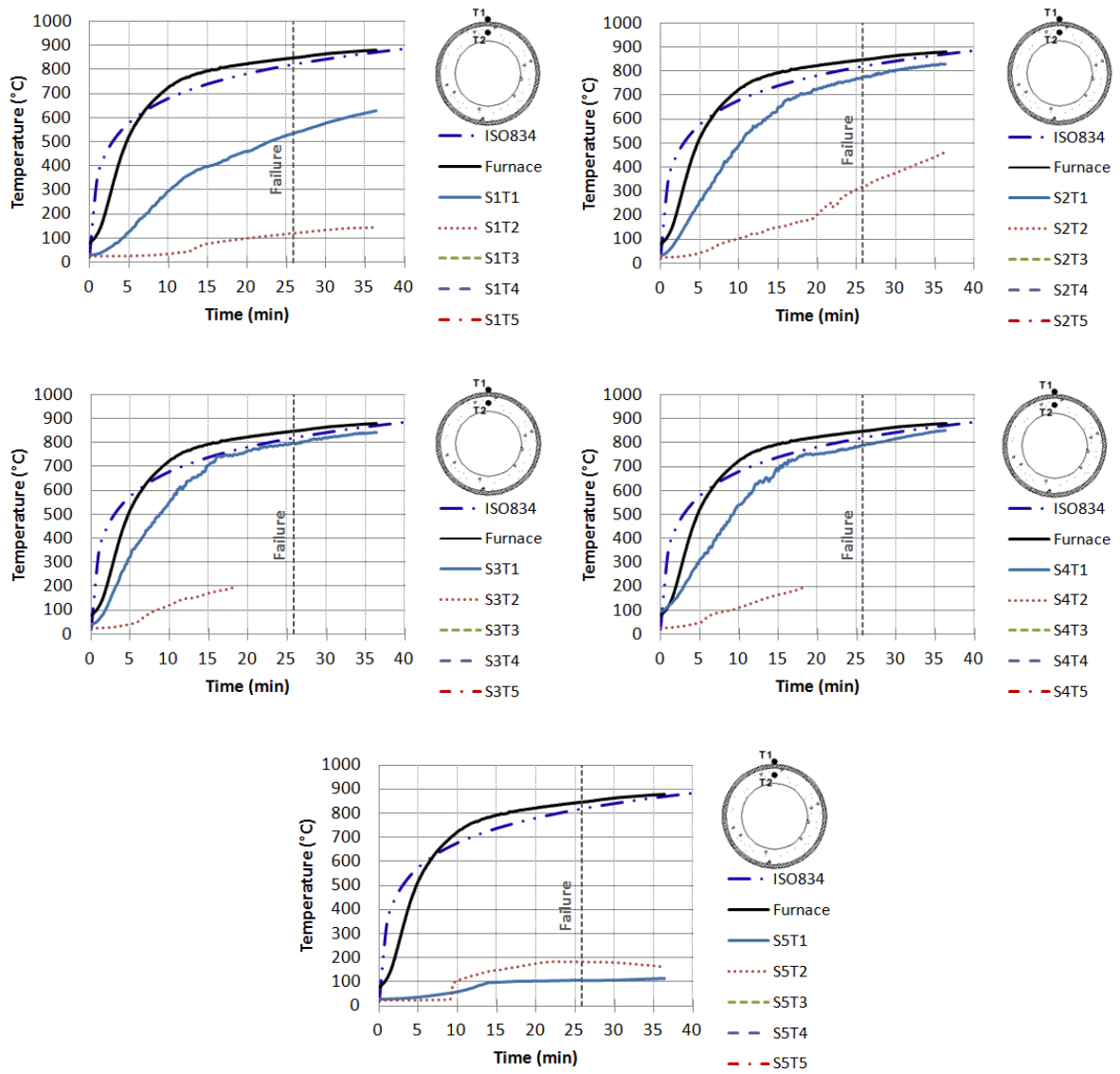


Figure B.13 – Distribution of temperature in cross-sections S1 to S5 for test column A13 168-RING-PC-30%-Klow.

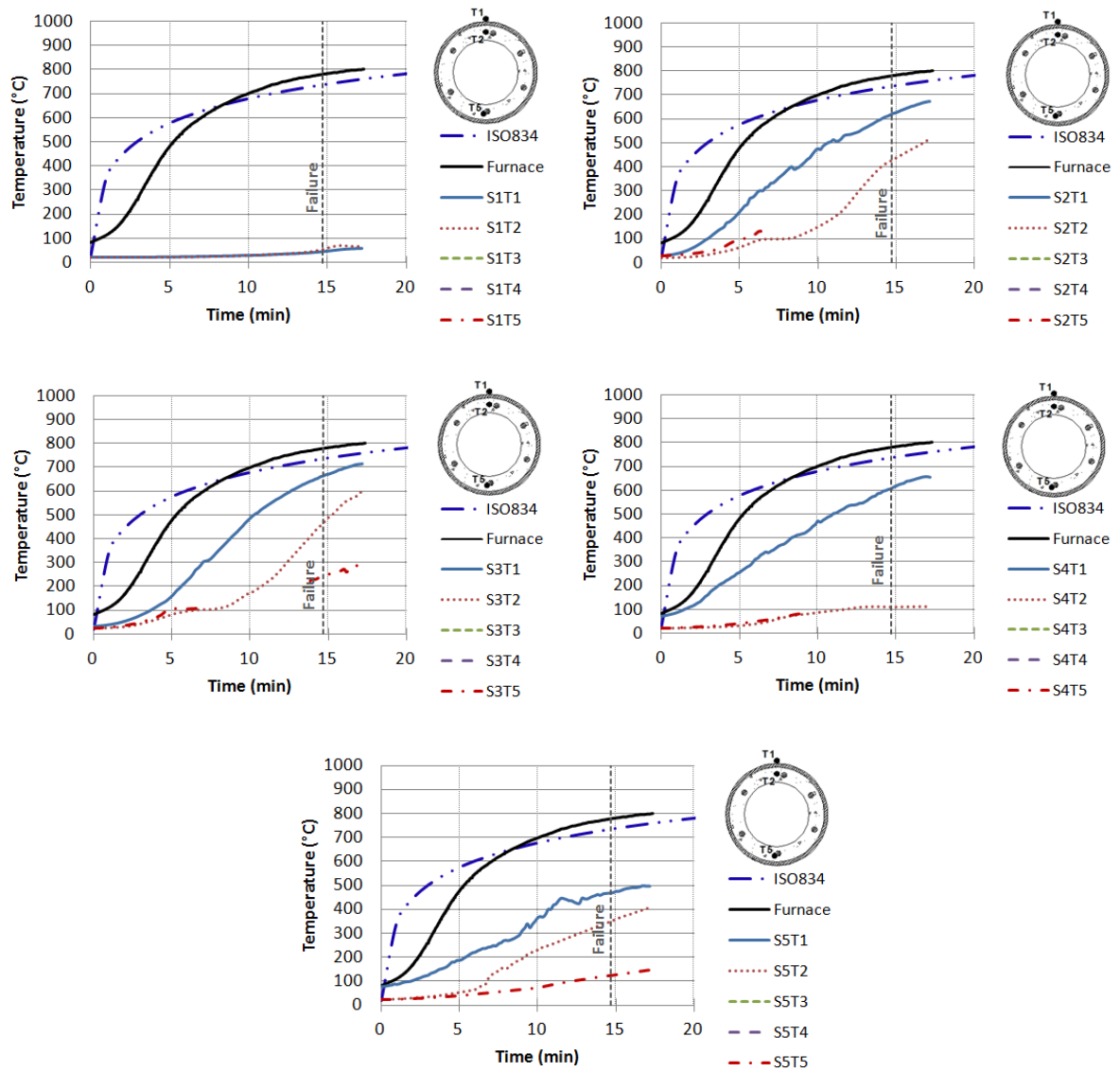


Figure B.14 – Distribution of temperature in cross-sections S1 to S5 for test column A14 168-RING-RC-30%-Klow.



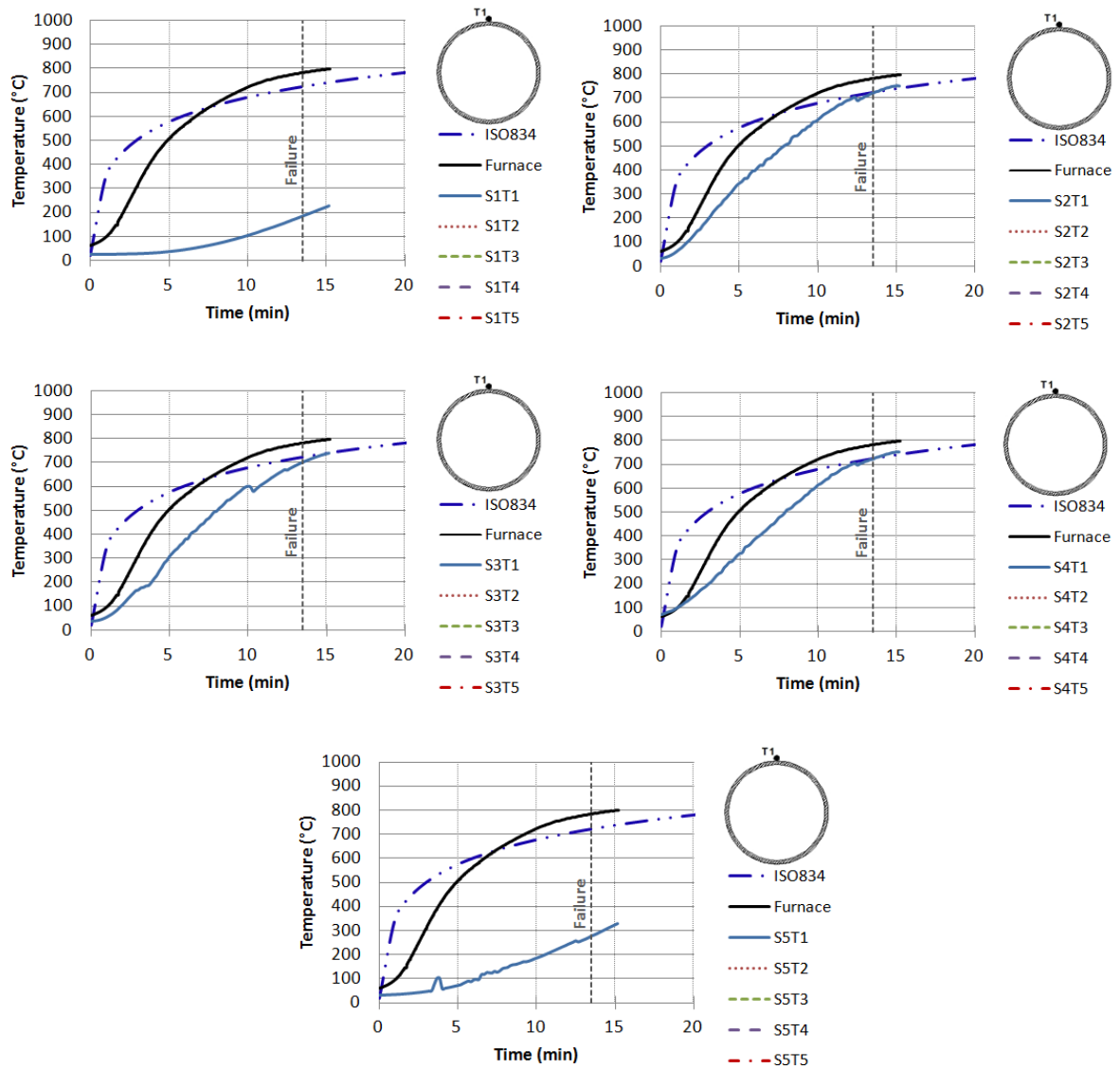


Figure B.15 – Distribution of temperature in cross-sections S1 to S5 for test column A15<sub>168-30%-Klow</sub>.

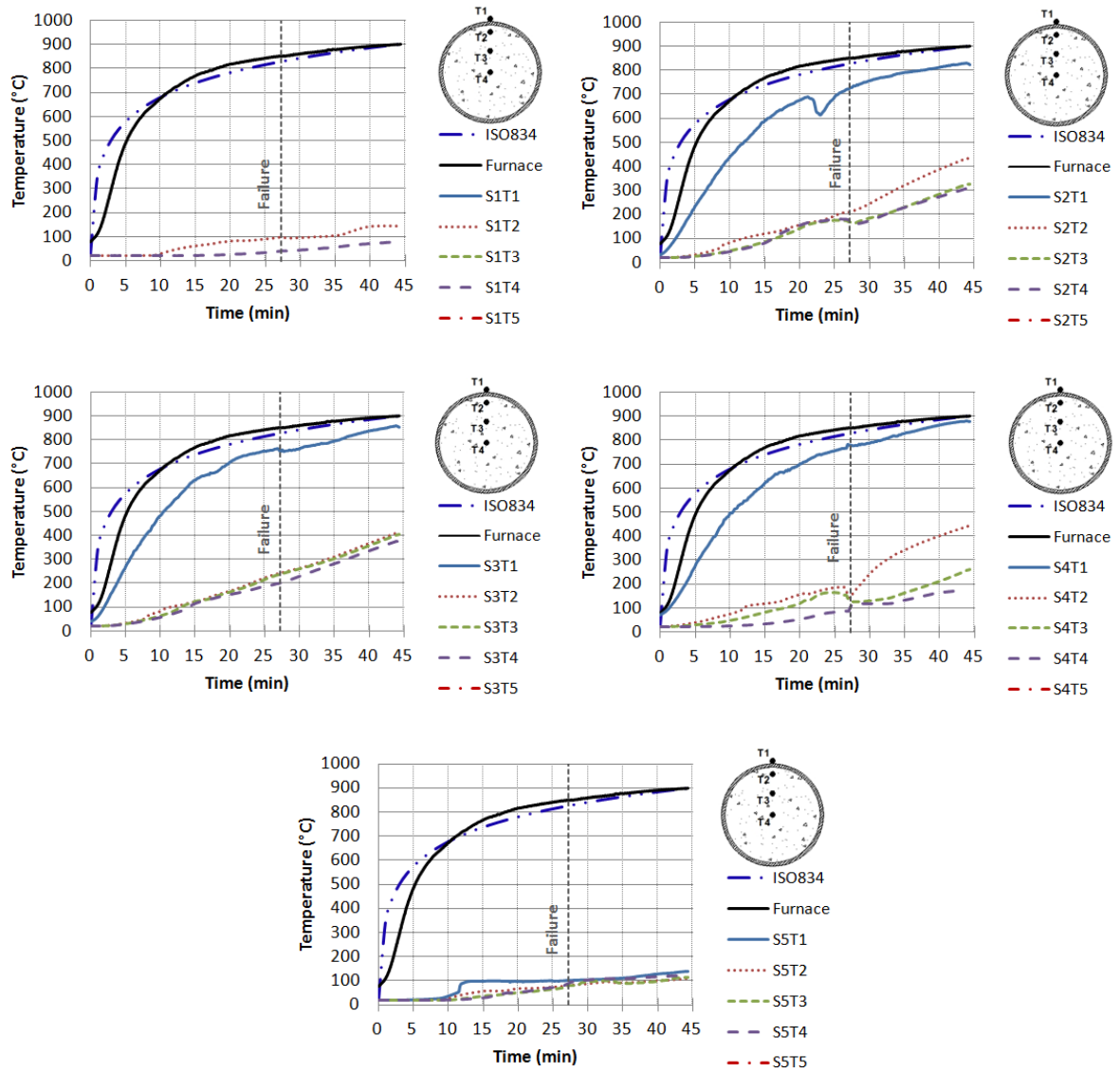


Figure B.16 – Distribution of temperature in cross-sections S1 to S5 for test column A16<sub>219-TOT-PC-30%-Klow</sub>.

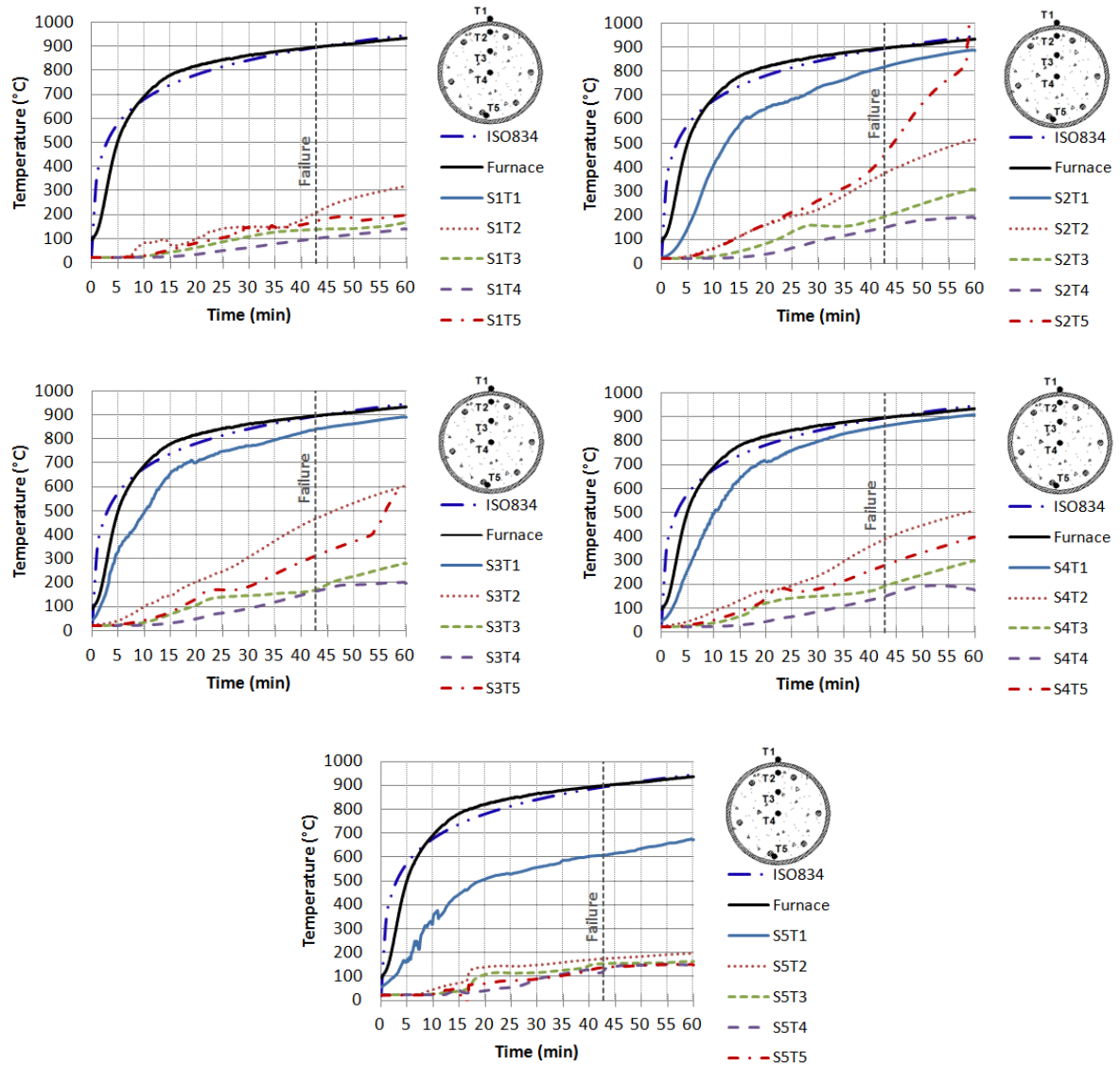


Figure B.17 – Distribution of temperature in cross-sections S1 to S5 for test column A17<sub>219-TOT-RC-30%-Klow</sub>.

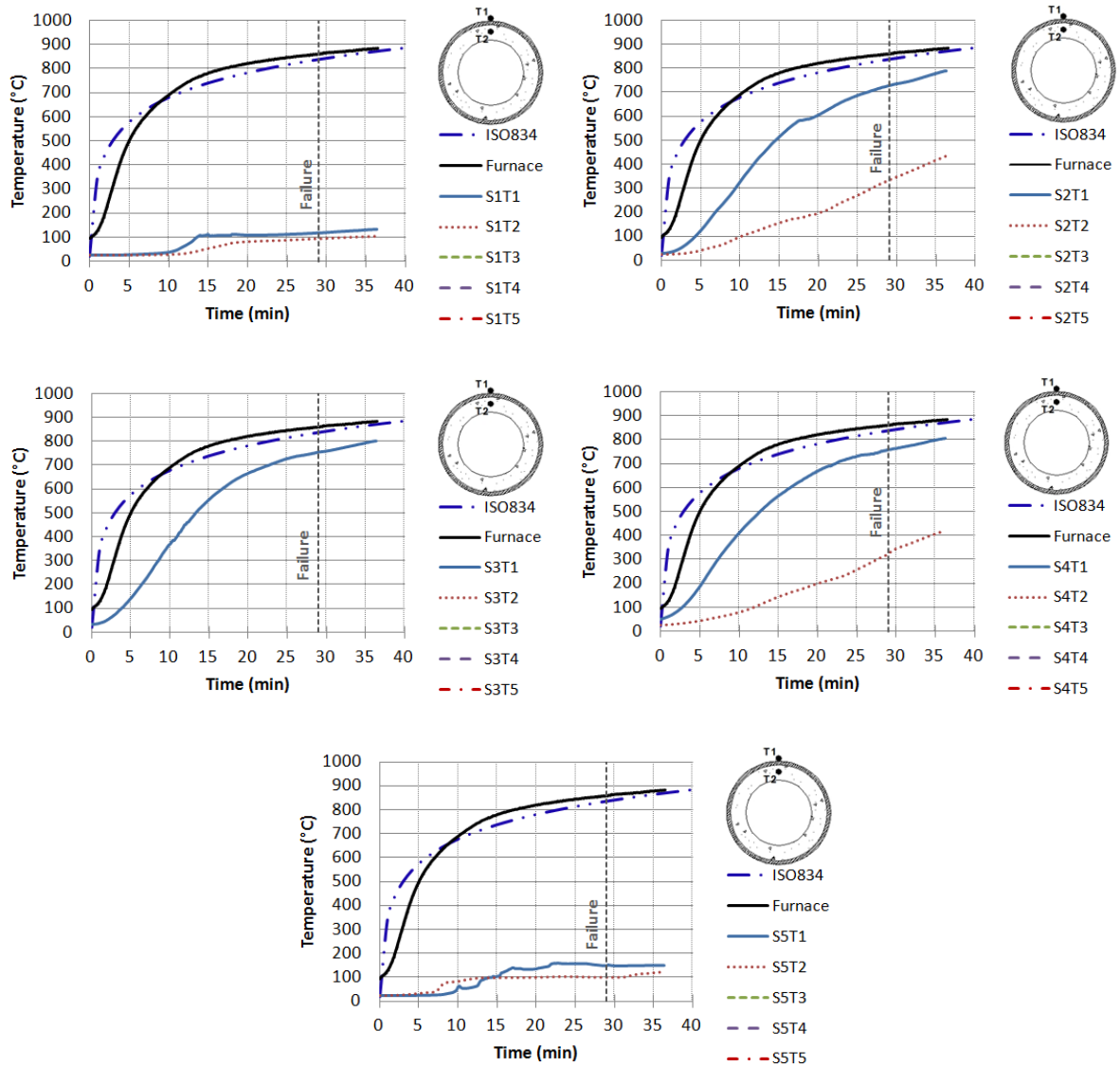


Figure B.18 – Distribution of temperature in cross-sections S1 to S5 for test column A18<sub>219-RING-PC-30%-Klow</sub>.

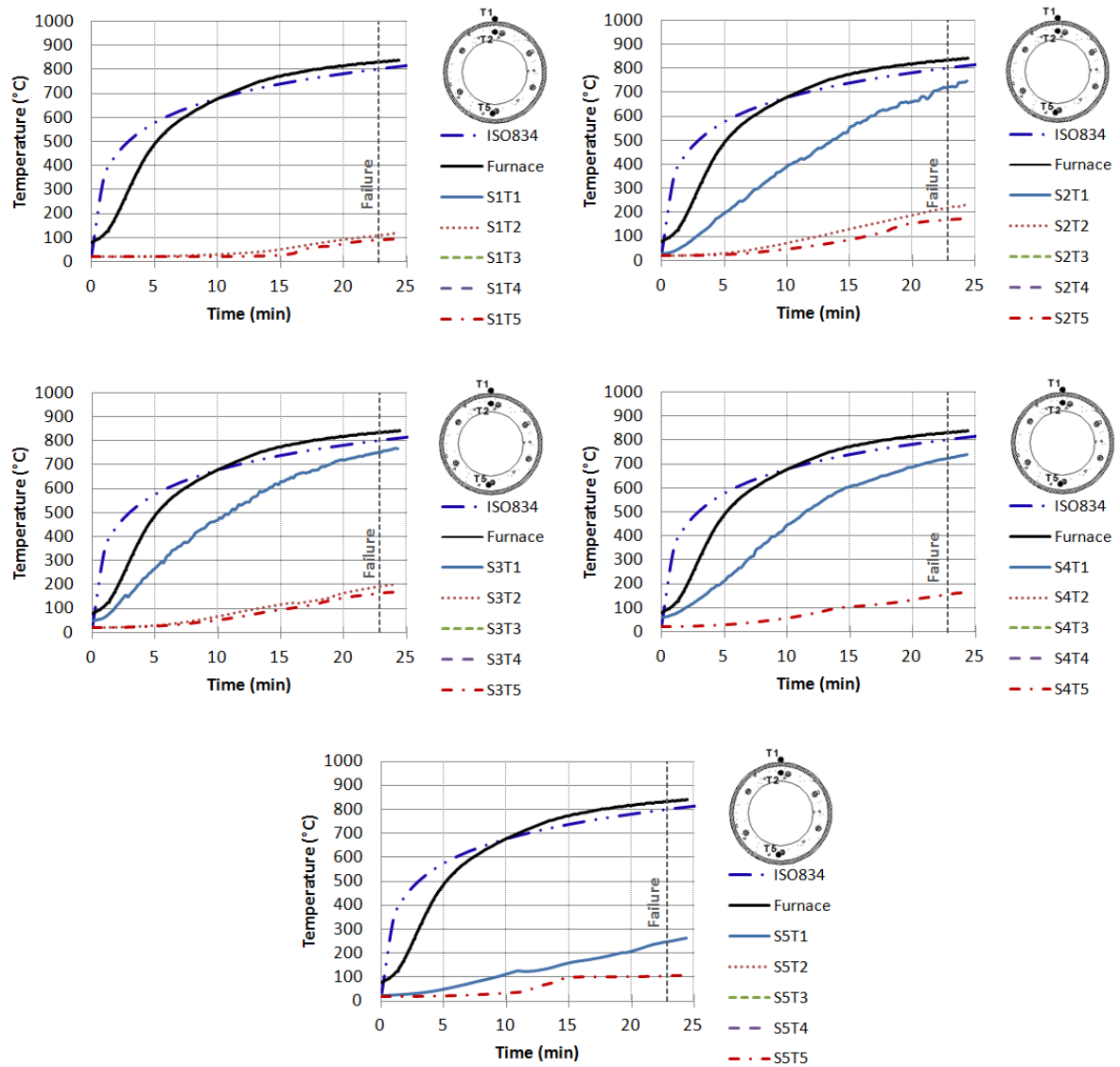


Figure B.19 – Distribution of temperature in cross-sections S1 to S5 for test column A19<sub>219-RING-RC-30%-Klow</sub>.

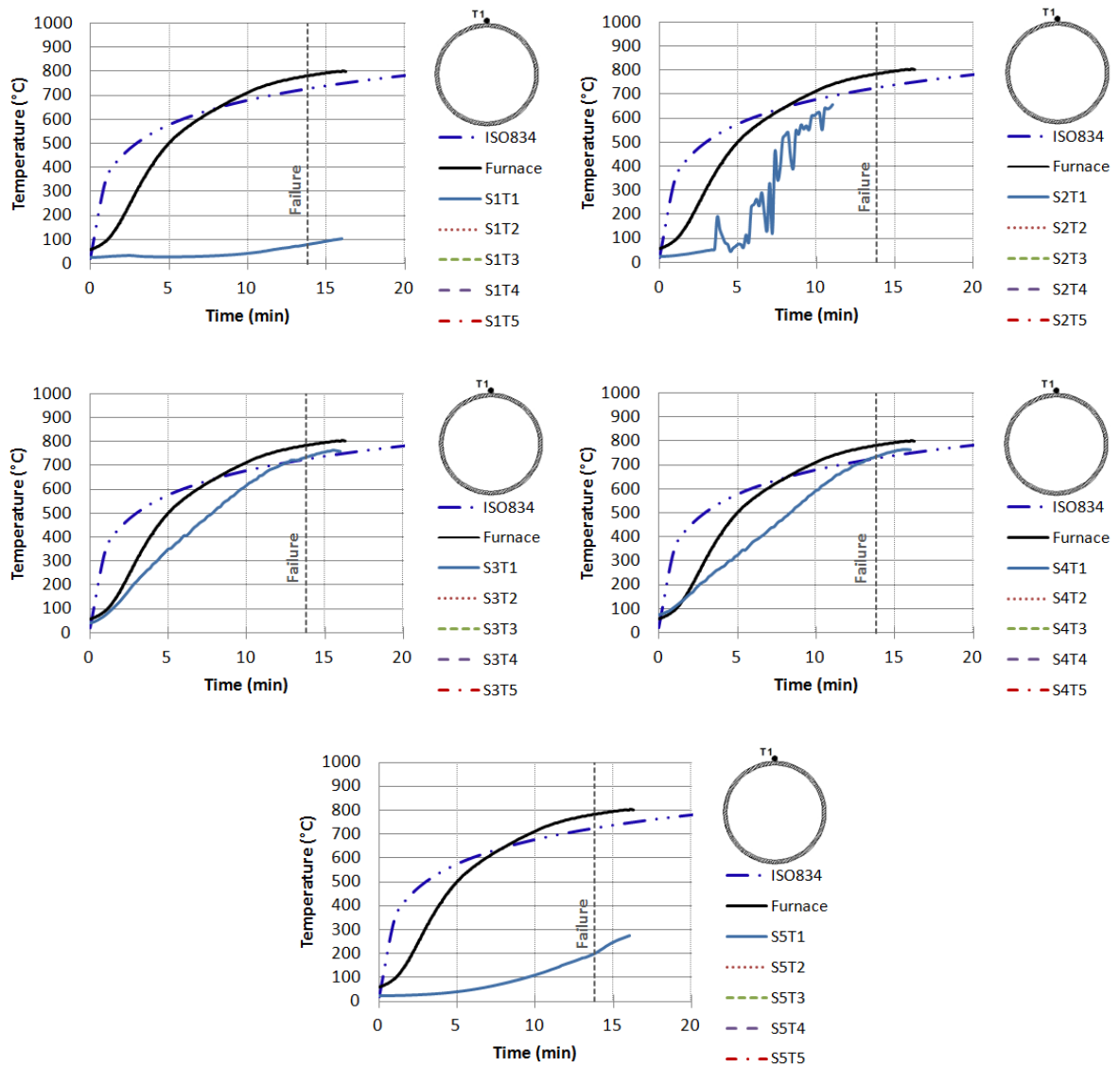


Figure B.20 – Distribution of temperature in cross-sections S1 to S5 for test column A20 219-30%-Klow.

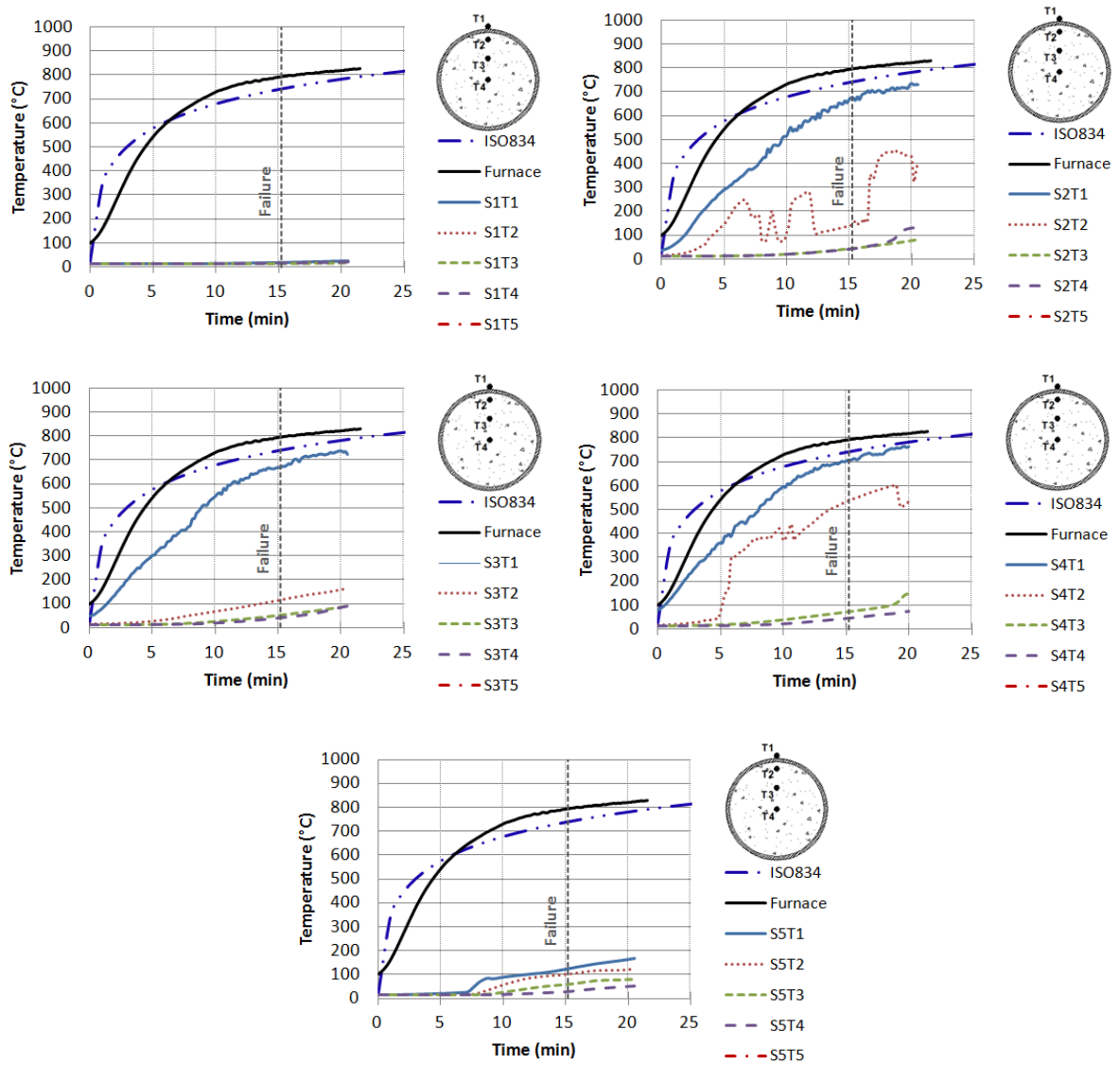


Figure B.21 – Distribution of temperature in cross-sections S1 to S5 for test column A21<sub>168-TOT-PC-70%-Khigh</sub>.

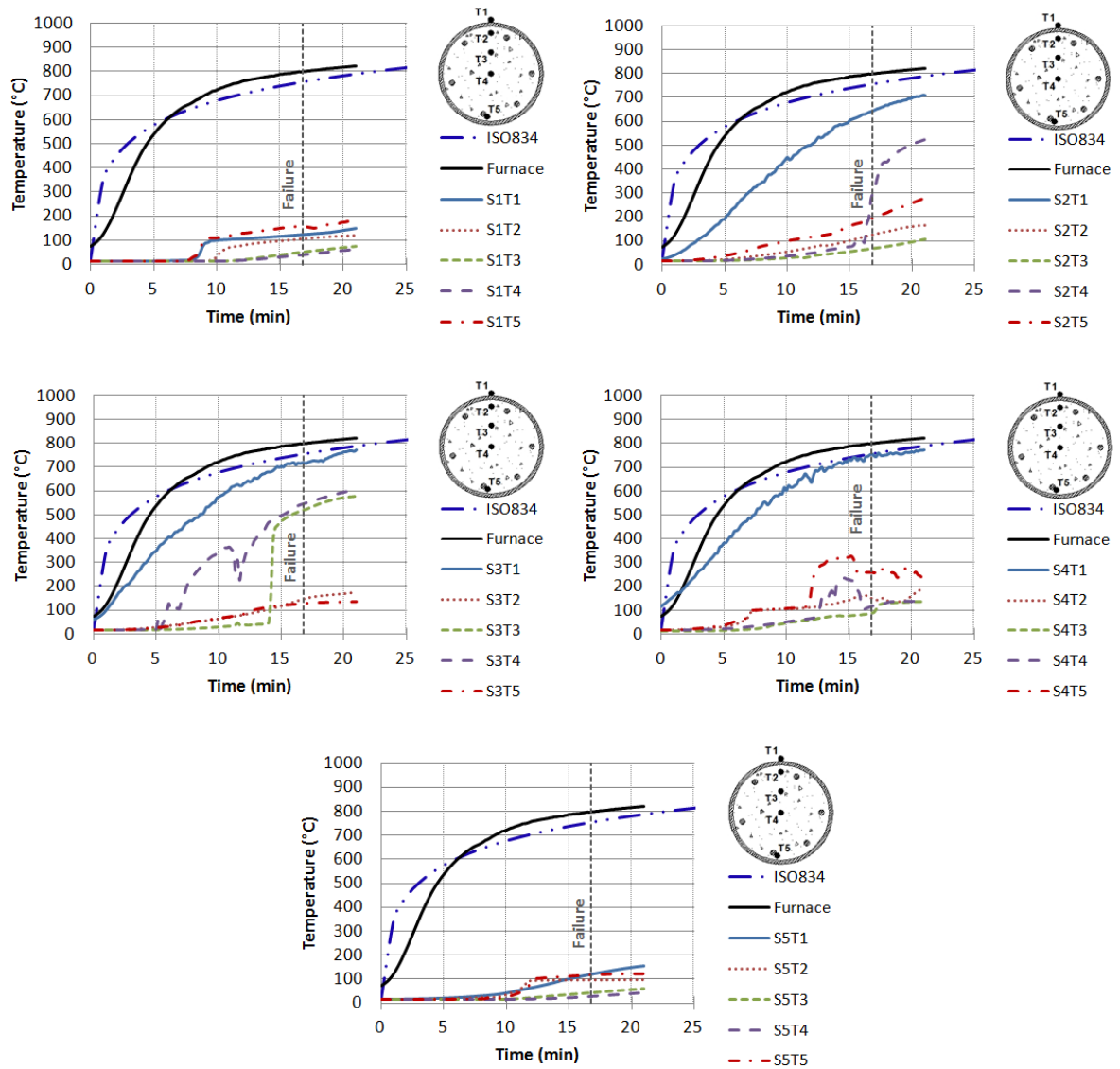


Figure B.22 – Distribution of temperature in cross-sections S1 to S5 for test column A22 168-TOT-RC-70%-Khigh.



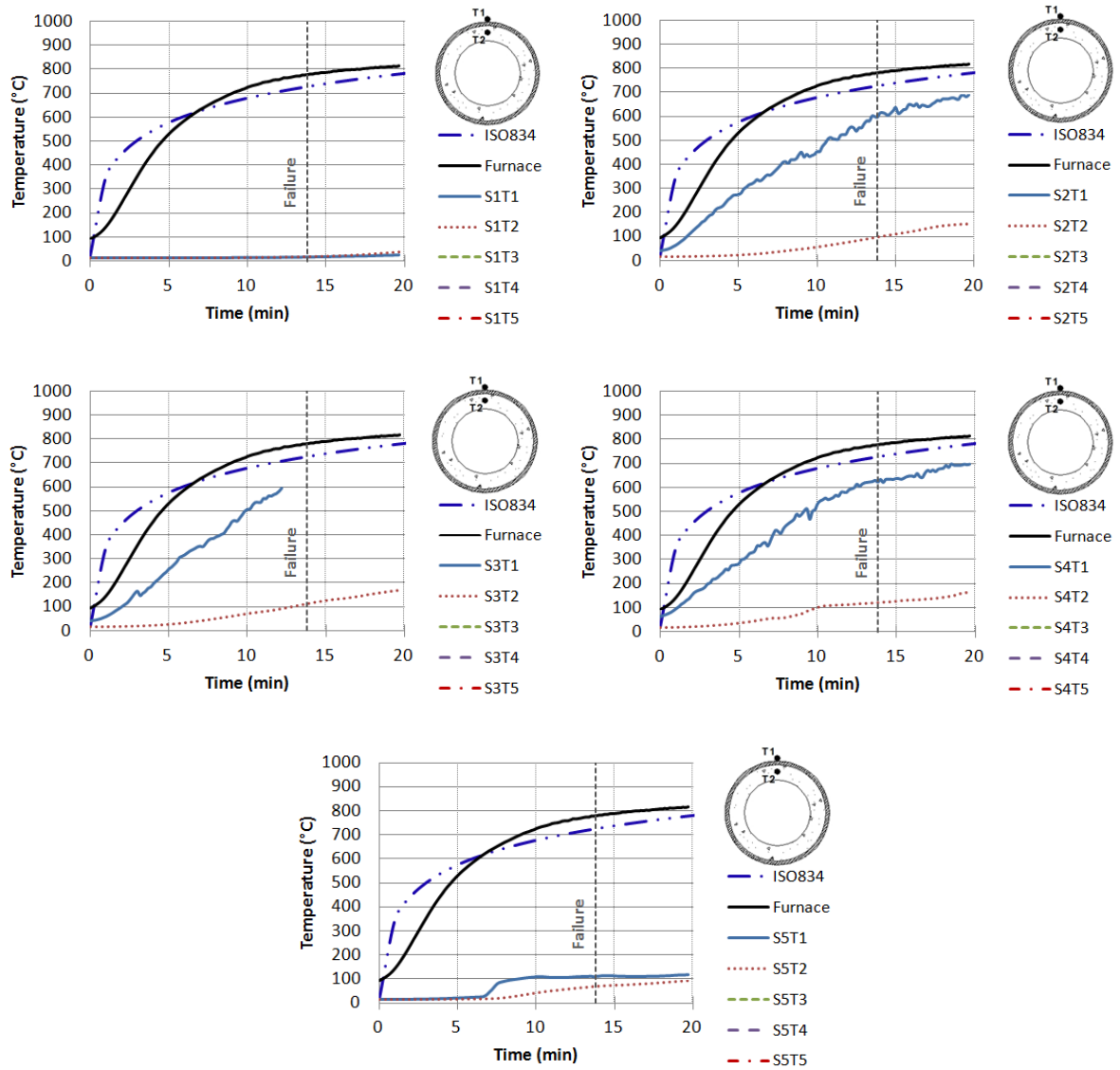


Figure B.23 – Distribution of temperature in cross-sections S1 to S5 for test column A23<sub>168-RING-PC-70%-Khigh-</sub>

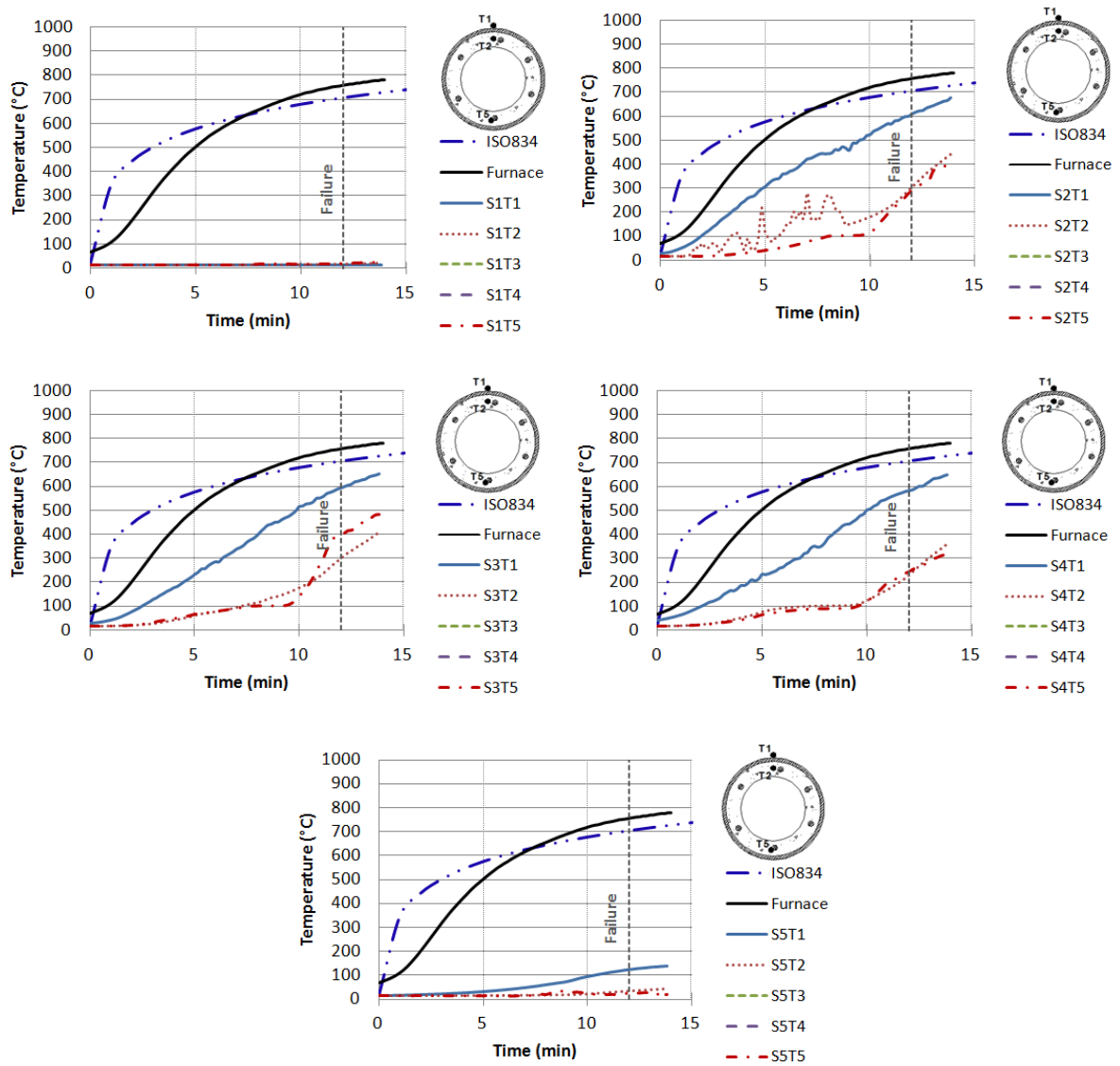


Figure B.24 – Distribution of temperature in cross-sections S1 to S5 for test column A24<sub>168-RING-RC-70%-Khigh</sub>

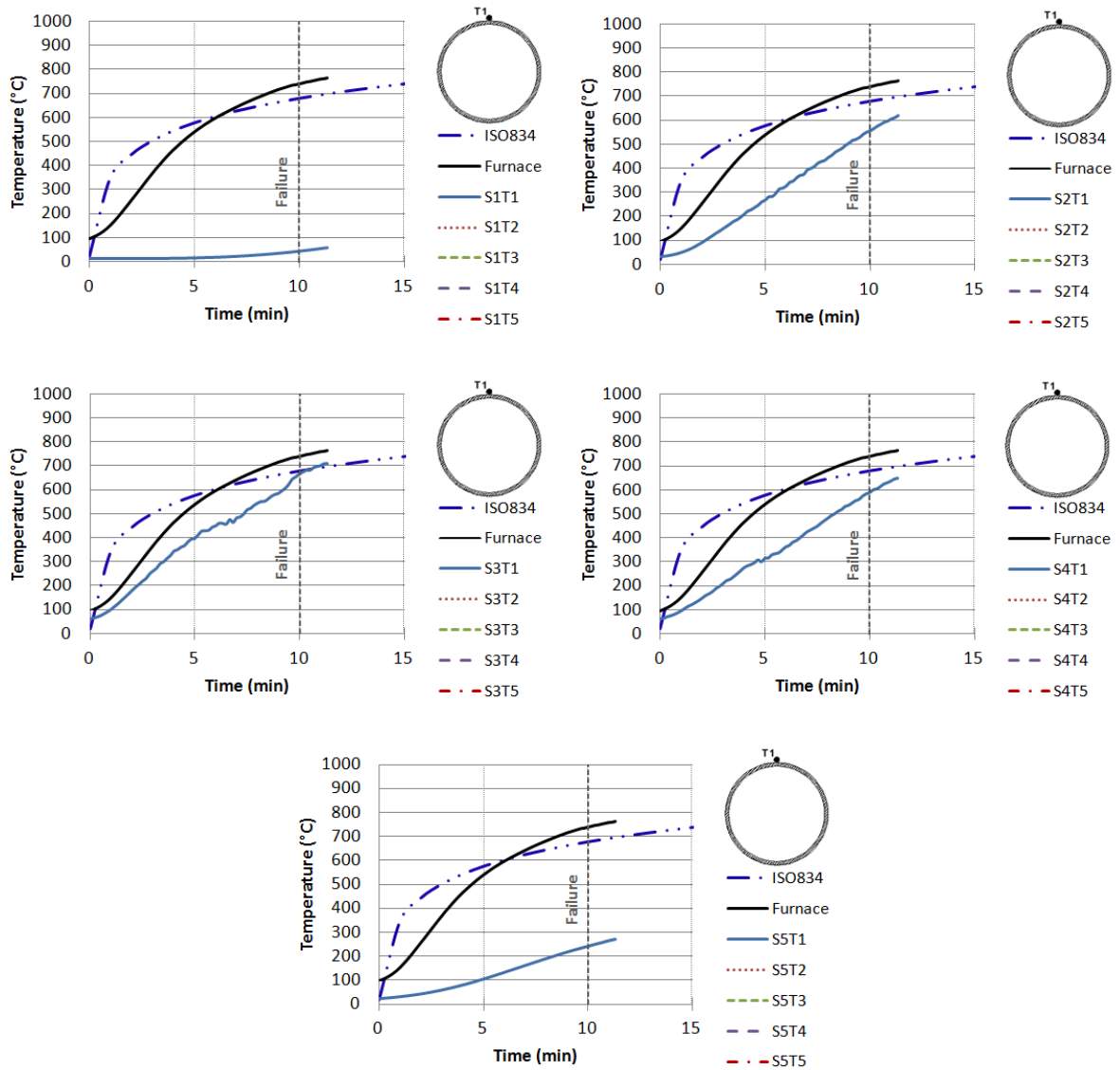


Figure B.25 – Distribution of temperature in cross-sections S1 to S5 for test column A25<sub>168-70%-Khigh</sub>.

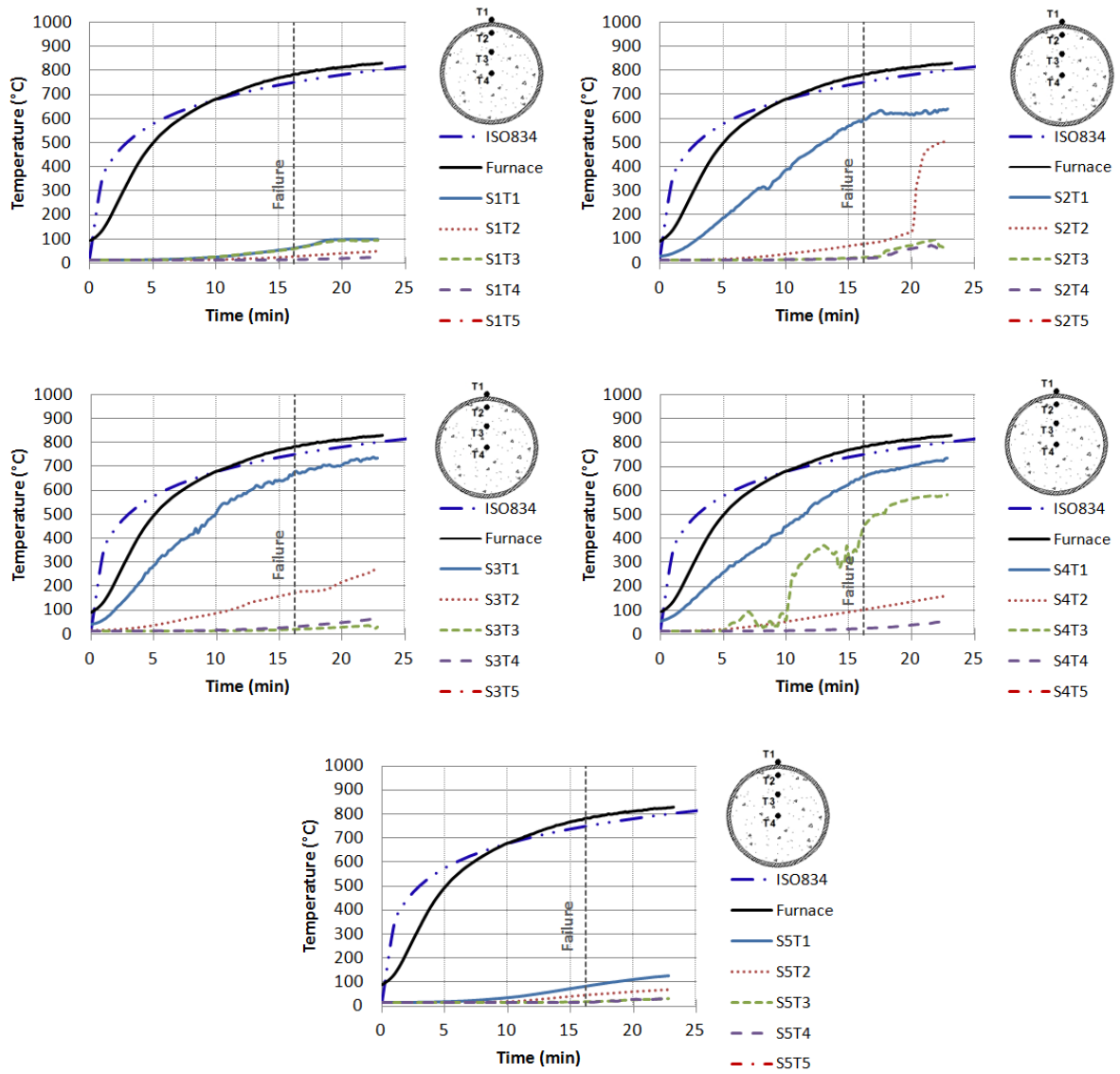


Figure B.26 – Distribution of temperature in cross-sections S1 to S5 for test column A26<sub>219-TOT-PC-70%-Khigh</sub>.

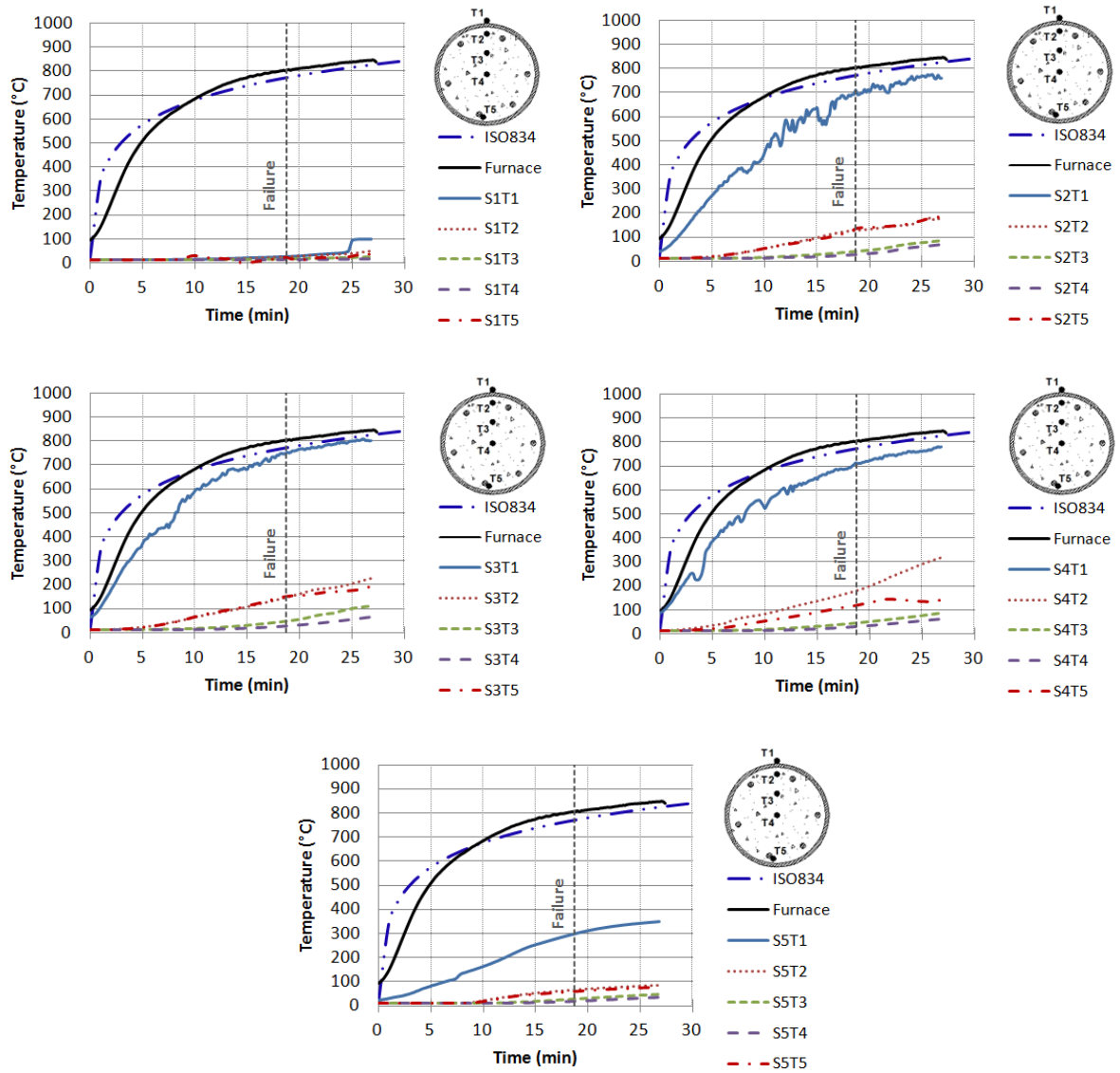


Figure B.27 – Distribution of temperature in cross-sections S1 to S5 for test column A27<sub>219-TOT-RC-70%-Khigh</sub>.

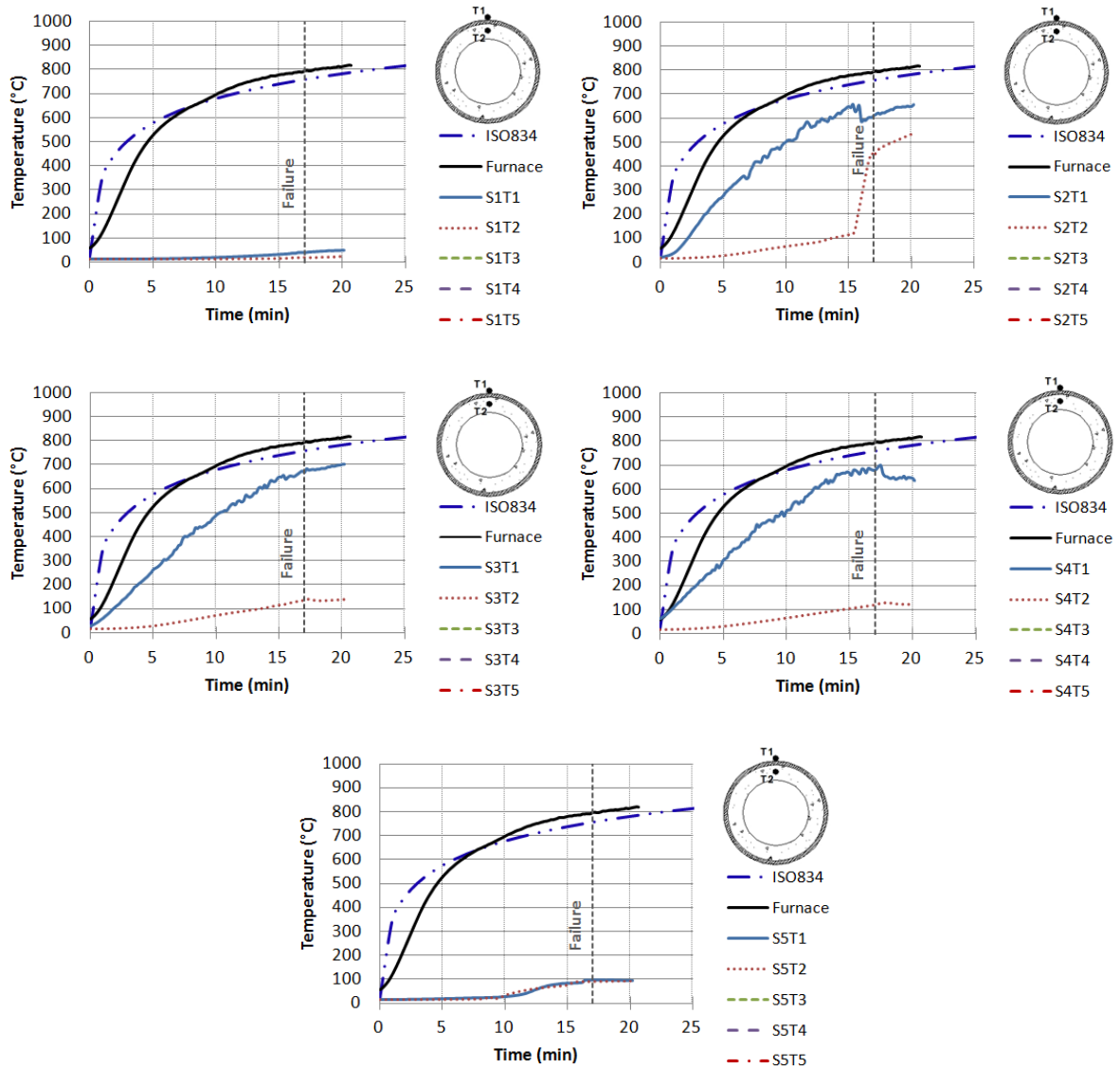


Figure B.28 – Distribution of temperature in cross-sections S1 to S5 for test column A28<sub>219-RING-PC-70%-Khigh</sub>.

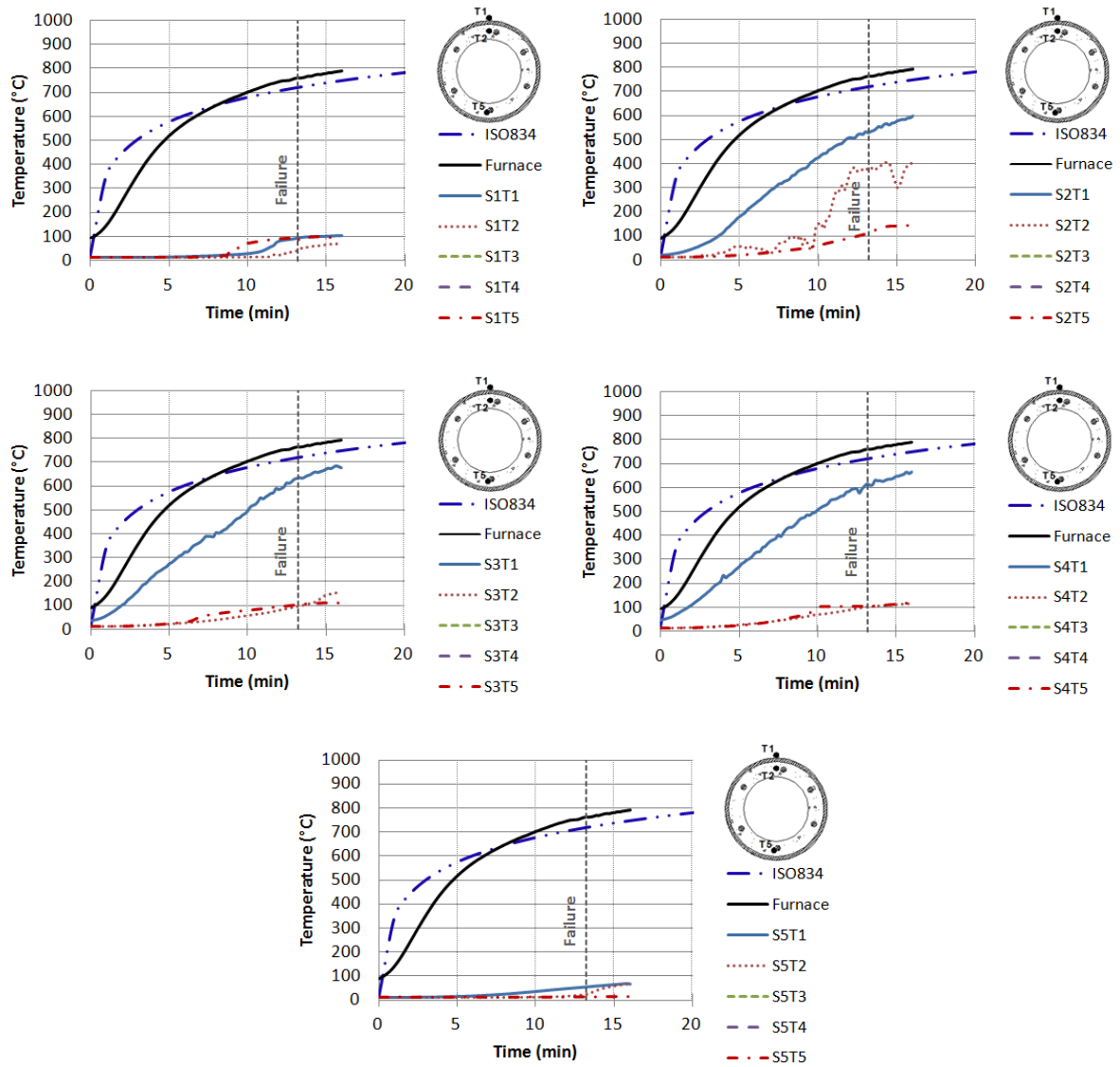


Figure B.29 – Distribution of temperature in cross-sections S1 to S5 for test column A29<sub>219-RING-RC-70%-Khigh</sub>.

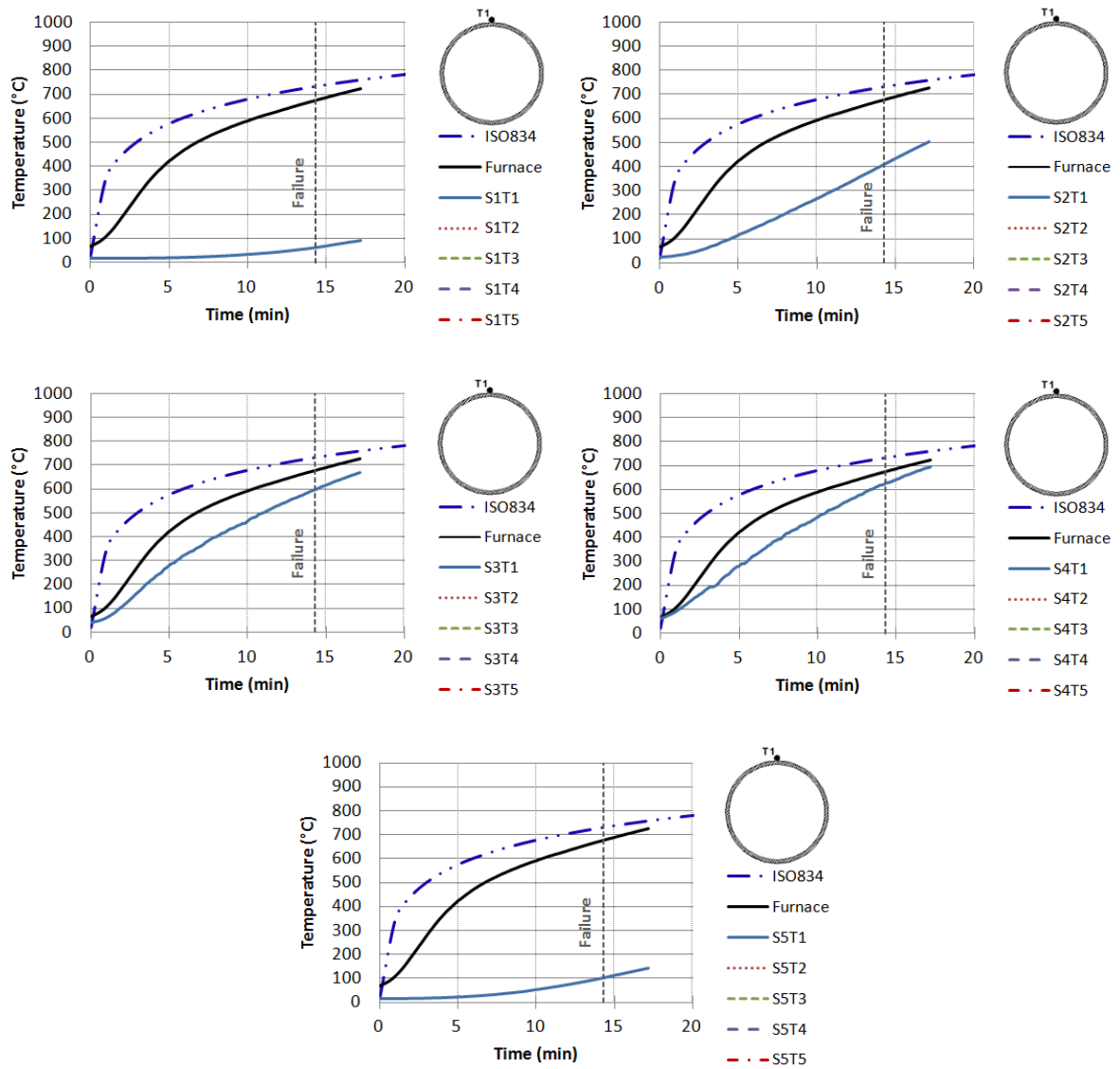


Figure B.30 – Distribution of temperature in cross-sections S1 to S5 for test column A30 219-70%-Khigh.



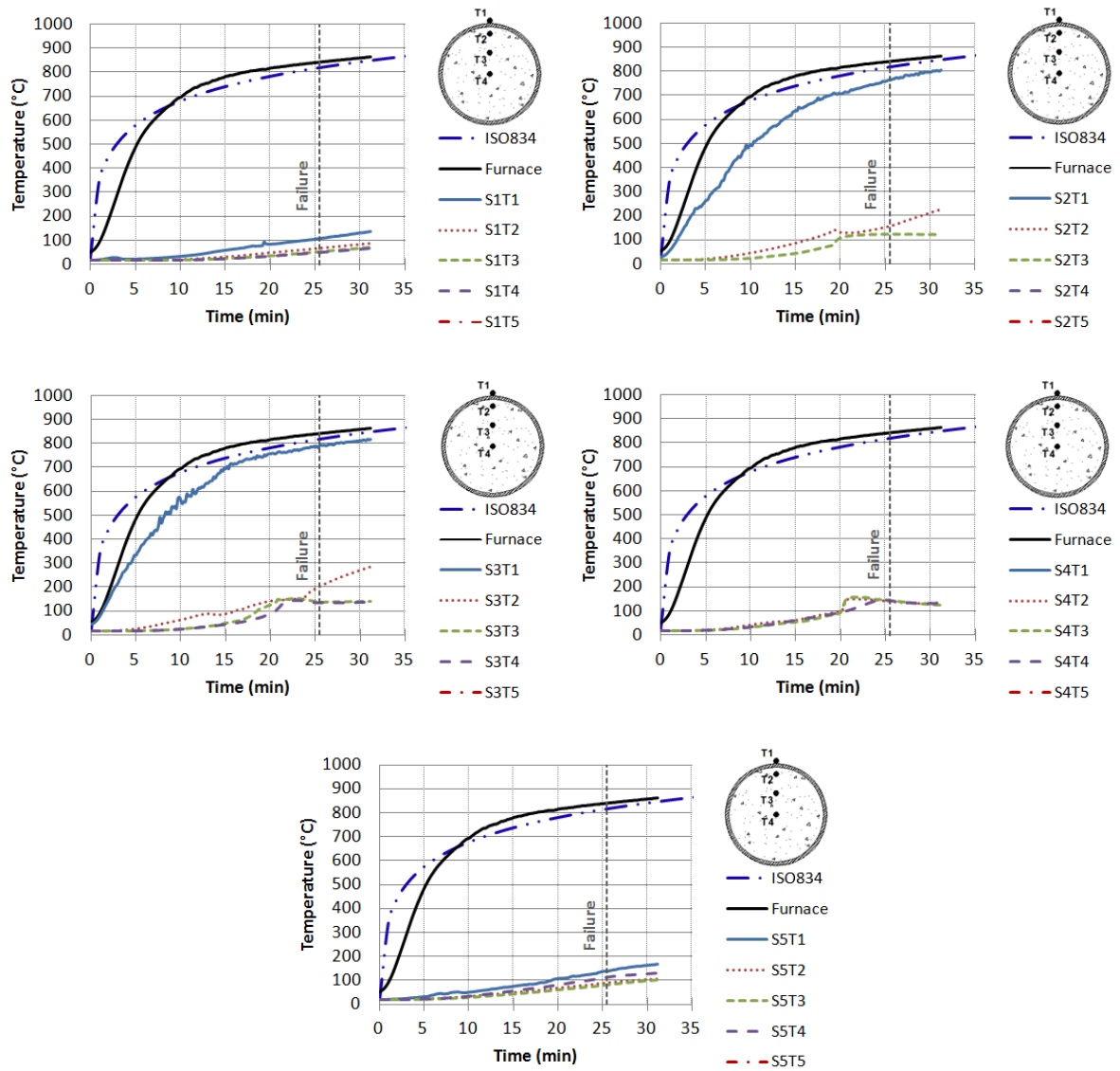


Figure B.31 – Distribution of temperature in cross-sections S1 to S5 for test column A31<sub>168-TOT-PC-30%-Khigh</sub>.

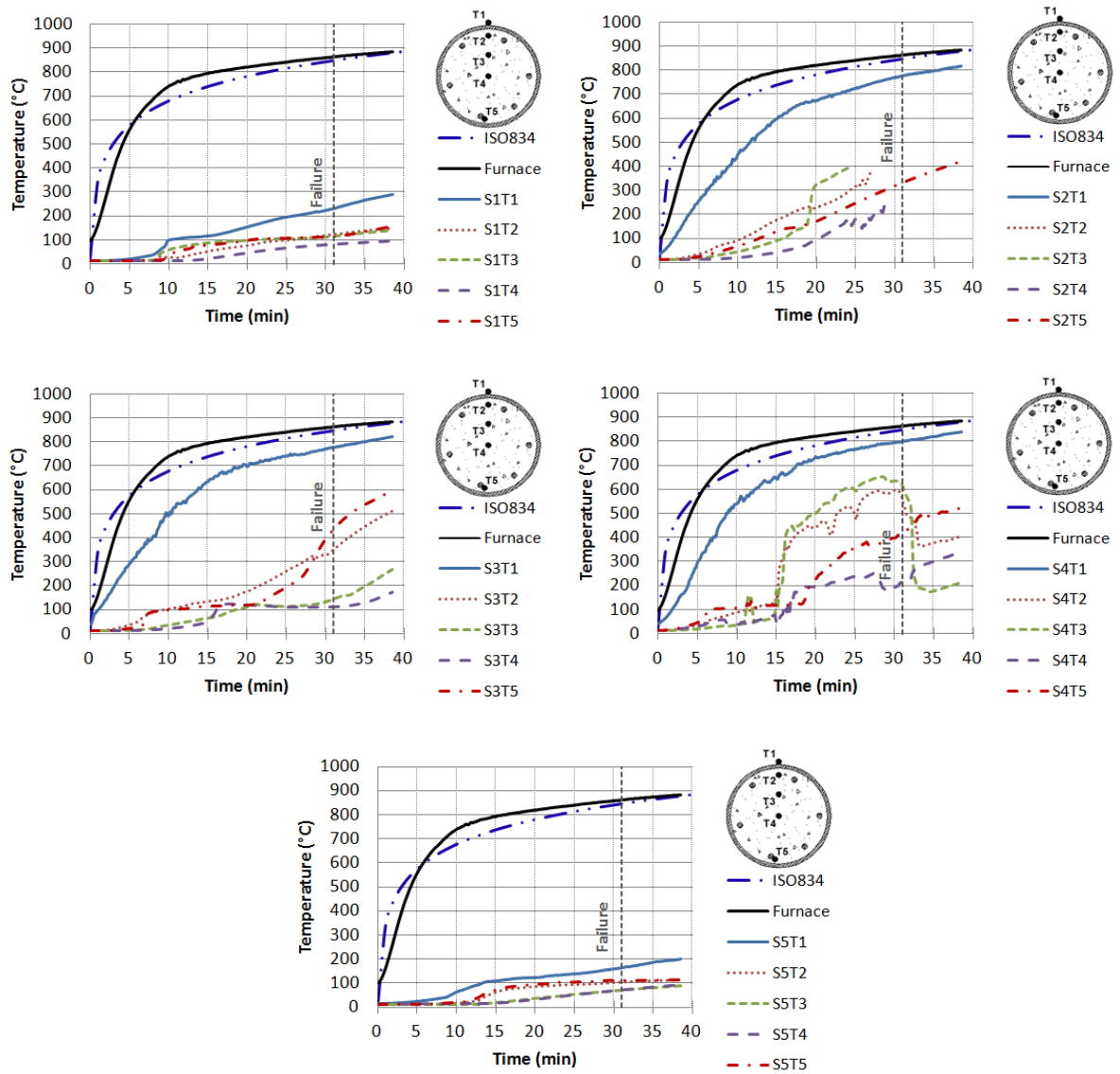


Figure B.32 – Distribution of temperature in cross-sections S1 to S5 for test column A32 168-TOT-RC-30%-Khigh-

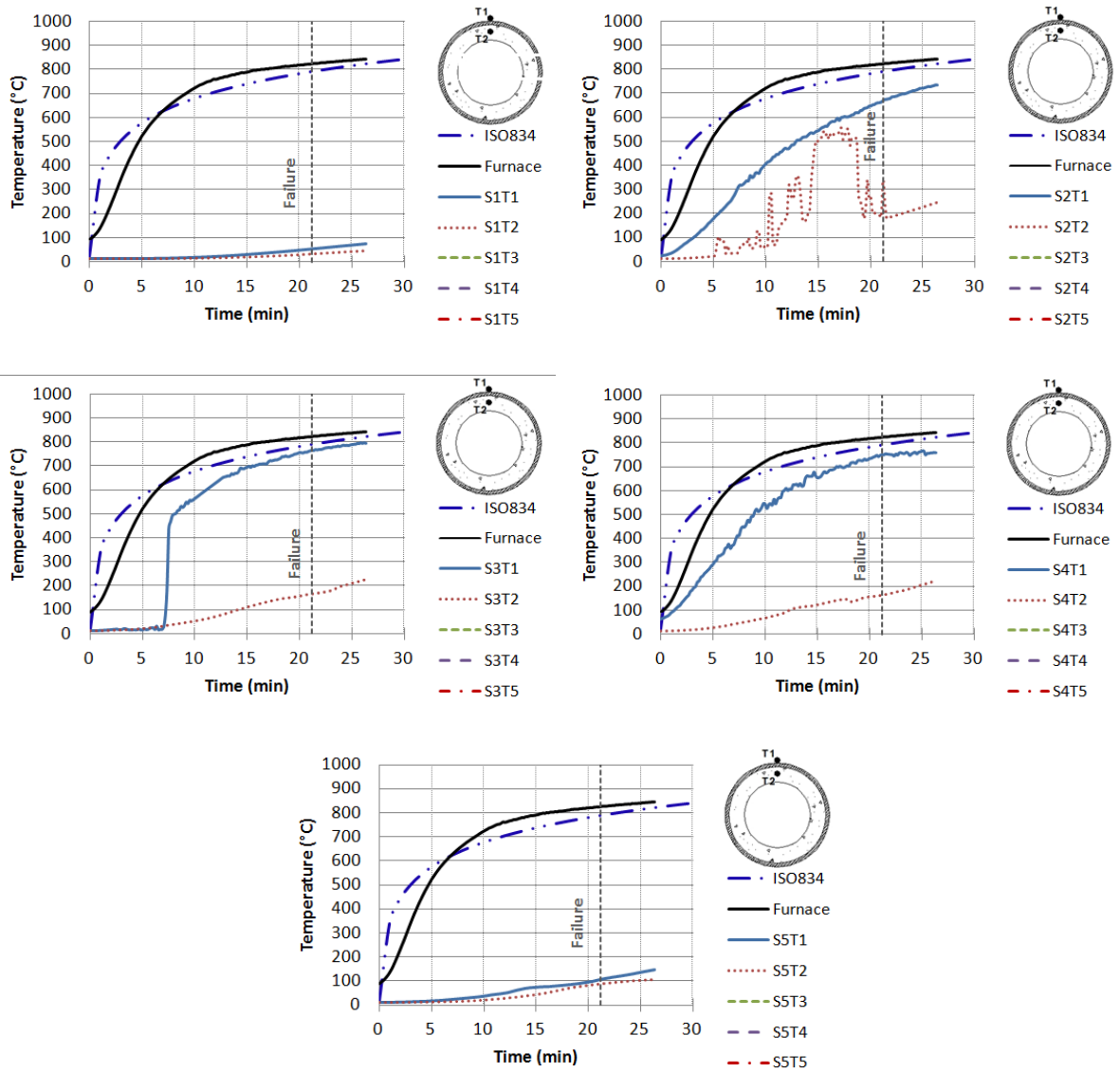


Figure B.33 – Distribution of temperature in cross-sections S1 to S5 for test column A33 168-RING-PC-30%-Khigh.

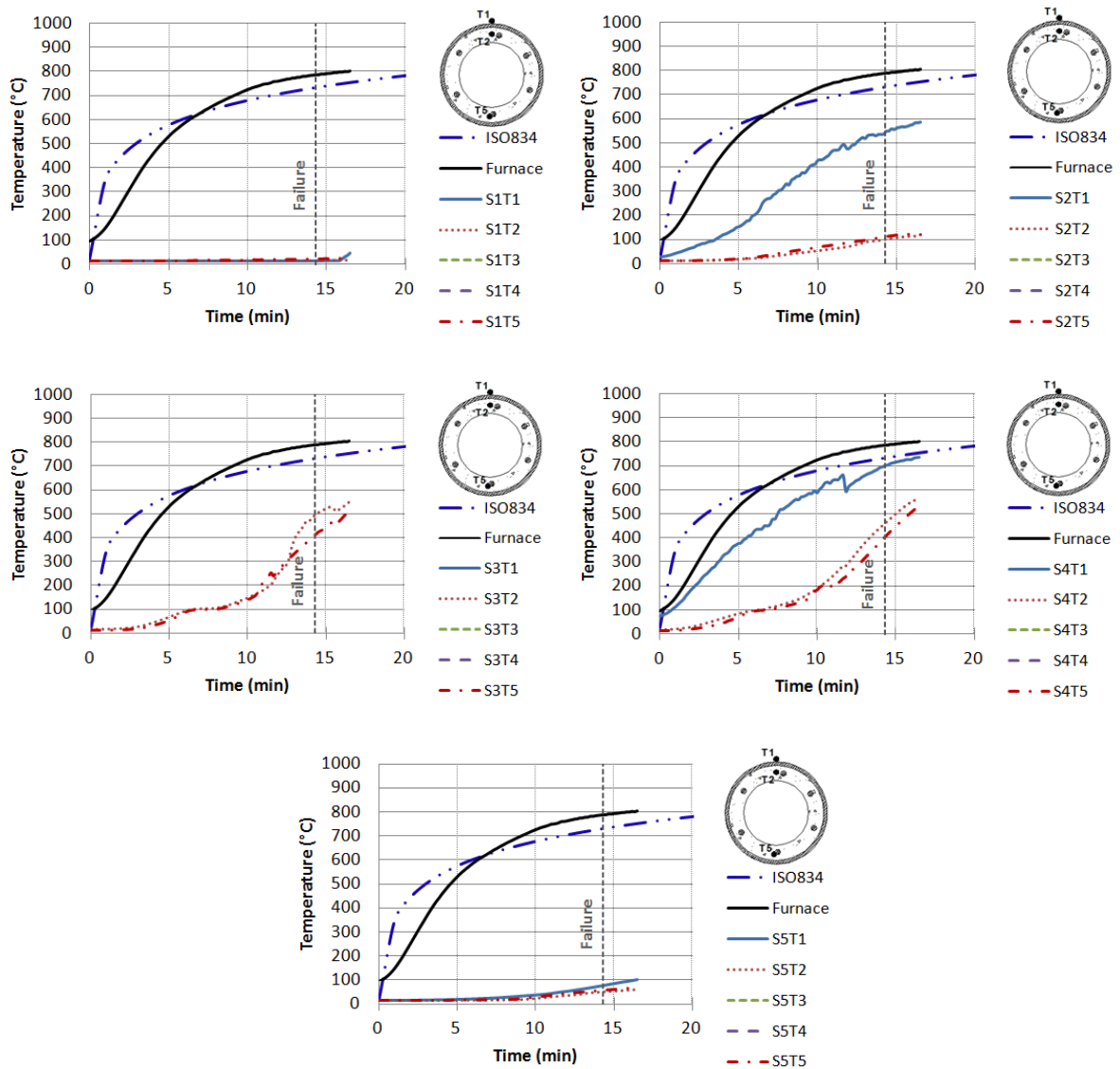


Figure B.34 – Distribution of temperature in cross-sections S1 to S5 for test column A34<sub>168-RING-RC-30%-Khigh</sub>.

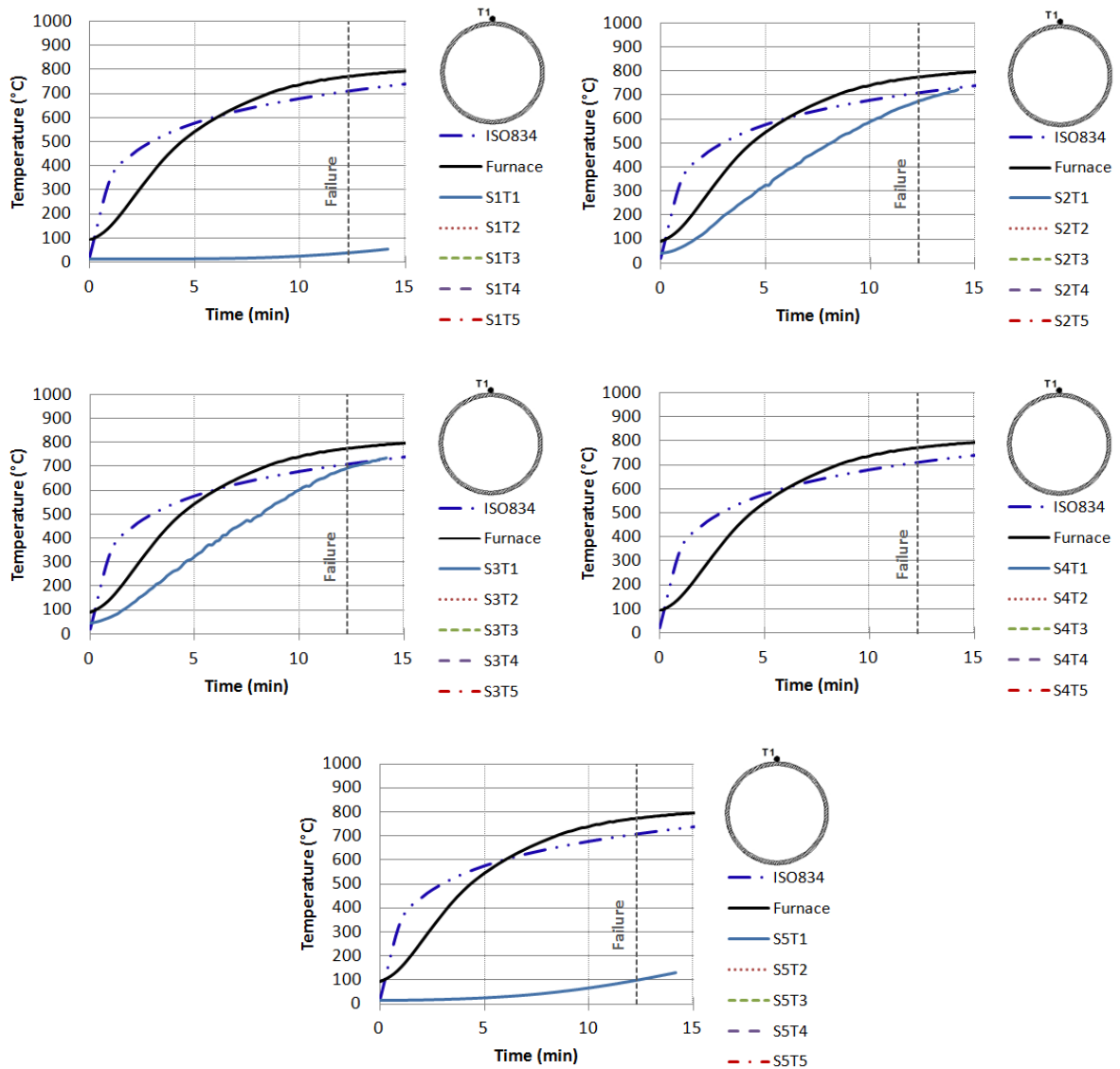


Figure B.35 – Distribution of temperature in cross-sections S1 to S5 for test column A35<sub>168-30%-Khigh</sub>.

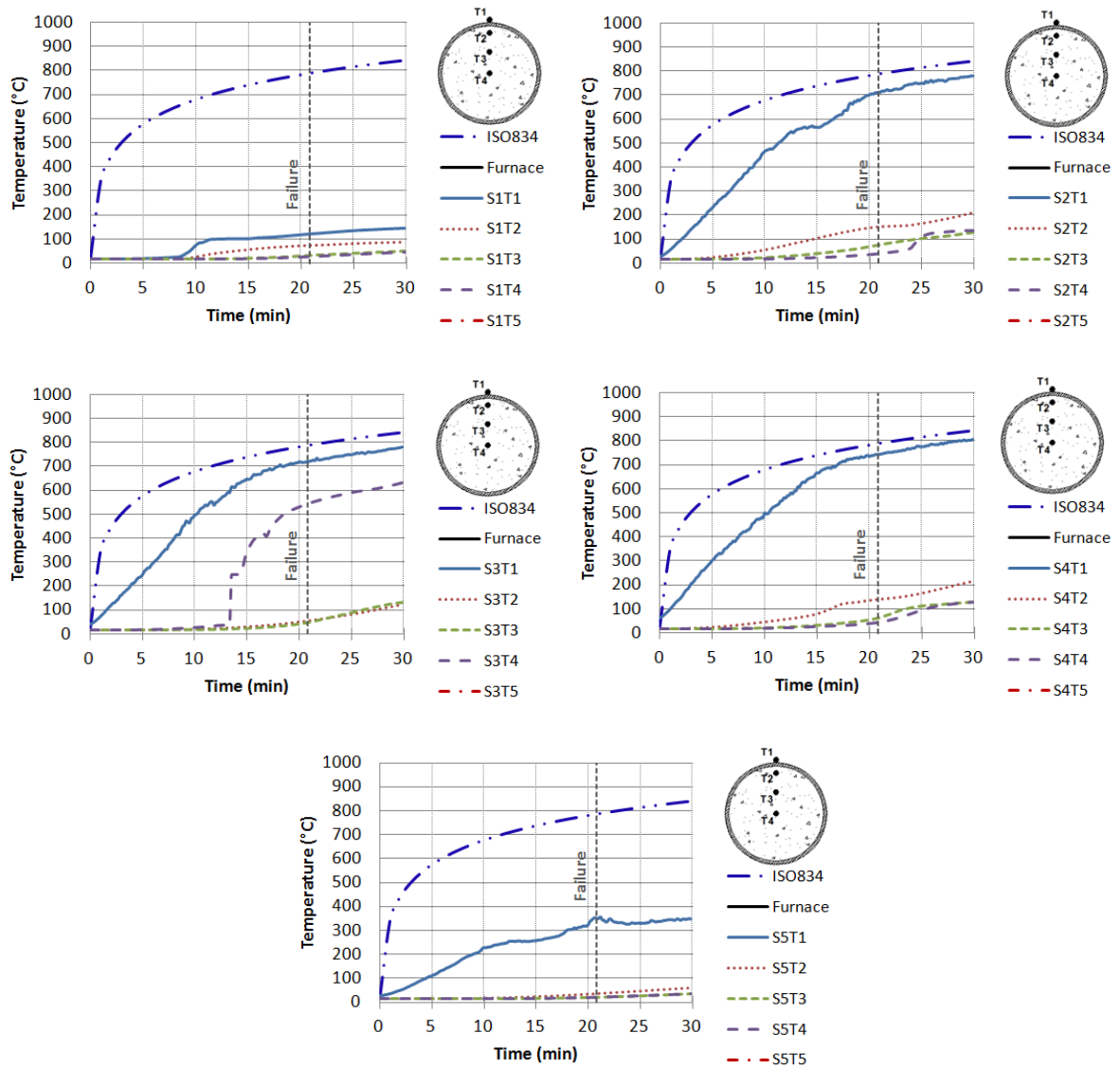


Figure B.36 – Distribution of temperature in cross-sections S1 to S5 for test column A36<sub>219-TOT-PC-30%-Khigh</sub>.

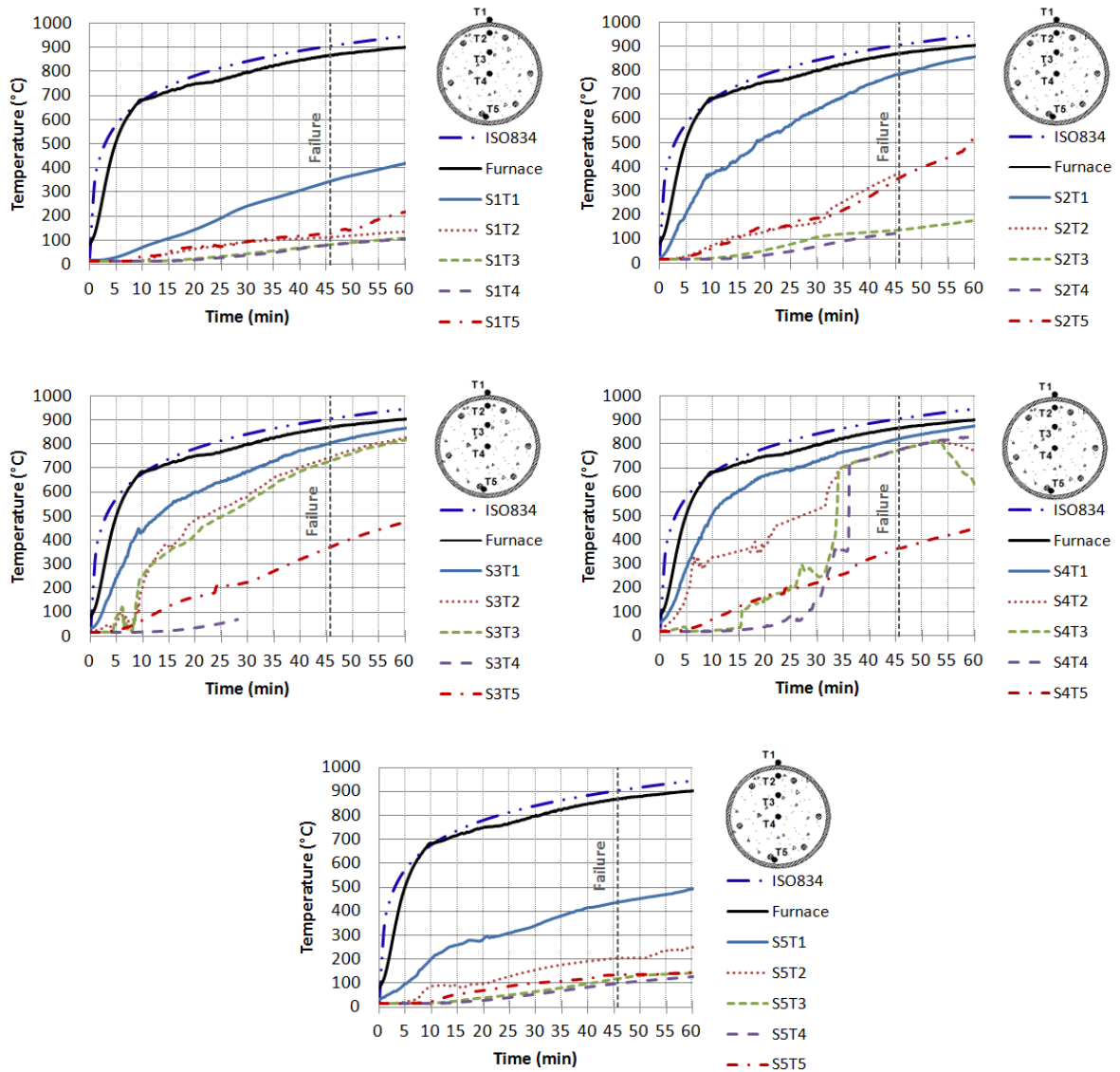


Figure B.37 – Distribution of temperature in cross-sections S1 to S5 for test column A37<sub>219-TOT-RC-30%-Khigh</sub>.

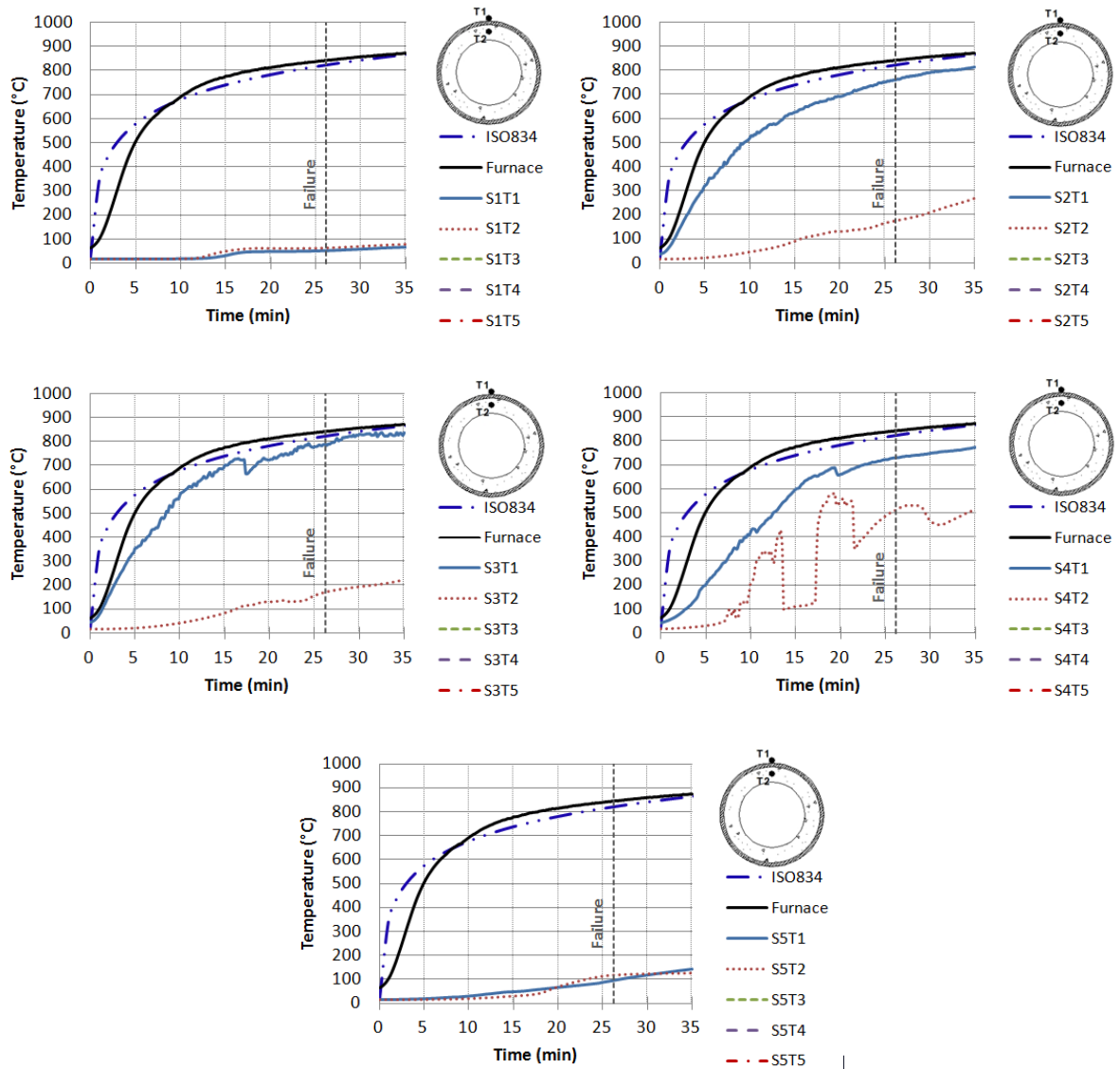


Figure B.38 – Distribution of temperature in cross-sections S1 to S5 for test column A38<sub>219-RING-PC-30%-Khigh</sub>.



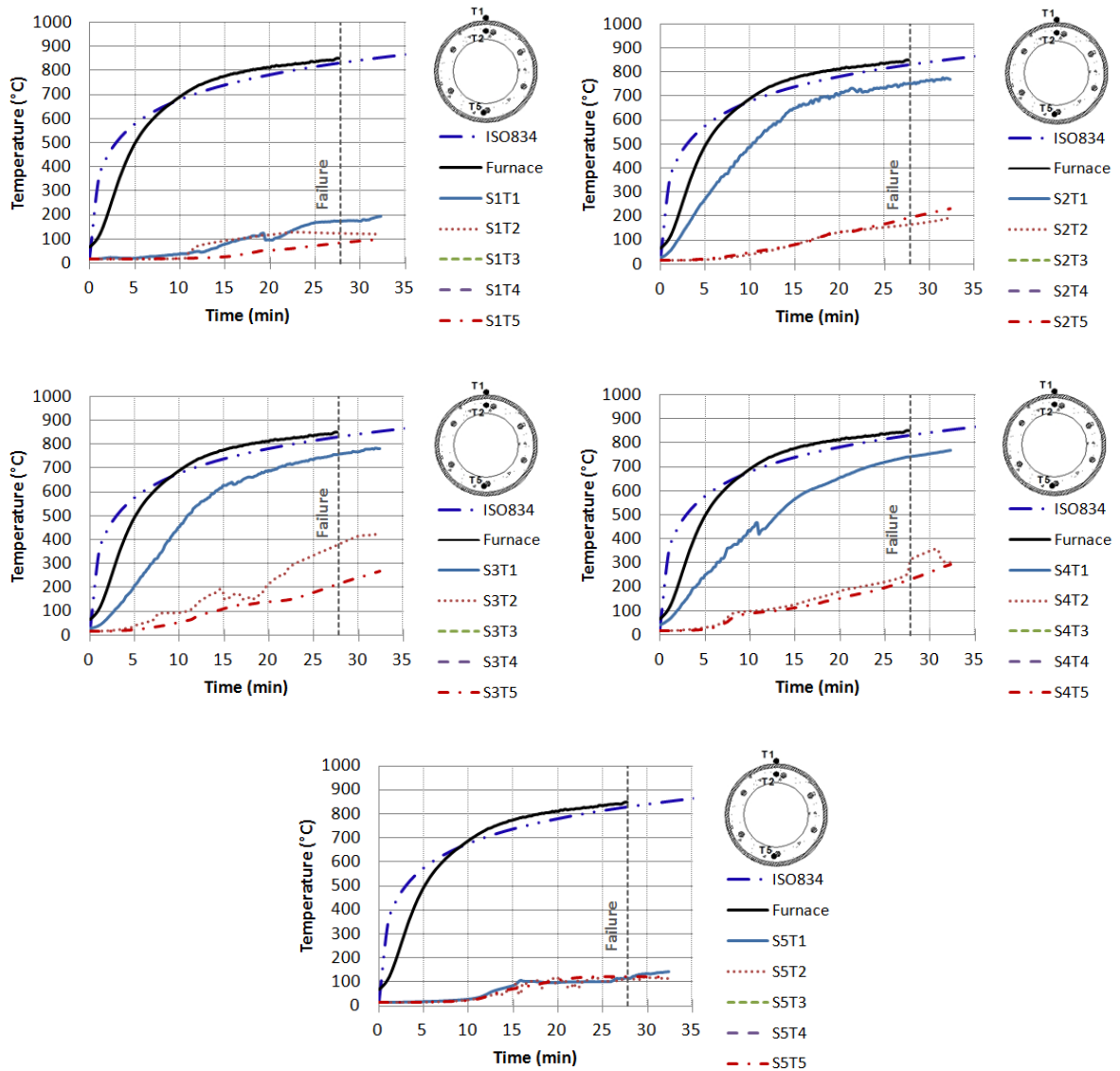


Figure B.39 – Distribution of temperature in cross-sections S1 to S5 for test column A39<sub>219-RING-RC-30%-Khigh</sub>.

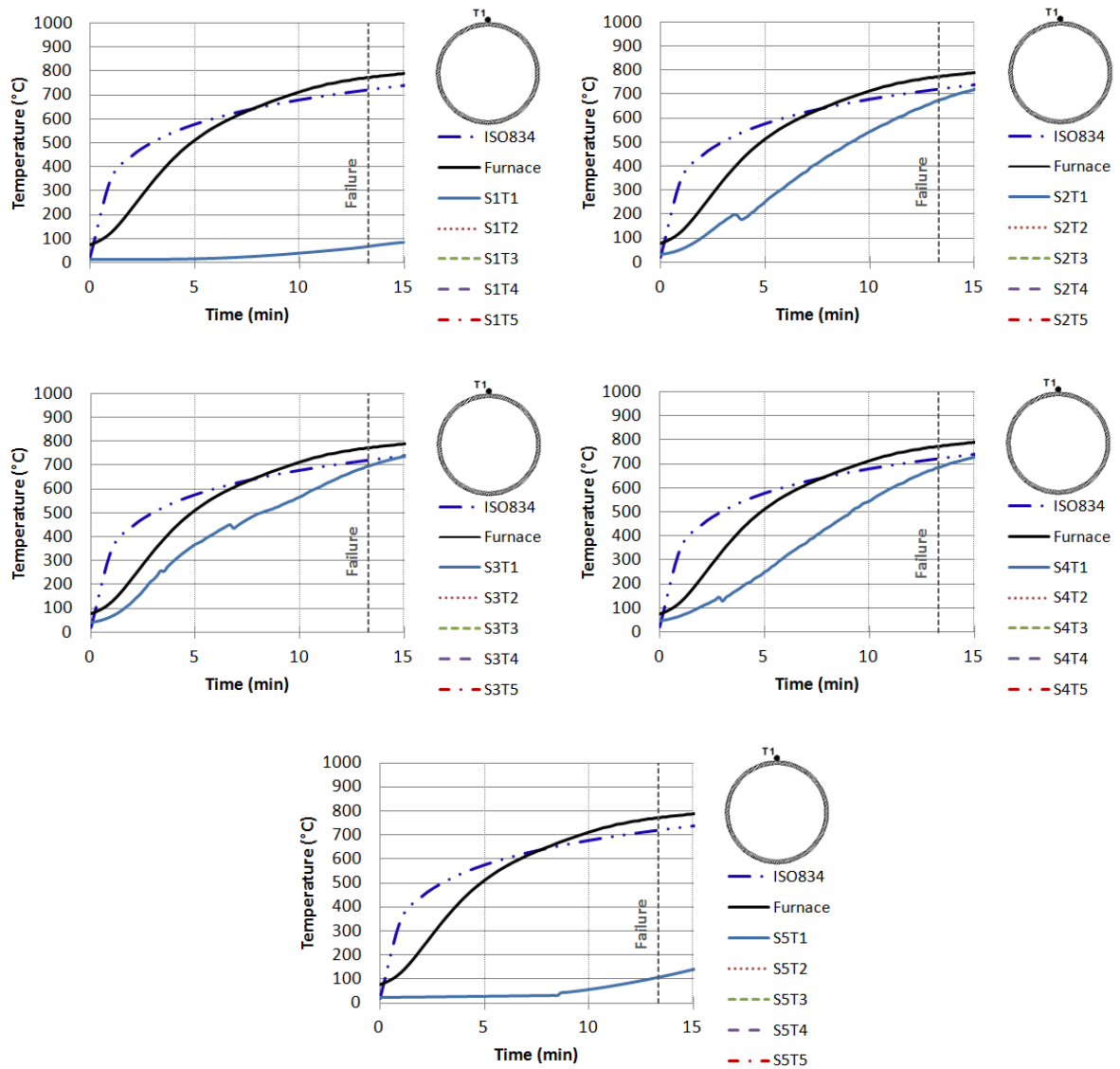


Figure B.40 – Distribution of temperature in cross-sections S1 to S5 for test column A40 219-30%-Khigh.

### APPENDIX C – Lateral deflections of tested columns

The lateral deflections of the columns were not presented in the main part of this thesis because there were not any well defined bending plan in the test columns, it was difficult to determine the lateral deflections and these results may be a bias in measurements.

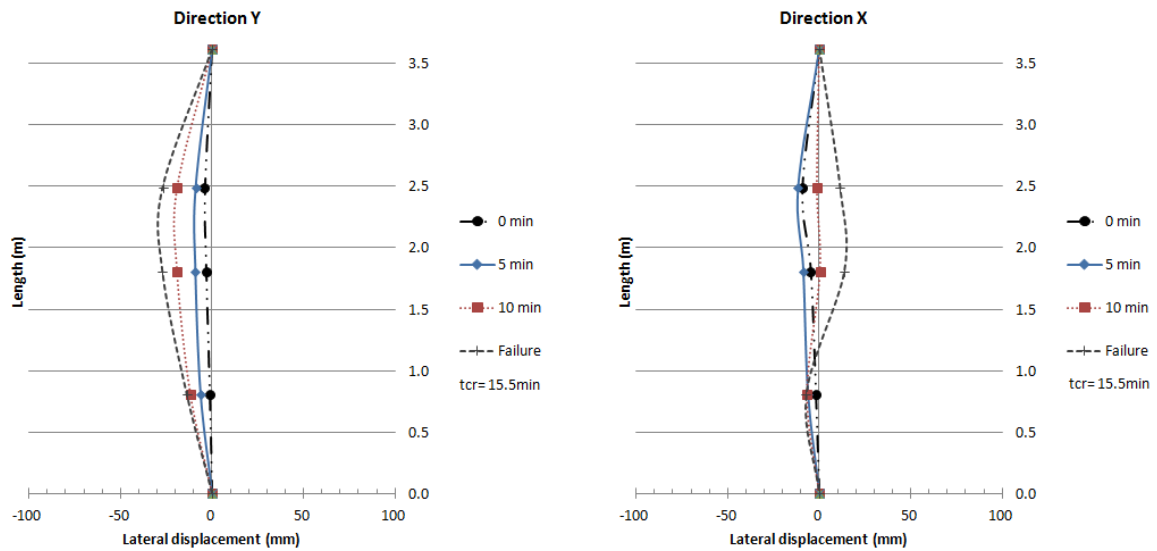


Figure C.1 – Lateral deflections in two perpendicular directions for test column A01 168-TOT-PC-70%-Klow.

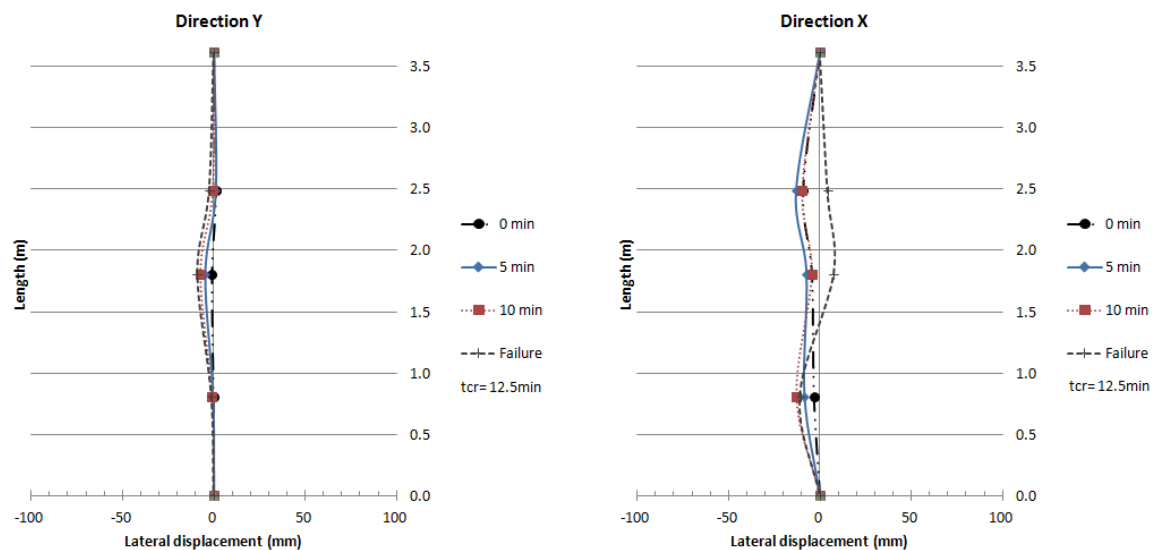


Figure C.2 – Lateral deflections in two perpendicular directions for test column A02 168-TOT-RC-70%-Klow.

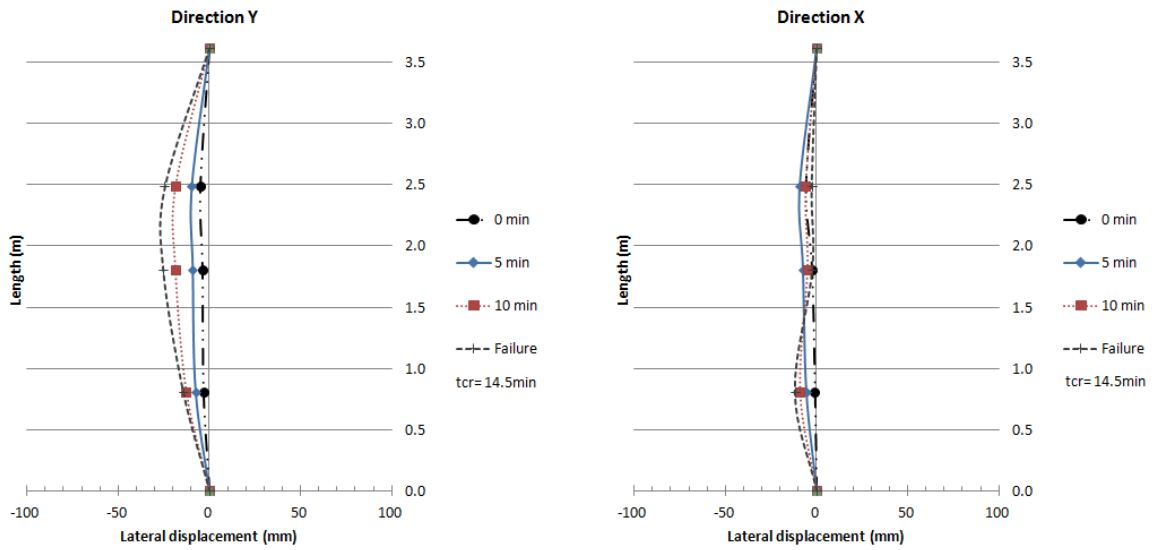


Figure C.3 – Lateral deflections in two perpendicular directions for test column A03<sub>168-RING-PC-70%-Klow</sub>.

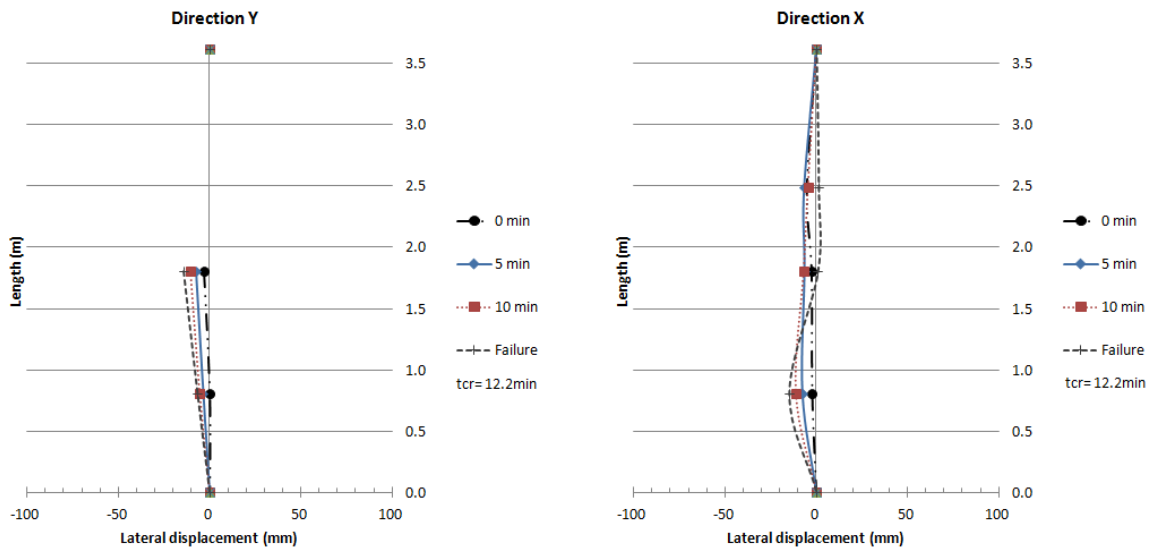


Figure C.4 – Lateral deflections in two perpendicular directions for test column A04<sub>168-RING-RC-70%-Klow</sub>.

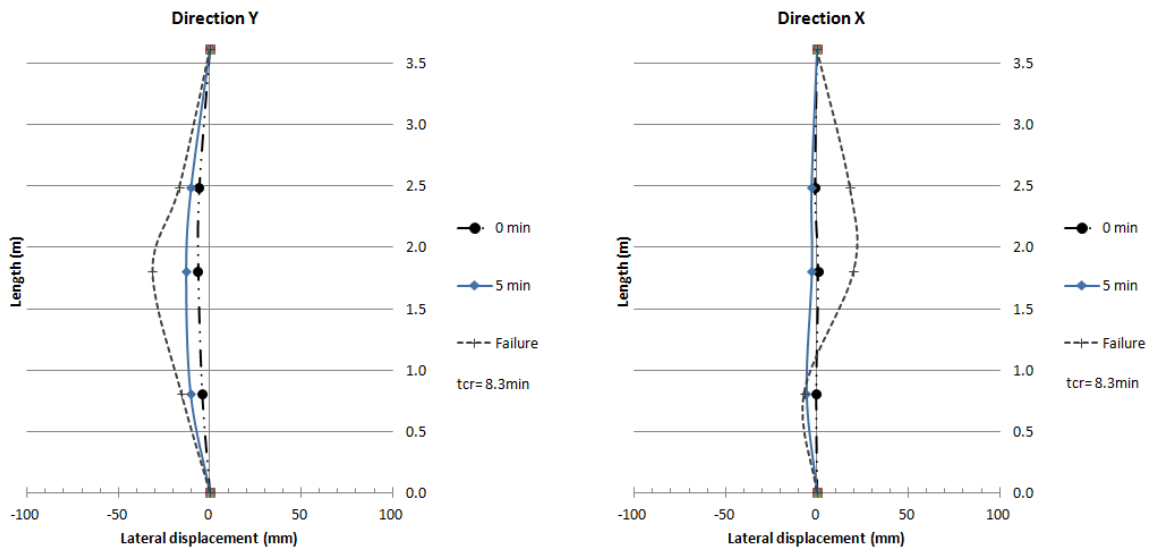


Figure C.5 – Lateral deflections in two perpendicular directions for test column A05<sub>168-70%-Klow</sub>.

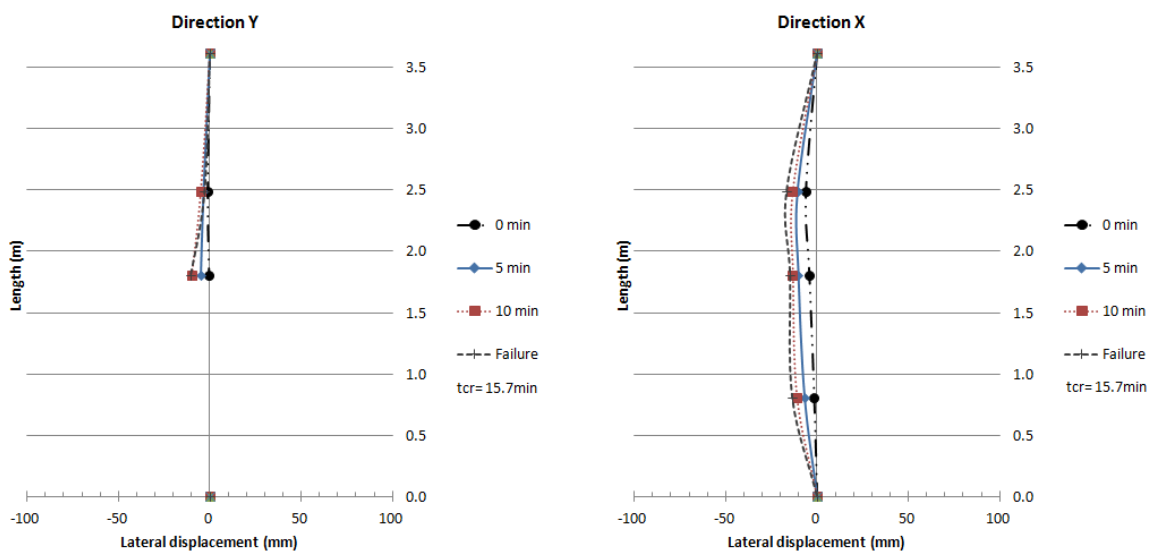


Figure C.6 – Lateral deflections in two perpendicular directions for test column A06<sub>219-TOT-PC-70%-Klow</sub>.

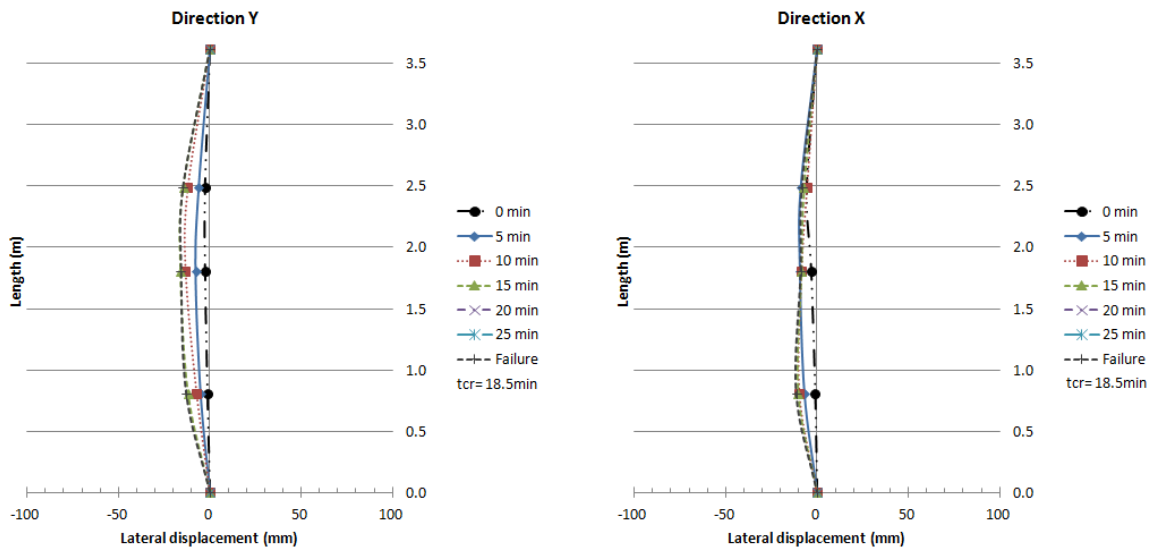


Figure C.7 – Lateral deflections in two perpendicular directions for test column A07<sub>219-TOT-RC-70%-Klow</sub>.

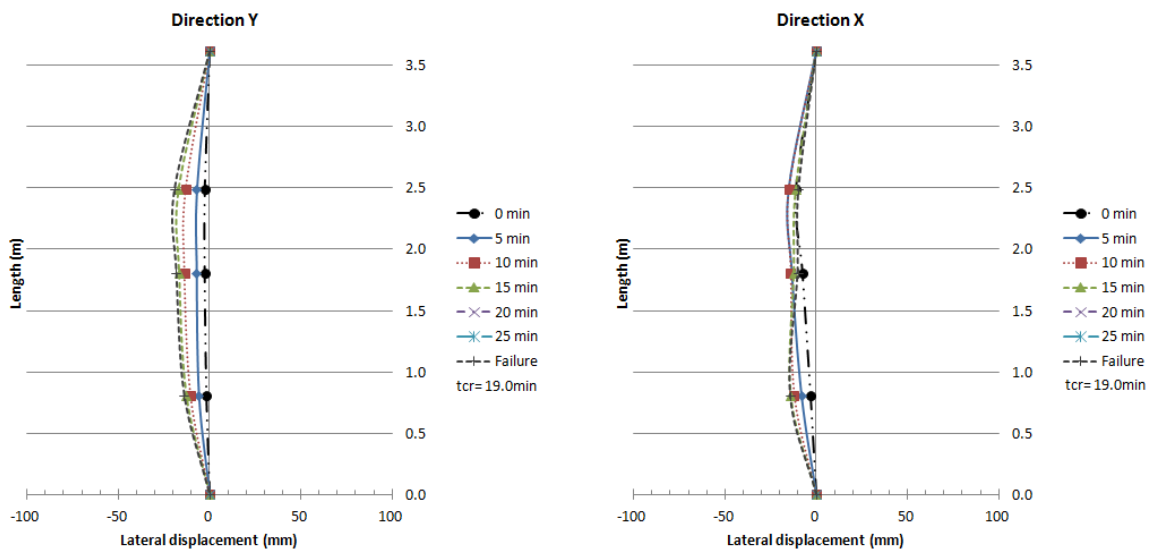


Figure C.8 – Lateral deflections in two perpendicular directions for test column A08<sub>219-RING-PC-70%-Klow</sub>.

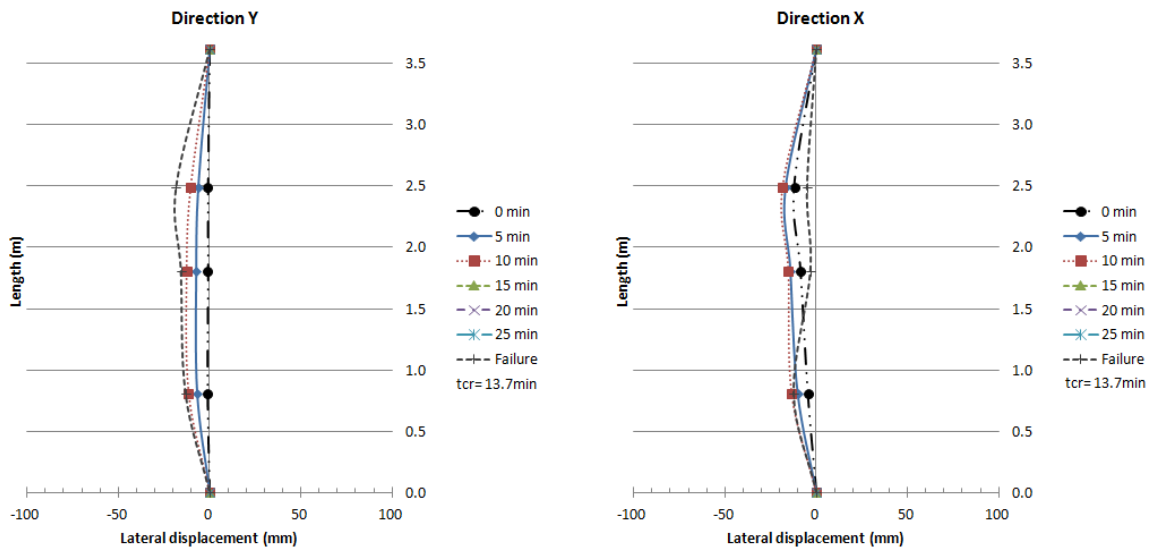


Figure C.9 – Lateral deflections in two perpendicular directions for test column A09<sub>219-RING-RC-70%-Klow</sub>.

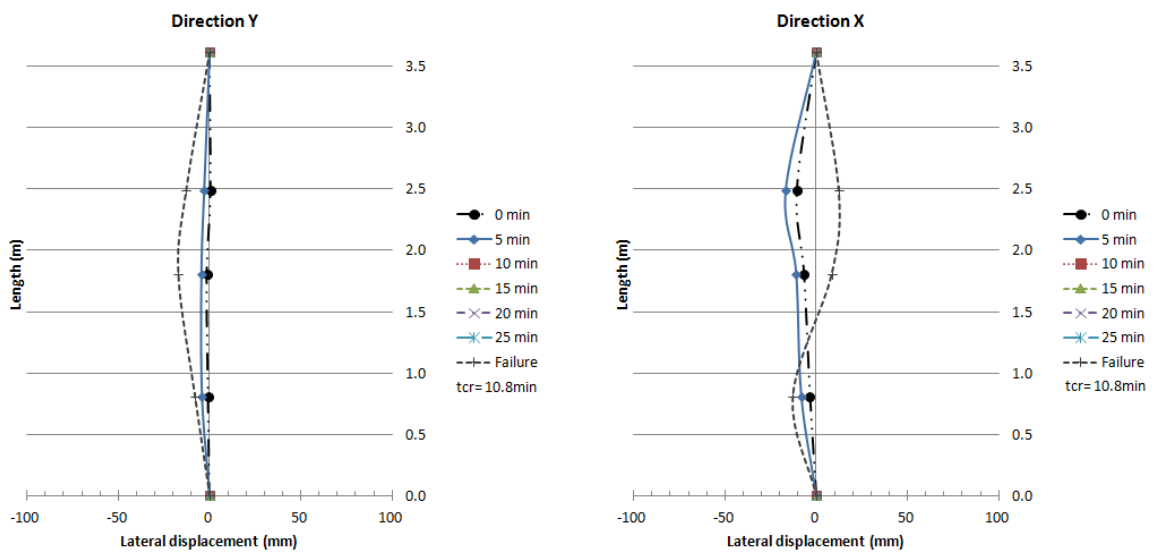


Figure C.10 – Lateral deflections in two perpendicular directions for test column A10<sub>219-70%-Klow</sub>.

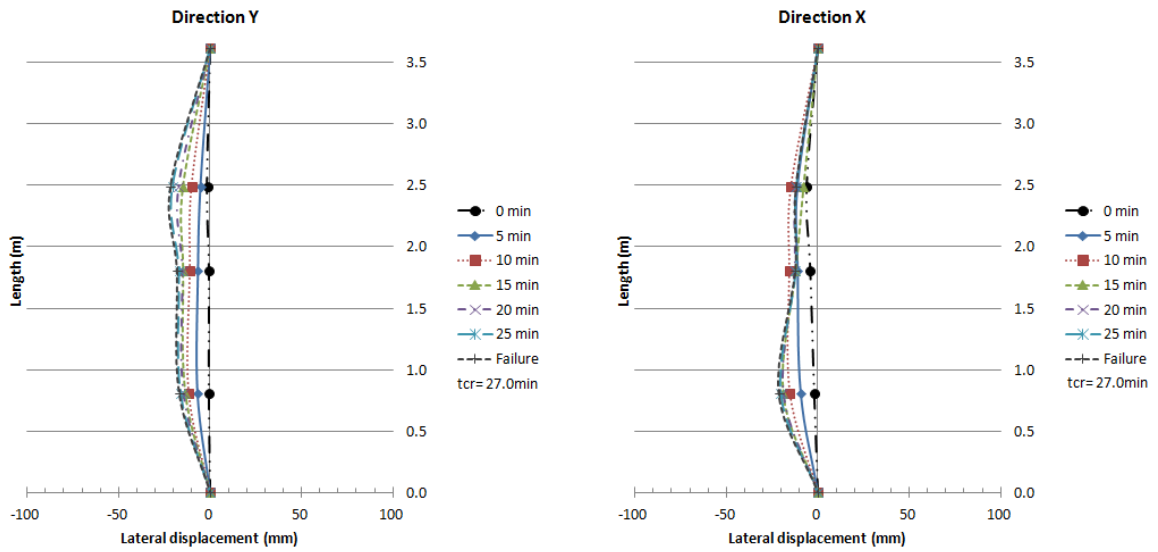


Figure C.11 – Lateral deflections in two perpendicular directions for test column A11<sub>168-TOT-PC-30%-Klow</sub>.

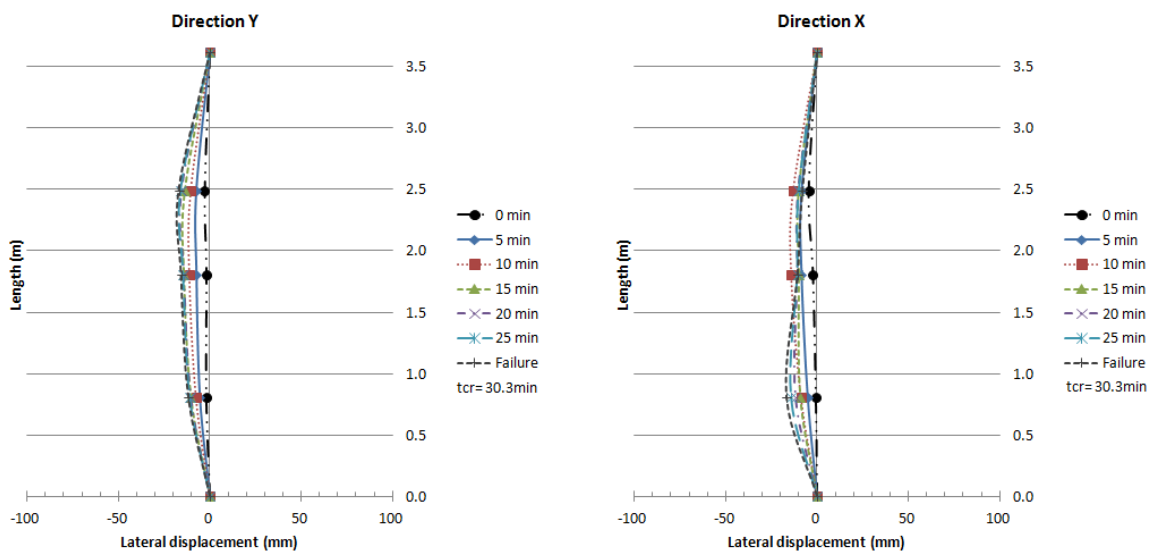


Figure C.12 – Lateral deflections in two perpendicular directions for test column A12<sub>168-TOT-RC-30%-Klow</sub>.



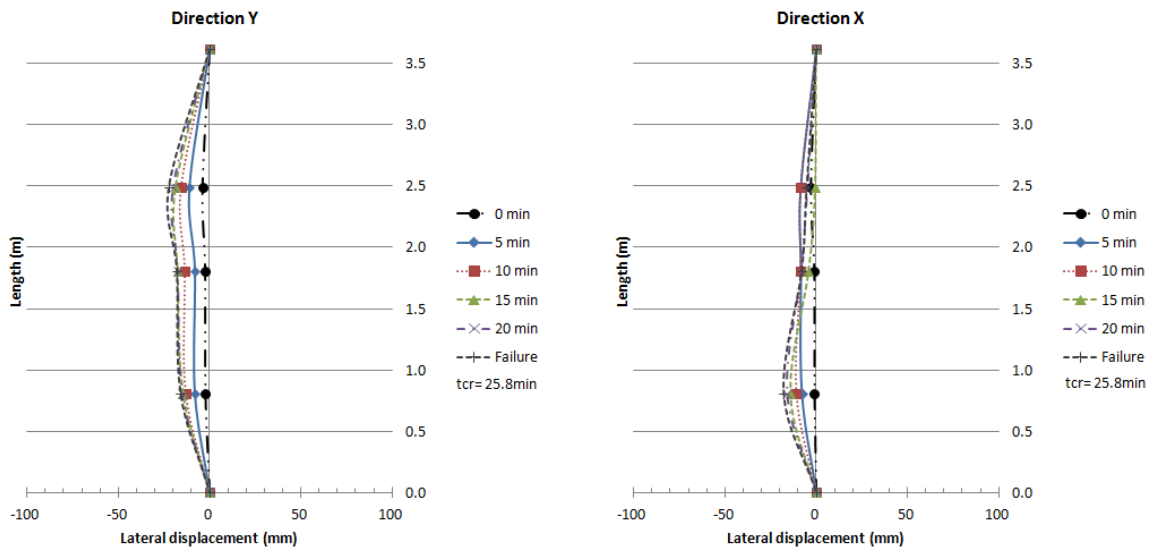


Figure C.13 – Lateral deflections in two perpendicular directions for test column A13<sub>168-RING-PC-30%-Klow</sub>.

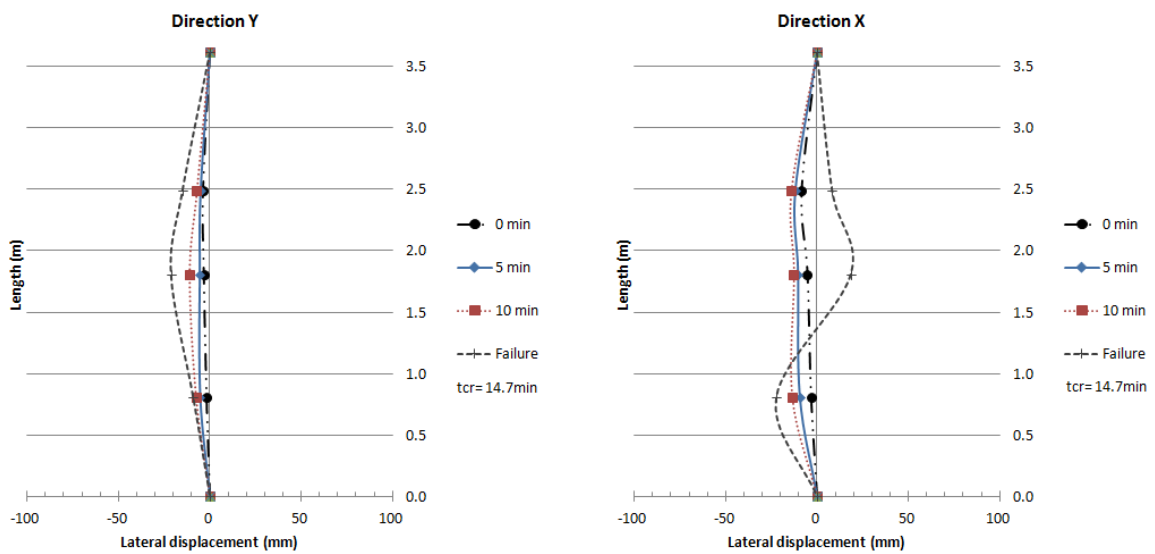


Figure C.14 – Lateral deflections in two perpendicular directions for test column A14<sub>168-RING-RC-30%-Klow</sub>.

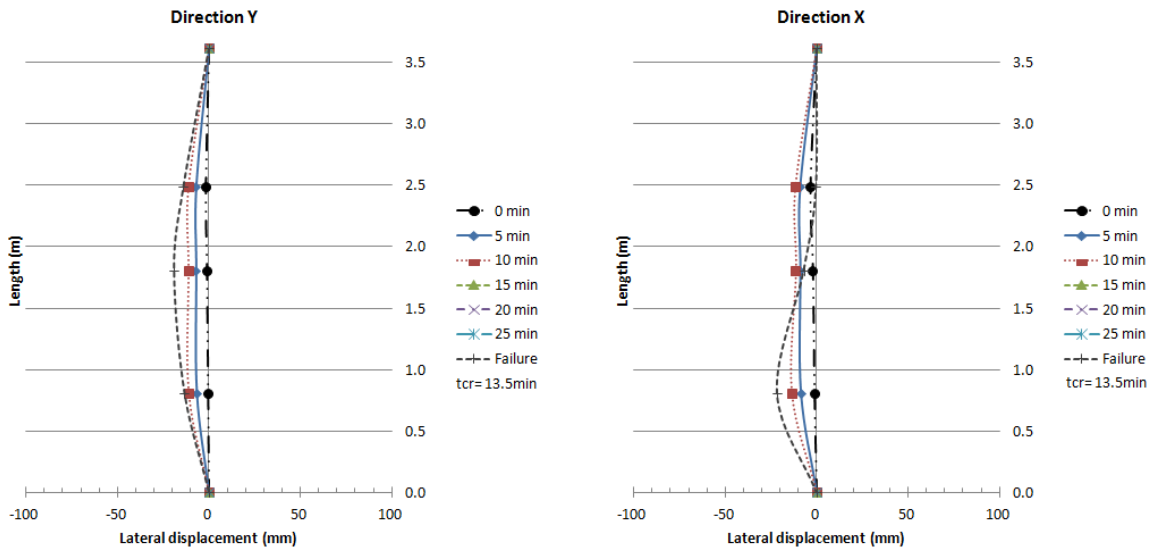


Figure C.15 – Lateral deflections in two perpendicular directions for test column A15<sub>168-30%-Klow</sub>.

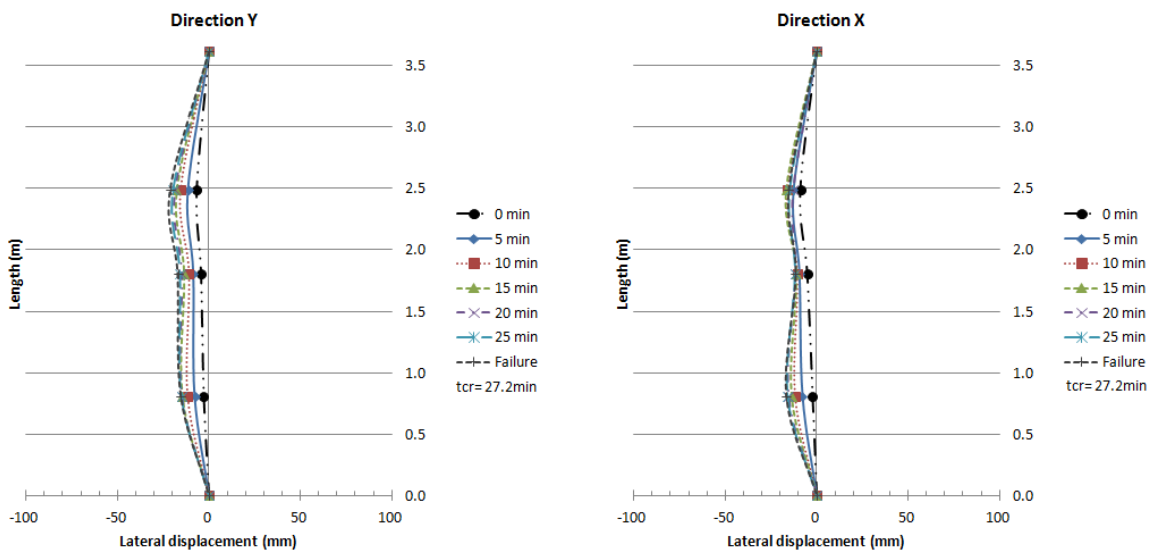


Figure C.16 – Lateral deflections in two perpendicular directions for test column A16<sub>219-TOT-PC-30%-Klow</sub>.

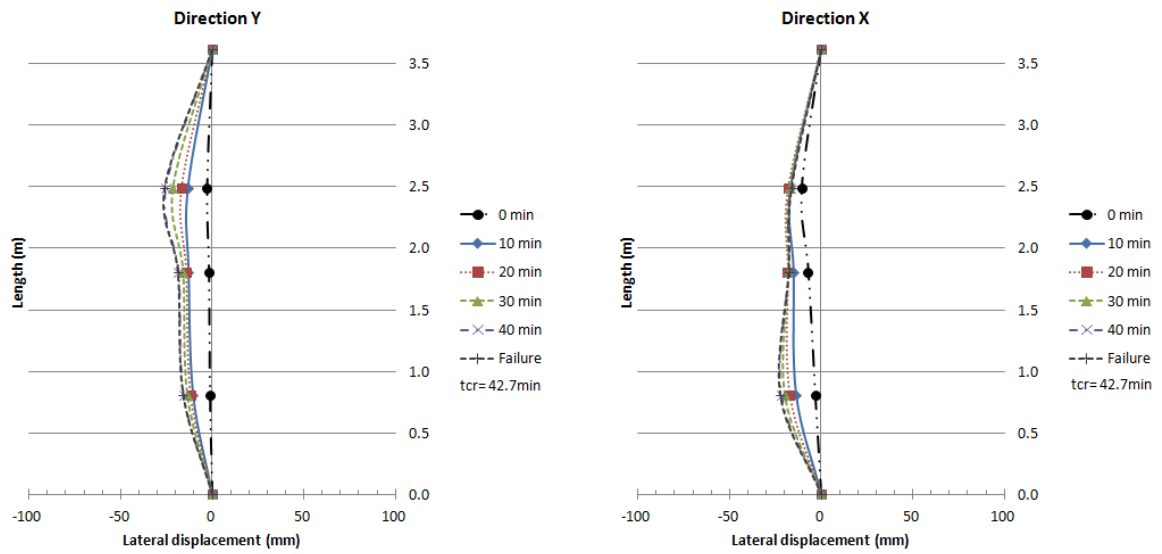


Figure C.17 – Lateral deflections in two perpendicular directions for test column A17<sub>219-TOT-RC-30%-Klow</sub>.

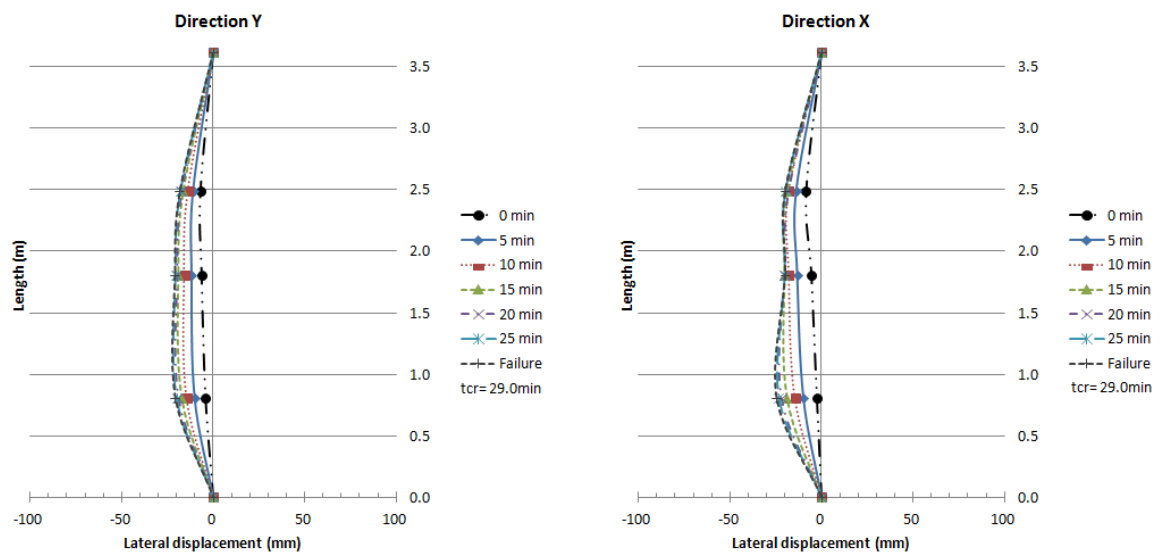


Figure C.18 – Lateral deflections in two perpendicular directions for test column A18<sub>219-RING-PC-30%-Klow</sub>.

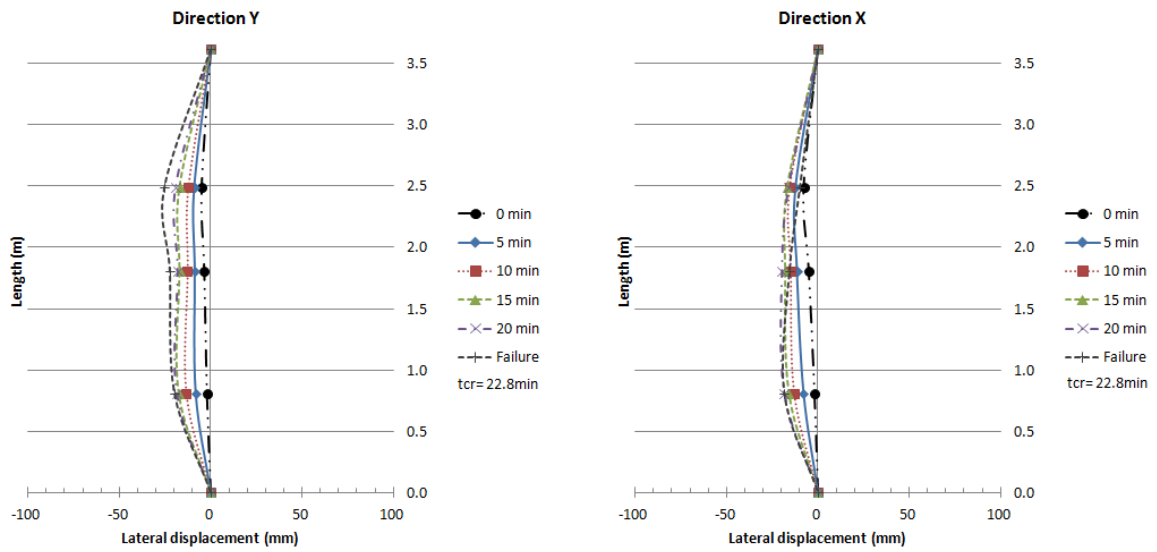


Figure C.19 – Lateral deflections in two perpendicular directions for test column A19<sub>219-RING-RC-30%-Klow</sub>.

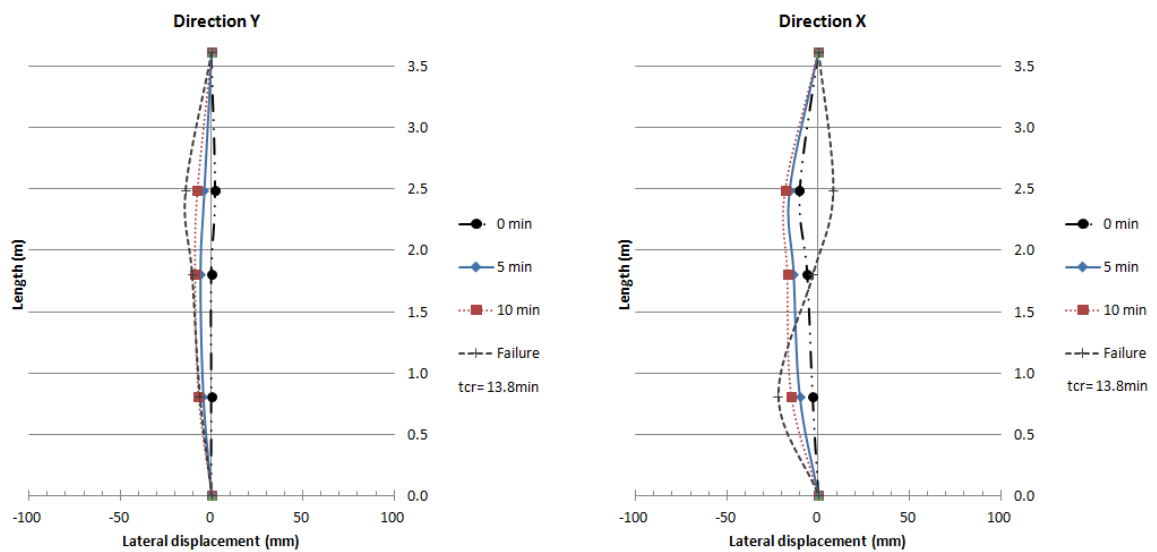


Figure C.20 – Lateral deflections in two perpendicular directions for test column A20<sub>219-30%-Klow</sub>.

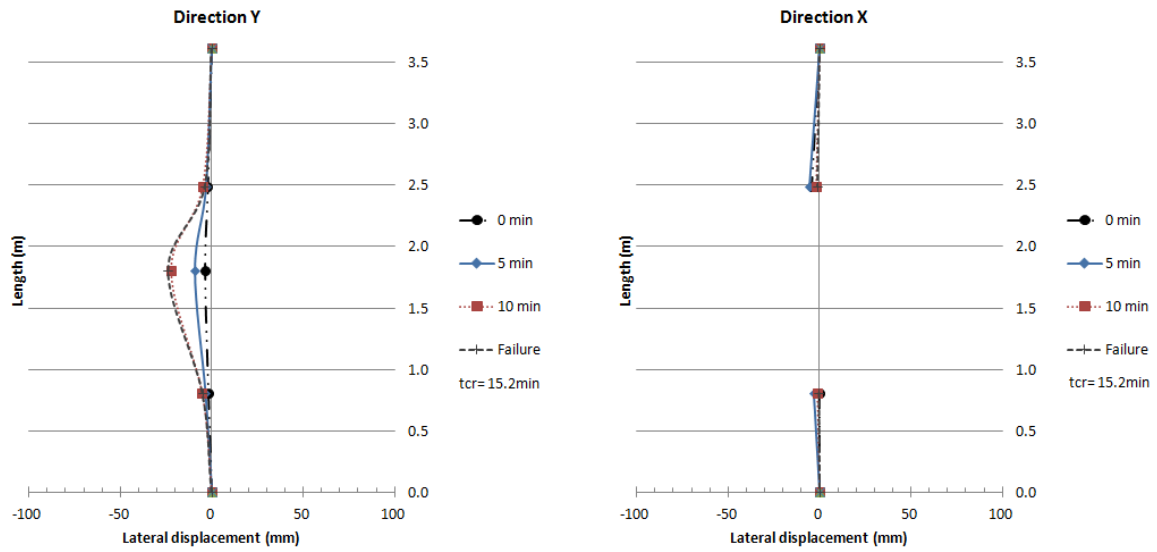


Figure C.21 – Lateral deflections in two perpendicular directions for test column A21<sub>168-TOT-PC-70%-Khigh</sub>.

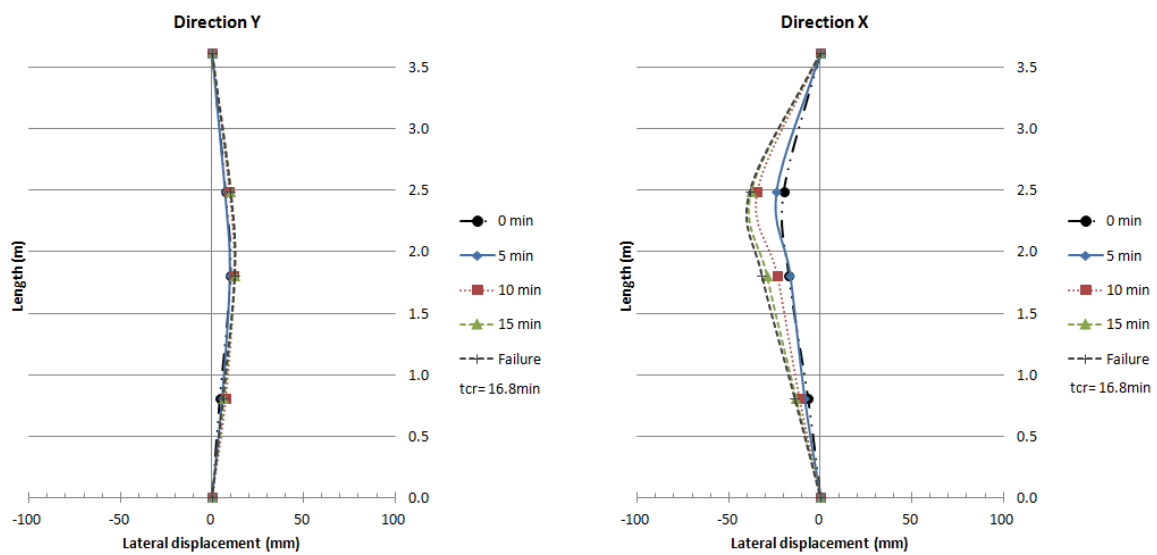


Figure C.22 – Lateral deflections in two perpendicular directions for test column A22<sub>168-TOT-RC-70%-Khigh</sub>.

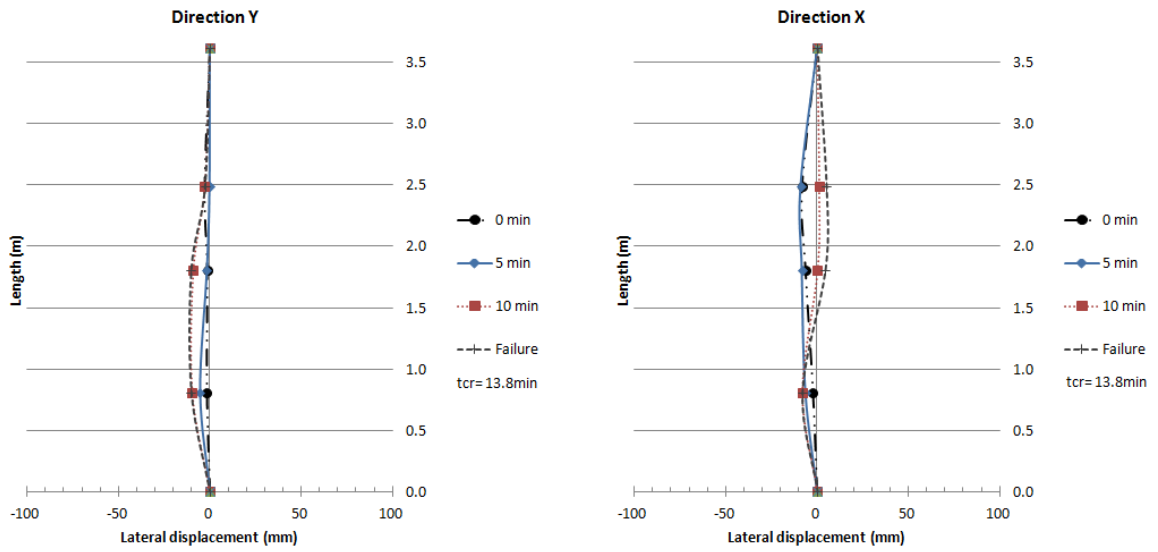


Figure C.23 – Lateral deflections in two perpendicular directions for test column A23<sub>168-RING-PC-70%-Khigh</sub>.

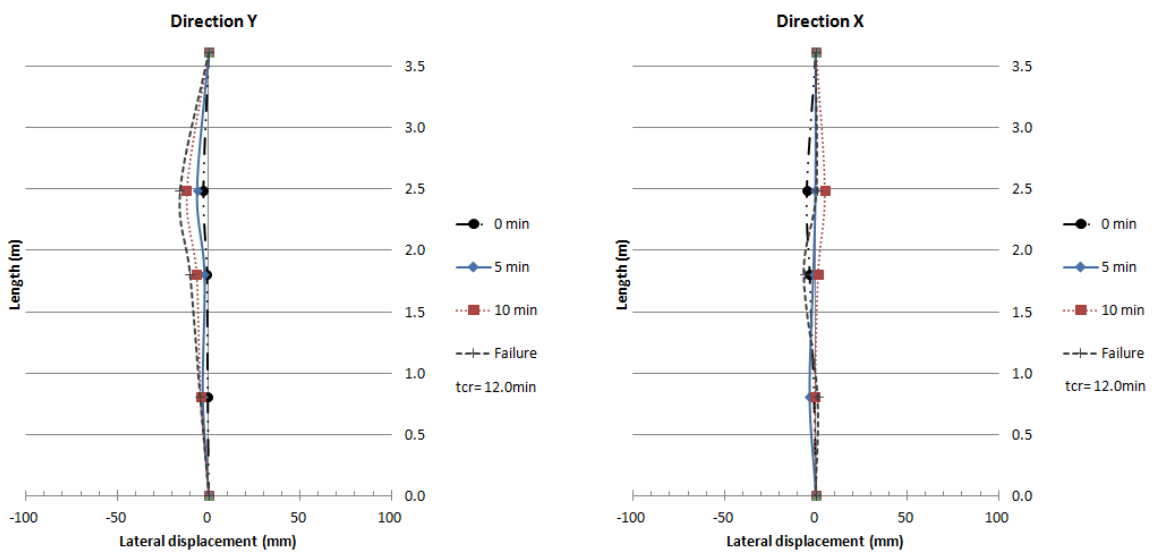


Figure C.24 – Lateral deflections in two perpendicular directions for test column A24<sub>168-RING-RC-70%-Khigh</sub>.

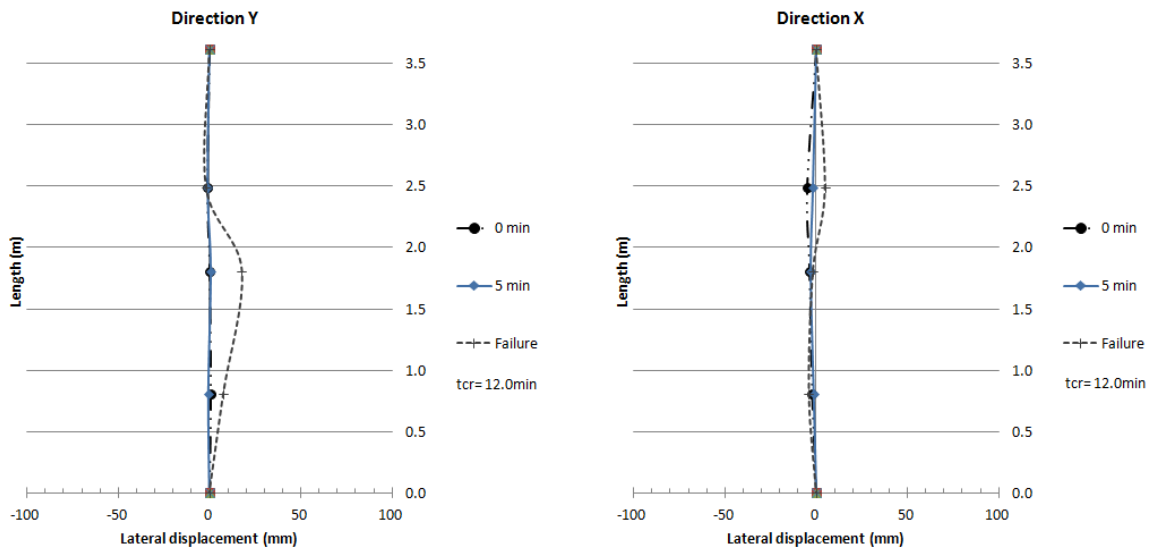


Figure C.25 – Lateral deflections in two perpendicular directions for test column A25<sub>168-70%-Khigh</sub>

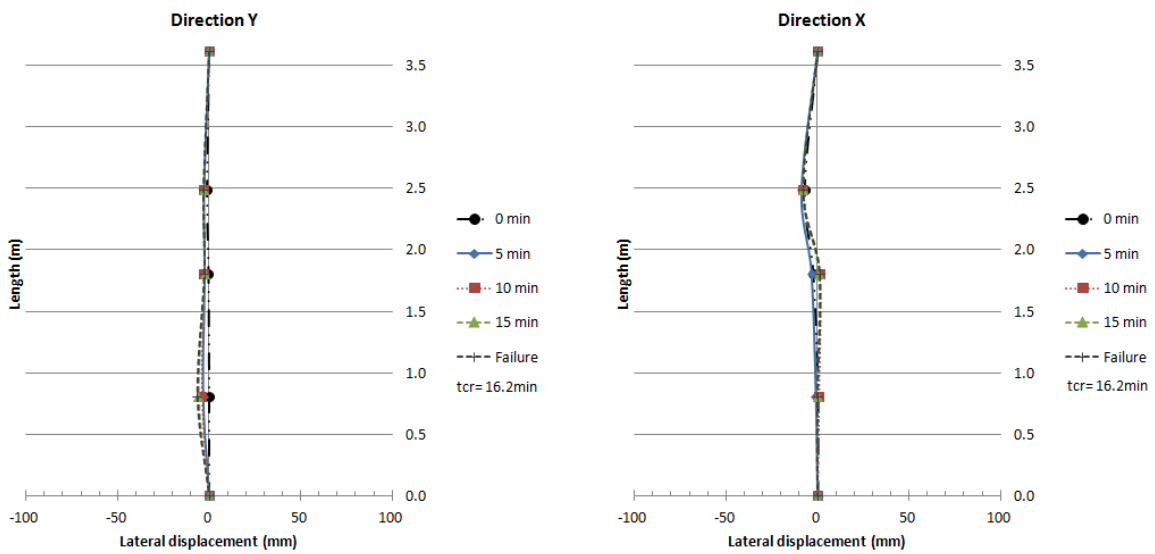


Figure C.26 – Lateral deflections in two perpendicular directions for test column A26<sub>219-TOT-PC-70%-Khigh</sub>

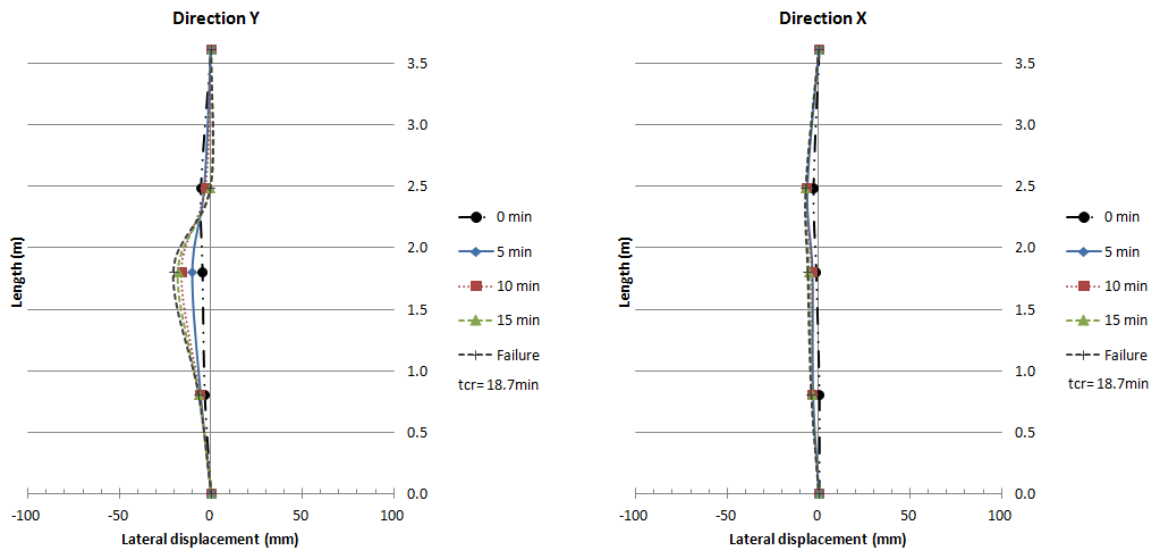


Figure C.27 – Lateral deflections in two perpendicular directions for test column A27<sub>219-TOT-RC-70%-Khigh</sub>.

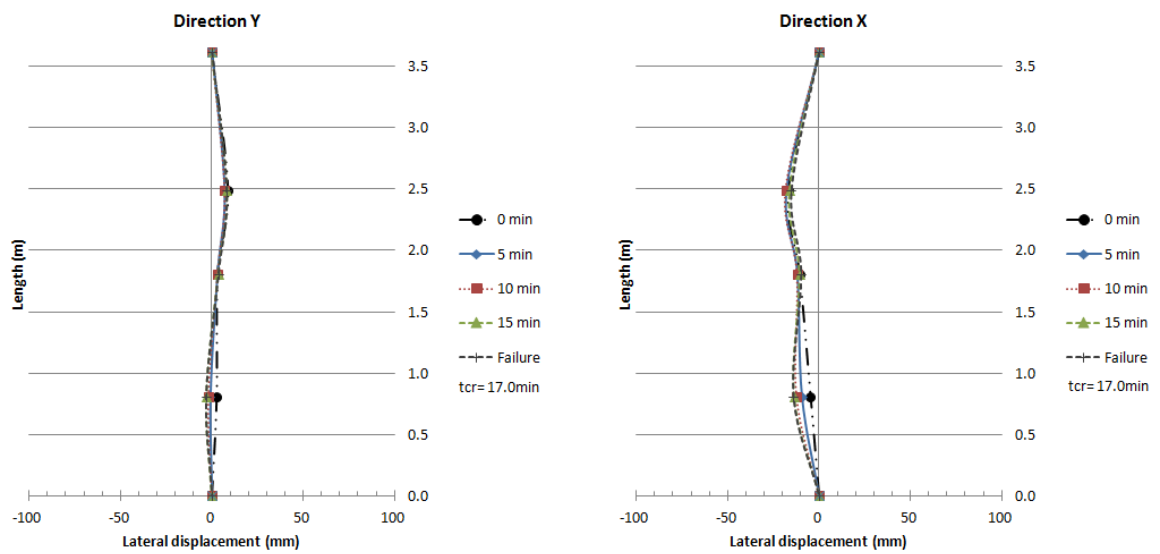


Figure C.28 – Lateral deflections in two perpendicular directions for test column A28<sub>219-RING-PC-70%-Khigh</sub>.



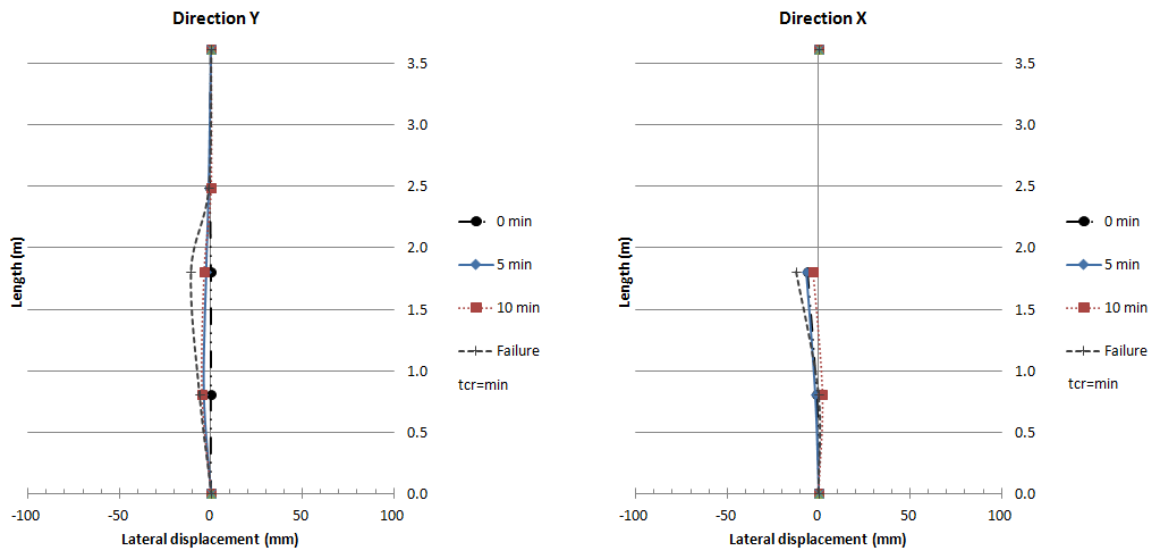


Figure C.29 – Lateral deflections in two perpendicular directions for test column A29<sub>219-RING-RC-70%-Khigh</sub>.

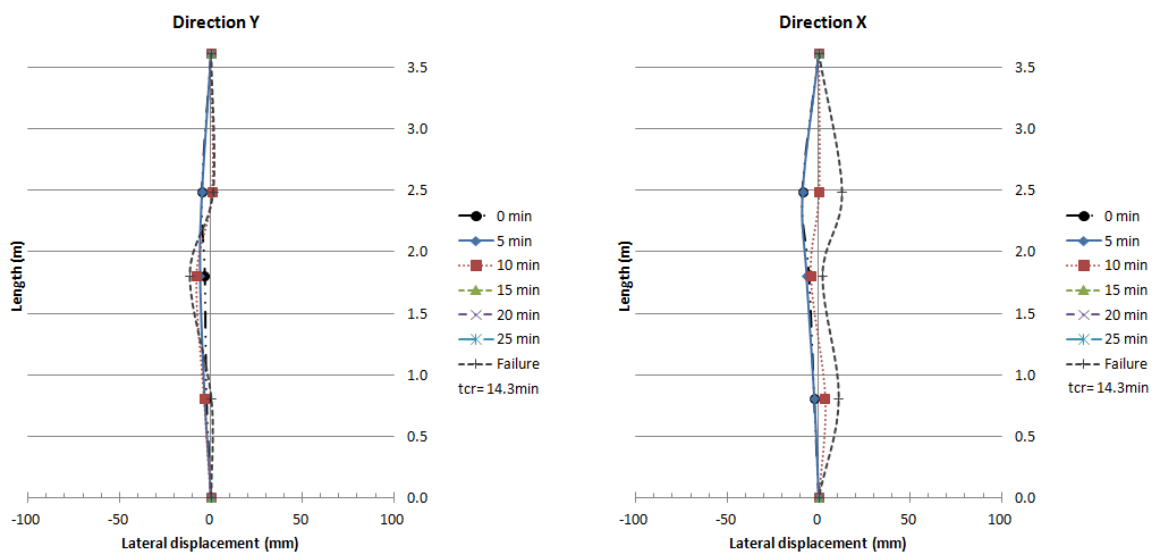


Figure C.30 – Lateral deflections in two perpendicular directions for test column A30<sub>219-70%-Khigh</sub>.

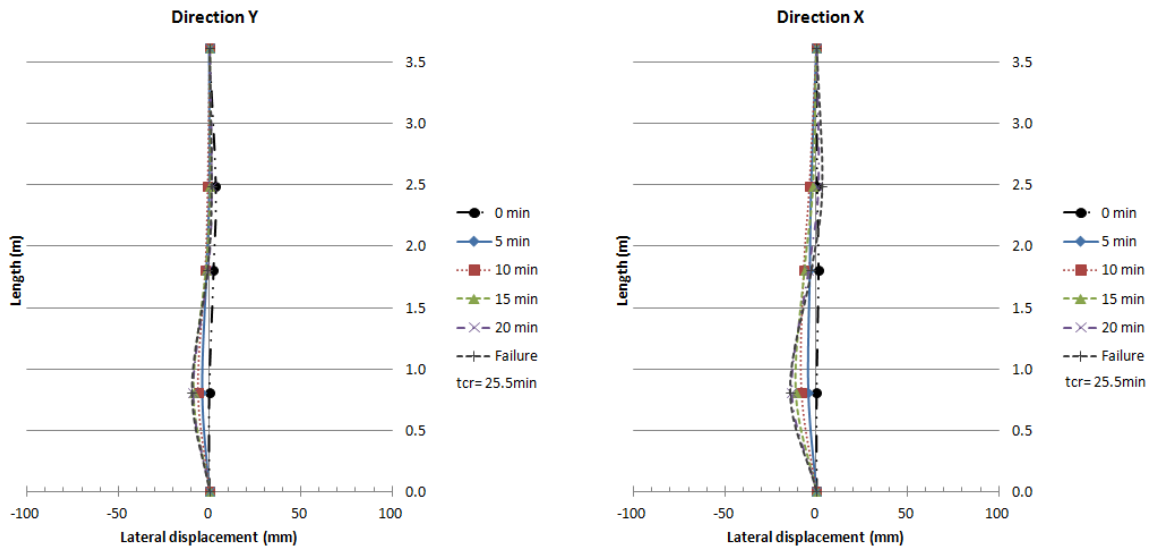


Figure C.31 – Lateral deflections in two perpendicular directions for test column A31<sub>168-TOT-PC-30%-Khigh</sub>.

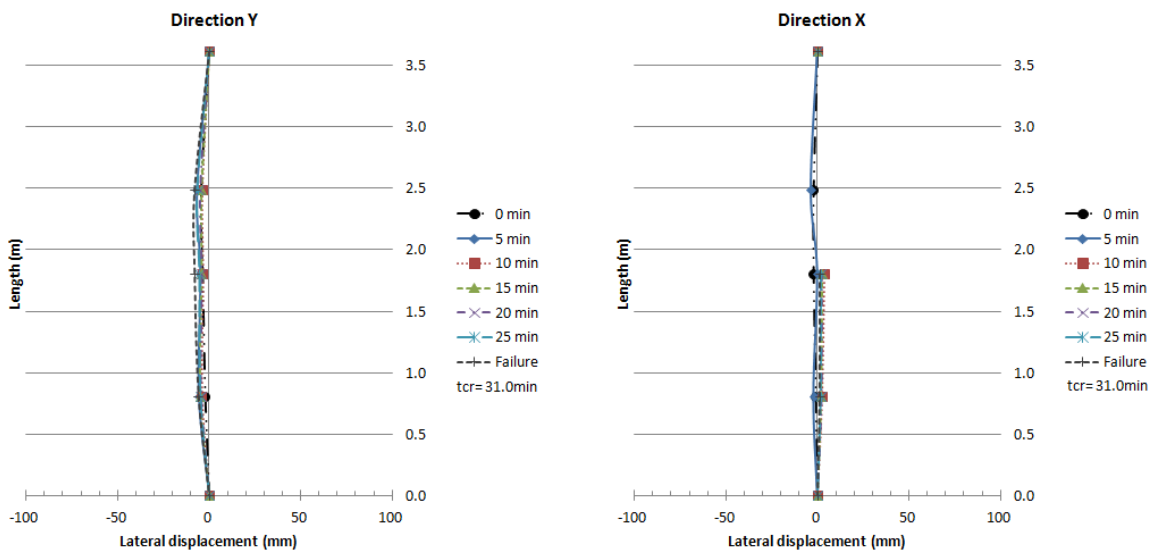


Figure C.32 – Lateral deflections in two perpendicular directions for test column A32<sub>168-TOT-RC-30%-Khigh</sub>.

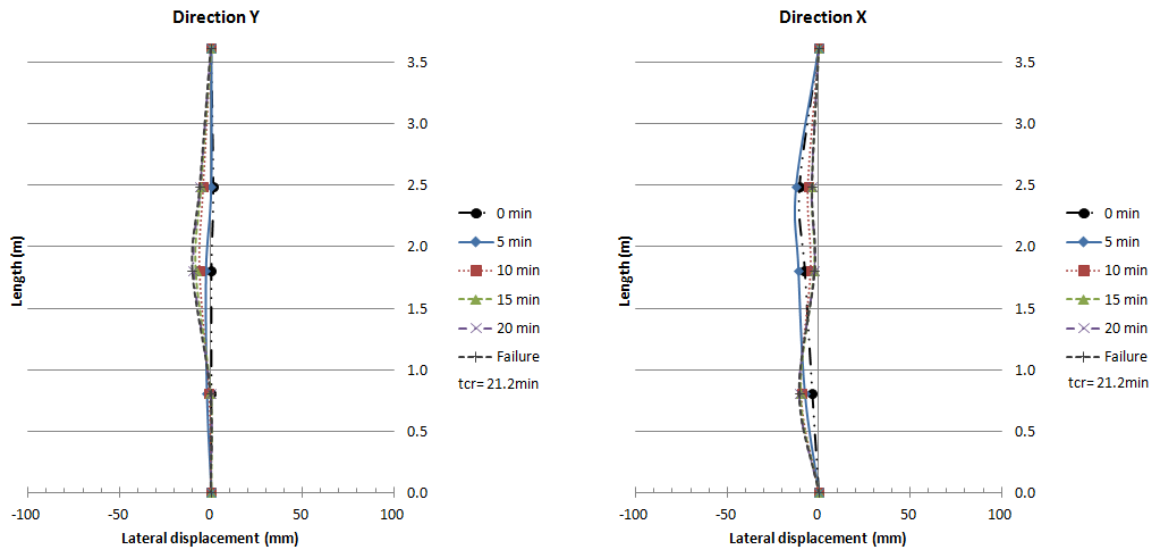


Figure C.33 – Lateral deflections in two perpendicular directions for test column A33<sub>168-RING-PC-30%-Khigh</sub>.

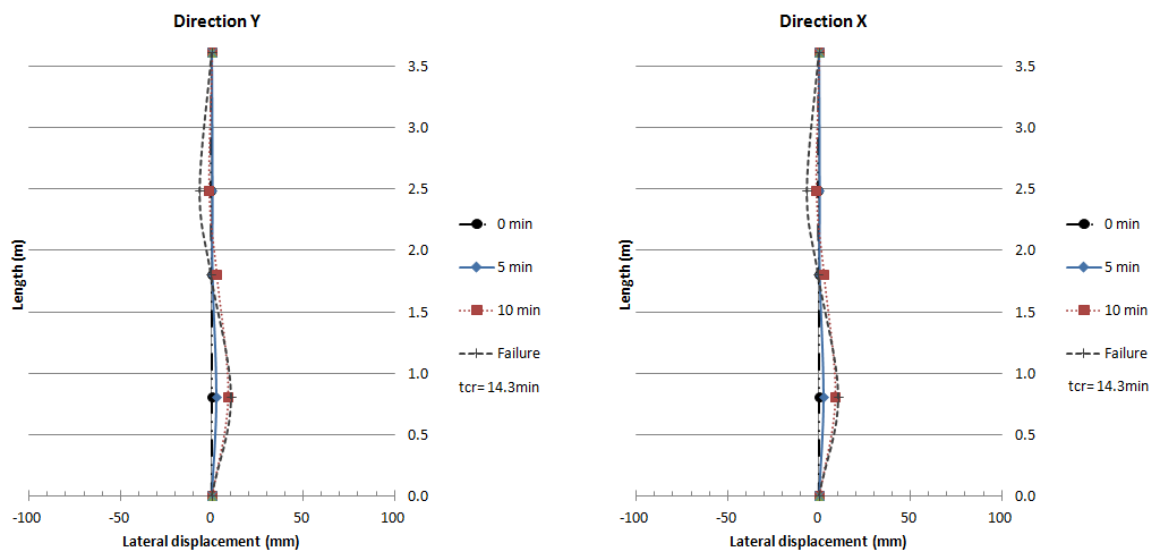


Figure C.34 – Lateral deflections in two perpendicular directions for test column A34<sub>168-RING-RC-30%-Khigh</sub>.

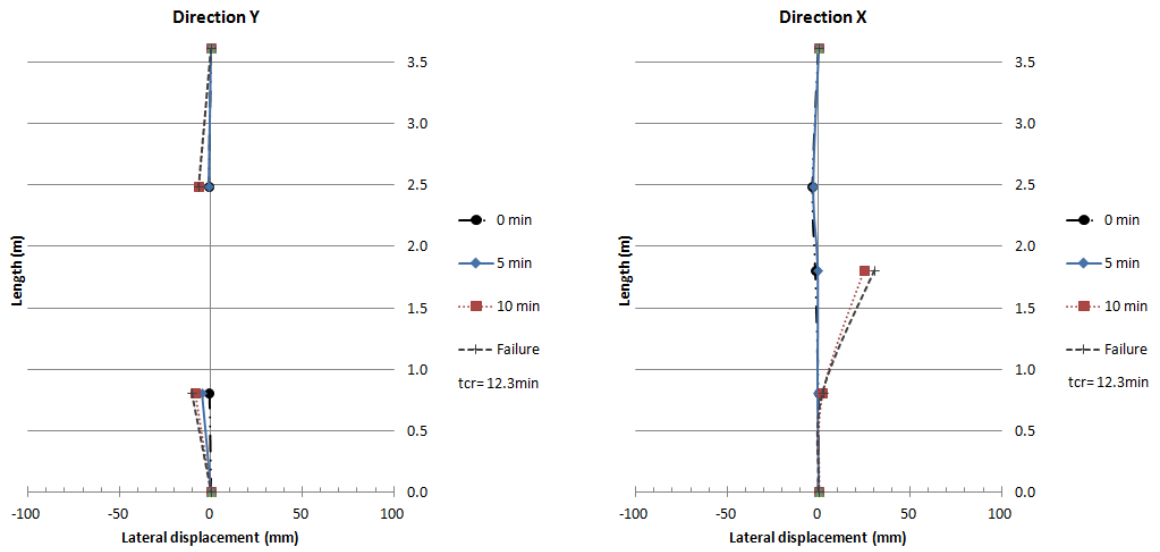


Figure C.35 – Lateral deflections in two perpendicular directions for test column A35<sub>168-30%-Khigh</sub>.

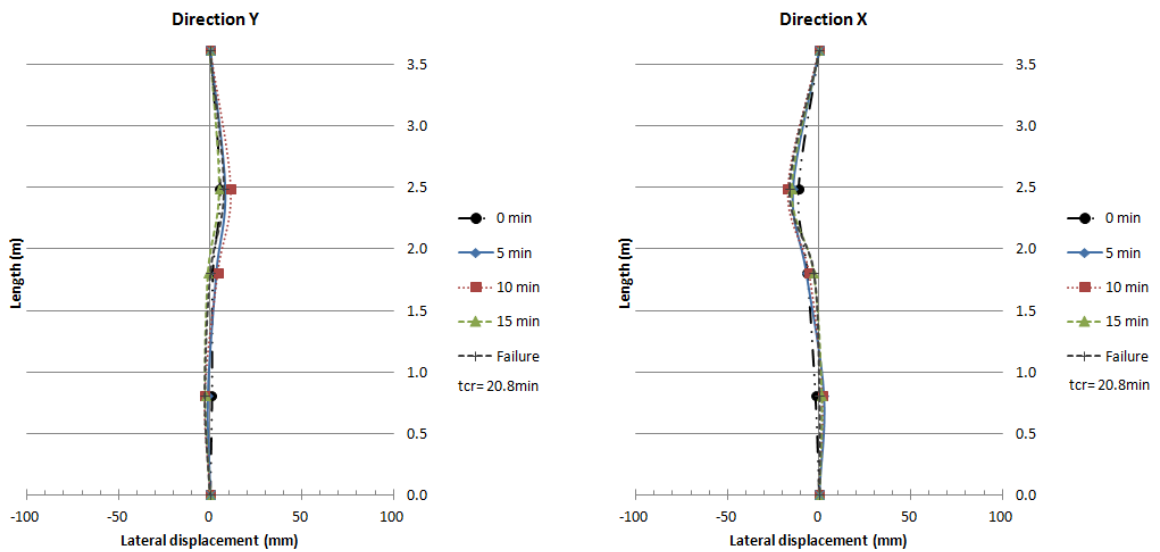


Figure C.36 – Lateral deflections in two perpendicular directions for test column A36<sub>219-TOT-PC-30%-Khigh</sub>.

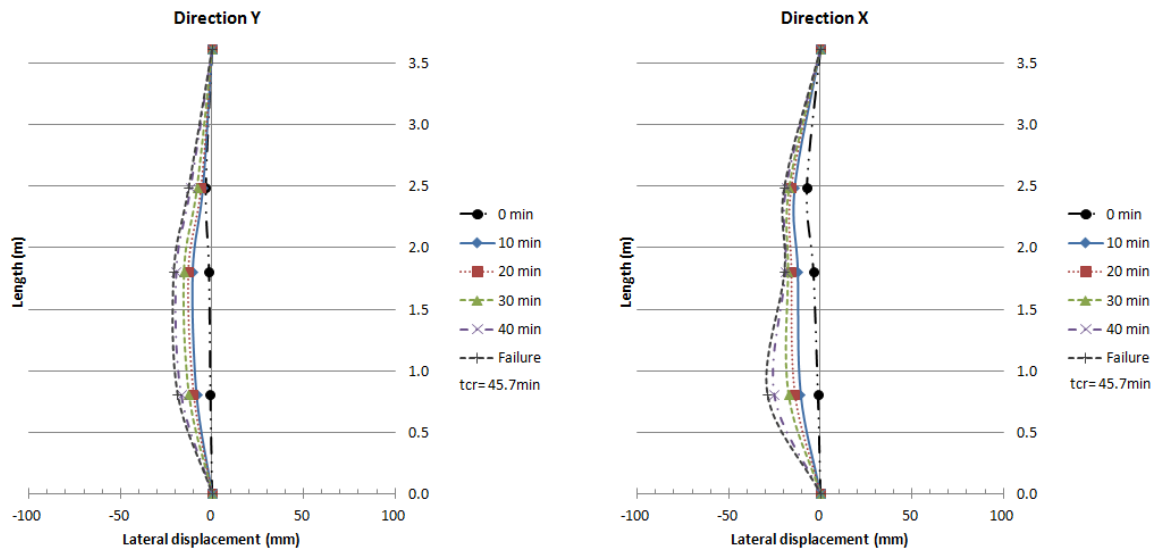


Figure C.37 – Lateral deflections in two perpendicular directions for test column A37<sub>219-TOT-RC-30%-Khigh</sub>.

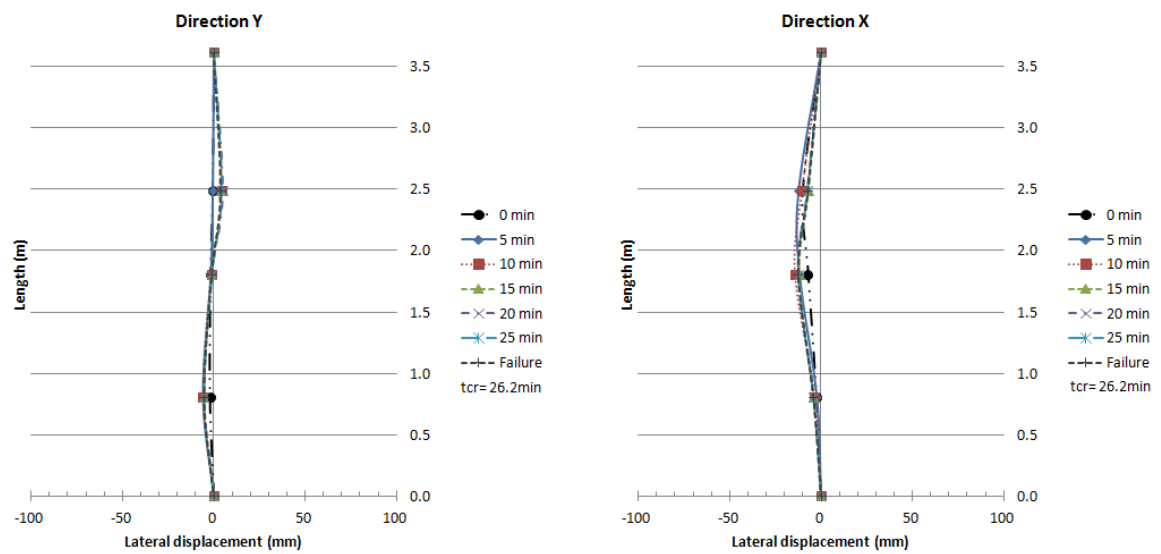


Figure C.38 – Lateral deflections in two perpendicular directions for test column A38<sub>219-RING-PC-30%-Khigh</sub>.

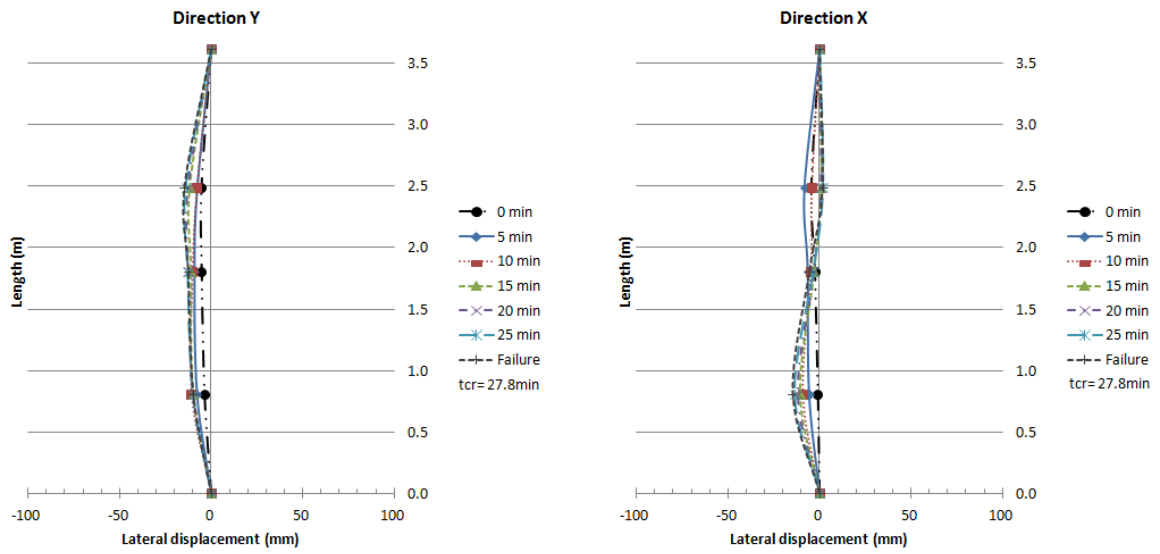


Figure C.39 – Lateral deflections in two perpendicular directions for test column A39<sub>219-RING-RC-30%-Khigh</sub>.

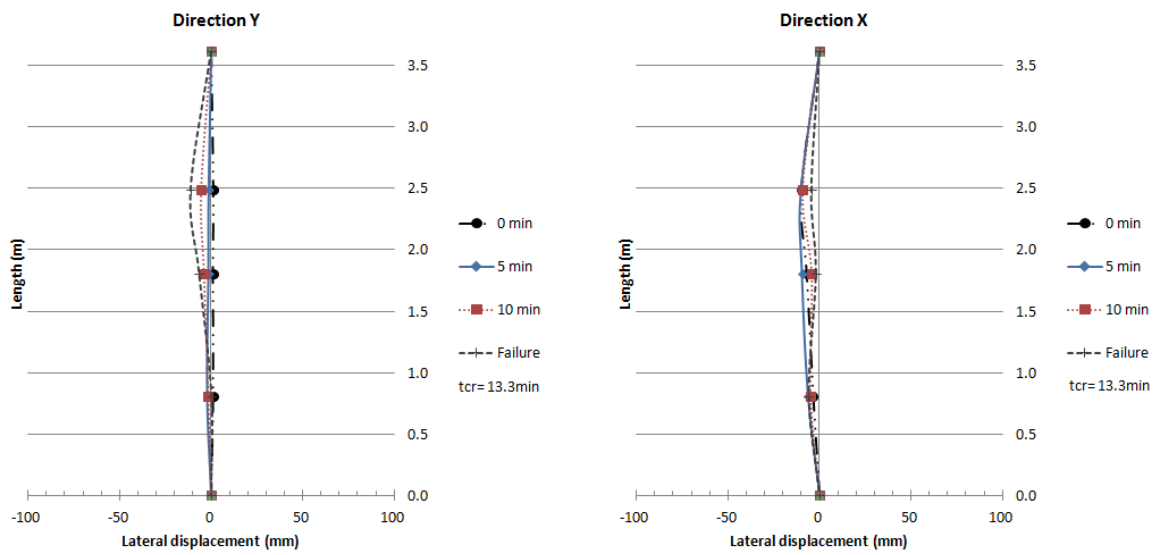


Figure C.40 – Lateral deflections in two perpendicular directions for test column A40<sub>219-30%-Khigh</sub>.

**APPENDIX D – Deformed shapes of tested columns**

Figure D.1 – Deformed shape of column  
A01 168-TOT-PC-70%-Klow.



Figure D.3 – Deformed shape of column  
A03 168-RING-PC-70%-Klow.



Figure D.2 – Deformed shape of column  
A02 168-TOT-RC-70%-Klow.



Figure D.4 – Deformed shape of column  
A04 168-RING-RC-70%-Klow.



Figure D.5 – Deformed shape of column  
A05 168-70%-Klow.



Figure D.7 – Deformed shape of column  
A07 219-TOT-RC-70%-Klow.



Figure D.6 – Deformed shape of column  
A06 219-TOT-PC-70%-Klow.



Figure D.8 – Deformed shape of column  
A08 219-RING-PC-70%-Klow.





Figure D.9 – Deformed shape of column  
A09 219-RING-RC-70%-Klow.



Figure D.11 – Deformed shape of column  
A11 168-TOT-PC-30%-Klow.



Figure D.10 – Deformed shape of column  
A10 219-70%-Klow.



Figure D.12 – Deformed shape of column  
A12 168-TOT-RC-30%-Klow.



Figure D.13 – Deformed shape of column  
A13 168-RING-PC-30%-Klow.



Figure D.15 – Deformed shape of column  
A15 168-30%-Klow.



Figure D.14 – Deformed shape of column  
A14 168-RING-RC-30%-Klow.



Figure D.16 – Deformed shape of column  
A16 219-TOT-PC-30%-Klow.



Figure D.17 – Deformed shape of column  
A17 219-TOT-RC-30%-Klow.



Figure D.19 – Deformed shape of column  
A19 219-RING-RC-30%-Klow.



Figure D.18 – Deformed shape of column  
A18 219-RING-PC-30%-Klow.



Figure D.20 – Deformed shape of column  
A20 219-30%-Klow.



Figure D.21 – Deformed shape of column  
A21 168-TOT-PC-70%-Khigh-



Figure D.23 – Deformed shape of column  
A23 168-RING-PC-70%-Khigh-



Figure D.22 – Deformed shape of column  
A22 168-TOT-RC-70%-Khigh-



Figure D.24 – Deformed shape of column  
A24 168-RING-RC-70%-Khigh-





Figure D.25 – Deformed shape of column  
A25 168-70%-Khigh.



Figure D.27 – Deformed shape of column  
A27 219-TOT-RC-70%-Khigh.



Figure D.26 – Deformed shape of column  
A26 219-TOT-PC-70%-Khigh.



Figure D.28 – Deformed shape of column  
A28 219-RING-PC-70%-Khigh.



Figure D.29 – Deformed shape of column  
A29 219-RING-RC-70%-Khigh.



Figure D.31 – Deformed shape of column  
A31 168-TOT-PC-30%-Khigh.



Figure D.30 – Deformed shape of column  
A30 219-70%-Khigh.



Figure D.32 – Deformed shape of column  
A32 168-TOT-RC-30%-Khigh.



Figure D.33 – Deformed shape of column  
A33 168-RING-PC-30%-Khigh.



Figure D.35 – Deformed shape of column  
A35 168-30%-Khigh.



Figure D.34 – Deformed shape of column  
A34 168-RING-RC-30%-Khigh.



Figure D.36 – Deformed shape of column  
A36 219-TOT-PC-30%-Khigh.



Figure D.37 – Deformed shape of column  
A37 219-TOT-RC-30%-Khigh-



Figure D.39 – Deformed shape of column  
A39 219-RING-RC-30%-Khigh-



Figure D.38 – Deformed shape of column  
A38 219-RING-PC-30%-Khigh-



Figure D.40 – Deformed shape of column  
A40 219-30%-Khigh-



## APPENDIX E – Fire tests on fibre reinforced concrete filled circular hollow (CFCH-FRC) columns

This appendix presents two Concrete Filled Circular Hollow (CFCH) columns that were filled with steel + polypropylene fibre reinforced concrete (FRC). The columns were tested in the same apparatus previously presented in this thesis. Table E.1 presents the concrete composition used in the casting of these columns.

Table E.1 – Steel + polypropylene fibre reinforced concrete composition.

<i>Composites</i>	<i>Quantity (Kg/m<sup>3</sup>)</i>
<b>Calcareous aggregate</b>	900
<b>Fine siliceous sand</b>	320
<b>Medium siliceous sand</b>	550
<b>Cement 52.5</b>	300
<b>Super - plasticizer Sika 3002HE</b>	3.2
<b>Water</b>	172
<b>steel fibers</b>	39.7
<b>polypropylene fiber</b>	2

The external diameters of the columns were 168.3 and 219.1mm and the length 3000mm. The concrete filling formed a ring around the inner wall of the steel tube and the ring thicknesses were 40 and 50mm respectively for the 168.3 and 219.1mm columns. The load level applied was 30% of the design value of the buckling load at room temperature ( $N_{ed}$ ) calculated as per EN1994-1-1 (2005) and the stiffness of the surrounding structure was 13kN/mm (axial stiffness), 4091 and 1992 kN m/rad (rotational stiffness in the main perpendicular directions). The heating rate followed the ISO834(1999) standard curve. Table E.2 presents the main parameters of these columns and its critical times and failure modes.

Thermocouples type K registered the evolution of temperatures along the time in the steel tube surface (T1) and in the concrete ring (T2). Five different sections were instrumented (S1 to S5) along the column length (Figure E.1).

Table E.2 – Test plan, critical times and failures modes of the fibre reinforced columns

<i>Ref.</i>	<i>Diameter (mm)</i>	<i>Degree of concrete filling</i>	<i>Relative slenderness <math>\bar{\lambda}</math></i>	<i>Serviceability load (kN) (%Ned)</i>	<i>Critical time (min)</i>	<i>Failure mode</i>
<b>A41</b>	168.3	Ring (40mm)	0.924	376 (30%)	28	global buckling
<b>A42</b>	219.1	Ring (50mm)	0.714	640 (30%)	31	global buckling

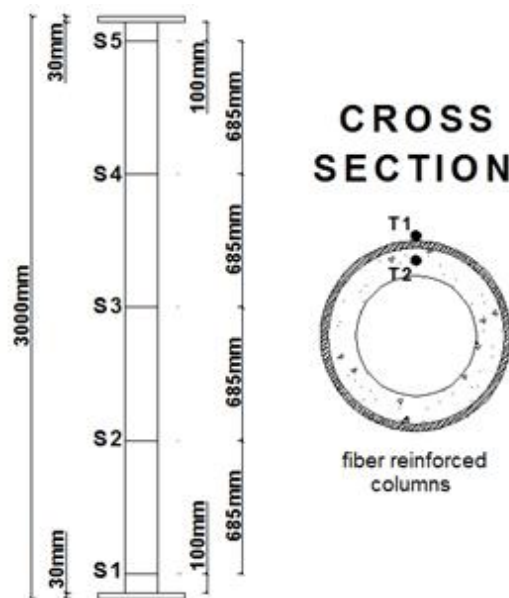


Figure E.1 – Position of thermocouples on the columns by height and cross-section

### ***Results of restraining forces and critical times***

Figures E.2 and E.3 present the relative restraining forces in function of the time for the tested columns. The results of CFCH-RC and CFCH-PC columns also were plotted for a comparison.

The graphs shows that the columns filled with plain concrete (PC) or fibre reinforced concrete (FRC) presented higher critical times, being even higher for those filled with fibre concrete.

The columns filled with fibre reinforced concrete (FRC) presented a small reduction in the restraining forces, maybe due to a better bonding strength between the concrete and the steel profile that reduced the thermal elongation of the column. Also these columns have higher stiffness than the others.

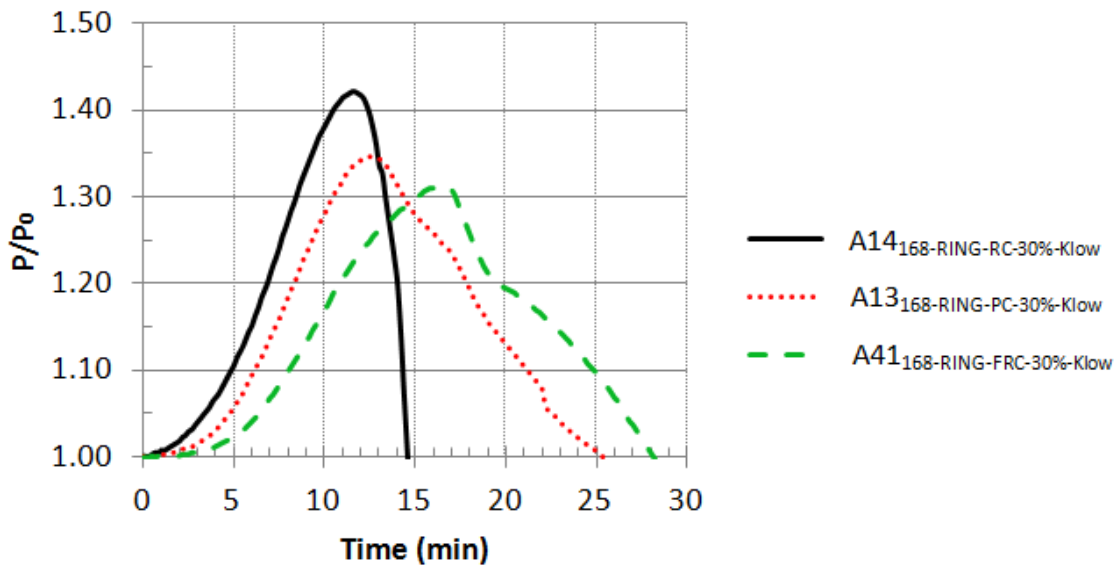


Figure E.2 – Restraining forces of CFCH columns with 168.3mm of diameter

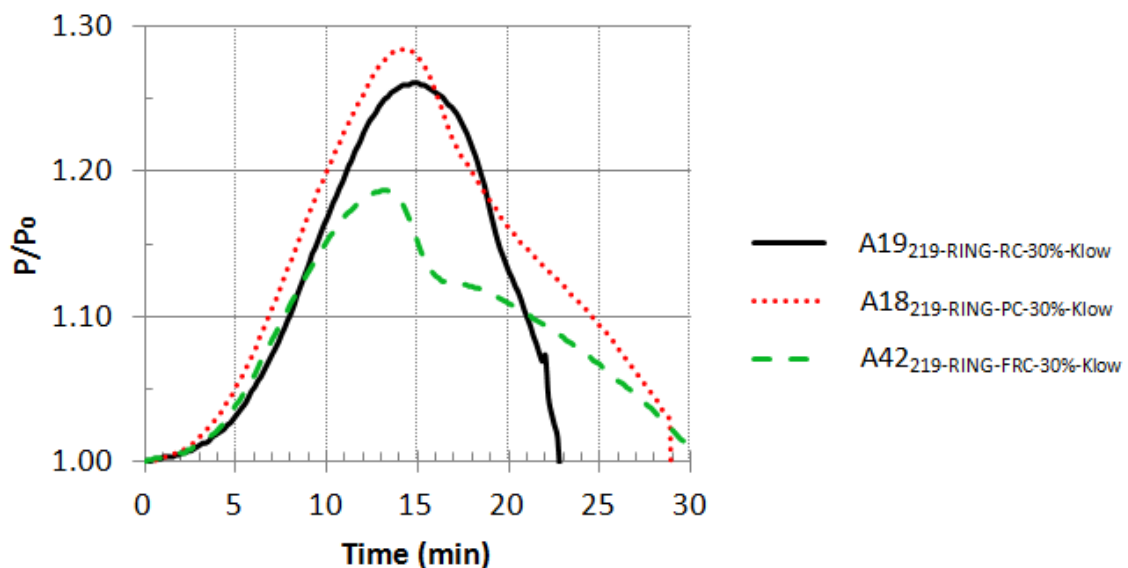


Figure E.3 – Restraining forces of CFCH columns with 219.1mm of diameter

The columns filled with steel reinforcing bars (RC) presented the worst behaviour in terms of critical times. However the restraining forces in these columns were slightly higher than in the others. The use of reinforcing steel bars in a concrete ring of small thickness is not a good solution. The steel bar instead of increasing the concrete strength, contributed due to expansion, to its excessive cracking and collapse. In this case the use of steel + polypropylene fibre concrete (FRC) proved to be a better solution.

The critical times of CFCH-PC and CFCH-FRC columns were very similar for both diameters (26 and 28min respectively for the columns with diameter of 168.3mm and 29 and 31min for the columns with 219.1mm). The critical times of the CFCH-RC are much smaller than others (15min for the column with diameter of 168.3mm and 23min for the column with 219.1mm) (Figures E.2 and E.3).

The critical times of the columns with 168.3mm of diameter (Figure E.2) were slight smaller than the ones of 219.1mm of diameter (Figure E.3), maybe due to the higher slenderness of the columns with smaller diameter.

### ***Results of axial deformations***

Figures E.4 and E.5 presents the axial deformations in function of the time for the tested columns. Again a comparison with similar CFCH ring columns was done.

In the restraining forces graphs (Figures E.2 and E.3) was observed that the CFCH-FRC columns presented the smaller relative restraining forces that corresponded to smaller axial deformations (Figures E.4 and E.5). The same justification advanced for the restraining forces is maybe also valid for this case. The maximum axial deformation was very similar for the two diameter of the column tested. They were around 8mm for the FRC and 12mm for the RC and PC columns.

### ***Failure mode***

In fact the columns were designed as pin-ended but the failure modes were more similar to pin-fixed-ended or fixed-fixed-ended columns (see Appendix D). The surrounding structure imposed some rotational restraint to the test columns that is usually not considered in the design.

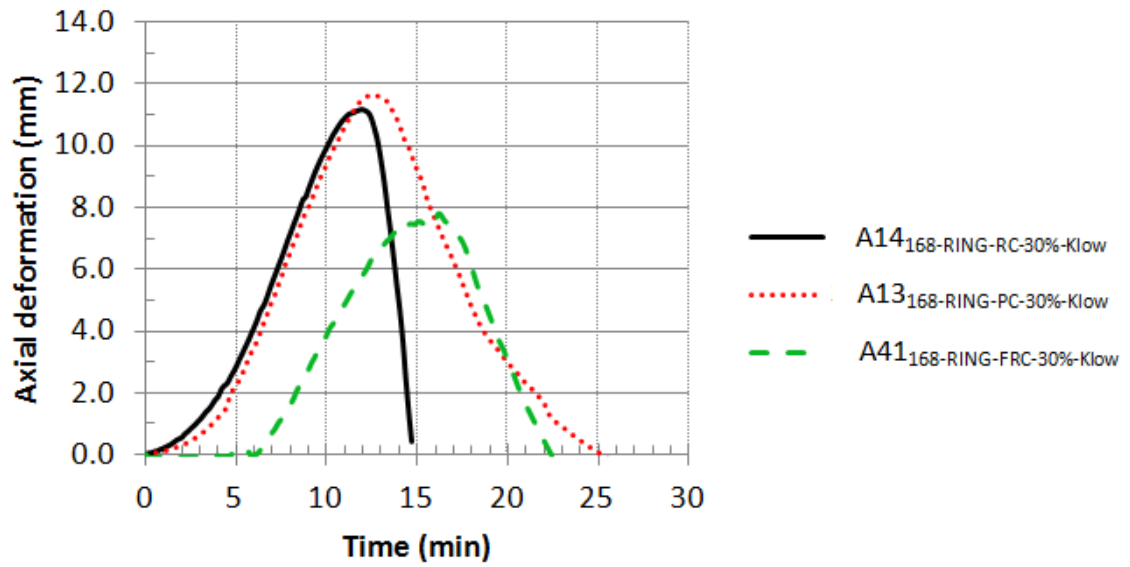


Figure E.4 – Axial deformations of CFCH columns with 168.3mm of diameter

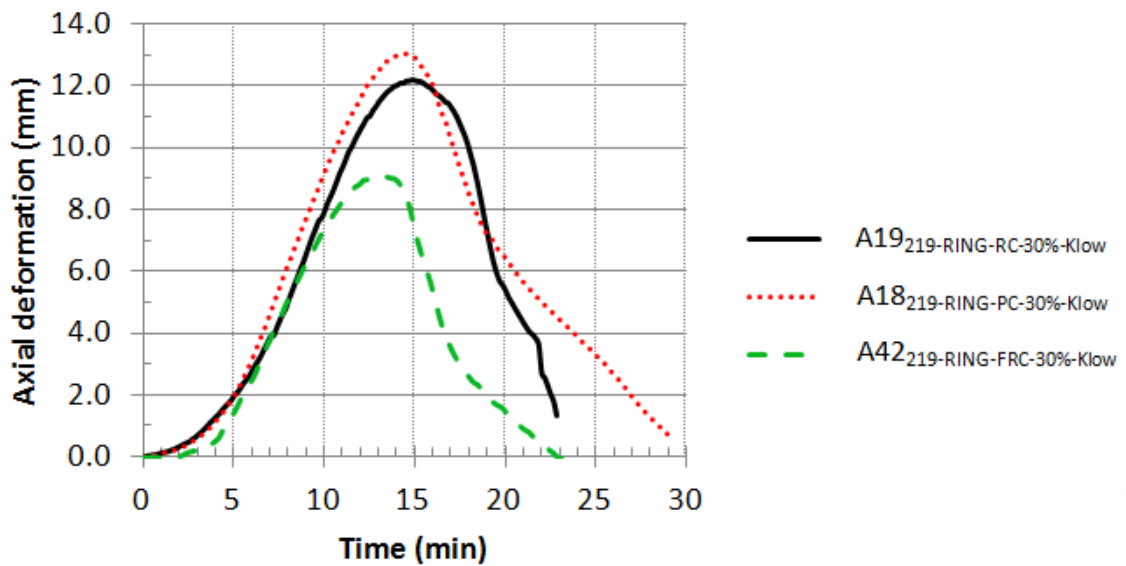


Figure E.5 – Axial deformations of CFCH columns with 219.1mm of diameter

The major failure mode of the columns was global buckling presenting the columns at the final stage a deformed shape in “S”. The higher deformation is slightly upward may be due to the furnace thermal gradient in height and/or the high stiffness of the steel piston for measuring the restraining forces that was located on the top of the test column connecting it to the 3D restraining frame.

In some cases, mainly the CFCH-PC and CFCH-RC columns, presented local buckling (see Appendix D). This suggests that the filling with steel fibre concrete (FRC) avoid the local buckling. The addition of polypropylene fibres could avoid the spalling of the concrete inside the columns, keeping intact the concrete ring longer and thus avoiding their local buckling

### ***Remarks***

The main conclusions about the fire performance of CFCH-FRC columns are:

- The concrete reinforcement with steel + polypropylene fibres (FRC) reduced the restraining forces and axial deformations and improved the fire performance in terms of critical times and avoiding the local buckling;
- It was observed sudden failure and shorter critical times for the CFCH-RC columns due to the small thickness of the concrete ring. Add steel fibres to the concrete in these columns are advisable.
- So, the use of steel + propylene fibre concrete (FRC) for filling CFCH columns can be a better solution than using plain (PC) or steel bar reinforced (RC) concrete especially in small diameters.